D I S S E R T A T I O N

submitted to the

Combined Faculty of Natural Sciences and Mathematics

of the

Ruperto-Carola University Heidelberg, Germany

for the degree of

Doctor of Natural Sciences

Presented by

M. Sc. Florian Köhler

born in Rathenow, Germany

Oral examination: October 10th, 2019

Epigenetic deregulation of lamina-associated domains in Hutchinson-Gilford Progeria Syndrome

Referees:

Prof. Dr. Frank Lyko

Dr. Sylvia Erhardt

‘All I know is that I know nothing.’ – Socrates

Zusammenfassung

Hutchinson-Gilford Progeria Syndrome (HGPS) ist eine seltene genetische Erkrankung, in der typischerweise altersassoziierte Symptome wie Arthritis, Lipodystrophie und Arteriosklerose bereits in jungem Alter auftreten. Zellen von HGPS Patienten exprimieren eine mutante Version des nukleären Hüllenproteins Lamin A, besser bekannt als Progerin. Gleichzeitig zeigen diese Zellen charakteristische Veränderungen an Histonmodifikationen, jedoch ist unklar, ob und inwieweit selbige einen Einfluss auf die Chromatinzugänglichkeit, DNA Methylierung sowie Genexpression in betroffenen Zellen haben.

In der vorliegenden Arbeit wurden epigenetische Veränderungen in primären Hautfibroblasten von HGPS Patienten mittels 'Assay for Transposase-Accessible Chromatin using Sequencing' (ATAC-seq), DNA Methylierunsanalysen und 'DNA Adenine Methyltransferase Identification using Sequencing' (Dam ID-seq) untersucht. Die Ergebnisse dieser Experimente zeigen, dass HGPS-spezifische Chromatinzugänglichkeits- und DNA Methylierungsveränderungen in so genannten ‚Lamina-assoziierten Domänen' (LADs), d.h. Genomregionen, welche in Kontakt mit der nukleären Lamina sind, angereichert vorkommen. Eine mechanistische Erklärung für diese Beobachtung lieferten gleichzeitige Veränderungen in der Lamin A-assoziierten LAD Landschaft, welche, in Kombination mit der epigenetischen Deregulierung der LADs, zur krankheitsspezifischen Genexpression von HGPS Fibroblasten beitragen. Unabhängig davon ließen sich die untersuchten Zellen anhand ihrer DNA Methylierungsprofile in zwei Subgruppen unterteilen, wovon eine ein im Durchschnitt rund ~ 10 Jahre höheres epigenetisches Alter als das durchschnittliche chronologische Alter aufwies. Dies lässt darauf schließen, dass zumindest in einem Teil von HGPS Patienten Merkmale eines fortgeschrittenen Alters auch auf epigenetischer Ebene manifestiert sind.

Zusammengenommen identifizieren die hierin gemachten Beobachtungen die epigenetische Deregulierung von LADs als ein kritisches und zuvor unerkanntes Merkmal von HGPS Zellen, welches einen Einfluss auf die krankheitsspezifische Genexpression hat. Daher erweitern diese die Forschung an dem Alterssyndrom nicht nur um eine neue epigenetische Komponente, sondern verbessern gleichzeitig unser Verständnis der ihm zugrundeliegenden molekularen Mechanismen.

Abstract

Hutchinson-Gilford Progeria Syndrome (HGPS) is a rare genetic disorder characterized by the onset of some age-related phenotypes including arthritis, lipodystrophy and atherosclerosis at a very early age. Cells from HGPS patients express a mutant version of the nuclear envelope component Lamin A (termed Progerin) and have previously been reported to exhibit characteristic histone modification changes. However, how these alterations affect the landscape of chromatin accessibility and global DNA methylation patterns or whether they are linked to disease-specific gene expression changes, is still unknown.

In this work, HGPS-specific epigenetic changes were analyzed in primary dermal fibroblasts using 'Assay for Transposase-Accessible Chromatin using Sequencing' (ATAC-seq), DNA methylation profiling and 'DNA Adenine Methyltransferase Identification using Sequencing' (Dam ID-seq). Importantly, HGPS cells exhibited chromatin accessibility and DNA methylation alterations enriched in lamina-associated domains (LADs). Strikingly, the epigenetic deregulation of LADs corresponded to changes in the Lamin A-associated LAD landscape in HGPS fibroblasts, thus yielding a mechanistic explanation for the observed dynamics. By integrating RNA-sequencing data into the analysis, both the epigenetic deregulation of LADs and the HGPS-specific changes in the LAD interactome were found to contribute to the pathological gene expression signature of patient fibroblasts. Independently of this, HGPS patients could be stratified into two subgroups based on their DNA methylation profiles, with one subgroup revealing an average epigenetic age acceleration of ~ 10 years. This confirms that at least in a subset of HGPS patients, characteristics of an advanced age are also manifested at the epigenetic level.

Taken together, the findings made herein identify the epigenetic deregulation of LADs as a critical and previously unrecognized feature of HGPS that is associated with disease-related gene expression patterns. Hence, they not only add a novel layer to the study of epigenetic changes in the progeroid disease but also significantly advance our understanding of its molecular pathology.

Table of Contents

List of Tables

List of Figures

List of Abbreviations (A→Z)

53BP1	*TP53 Binding Protein 1*
AP1	*Activating Protein 1*
ATAC-see	*Assay for Transposase-Accessible Chromatin using Microscopy*
ATAC-seq	*Assay for Transposase-Accessible Chromatin using Sequencing*
BAF	*Barrier-to-autointegration*
C-terminal	*Carboxy-terminal*
cDNA	*coding DNA*
COL4A1	*Collagen Type IV Alpha 1 Chain*
COL4A5	*Collagen Type IV Alpha 5 Chain*
Dam	*DNA adenine methyltransferase*
Dam ID-seq	*DNA Adenine Methyltransferase Identification using Sequencing*
ddH_2O	*Double-destilled Water*
DMEM	*Dulbecco's Modified Eagle Medium*
DMSO	*Dimethyl Sulfoxide*
DNA	*Deoxribonucleic Acid*
DNMTs	*DNA Methyltransferases*
dNTP	*deoxy Nucleotidetriphosphate Triphosphate*
DPT	*Dermatopontin*
DTT	*Dithiothreitol*
ECM	*Extracellular Matrix*
EDIL3	*EGF Like Repeats And Discoidin Domains 3*
EDTA	*Ethylenediaminetetraacetic Acid*
EHMT2/G9A	*Euchromatic Histone Lysine Methyltransferase 2*
ESC	*Embryonic Stem Cell*
EtOH	*Ethanol*
EZH2	*Enhancer Of Zeste 2 Polycomb Repressive Complex 2*
FACS	*Fluorescence-activated Cell Sorting*
FBS	*Fetal Bovine Serum*
FDR	*False Discovery Rate*
FISH	*Fluorescence In Situ Hybridization Hybridization*
FTI	*Farnesyltransferase Inhibitor*
GO	*Gene Ontology*
GSEA(s)	*Gene Set Enrichment Analysis*
HEPES	*Hydroxyetyl-Piperazineethane-Solfonic Acid*
HMD	*Highly Methylated Domain*
HP1	*Heterochromatin Protein 1*
HRP	*Horseradish Peroxidase*
IF	*Immunofluorescence*
IGFBP7	*Insulin Like Growth Factor Binding Protein 7*
iPSC	*induced Pluripotent Stem Cell*
IPTG	*Isopropyl β-D-1-Thiogalactopyranoside*
KEGG	*Kyoto Encyclopedia of Genes and Genomes*

LAD(s)	*Lamina-associated Domain(s)*
LAP2α	*Lamina-associated polypeptide 2α*
LB Agar	*Lysogeny Broth Agar*
LBR	*Lamin B Receptor*
LINEs	*Long Interspersed Nuclear Elements*
LMNA	*Lamin A Gene*
miR-9	*micro RNA-9*
mRNA	*Messenger RNA*
MSCs	*Mesenchymal Stem Cells*
MSigDB	*Molecular Signatures Database*
N-terminal	*Amino-terminal*
ncRNA	*non-coding RNA*
NEB	*New England Biolabs*
NGS	*Next Generation Sequencing*
NHEJ	*Non-homologous End Joining*
NRF2	*Nuclear Factor Erythroid 2-related Factor 2*
OD_X	*Optical Density at Wavelength X nm*
PARP1	*Poly(ADP-Ribose) Polymerase 1*
PBS	*Phosphate-buffered Saline*
PBT	*PBS with Tween 20*
PCA	*Principal Component Analysis*
PCR	*Polymerase Chain Reaction*
PEI	*Polyethylenimine*
PFA	*Paraformaldehyde*
pH	*Hydrogen Ion Concentration*
PI	*Propidium Iodide*
PMD	*Partially Methylated Domain*
pRb	*Retinoblastoma Protein*
PRF	*Progeria Research Foundation*
PRR14	*Proline-rich 14*
qPCR	*Quantitative PCR*
RNA	*Ribonucleic Acid*
RNA-seq	*RNA Sequencing*
RT	*Reverse Transcription*
SAHF	*Senescence-associated Heterochromatin Foci (SAHF)*
SDS	*Sodium Dodecyl Sulfate*
SDS-PAGE	*Sodium Dodecyl Sulfate - Polyacrylamide Gel Electrophoresis*
shRNA	*short-hairpin RNA*
SIRT6	*Sirtuin 6*
solo-WCGW	*Single CpG Flanked By A or T on both Sides*
SREBP1	*Sterol Regulatory Element-binding Protein 1*
SSC	*Saline-Sodium Citrate*
SUN1	*Sad1 And UNC84 Domain Containing 1*
SUV39H1/2	*Suppressor Of Variegation 3-9 Homolog 1/2*

TAE	*Tris-acetate-EDTA*
TBE	*Tris-borate-EDTA*
TEAD	*TEA Domain Transcription Factor*
TFBS(s)	*Transcription Factor Binding Site(s)*
TRF2	*Telomere Repeat-binding Factor 2*
TWIST2	*Twist Family BHLH Transcription Factor 2*
UV	*Ultraviolet*
v/v	*Volume/Volume*
VSMCs	*Vascular Smooth Muscle Cells*
w/v	*Weight/Volume*
WB	*Western Blot*
XPA	*Xeroderma Pigmentosum Group A*
ZMPSTE24	*Zinc Metallopeptidase STE24*

Units (A→Z)

bp	*Base Pairs*
cm	*Centimeter*
d	*Day(s)*
g	*Standard Gravity (9.81 m/s^2)*
kb	*Kilobases*
kDa	*Kilodalton*
l	*Liter*
M	*Molar (mol/l)*
Mb	*Megabases*
mg	*Milligram(s)*
min	*Minute(s)*
ml	*Milliliter*
mM	*Millimolar (mmol/l)*
mm	*Millimeter*
ng	*Nanogram(s)*
nm	*Nanometer*
s	*Second(s)*
μg	*Microgram(s)*
μl	*Microliter*
μM	*Micromolar (μmol/l)*
μm	*Micrometer*
W	*Watt*

1. Introduction

1.1. Epigenetic changes are a hallmark of aging

The process of aging is characterized by a continuous loss of function at the cellular, tissue and organismal level. Epigenetic changes represent one of the hallmarks of this process (López-Otín *et al.*, 2013). They involve molecular alterations that are not encoded in the underlying genomic sequence but instead control gene expression '*epi-*' genetically, i.e. 'on top of' the level of the DNA. A cell's epigenome is much more dynamic than the more static genome; in fact, epigenetic changes can occur in response to external stimuli, allowing the organism to adapt to a changing environment. As such, the epigenome needs to be stringently controlled and demands a sophisticated regulatory landscape, which involves DNA methylation, post-translational modifications of histones, chromatin remodeling and non-coding RNAs (ncRNAs). During aging, this multilayered regulatory system is subject to a loss of fidelity and functional decline, culminating in altered gene expression, the activation of transposable elements and genomic instability.

1.1.1. DNA methylation dynamics during aging

DNA methylation involves the transfer of a methyl group from the donor S-adenosylmethyonine to the 5' position of a cytosine, creating 5-methylcytosine. In mammals, this reaction is catalyzed by the activity of the DNA methyltransferases (DNMTs) DNMT1, DNMT3A and DNMT3B, and occurs predominantly in the context of CpG dinucleotides (Bird, 2002; Lyko, 2018). 28 million CpGs are present in the human genome, 60-80 % of which are methylated in somatic cells (Smith and Meissner, 2013). The remaining 20-40 % are frequently clustered in regions known as CpG islands, which are often found in or close to regulatory elements (Deaton and Bird, 2011). Historically, the presence of the modification has been linked to the suppression of transposable elements, X-chromosome inactivation, genomic imprinting and heterochromatin formation (Li, Beard and Jaenisch, 1993; Singer-Sam J, 1993; Jones and Takai, 2001; Smith and Meissner, 2013; Rose and Klose, 2014). However, more recent data suggest that it also has a role in transcriptional regulation, marking regions of active gene expression and preventing aberrant transcription initiation (Baubec *et al.*, 2015; Neri *et al.*, 2017).

DNA methylomes become more divergent with age (Fraga *et al.*, 2005; Heyn *et al.*, 2012; Bormann *et al.*, 2016). This process includes the accumulation of stochastic changes, commonly referred to as epigenetic drift, as well as the occurrence of more directional alterations (Figure 1) (Horvath, 2013; Teschendorff, West and Beck, 2013; Issa, 2014; Zampieri *et al.*, 2015). For example, in various aging mammalian cells and tissues, DNA methylation levels tend to decline at megabase scale in AT-rich, lamina-associated genomic regions (Heyn *et al.*, 2012; Pérez *et al.*, 2018; Zhou *et al.*, 2018). This hypomethylation also occurs at repetitive sequences like Alu elements, possibly contributing to increased genomic instability (Figure 1) (Bollati *et al.*, 2009; Jintaridth and Mutirangura, 2010; Zampieri *et al.*, 2015). In addition, aging DNA methylomes are frequently characterized by site-specific DNA hypermethylation,

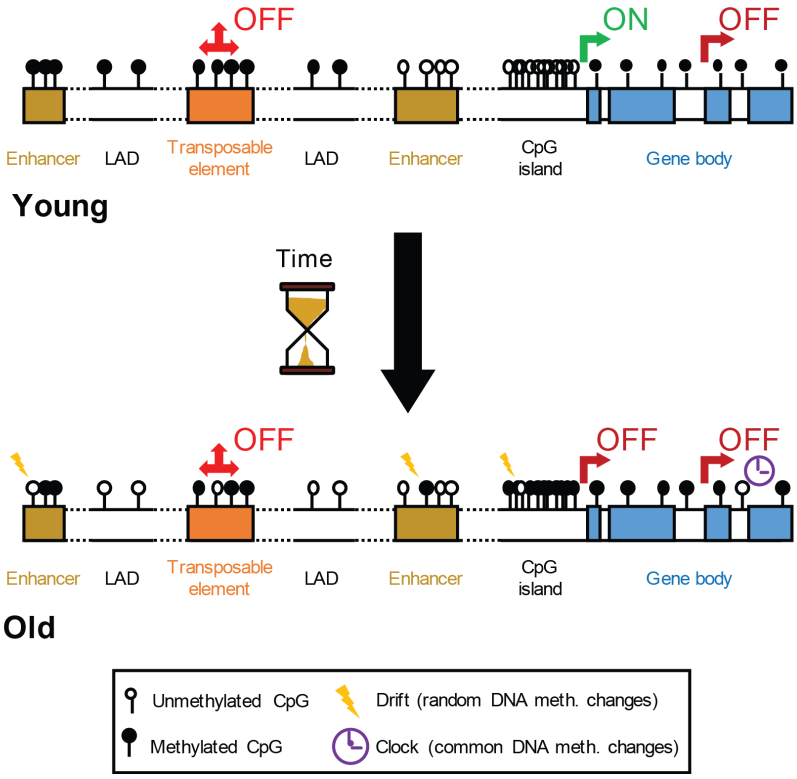

Figure 1: DNA methylation changes occurring during aging. Mammalian DNA methylomes become more divergent with age. This process includes stochastic changes (referred to as 'epigenetic drift') as well as more directional ones. Hypomethylation occurs at lamina-associated domains (LADs) and repetitive sequences like transposable elements, whereas promoter-associated CpG islands frequently gain DNA methylation, thus silencing gene expression. Many of the underlying dynamics can be tracked with recently developed epigenetic age predictors, which use the methylation status of a selected number of 'clock CpGs'. Adapted from Köhler and Rodriguez-Paredes, 2019. meth. = methylation.

predominantly at promoter-associated CpG islands (Figure 1) (Heyn *et al.*, 2012; Yuan *et al.*, 2015). Interestingly, both large-scale DNA hypomethylation, as well as localized hypermethylation are also observed in many cancer cells, thus underscoring the intricate relationship between aging and tumorigenesis (Lister *et al.*, 2009; Hansen *et al.*, 2011; Pérez *et al.*, 2018; Rodríguez-Paredes *et al.*, 2018).

Some of these age-associated changes can be tracked by so-called DNA methylation clocks. Using the methylation status of a few hundred CpGs, these algorithms predict the epigenetic age for a variety of tissues and organisms with high accuracy (Hannum *et al.*, 2013; Horvath, 2013; Stubbs *et al.*, 2017; Thompson *et al.*, 2017; Horvath *et al.*, 2018). The original pan-tissue predictor, for instance, used the methylation status of 353 human CpGs for the estimation of a DNA methylation age with an average error of 3.6 years (Horvath, 2013). Based on deviations between chronological and DNA methylation age, this and other clocks also yield information about the biological age of a tissue or individual, allowing the identification of an advanced or decelerated aging process (Field *et al.*, 2018; Horvath and Raj, 2018). An age acceleration has, for example, been reported in Alzheimer's disease, 'human immunodeficiency virus' (HIV) infection or obesity, while an age deceleration is a characteristic of many cancers (Horvath *et al.*, 2014; Horvath and Levine, 2015; Quach *et al.*, 2017; Rodríguez-Paredes *et al.*, 2018). At the same time, an accelerated DNA methylation clock is associated with an increased risk of cancer, cardiovascular disease and all-cause mortality (Marioni *et al.*, 2015; Christiansen *et al.*, 2016; Zheng *et al.*, 2016; Ambatipudi *et al.*, 2017; Durso *et al.*, 2017). Importantly, the dynamics underlying these changes are not restricted to the relatively small sets of CpGs selected to yield the most accurate age prediction but instead reflect broader trends in the DNA methylome affecting thousands of candidate clock sites (Figure 1) (Wang *et al.*, 2017; Field *et al.*, 2018; Horvath and Raj, 2018). As such, they likely represent a part of a more general aging signature, which also involves other layers of the epigenome (Booth and Brunet, 2016; Horvath and Raj, 2018).

1.1.2. Chromatin alterations during aging

One of these additional epigenomic layers is the functional organization of chromatin. Structurally, chromatin is composed of nucleosomes, which are formed by 147 base pairs of DNA wrapped around an octamer of core histones containing dimers of each of the four histone proteins H2A, H2B, H3 and H4 (Kornberg, 1974; Luger *et al.*, 1997). Additional components like the linker histone H1 or the 'Heterochromatin Protein 1' (HP1) facilitate the formation of higher-

order structures and the condensation into inaccessible heterochromatin (Maison and Almouzni, 2004; Hergeth and Schneider, 2015). In contrast to the highly accessible euchromatic parts of the genome, repressive heterochromatic regions ensure the silencing of genes and transposable elements, the 3D organization of the genome and the suppression of recombination (Grewal and Jia, 2007; van Steensel and Belmont, 2017; Allshire and Madhani, 2018). The condensation of chromatin is also facilitated or impeded by post-translational modifications on protruding amino (N)-terminal histone tails. Most prominently, methylation of lysine 9 and 27 on histone H3 (H3K9me2/3 and H3K27me3, respectively), and methylation of lysine 20 on histone H4 (H4K20me3) are associated with a heterochromatic status (Black, Van Rechem and Whetstine, 2012; Hyun *et al.*, 2017; Wiles and Selker, 2017). On the other hand, methylation of lysine 4, 36 and 79 (H3K4me3, H3K36me3 and H3K79me2/3, respectively), as well as acetylation of lysine 27 (H3K27ac), on histone H3 are related to accessible, transcriptionally active chromatin or active enhancers (Creyghton *et al.*, 2010; Wagner and Carpenter, 2012; Farooq *et al.*, 2016; Hyun *et al.*, 2017).

Many of these chromatin marks undergo profound changes in aging cells. Diminishing levels of core histone proteins, for example, are a conserved feature of cellular aging that has been observed in yeast, worms and human primary fibroblasts (Feser *et al.*, 2010; O'Sullivan *et al.*, 2010; Ni *et al.*, 2012). Furthermore, histone modifications are subject to age-associated alterations, as the function and abundance of the underlying enzymes change. Levels of the H4K16ac, a modification associated with open chromatin and transcription (Verdone, Caserta and Mauro, 2005; Zhang, Erler and Langowski, 2017), increase during cellular aging of yeast and human fibroblasts, whereas levels of H3K56ac, a marker of elevated nucleosome turnover (Li *et al.*, 2008), decrease (Dang *et al.*, 2009; O'Sullivan *et al.*, 2010). These dynamics have been identified as drivers of cellular aging in yeast (O'Sullivan *et al.*, 2010; Pal and Tyler, 2016). Consistently, restoring the activity of sirtuins, a conserved class of histone deacetylases, through chemical interventions or caloric restriction is associated with health- and lifespan extension in mammalian cells (Cantó and Auwerx, 2009; Giblin, Skinner and Lombard, 2014; Bonkowski and Sinclair, 2016). Age-related trends in the level of histone methylation primarily involve the loss of heterochromatic marks (Booth and Brunet, 2016). H3K9me3 levels are reduced in aging invertebrates, as well as in dermal fibroblasts from aged human donors and in mesenchymal stem cells (MSCs) from the premature aging disease Werner syndrome (Scaffidi and Misteli, 2006; Wood *et al.*, 2010; Ni *et al.*, 2012; Zhang *et al.*, 2015). Depletion of H3K9me3 in these cells is frequently accompanied by a loss of the alpha and gamma isoforms of HP1 (Scaffidi and Misteli, 2006; Benayoun, Pollina and Brunet, 2015; Zhang *et al.*, 2015), which is

unsurprising, given the close interaction between the two heterochromatic marks (Lehnertz *et al.*, 2003; Watanabe *et al.*, 2018). Similarly, large-scale losses of H3K27me3 occur in senescent fibroblasts (Shah *et al.*, 2013), although in aging non-senescent hematopoietic stem cells these changes appear to be context-dependent (Sun *et al.*, 2014). Together, these alterations are part of a more global redistribution of heterochromatin in aging and senescence (Tsurumi and Li, 2012; Sun *et al.*, 2018). However, age-related histone modification changes also include the active chromatin marks H3K4me3 and H3K36me3. H3K4me3 shows distinct deposition patterns in aging murine hematopoietic stem cells and senescent human fibroblasts (Shah *et al.*, 2013; Sun *et al.*, 2014), while loss of H3K36me3 in yeast and worms is correlated with diminished transcriptional fidelity and shorter lifespan (Pu *et al.*, 2015; Sen *et al.*, 2015). These examples represent only a minuscule fraction of the age-associated histone modification changes that have been identified in model organisms to date and that will likely be discovered in the future. In sum, they underlie the functional disorganization of chromatin observed during aging and contribute to the deregulation of transcriptional programs characteristic of aged cells (Sen *et al.*, 2016).

1.2. The nuclear lamina - a fibrous layer with complex functions

Metazoan nuclear envelopes are composed of an inner nuclear membrane, a 40-50 nanometer (nm) perinuclear space spanned by nuclear pore complexes, and an outer nuclear membrane (Grossman, Medalia and Zwerger, 2012; Burke and Stewart, 2013). Whereas the outer nuclear membrane connects the nucleus with the endoplasmic reticulum, the inner nuclear membrane is lined at its nuclear face by a thin protein network called the nuclear lamina (Fawcett, 1966; Gerace and Huber, 2012; Burke and Stewart, 2013).

1.2.1. Structure and function of the nuclear lamina

The nuclear lamina is a fibrous meshwork, whose main components are type V intermediate filament proteins called lamins (Fawcett, 1966; Parry, Conway and Steinert, 1986). These proteins contain a central α-helical rod domain flanked by a short (~ 30 amino acids) N-terminal and a long (185-277 amino acids) carboxy (C)-terminal globular domain, the latter of which includes a immunoglobulin-like fold (Fisher, Chaudhary and Blobel, 1986; Dhe-Paganon *et al.*, 2002; Capell and Collins, 2006). In solution, lamin monomers form parallel homodimers, which further assemble into head-to-tail polymers in a partly staggered fashion to form ~ 3.5 nm thick

filaments (Figure 2A) (Stuurman, Heins and Aebi, 1998; Ben-Harush *et al.*, 2009; Turgay *et al.*, 2017).

Two types of lamins have been identified in mammalian nuclei, A- and B-type lamins (Peter *et al.*, 1989; Vorburger *et al.*, 1989). In human cells, a single gene, *LMNA*, encodes the A-type lamins Lamin A, Lamin AΔ10, Lamin C and Lamin C2. An alternative splice site in intron 10 generates Lamin C, which is produced in similar amounts as Lamin A (Lin and Worman, 1993; Capell and Collins, 2006). The expression of Lamin C2 is restricted to testis, while Lamin AΔ10, generated through the deletion of exon 10, has only been found in cells from colon, lung and breast carcinomas (Machiels *et al.*, 1996; Hutchison, 2002).

The B-type lamins Lamin B1 and B2, on the other hand, are encoded by *LMNB1* and *LMNB2*, respectively, with the latter coding for an additional, testis-specific variant (Lamin B3) through alternative splicing (Peter *et al.*, 1989; Vorburger *et al.*, 1989; Furukawa and Hotta, 1993; Lin F and Worman HJ, 1995).

Interestingly, A- and B-type lamins are not equally expressed throughout development. That is, early mouse embryonic cells express B-type but not A-type lamins, the latter of which do not emerge until the appearance of differentiated tissues (Stewart and Burke, 1987; Rober, Weber and Osborn, 1989). From the above observation, as well as knock-down studies in cultured mammalian cells, it was initially concluded that B-type lamins represent essential cellular factors, while A-type lamins might be dispensable (Stewart and Burke, 1987; Harborth *et al.*, 2001). However, mice lacking *Lmnb1* and *Lmnb2* were later reported to survive until birth, suggesting that B-type lamins are not essential during embryonic development, although their absence leads to postnatal defects, especially in neuronal lineages (Kim *et al.*, 2011; Yang *et al.*, 2011). At the tissue level, Lamin A and C are present in differentiated somatic cells but absent from certain cells of the hematopoietic system, embryonic stem cells (ESCs) and induced pluripotent stem cells (iPSCs) (Rober *et al.*, 1990; Constantinescu *et al.*, 2006; Dechat *et al.*, 2008; Liu *et al.*, 2011). Conversely, B-type lamins are expressed in all nucleated cell types but become downregulated during replicative and oncogene-induced senescence (Shimi *et al.*, 2011; Freund *et al.*, 2012; Burke and Stewart, 2013).

High-resolution microscopy studies have revealed that A- and B-type lamins are similar with respect to their structural assembly but that they form separate meshworks at the nuclear rim (Goldberg *et al.*, 2008; Shimi *et al.*, 2015; Turgay *et al.*, 2017). More specifically, the ~ 3.5 nm thick polymers form distinct meshworks containing filaments of different length and regions of varying density (Figure 2B) (Turgay *et al.*, 2017). Furthermore, there is evidence that both lamin meshworks interact and influence each other's organization, although they may serve different

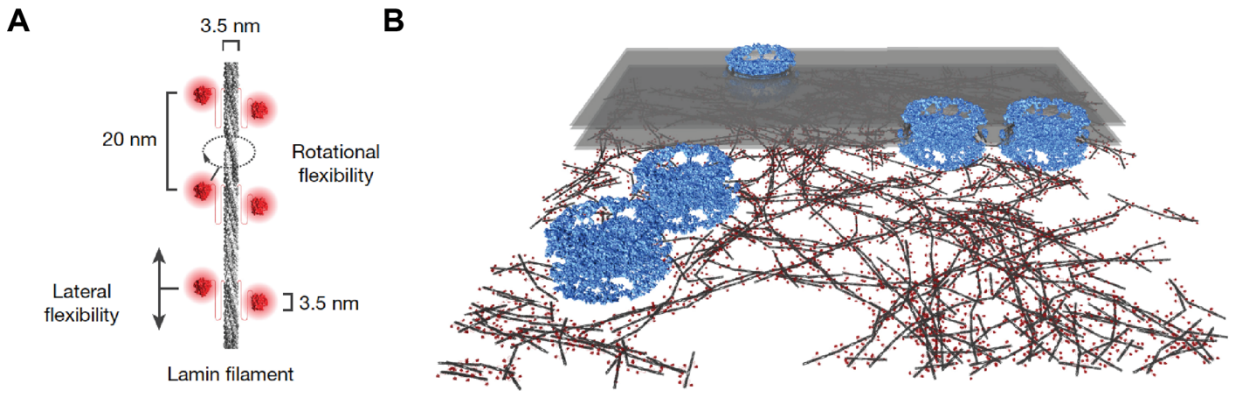

Figure 2: A-type lamin filament structure and assembly. (A) Cryo-electron tomography-based model of lamin filament assembly showing 3.5 nm rod filament (grey) and lateral globular domains (red). Adapted from Turgay *et al.,* 2017. **(B)** Cryo-electron tomography-based model of lamin meshwork at the nuclear envelope. Lamin filaments (as shown in (A), in dark grey) assemble into a thin fibrous meshwork at face of the inner nuclear membrane. The outer and inner nuclear membrane (transparent grey layers) are permeated by nuclear pore complexes (blue). Adapted from Turgay *et al*., 2017.

structural functions (Dechat *et al.*, 2008; Guo *et al.*, 2014; Shimi *et al.*, 2015). Loss of Lamin A/C renders nuclei more sensitive to mechanical stress, which is why it has been suggested that A-type lamins are responsible for the stiffness of the nucleus (Sullivan *et al.*, 1999; Lammerding *et al.*, 2006; Swift *et al.*, 2013). The structural role of B-type lamins, in contrast, is less well defined, but they are likely to contribute to the elasticity of the nuclear envelope (Swift and Discher, 2014; Osmanagic-Myers, Dechat and Foisner, 2015). Intriguingly, there is an additional, highly dynamic fraction of A-type lamins in the nuclear interior (Dechat, Gesson and Foisner, 2010). Initially considered as a transient, non-assembled pool, it has more recently been linked to functions fundamentally distinct from the mechanical role at the nuclear periphery, including transcriptional signaling and higher-order chromatin organization (Dechat, Gesson and Foisner, 2010; Gesson, Vidak and Foisner, 2014; Naetar, Ferraioli and Foisner, 2017).

Aside from their role as structural building blocks, lamins participate in multiple nuclear processes including DNA replication, transcription, DNA repair and chromatin organization (Dechat *et al.*, 2008; Burke and Stewart, 2013; de Leeuw, Gruenbaum and Medalia, 2018). B-type lamins, for example, assemble into a matrix-like network during mitosis, ensuring proper microtubule and spindle assembly (Tsai *et al.*, 2006). At the same time, an intact Lamin B1 nucleoskeleton is essential for the maintenance of RNA Polymerase II-dependent transcription

(Dechat *et al.*, 2008; Tang *et al.*, 2008). A-type lamins also regulate transcription, as transcription factors such as the activating protein 1 (AP1) family member c-Fos, retinoblastoma protein (pRb), and sterol regulatory element-binding protein 1 (SREBP1) colocalize with Lamin A/C at the nuclear lamina (Johnson *et al.*, 2004; Capanni *et al.*, 2005; Ivorra *et al.*, 2006; Heessen and Fornerod, 2007). Moreover, genome integrity is dependent on functional lamins, as they stabilize telomeres and regulate the DNA damage response by interacting with DNA repair factors like 'TP53 binding protein 1' (53BP1) (Gonzalo, 2014; Gibbs-Seymour *et al.*, 2015; Gonzalo and Eissenberg, 2016). Finally, by binding directly and indirectly to chromatin, they exert a central role in chromosome organization inside the nucleus (Dechat *et al.*, 2008; Dechat, Adam and Goldman, 2009).

1.2.2. The role of the nuclear lamina in epigenetic regulation

Lamins directly and indirectly tether chromatin to the nuclear envelope. The observation that human A- and B-type lamins interact with DNA *in vitro* (Shoeman and Traub, 1990; Gruenbaum and Foisner, 2015), led to the belief that lamins directly sequester chromatin to the nuclear periphery. This view is supported by findings in *Drosophila* cells, where multiple genes become detached from the nuclear lamina in response to the depletion of a single B-type lamin (Shevelyov *et al.*, 2009; Kohwi *et al.*, 2013), and in *C.elegans*, where a transgene array can be sequestered to the nuclear lamina by the only lamin, LMN-1 (Mattout *et al.*, 2011). It was later demonstrated that in mammalian cells, peripheral heterochromatin is anchored at the nuclear envelope through a Lamin A/C-dependent mechanism but is complemented by a 'Lamin B receptor' (LBR)-dependent one (Yokochi *et al.*, 2009; Kind *et al.*, 2013; Solovei *et al.*, 2013). This redundancy likely explains, why a depletion of all lamins does not significantly alter the landscape of lamina-located genomic loci or the expression of lamina-associated genes in mouse embryonic stem cells (Amendola and van Steensel, 2015; Zheng, Kim and Zheng, 2015; Zheng *et al.*, 2018). In fact, in addition to LBR, several non-lamin proteins, including 'Barrier-to-autointegration' (BAF), the nuclear lamina component 'Proline-rich 14' (PRR14) and the transmembrane protein emerin, have been reported to contribute to chromatin tethering to the nuclear envelope (Berk, Tifft and Wilson, 2013; Poleshko *et al.*, 2013; Amendola and van Steensel, 2015; Jamin and Wiebe, 2015; Zheng, Kim and Zheng, 2015).

Crucially, heterochromatin plays a central role in directing DNA to the nuclear lamina. Both PRR14 and LBR bind to HP1 (Olins *et al.*, 2010; Poleshko *et al.*, 2013), a heterochromatin mark known to be associated with H3K9me2/3 (Bannister *et al.*, 2001; Lachner *et al.*, 2001). In line with this, depletion of 'Suppressor Of Variegation 3-9 Homolog 1/2' (SUV39H1/2) and

'Euchromatic Histone Lysine Methyltransferase 2' (EHMT2/G9A), the enzymes that catalyze methylation of H3K9, relaxes or abolishes chromatin-lamina interactions, indicating that methylation of this histone mark is critical for lamina binding (Pinheiro *et al.*, 2012; Bian *et al.*, 2013; Kind *et al.*, 2013; Harr *et al.*, 2015). Likewise, the heterochromatic histone marks H3K27me3 and H4K20me3 have been reported to be involved in lamina tethering, although their role remains less well defined (Olins *et al.*, 2010; Harr *et al.*, 2015). It is important to note, however, that lamins can also interact with euchromatin, as the nucleoplasmic fraction of Lamin A/C associates with euchromatic regions through an interaction with 'Lamina-associated polypeptide 2α' (LAP2α) (Gesson *et al.*, 2016).

Genomic regions in contact with the nuclear lamina are known as 'Lamina-associated domains' (LADs) (Figure 3). Mammalian nuclei contain between 1,000 and 1,500 of such domains, typically 10 kb - 10 Mb in size (van Steensel and Belmont, 2017). In some human and murine cell types, they can constitute up to one-third of the genome, thus making them an important characteristic of mammalian epigenomes (van Steensel and Belmont, 2017). LADs are enriched for AT-rich DNA and are characterized by low gene density, low transcriptional levels and an enrichment of the heterochromatin marks H3K9me2/3, as well as H3K27me3 at their boundaries (Figure 3) (Guelen *et al.*, 2008; Wen *et al.*, 2009; Peric-Hupkes *et al.*, 2010; Kind *et al.*, 2013; Harr *et al.*, 2015). Some LADs are conserved between different cell types (constitutive LADs), whereas others vary (facultative LADs) (Peric-Hupkes *et al.*, 2010; Meuleman *et al.*, 2013). Constitutive LADs are enriched for AT-rich DNA sequences and 'Long interspersed nuclear elements' (LINEs), and are especially gene-poor (Meuleman *et al.*, 2013; van Steensel and Belmont, 2017). Although the underlying DNA sequences differ, the genomic position and sizes of constitutive LADs are highly conserved between human and mouse genomes (Meuleman *et al.*, 2013), suggesting that they represent a structural backbone anchoring chromatin to the nuclear lamina at specific positions (van Steensel and Belmont, 2017). Facultative LADs, on the other hand, are more gene-dense and less conserved (Meuleman *et al.*, 2013). Importantly, many LADs also vary between mother and daughter cells, indicating a certain randomization after mitosis (Figure 3) (Kind *et al.*, 2013). In fact, single-cell-based experiments with human myeloid leukemia cells have revealed that every LAD has a specific contact frequency at the nuclear lamina (Kind *et al.*, 2015). One explanation for this phenomenon comes from the observation, that LADs partially overlap with nucleoli-associated domains and that the two can switch positions after mitosis (van Koningsbruggen *et al.*, 2010; Kind *et al.*, 2013; van Steensel and Belmont, 2017).

An important question with regard to the LAD interactome is how relative gene positioning affects gene expression. While 5-10 % of LAD-related genes are expressed at high levels, the large majority of them are transcriptionally silent (Guelen *et al.*, 2008; Peric-Hupkes *et al.*, 2010). Consistently, genes gaining nuclear lamina contact during differentiation often get downregulated, whereas genes released to the nuclear interior become activated (Pickersgill *et al.*, 2006; Peric-Hupkes *et al.*, 2010; Lund *et al.*, 2013; Robson *et al.*, 2016). These dynamics seem to be dependent on the heterochromatic nature of LADs, as artificial tethering of reporter genes to the nuclear lamina results in their downregulation (Akhtar *et al.*, 2013), and depletion of H3K9me2 leads to an upregulation of LAD-located genes in mouse embryonic stem cells (Yokochi *et al.*, 2009).

Interestingly, despite their heterochromatic nature, LADs do not contain high levels of cytosine methylation. In fact, they largely overlap with 'Partially methylated domains' (PMDs), i.e., expansive genomic regions with <70 % average methylation, and thus differ strongly from 'Highly methylated domains' (HMDs), which feature >70 % average methylation levels (Lister *et al.*, 2009; Schroeder *et al.*, 2011). PMDs have been shown to become hypomethylated as a consequence of accumulated cell divisions during cell culture, as well as in aging and cancer

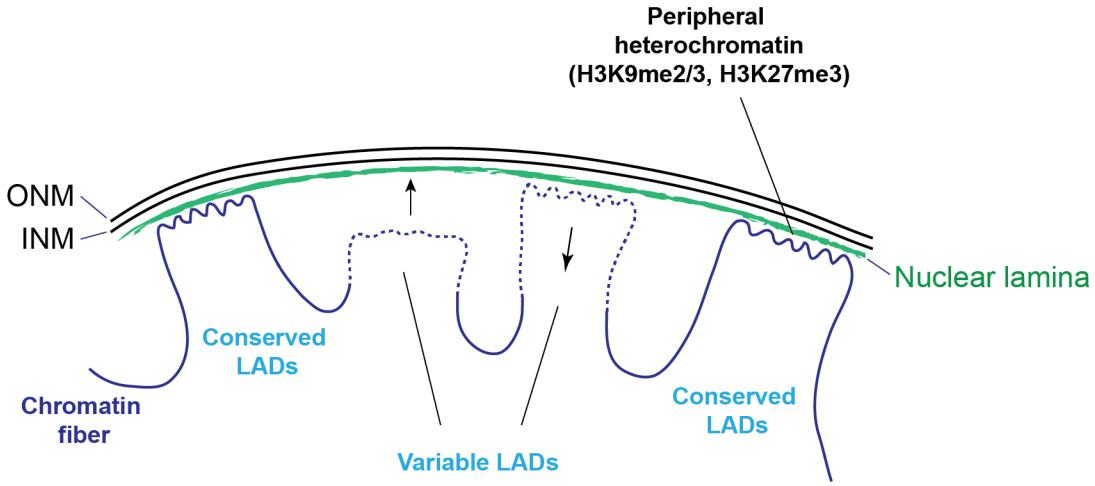

Figure 3: Schematic model of conserved and variable lamina-associated domains (LADs). Genomic regions in contact with the nuclear lamina are enriched for AT-rich DNA and are characterized by low gene density, low transcriptional levels and an enrichment of the heterochromatin marks H3K9me2/3, as well as H3K27me3 at their boundaries. Some LADs are conserved between different cell types, whereas others vary. Additionally, many LADs are shuffled between mother and daughter cells, giving each LAD its own contact frequency. ONM = outer nuclear membrane, INM = inner nuclear membrane.

(Lister *et al.*, 2009; Berman *et al.*, 2012; Salhab *et al.*, 2018; Zhou *et al.*, 2018). This phenomenon has been attributed to both their replication late in S-phase and the absence of H3K36me3 (Aran *et al.*, 2011; Salhab *et al.*, 2018; Zhou *et al.*, 2018).

1.2.3. Nuclear lamina alterations in aging and disease

Due to its central role in various cellular processes, it is not surprising that malfunction of the nuclear lamina has been associated with a multitude of human disorders, collectively called laminopathies. In fact, more than 400 mutations are described for *LMNA* alone, making it one of the genes with the largest known number of disease-causing mutations in the human genome (Burke and Stewart, 2013; Briand and Collas, 2018). Diseases involving mutations in this gene share an accumulation of symptoms in mesenchymal tissues and comprise forms of lipodystrophy, muscular dystrophy, cardiomyopathy and progeria (Dittmer and Misteli, 2011). Prominent examples of *LMNA*-related conditions are atypical Werner syndrome, mandibuloacral dysplasia, Emery-Dreifuss muscular dystrophy, restrictive dermopathy and Hutchinson-Gilford Progeria Syndrome (Capell and Collins, 2006).

Significantly less mutations have been reported for B-type lamins, which has been interpreted as a reflection of their importance for cell viability (Dittmer and Misteli, 2011). The few known laminopathies involving *LMNB1/2* mutations include autosomal-dominant leukodystrophy, a neurological disorder that is caused by a duplication of *LMNB1*, and acquired partial lipodystrophy, which is driven by a number of rare missense mutations in *LMNB2* (Hegele *et al.*, 2006; Padiath *et al.*, 2006).

Lamins also play a role in malignancies. In general, an altered nuclear morphology is a recognized characteristic of cancer cells and many cancer types show differential expression of lamins, although these changes are not unidirectional (Zink, Fischer and Nickerson, 2004; Irianto *et al.*, 2016). Instead, they appear to be dependent on the tumor context: whereas higher A- and B-type lamin expression confers increased mechanical resistance in solid tumors, their downregulation results in lower nuclear rigidity and increased deformability, allowing migrating cells to squeeze through interstitial spaces or capillaries (Ho *et al.*, 2012; Irianto *et al.*, 2016; Alvarado-Kristensson *et al.*, 2019). Additionally, reduced lamin expression has been associated with lower levels of differentiation in tumor cells and poor prognosis (Foster *et al.*, 2010; Chow, Factor and Ullman, 2012; Sakthivel and Sehgal, 2016).

As lamins do not only serve mechanical purposes but also function in chromatin regulation, alterations in the LAD structure may also be of crucial importance in aging and disease. For example, the hypomethylation of PMDs, overlapping to a large extent with LADs, is a well

established characteristic of cancer epigenomes (Salhab *et al.*, 2018; Zhou *et al.*, 2018). Initially identified in colon cancer (Berman *et al.*, 2012), PMD hypomethylation has recently been demonstrated to represent an almost universal feature of 33 different cancer types, specifically in the context of single CpGs that are flanked by an A or T (solo-WCGWs) (Zhou *et al.*, 2018). Tracking the mitotic history of a cell or tissue, the trend arises during fetal development, becomes more apparent with age, and is thought to allow the mobilization of retrotransposons like LINE-1 (Lee *et al.*, 2012; Tubio *et al.*, 2014; Salhab *et al.*, 2018; Zhou *et al.*, 2018). This, in turn, can lead to chromosomal aberrations and tumorigenesis (Solyom *et al.*, 2012; Helman *et al.*, 2014). A dramatic redistribution of LAD-related heterochromatin is also observed in senescent cells, ultimately driving the formation of 'senescence-associated heterochromatin foci' (SAHF), a prominent senescence marker (Chandra *et al.*, 2015; Lenain *et al.*, 2017). Interestingly, whether comparable changes occur in laminopathies, is still an open question. In fact, very few studies have investigated the consequences of lamin mutations on the LAD interactome to date. Considerable LAD rearrangements have been identified in cells carrying *LMNA* mutations that cause congenital muscle dystrophy, lipodystrophy and Emery-Dreifuss muscle dystrophy, respectively (Perovanovic *et al.*, 2016; Barateau *et al.*, 2017; Oldenburg *et al.*, 2017). However, the limited availability of data in this field emphasizes the need for further studies to help address the question whether similar epigenomic changes occur in progeroid diseases or during physiological aging.

1.3. The progeroid disease Hutchinson-Gilford Progeria Syndrome (HGPS)

1.3.1. Background, course and phenotype

Hutchinson-Gilford Progeria Syndrome (HGPS), first described by Dr. Jonathan Hutchinson in 1886 and again in more detail in 1897 by Dr. Hastings Gilford (Hutchinson, 1886; Gilford, 1904), is a segmental and rare genetic disorder that is characterized by the onset of some age-related phenotypes at a very early age (Hennekam, 2006; Merideth *et al.*, 2008). It has been estimated to affect between one in four to eight million live births, although newer evidence suggests that the actual prevalence might be lower (Hennekam, 2006; The Progeria Research Foundation, 2019). Worldwide, 350-400 children are thought to live with the disease at any time, with similar prevalence in both sexes and all races (The Progeria Research Foundation, 2019).

HGPS patients usually appear normal at birth and are diagnosed within the first years of life owing to a failure to thrive and a loss of subcutaneous fat and hair (Hennekam, 2006).

Figure 4: Phenotypic characteristics of Hutchinson-Gilford Progeria Syndrome (HGPS). Manifestation of characteristic facial appearance, alopecia and lipodystrophy in an HGPS patient (adapted from Hennekam 2006).

Additional symptoms develop gradually, including a characteristic facial appearance (Figure 4), more severe lipodystrophy, loss of muscle mass and the stiffening of joints (Hennekam, 2006; Merideth *et al.*, 2008). Premature death occurs at an average age of 14.6 years due to progressive atherosclerosis in the vascular system, resulting in an increased risk of myocardial infarction and stroke (Hennekam, 2006; Merideth *et al.*, 2008; Hamczyk, del Campo and Andrés, 2018).

Symptoms are generally concentrated in tissues of mesenchymal origin, with adipose tissue, bone, cartilage and the cardiovascular system among the most affected. For example, osteolysis of the phalanges, clavicles, mandible or cranium is present in almost all patients, as are the thinning and drying of skin, causing blood vessels to become prominently visible (Hutchinson, 1886; Hennekam, 2006; Merideth *et al.*, 2008). Decreased joint mobility and contractures are equally common, resulting in a limited range of motion (Hennekam, 2006; Merideth *et al.*, 2008). Some of the most severe disease-associated alterations, however, occur in the cardiovascular system. Structural and functional HGPS-specific cardiovascular changes include vascular stiffening, calcification and fibrosis, atherosclerosis, ventricular hypertrophy, as well as cardiac fibrosis (Merideth *et al.*, 2008; Hamczyk, del Campo and Andrés, 2018). Complications arising from these, i.e., myocardial infarctions and intracranial bleeding, are the

most common causes of death in HGPS patients (Hennekam, 2006; Hamczyk, del Campo and Andrés, 2018).

Interestingly, cognitive development is unaffected and individuals with HGPS do not suffer from neurodegenerative diseases. This may be a consequence of the expression of micro RNA-9 (miR-9), which specifically represses neuronal expression of Lamin A and Progerin (Nissan *et al.*, 2012). Likewise, other typically age-related maladies, such as diabetes, chronic kidney failure or malignancies, are rare in classical HGPS patients (Kubben and Misteli, 2017), thus underscoring the segmental nature of the disease.

1.3.2. Disease mechanism and molecular characteristics of HGPS cells

The molecular basis of HGPS remained unknown until 2003, when two research groups discovered that the disorder is caused by mutations in the *LMNA* gene (De Sandre-Giovannoli *et al.*, 2003; Eriksson *et al.*, 2003). At least six mutations in the gene can cause HGPS, but more than 90 % of patients carry a heterozygous substitution in exon 11 (1824C>T) (De Sandre-Giovannoli *et al.*, 2003; Eriksson *et al.*, 2003; Capell and Collins, 2006). The *de novo* mutation alters splicing of the *LMNA* transcript, resulting in the deletion of 150 base pairs, i.e., 50 amino acids, near the carboxyl-terminus of Lamin A, leaving Lamin C unaffected (De Sandre-Giovannoli *et al.*, 2003; Eriksson *et al.*, 2003). Crucially, the truncated part of the protein contains an endoproteolytic cleavage site, which is used by the protease 'Zinc Metallopeptidase STE24' (ZMPSTE24) to remove a farnesyl residue added to pre-Lamin A during post-translational processing (Figure 5) (Sinensky *et al.*, 1994; Bergo *et al.*, 2002; Pendás *et al.*, 2002). Similar to Ras proteins, pre-Lamin A, Lamin B1 and B2 usually undergo farnesylation by protein farnesyltransferase at a C-terminal CAAX motif (C = cysteine, A = an aliphatic amino acid, X = any amino acid), a modification facilitating their interaction with the hydrophobic nuclear membrane (Zhang and Casey, 1996; Capell and Collins, 2006; Young *et al.*, 2013). Because this residue cannot be removed during the processing of mutant pre-Lamin A in HGPS, the protein, commonly referred to as 'Progerin', remains permanently farnesylated and attached to the nuclear lamina. There, its accumulation leads to a characteristic molecular phenotype that involves lobulation and wrinkling of the nuclear envelope (Eriksson *et al.*, 2003; Goldman *et al.*, 2004; Scaffidi and Misteli, 2005) (Figure 6). Intriguingly, Progerin is also expressed in cultured normal fibroblasts (Scaffidi and Misteli, 2006; Cao *et al.*, 2007) and in aging skin (McClintock *et al.*, 2007), thus suggesting that the mutant protein might have role in physiological aging, as well.

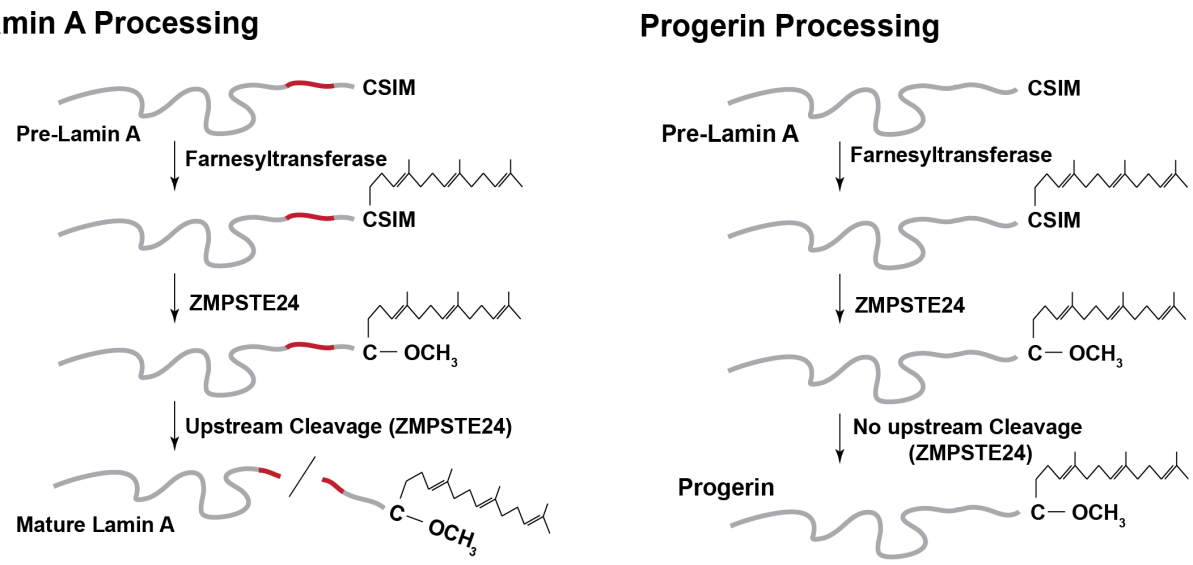

Figure 5: Post-translational processing of Lamin A and Progerin. Pre-lamin A is farnesylated by farnesyltransferase at its C-terminal CAAX motif (the polypeptide contains the C-terminal amino acids cysteine (C), serine (S), isoleucine (I) and methionine (M)). Subsequently, the three terminal amino acids are cleaved off by ZMPSTE24, and the farnesylated cysteine undergoes carboxymethylation. A second cleavage step by the same enzyme removes the 15 C-terminal amino acids plus the farnesyl group. This final step cannot occur in the processing of mutant Pre-lamin A, as aberrant splicing results in the absence of 50 amino acids that contain the endoproteolytic cleavage site (in red).

Although very few patient-derived cell lineages are available for studying, some success has been made with regard to characterizing the expression of Progerin in different cell types. Mesodermal lineages including MSCs, fibroblasts, vascular smooth muscle cells (VSMCs) and endothelial cells exhibit high levels of the protein, whereas iPSCs and neural progenitors express only low amounts (Liu *et al.*, 2011; Zhang *et al.*, 2011). These variations result from the inherent tissue-related differences in the expression of A-type lamins (Zhang *et al.*, 2011), the general downregulation of A-type lamins in pluripotent cell types (Constantinescu *et al.*, 2006) and, as mentioned before, the expression of lineage-specific ncRNAs regulating *LMNA* transcript levels (Nissan *et al.*, 2012). How they lead to the severe pathologies observed at the organismal level is a matter of ongoing research. The exhaustion of mesenchymal stem cell pools, as a consequence of altered Wnt signaling and increased hypoxia sensitivity, has been suggested to thwart the substitution of cells in affected tissues, for example (Halaschek-Wiener and Brooks-Wilson, 2007; Meshorer and Gruenbaum, 2008; Hernandez *et al.*, 2010; Zhang *et al.*, 2011; Kubben *et al.*, 2016). Additionally, with regard to atherosclerosis in particular, the

Progerin-related premature death of VSMCs has recently been demonstrated to constitute a central driving force (Zhang, Xiong and Cao, 2014; Hamczyk, del Campo and Andrés, 2018).

At the cellular level, the dominant-negative role of Progerin at the nuclear lamina has been linked to a multitude of disease-related changes (Broers *et al.*, 2006; Vidak and Foisner, 2016; Kubben and Misteli, 2017). Most prominent are characteristic malformations of the nuclear envelope (Eriksson *et al.*, 2003; Goldman *et al.*, 2004; Scaffidi and Misteli, 2006), but other structural aberrations have been demonstrated in HGPS nuclei. They include a clustering of nuclear pores (Goldman *et al.*, 2004), altered nuclear mechanical properties such as increased stiffness and thickening of the lamina (Dahl *et al.*, 2006), as well as higher susceptibility to physical stress (Verstraeten *et al.*, 2008; Zhang *et al.*, 2011). Molecularly, these are accompanied by an impaired mobility of the nuclear envelope component 'Sad1 And UNC84 Domain Containing 1' (SUN1), a decrease in the levels of Lamin B1, and a loss of the nucleoplasmic fraction of Lamin A/C, all of which have been reported in Progerin-expressing nuclei (Scaffidi and Misteli, 2005; Shimi *et al.*, 2011; Chen *et al.*, 2014; Vidak *et al.*, 2015).

Aside from structural alterations, HGPS fibroblasts are characterized by abnormal

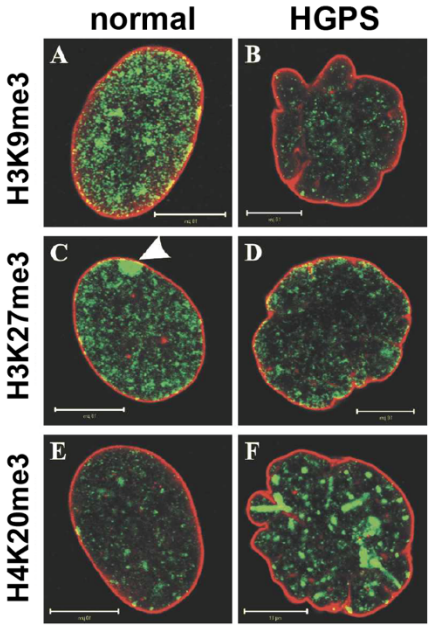

Figure 6: Nuclear malformation and characteristic epigenetic alterations in Progerin-expressing cells. Lamin A-staining (in red) reveals characteristic nuclear lobulation in HGPS fibroblasts. H3K9me3 (A, B) and H3K27me3 (C, D) levels are reduced in HGPS nuclei, whereas H4K20me3 (E, F) levels are elevated (all in green). The arrowhead indicates the inactive X chromosome, which is enriched in H3K27me3. Scale bar = 10 μm. Adapted from Dechat *et al.,* 2008.

chromosome segregation and mitotic defects (Goldman *et al.*, 2004; Cao *et al.*, 2007), as well as a compromised DNA damage response. The latter involves the persistence of DNA damage foci marked by phosphorylated histone H2AX, the delayed recruitment of the repair factors 53BP1 and Rad51, and a mislocalization of the nucleotide excision repair factor 'Xeroderma Pigmentosum Group A' (XPA) to DNA double-strand breaks (Liu *et al.*, 2005, 2008; Scaffidi and Misteli, 2006). Disrupted DNA damage signaling in HGPS cells is especially prominent at telomeres, triggering chromosomal aberrations, increased telomere shortening and premature senescence (Allsopp *et al.*, 1992; Decker *et al.*, 2009; Gonzalez-Suarez *et al.*, 2009; Benson, Lee and Aaronson, 2010; Kan Cao *et al.*, 2011; Wheaton *et al.*, 2017). These changes are aggravated by heightened oxidative stress, as Progerin reduces antioxidant expression by sequestering 'nuclear factor erythroid 2-like 2' (NRF2), a central transcriptional activator of antioxidant genes (Lewis *et al.*, 2010), away from its target genes in the nuclear interior (Viteri, Chung and Stadtman, 2010; Datta, Snow and Paschal, 2014; Kubben *et al.*, 2016). The damage to proteins by reactive oxygen species and the accumulation of Progerin place additional stress on the proteasome, whose activity is decreased in HGPS cells (Viteri, Chung and Stadtman, 2010; Kubben *et al.*, 2016).

1.3.3. Known epigenetic alterations in HGPS

Epigenetic changes are one of the hallmarks of aging and have also been identified in Progerin-expressing cells, although predominantly at the level of histone modifications. In analogy to physiological aging, a global loss of heterochromatin-specific factors has been noted in HGPS fibroblasts (Scaffidi and Misteli, 2006). More specifically, HGPS cells display lower levels of the repressive chromatin marks H3K9me3, H3K27me3 and HP1 (Figure 6) (Scaffidi and Misteli, 2006; Shumaker *et al.*, 2006; Dechat *et al.*, 2008), and electron microscopy-based studies have determined that these changes are especially prominent near the nuclear lamina (Goldman *et al.*, 2004; McCord *et al.*, 2013). These dynamics are accompanied by a downregulation of the enzymes responsible for the methylation of H3K9 and H3K27, SUV39H1/2 and 'Enhancer Of Zeste 2 Polycomb Repressive Complex 2' (EZH2), respectively (Shumaker *et al.*, 2006; McCord *et al.*, 2013). Conversely, H3K4me3, a heterochromatic mark primarily associated with centromeres and telomeres (Schotta *et al.*, 2004; Gonzalo *et al.*, 2005), accumulates and clusters in late-passage HGPS cells (Figure 6) (Shumaker *et al.*, 2006; Dechat *et al.*, 2008), thus emphasizing that the landscape of chromatin alterations in Progerin-expressing cells is complex. In this respect, Hi-C experiments revealed that late-passage HGPS

fibroblasts are characterized by disrupted chromatin organizational patterns involving the loss of active and inactive chromatin compartments (McCord *et al.*, 2013; Chandra *et al.*, 2015).

It has also been reported that fibroblasts from HGPS patients express lower levels of 'Sirtuin 6' (SIRT6), a histone and non-histone protein acetylase contributing to the repair of DNA double-strand breaks (Mao *et al.*, 2011), and that Progerin compromises SIRT6 activity (Endisha *et al.*, 2015; Ghosh *et al.*, 2015). Similarly, Progerin impairs SIRT6-mediated mono-ADP ribosylation of 'Poly(ADP-Ribose) Polymerase 1' (PARP1) (Zhang, Xiong and Cao, 2014; Ghosh *et al.*, 2015), a critical step in 'non-homologous end joining' (NHEJ)-mediated DNA repair (Mao *et al.*, 2011). Histone SUMOylation may also be affected, as HGPS fibroblasts reveal reduced nuclear SUMO2/3 levels and a relocalization of Ubc9, an enzyme responsible for the SUMOylation of histones (Shiio and Eisenman, 2003), to the cytoplasm (Kelley *et al.*, 2011).

Less is known about the role of DNA methylation in HGPS. An initial study by Liu and colleagues identified 586 differentially methylated autosomal genes in HGPS fibroblasts (Liu *et al.*, 2011) but was restrained by the technological limitations of bisulfite padlock probes, which allow the targeted quantification of DNA methylation at a limited number of CpGs (Deng *et al.*, 2009). Another analysis using the more advanced Infinium HumanMethylation450 BeadChip arrays demonstrated substantial DNA methylation alterations in a set of aging-related genes in progeria patients (Heyn, Moran and Esteller, 2013). Nevertheless, this work could not answer the question of HGPS-specific DNA methylation changes, because the authors used a set of adult onset, i.e., non-classical progeria samples for their comparisons (Heyn, Moran and Esteller, 2013). Finally, the most compelling evidence for the existence of considerable DNA methylation changes in the disease comes from the recent observation that fibroblasts from some HGPS patients exhibit an elevated 'DNA methylation age' (Horvath *et al.*, 2018). However, no further specification of these changes has been performed to date, thus highlighting the need for a technologically more advanced and comprehensive characterization of DNA methylation aberrations in the disease.

2. Aims of the thesis

Some epigenetic changes have been identified in HGPS, however, primarily at the level of histone modifications. How they affect chromatin accessibility in the disease has not been specified to date. Similarly, although there is some evidence for DNA methylation alterations in patient cells, their nature and quantity has yet to be comprehensively studied. Lastly, it is unknown whether HGPS-specific changes in these layers contribute to the pathology of the disease.

2.1. Characterization of epigenetic changes in HGPS

To answer these questions, the central aim of this work was to characterize HGPS-specific epigenetic changes genome-wide with the use of high-throughput technology. To this end, chromatin accessibility dynamics in primary HGPS cells were profiled using the 'Assay for Transposase-Accessible Chromatin using sequencing' (ATAC-seq). Disease-associated DNA methylation patterns, on the other hand, were assessed using MethylationEPIC BeadChips, i.e., 'state-of-the-art' epigenomic arrays, which interrogate the DNA methylation status of more than 850,000 CpGs.

2.2. Defining the HGPS-specific LAD interactome

The LAD interactome represents a key epigenomic regulatory layer and is likely to play a crucial role in laminopathies. Surprisingly, the nature and extent of changes in the LAD structure of HGPS primary cells is still unknown. Another goal of the present study was therefore to quantitatively and qualitatively characterize the LAD landscape of Progerin-expressing cells, and to address the question whether potential changes at this level coincide with alterations in chromatin accessibility and DNA methylation.

2.3. Exploring the role of epigenetic changes in HGPS pathology

While some expression changes have been identified in HGPS, previous studies were performed with a relatively small number of samples and restricted by the technological limits of gene expression arrays. Hence, another aim of this work was to analyze the HGPS transcriptome using high-throughput bulk RNA sequencing (RNA-seq) with one of the largest sets of primary samples studied to date. Ultimately, integrating these observations with the HGPS-specific LAD-, chromatin accessibility and DNA methylation data was going to better define the role epigenomic aberrations play in the pathology of the disease.

3. Results

3.1. Characterization of the fibroblast model system

For the experimental analyses, primary skin fibroblasts from nine patients diagnosed with the classic form of Hutchinson-Gilford Progeria Syndrome, as well as six unaffected controls (see Table 10), were obtained. The group of controls contained fibroblasts from four age-matched, i.e., young donors, and fibroblasts from two genetically matched individuals, i.e., parents of one of the HGPS patients. The HGPS samples were divided into an HGPS young (<8 years) and an HGPS old (>8 years) subgroup whenever appropriate. Furthermore, all cell lines were initially tested for the presence of the classic HGPS mutation (1824C>T), characteristic nuclear morphology changes and Progerin expression at the transcript and protein levels.

3.1.1. Verification of mutational status and Progerin expression

Using Sanger sequencing with primers amplifying the region of interest in the *LMNA* gene, all cell lines were analyzed for the presence of the classic HGPS mutation (1824C>T). As expected, HGPS samples revealed mixed cytosine/thymine signals at position 1824 (Figure S34), indicative of the heterozygous presence of the mutation. Control cell lines, in contrast, exhibited uniform cytosine-specific signal, verifying the absence of the mutation (Figure S34).

Subsequently, expression of the mutant ∆150 *LMNA* mRNA and Progerin protein was quantified in all cell lines. Using primers designed to specifically amplify either ∆150 *LMNA* or a control *LMNA* mRNA (Figure 7A), strong expression of the progerin-specific transcript was detected in HGPS cells from both young and old patients (Figure 7B and C). Interestingly, the ∆150 *LMNA* transcript was also detected in some of the control samples, albeit at considerably lower levels (Figure 7B). However, it did not result in the expression of detectable amounts of Progerin protein, which was restricted to HGPS samples only (Figure 8).

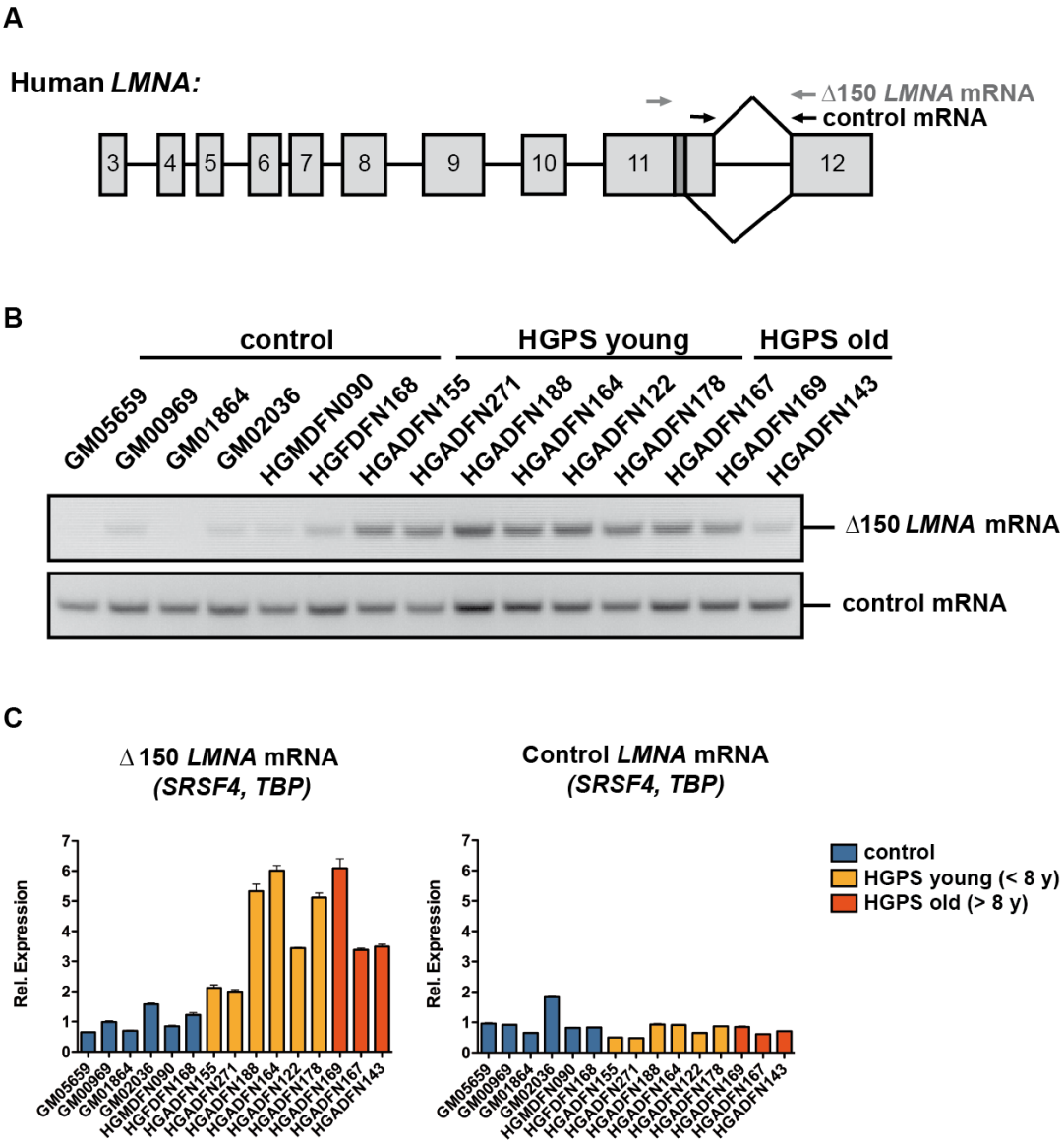

Figure 7: Δ150 *LMNA* mRNA expression in the sample set. (A) Schematic representation of the *LMNA* gene, exons 3-12. The location of the 1824C>T mutation (in dark grey) and those of the oligos used for the amplification of the Δ150 *LMNA* mRNA, as well as an unaffected control mRNA, are indicated. (**B)** Detection of Δ150 *LMNA* and control mRNA in sample set using RT-PCR. **(C)** qRT-PCR-based quantification of Δ150 *LMNA* and control mRNA levels relative to *SRSF4* and *TBP* levels in the sample set.

Figure 8: Progerin protein expression in the sample set. Immunoblot of total protein extracts (20 μg) from all samples. Lamin A, Progerin and Lamin C were detected using a mouse α-Lamin A/C antibody. Lamin C signal was used as a loading control.

3.1.1. HGPS fibroblasts reveal characteristic nuclear morphology changes

Alterations in the structure of the nuclear lamina resulting from the expression of Progerin are one of the most characteristic and commonly used phenotypic markers of HGPS cells (Eriksson *et al.*, 2003; Liu *et al.*, 2011; Zhang *et al.*, 2011; Shimi, Butin-Israeli and Goldman, 2012; Miller *et al.*, 2013). To verify their presence or absence in the primary fibroblasts, immunofluorescence experiments using an α-Lamin A/C antibody were performed. As shown in Figure 9A and Figure S35, HGPS nuclei were characterized by a wide range of malformations including characteristic

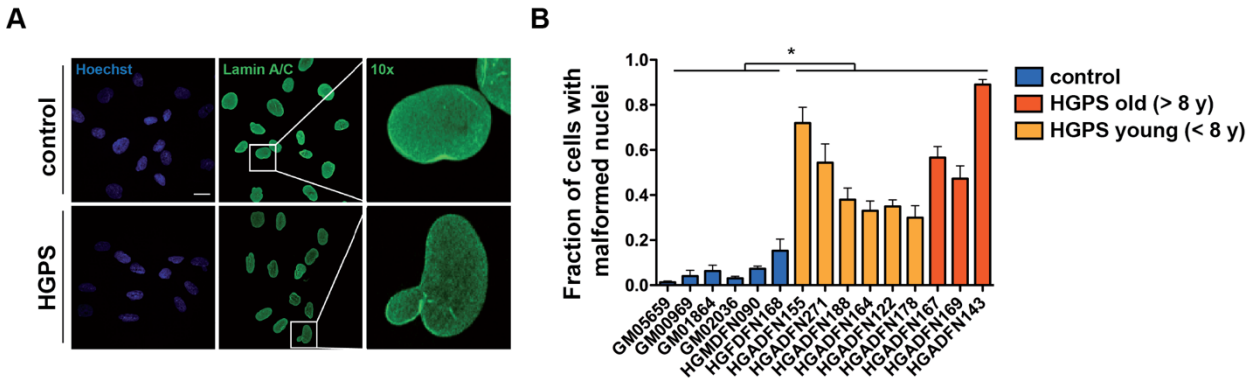

Figure 9: Nuclear malformation in HGPS fibroblasts. (A) Immunofluorescence of Lamin A/C confirms characteristic nuclear malformations in HGPS nuclei. The range of nuclear morphologies scored as 'malformed' is shown in Figure S35. Scale bar = 10 μm. Magnification: 10x**. (B)** Quantification of (A) in fibroblast samples. Bars represent the mean of three technical replicates with 100 cells counted per replicate. *P<0.01, unpaired t-test.

wrinkling and lobulation of the nuclear lamina. These morphologies were substantially more frequent in patient-derived cells: In HGPS samples, the fraction of cells with dysmorphic nuclei ranged from 30-89 %, whereas only 3-15 % of control cells exhibited similar changes ($P<0.01$, unpaired t-test; Figure 9B). Additionally, despite a slight trend towards higher levels of malformation in samples from older patients, no correlation between patient age and the fraction of dysmorphic nuclei was found (Figure 9B and Table 10). These results confirm that the reported nuclear alterations, while mostly absent in control samples, are indeed present in the obtained HGPS fibroblasts.

3.1.2. HGPS cells exhibit minimal cell cycle changes

In addition to the distinctive nuclear phenotype, HGPS cells are characterized by premature cellular senescence and persistent DNA damage foci (Allsopp *et al.*, 1992; Liu *et al.*, 2005; Scaffidi and Misteli, 2006). However, early-passage HGPS fibroblasts have been reported to divide normally, without obvious defects (Bridger and Kill, 2004; Goldman *et al.*, 2004; Paradisi *et al.*, 2005). This raises the question whether cell cycle dynamics are noticeably altered in HGPS fibroblasts. To answer this question, HGPS and control samples were subjected to a Propidium Iodide (PI) staining, followed by 'Fluorescence-activated Cell Sorting' (FACS) analysis of DNA content. In brief, despite minor variations in the proportion of cells in G1, S or G2/M phase, respectively (Figure 10A), no significant differences were found when comparing cell cycle populations from two HGPS and two control samples (Figure 10B, unpaired t-test for all). The large majority of HGPS fibroblasts contained DNA content indicative G1 phase, a minority exhibited intermediate DNA content reflecting ongoing S phase, and a slightly larger fraction revealed DNA content characteristic of G2/M phase (Figure 10A and B). However, control cells were characterized by a highly similar distribution, thus indicating that population-scale cell cycle differences in the obtained HGPS samples are limited and should not constitute a decisive factor in the analysis of epigenetic alterations.

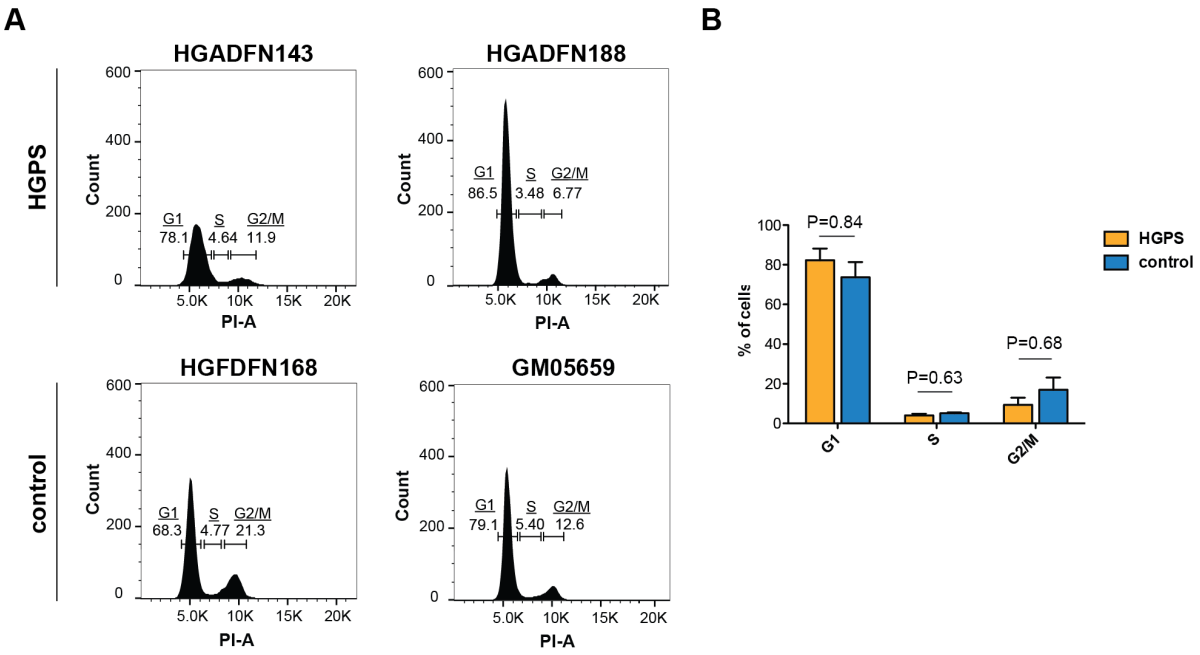

Figure 10: Propidium iodide (PI) staining reveals no broad cell cycle changes in HGPS cells. (A) PI staining of two HGPS and two control cell lines analyzed by FACS. The percentages of cells in G1, S and G2/M phase are indicated. (**B)** Quantification of (A). P-values as indicated (all: unpaired t-test).

3.2. HGPS-specific chromatin accessibility changes are enriched in LADs

Widespread histone modification changes are an established characteristic of HGPS fibroblasts (Scaffidi and Misteli, 2006; Shumaker *et al.*, 2006; McCord *et al.*, 2013). Moreover, cells from affected individuals show a decompaction of heterochromatin similar to senescent cells (McCord *et al.*, 2013; Chandra *et al.*, 2015). The question therefore arises, to which extent these epigenetic alterations change the chromatin accessibility landscape in the disease. To address this question, ATAC-see/seq experiments were performed in early-passage fibroblasts from HGPS patients and control individuals.

3.2.1. ATAC-see reveals single-cell-dependent chromatin accessibility changes in HGPS fibroblasts

Chen *et al.* recently developed a method to visualize the accessible fraction of the genome in individual cells (Chen *et al.*, 2016). The technique, referred to as ‘ATAC-see’, is based on the

integration of fluorescent oligos into accessible chromatin by Tn5 transposase, enabling the visualization of decompacted regions under the microscope. To find out whether the epigenetic changes reported in HGPS cells entail significant changes at the level of chromatin accessibility, ATAC-see experiments were performed with HGPS and control fibroblasts. As shown in Figure 11A and in Figure S36, normal nuclei revealed a number of clearly distinguishable, bright foci, signaling high chromatin accessibility, as well as broad regions with low signal intensity, representing more heterochromatic fractions of the genome. Importantly, these foci did not overlap with Lamin A/C signal, confirming that regions associated with the nuclear lamina are predominantly heterochromatic and low in transcriptional activity (Figure 11A and Figure S36). In striking contrast, in many visibly malformed nuclei, ATAC-see foci were entirely absent and

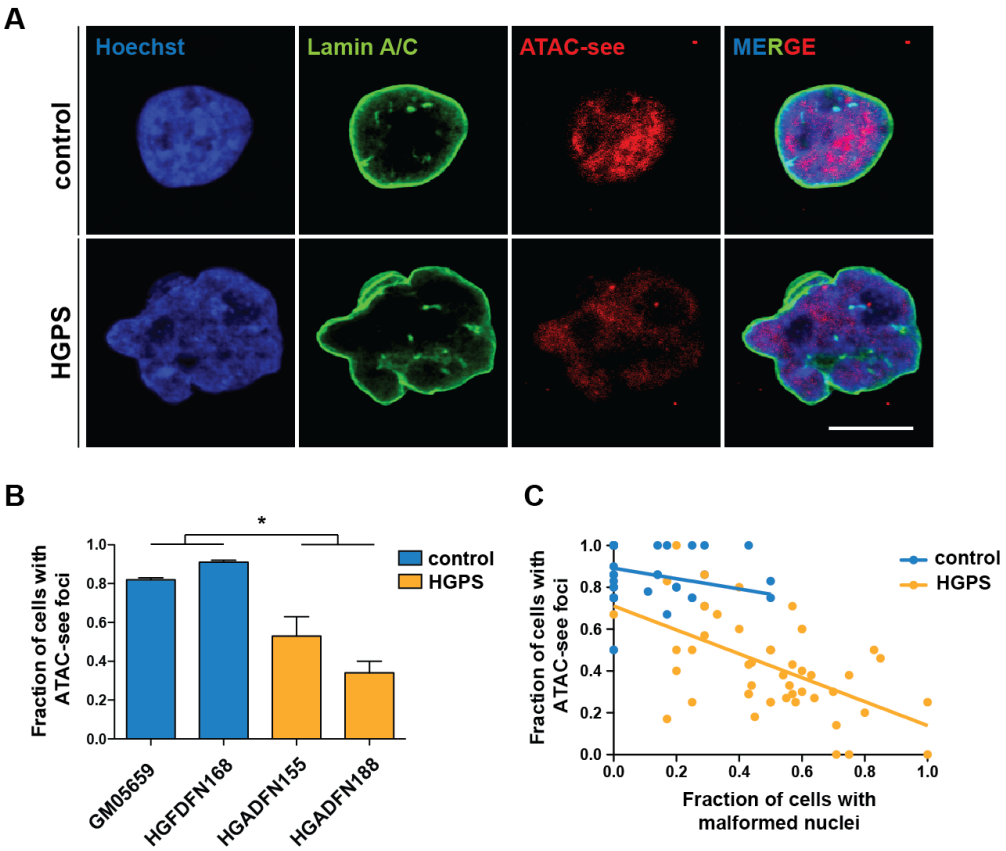

Figure 11: ATAC-see reveals loss of highly accessible chromatin foci in severely malformed HGPS nuclei. (A) Representative ATAC-see signal in control and severely malformed HGPS nuclei. Note the loss of bright foci, i.e., highly accessible chromatin in HGPS. Scale bar = 10 μm. **(B)** Quantification of the fraction of cells with ATAC-see foci in HGPS and control samples (P=0.01, unpaired t-test). **(C)** Correlation of (B) with the fraction of cells with malformed nuclei (R^2 = 0.30, P<0.0001).

the nucleoplasm revealed more intermediate signals, indicating at least a partial loss of eu- and heterochromatic compartments (Figure 11A and Figure S36). HGPS samples exhibited significantly (P=0.01, unpaired t-test) less cells with ATAC-see foci (Figure 11B) and, consistent with the previous observations, substantially more nuclei with malformations. Accordingly, the fraction of cells containing ATAC-see foci was significantly (P<0.0001, R^2 = 0.30) negatively correlated with the fraction of cells showing severe nuclear malformation (Figure 11C), thus suggesting a link between lamina integrity and chromatin accessibility in dermal fibroblasts.

In summary, these findings indicate that the reported HGPS-specific epigenetic changes are indeed accompanied by significant chromatin accessibility changes, at least in the subpopulation of cells with severe lamina anomalies. At the same time, they reveal considerable variation at the single-cell level and thus highlight the potential impact of population heterogeneity on the study of epigenetic alterations in HGPS fibroblasts.

3.2.2. ATAC-seq: Genome-wide chromatin accessibility changes are limited but enriched in LADs

To quantify chromatin accessibility changes in HGPS fibroblasts genome-wide, the accessible genome of two control and six HGPS fibroblast samples was profiled using ATAC-seq. In contrast to ATAC-see, this technique relies on the transposase-based integration of sequencing adaptors into open chromatin sites, followed by next-generation sequencing (Buenrostro *et al.*, 2015).

As shown for chromosome 11 in Figure 12A, global accessibility profiles of HGPS and control cells appeared highly similar, indicating limited population-level alterations. Likewise, the two groups were not clearly distinguishable in a principal component analysis (PCA) (Figure S37). Nevertheless, after removal of sex chromosome-associated peaks, 545 significantly (q<0.05, Benjamini-Hochberg) differentially accessible autosomal regions were identified, 397 and 148 of which gained and lost accessibility in HGPS, respectively (Figure 12B and C). About half of these were located in genes, about one third mapped to intergenic regions and a minor fraction to active and poised enhancers (Figure 13A).

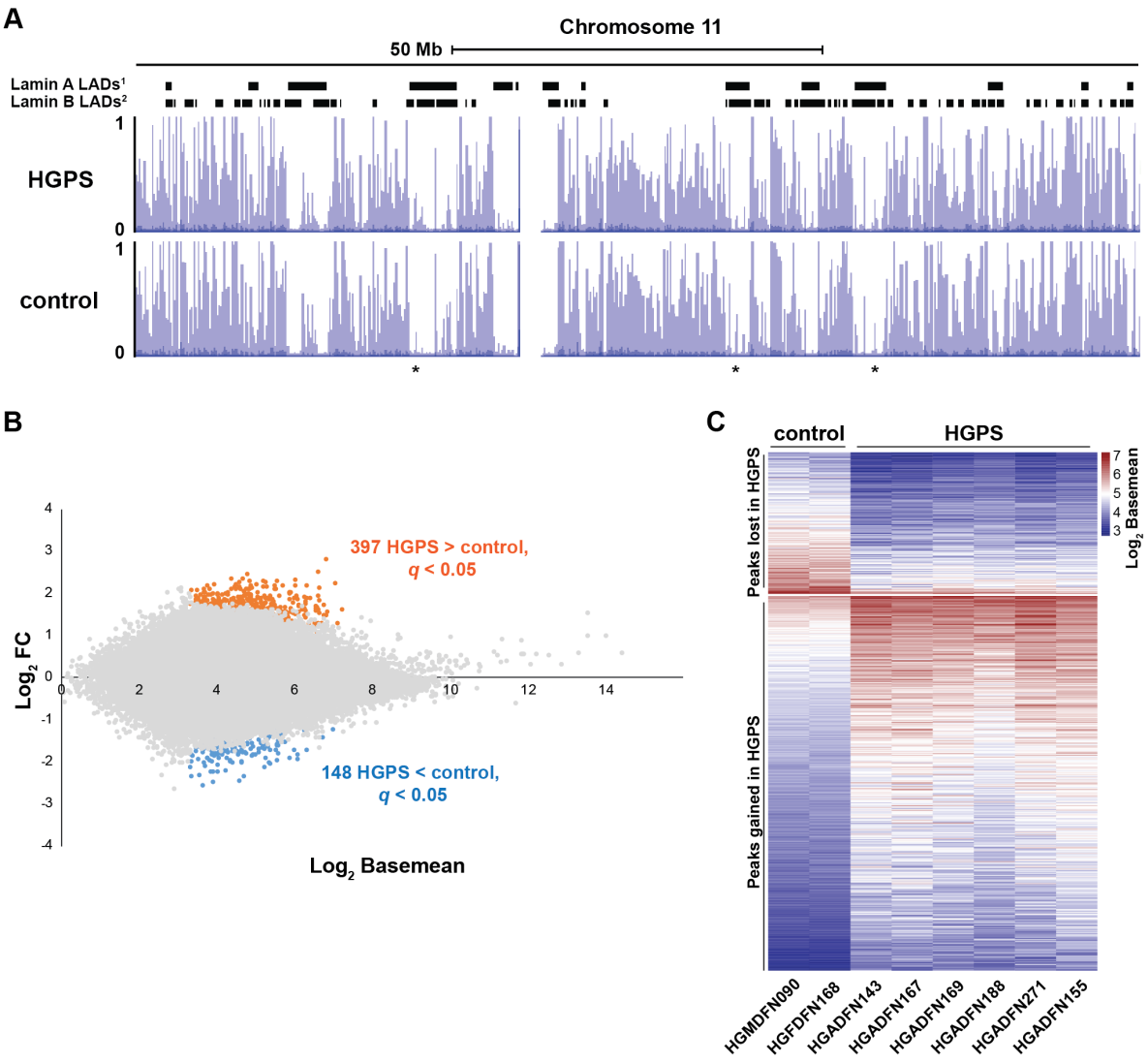

Figure 12: ATAC-seq reveals defined population-level changes in HGPS fibroblasts. **(A)** Average scaled ATAC-seq signal for chromosome 11 in HGPS and control cells with locations of previously identified LADs ([1]Lund *et al.,* 2015, [2]Guelen *et al.*, 2008). Stars indicate the location of visible differences between both tracks. **(B)** 545 regions were found to exhibit significant (q < 0.05, Benjamini-Hochberg) differences in chromatin accessibility between HPS and control cells. (**C)** Heat map representation of the 545 differentially accessible regions (peaks) in all samples.

Given the role of the nuclear envelope in the disease and the previously reported alterations to the peripheral heterochromatin landscape in affected cells (Scaffidi and Misteli, 2006; Shumaker *et al.*, 2006; McCord *et al.*, 2013), major accessibility changes could be expected in regions proximal to the nuclear lamina. Importantly, analyzing the spatial distribution of HGPS-specific chromatin accessibility alterations yielded several lines of evidence in support of this hypothesis: first, Lamin A LAD-associated peaks were strongly and significantly (P<0.05, Fisher's exact test)

overrepresented among regions that gained (2.6-fold) or lost (3.3-fold) accessibility in HGPS, respectively (Figure 13B). Interestingly, accessibility changes in regions overlapping with Lamin B were also slightly above expected levels (Figure 13B) - likely a result of the partial overlap of Lamin A- and Lamin B-associated LADs (Figure 12A).

Second, the relatively gene-poor chromosome 18, which shows multiple LAD contacts in proliferating cells and is often found near the nuclear periphery (Meaburn *et al.*, 2007; Kind *et al.*, 2015), exhibited over 7 times more differentially accessible regions than the similarly sized, gene-rich and more centrally located chromosome 19 (Figure 13C).

Third, chromatin accessibility changes were slightly, but significantly (P=5.61e-04 and P=2.66e-05, Fisher's Exact test) enriched in genomic regions characterized by the presence of

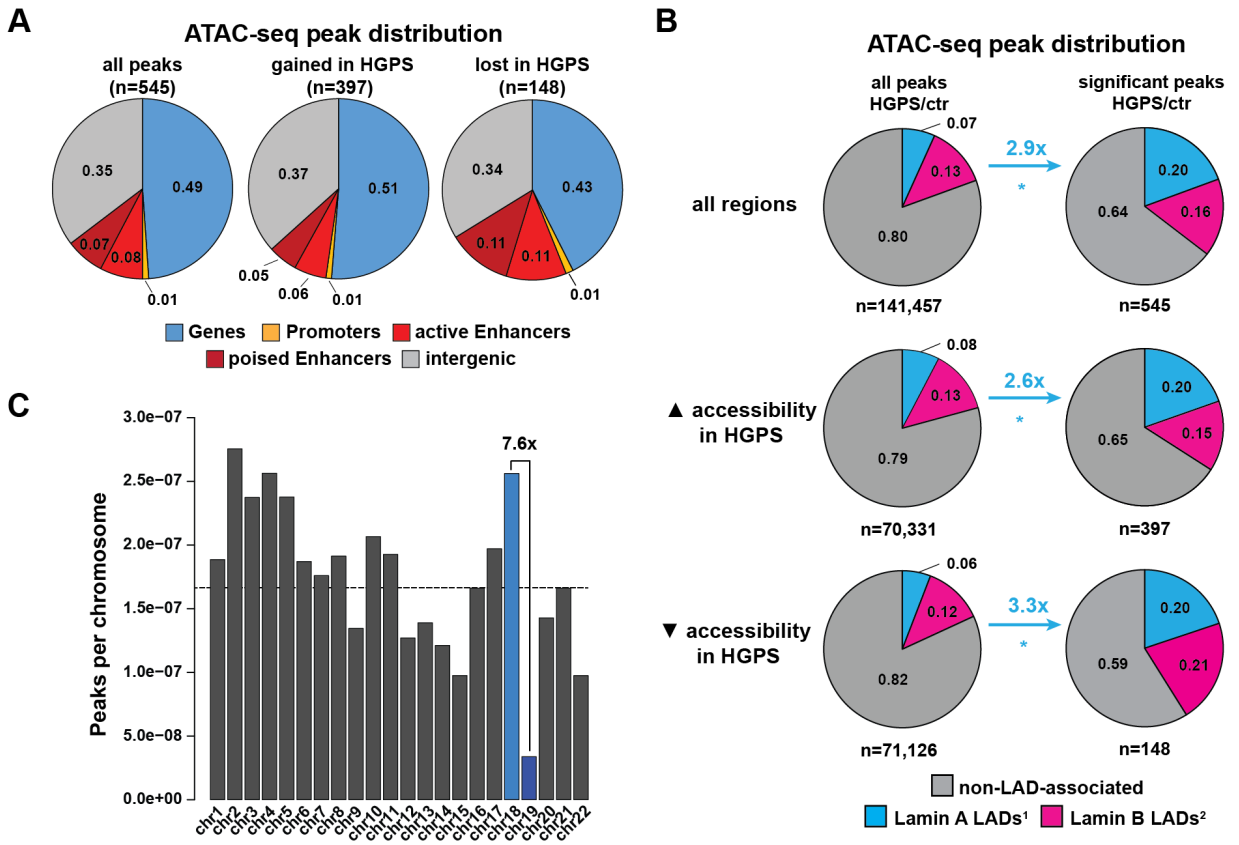

Figure 13: Genome-wide chromatin accessibility changes are enriched in Lamina-associated domains (LADs). (A) Distribution of ATAC-seq peaks across genes, promoters and enhancers. (**B)** Distribution of ATAC-seq peaks across Lamin A-([1]Lund *et al.*, 2015), Lamin B-([2]Guelen *et al.*, 2008) and non-LAD-associated regions (*P<0.05; Fisher's Exact test). Ctr = control. (**C)** Relative distribution of differentially accessible regions (peaks) across chromosomes. Chromosome 18 revealed 7.6 times more differentially accessible regions than chromosome 19. Mean = 1.66e-07 peaks per chromosome.

H3K9me2 and H3K9me3 (Figure 14A), two prominent LAD markers (Guelen *et al.*, 2008; Wen *et al.*, 2009; Kind *et al.*, 2013). In contrast, differentially accessible regions were significantly underrepresented in parts of the genome containing markers of active transcription, including promoter-associated H3K4me3 (P<2.20e-16), H3K27ac (P=1.27e-03) or gene body-associated H3K36me3 (P=3.15e-06) (Figure 14A, Fisher's Exact test for all).

Fourth, a HOMER transcription factor binding site (TFBS) enrichment analysis revealed that the differentially accessible regions are highly enriched (q<0.01, Benjamini-Hochberg) with

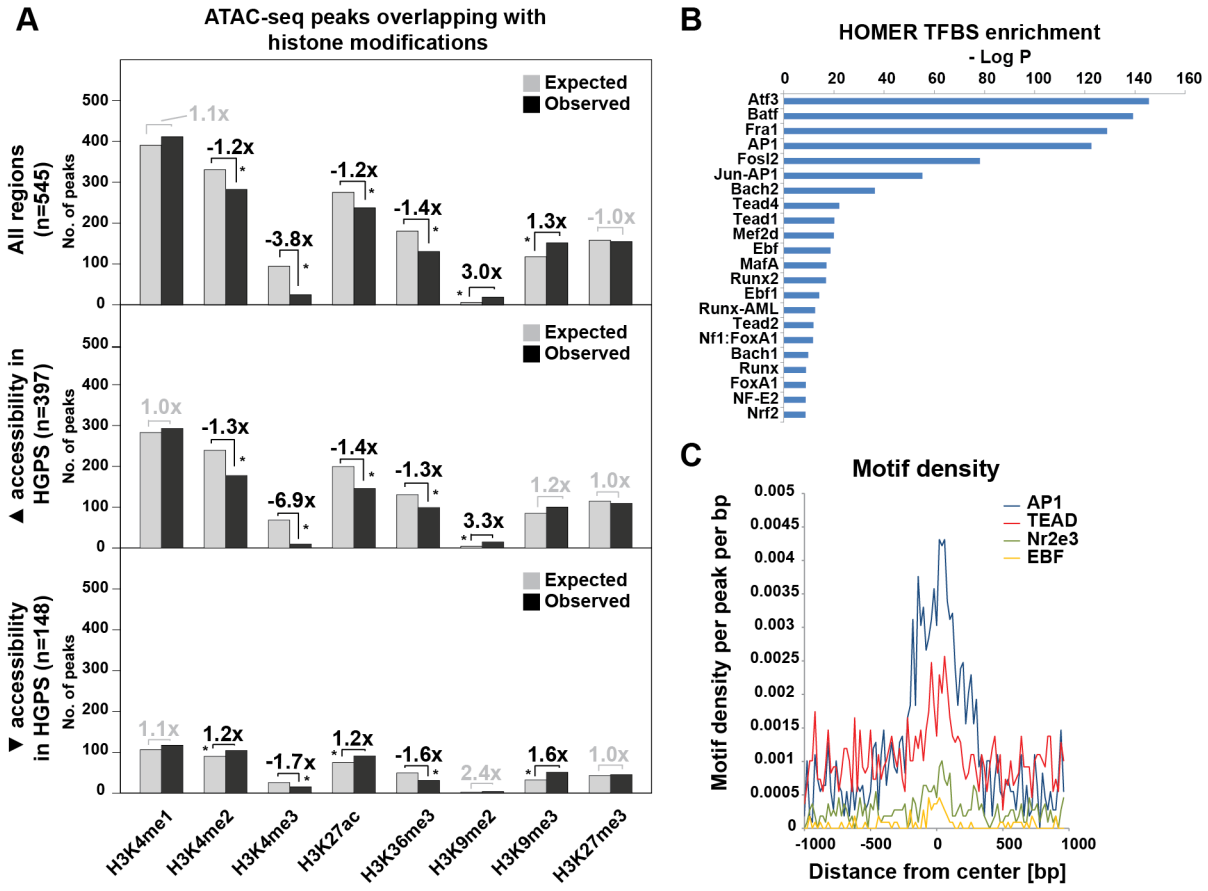

Figure 14: Chromatin accessibility changes are enriched in regions marked by H3K9me3 and the presence of AP1 transcription factor binding sites (TFBSs). (A) Overlap of ATAC-seq peaks with the indicated histone modifications (Fold changes as indicated, *P<0.05, Fisher's Exact test). The expected number of peaks was calculated based on the fraction of all (including non-significant (q<0.05, Benjamini-Hochberg)) peaks overlapping with a certain histone modification normalized to the number of peaks significantly (q<0.05, Benjamini-Hochberg) gaining or losing accessibility, or both. No. = number. **(B)** NRF2 binding motifs are among the TFBSs enriched in the differentially accessible regions (NRF2: q=1.80e-03, Benjamini-Hochberg). **(C)** Motif density plot showing an enrichment of AP1 family member TFBSs in the differentially accessible regions. Motif densities were calculated using the HOMER motif density tool for top *de novo* motifs.

binding sites of 'Activator Protein 1' (AP1) family members, which have previously been shown to be associated with the nuclear lamina in mammalian cells (Ivorra *et al.*, 2006) (Figure 14B and C). In addition, this analysis identified several members of the 'TEA Domain' (TEAD) family of transcription factors, which play key roles in the Hippo signaling pathway, a developmental signaling pathway controlling organ size (Zhao *et al.*, 2010), and regulate development, tissue homeostasis and tumorigenesis (Pobbati and Hong, 2013; Lin, Park and Guan, 2017). Finally, binding sites of 'Nuclear factor erythroid 2-related factor 2' (NRF2), whose sequestration to the nuclear lamina has recently been reported as a key driver of oxidative stress in HGPS cells (Kubben *et al.*, 2016), were also found significantly ($q<0.01$, Benjamini-Hochberg) enriched in the differentially accessible regions (Figure 14B).

Taken together, these results provide evidence that population-level HGPS-specific chromatin accessibility changes, while limited in quantity, are concentrated in regions of the genome that are in contact with the nuclear lamina, depleted of markers of active transcription and that contain binding sites of several transcriptional regulators.

3.3. HGPS cells show widespread DNA methylation changes enriched in LADs

HGPS-specific DNA methylation patterns have not been comprehensively analyzed to date. To obtain a clearer picture of the HGPS methylome and to investigate whether the LAD-related chromatin accessibility changes are accompanied by alterations at the level of DNA methylation, Infinium MethylationEPIC BeadChip-mediated methylome profiling was performed. These arrays capture the methylation status of more than 850,000 single CpGs in the human genome and therefore represent a cost-effective method to comprehensively investigate potential genome-level methylation changes.

3.3.1. General features of the HGPS DNA methylome

Genomic DNA from nine HGPS patients and six healthy controls was submitted for MethylationEPIC BeadChip-mediated analysis of DNA methylation patterns. After normalization (see Methods, Section 6.2.15.2), 19,759 significantly ($P<0.05$, F-test) differentially methylated autosomal probes were identified, 15,554 and 4,205 of which were hyper- and hypomethylated in HGPS, respectively (Figure 15A). HGPS samples also clustered separately from control samples in a PCA based on the methylation of all probes, albeit with limited differences (Figure

15B). In line with this, median methylation levels of individual HGPS samples were similar to those of control samples, showing no general trend towards HGPS-specific hyper- or hypomethylation and substantial between-sample variation (Figure 15C).

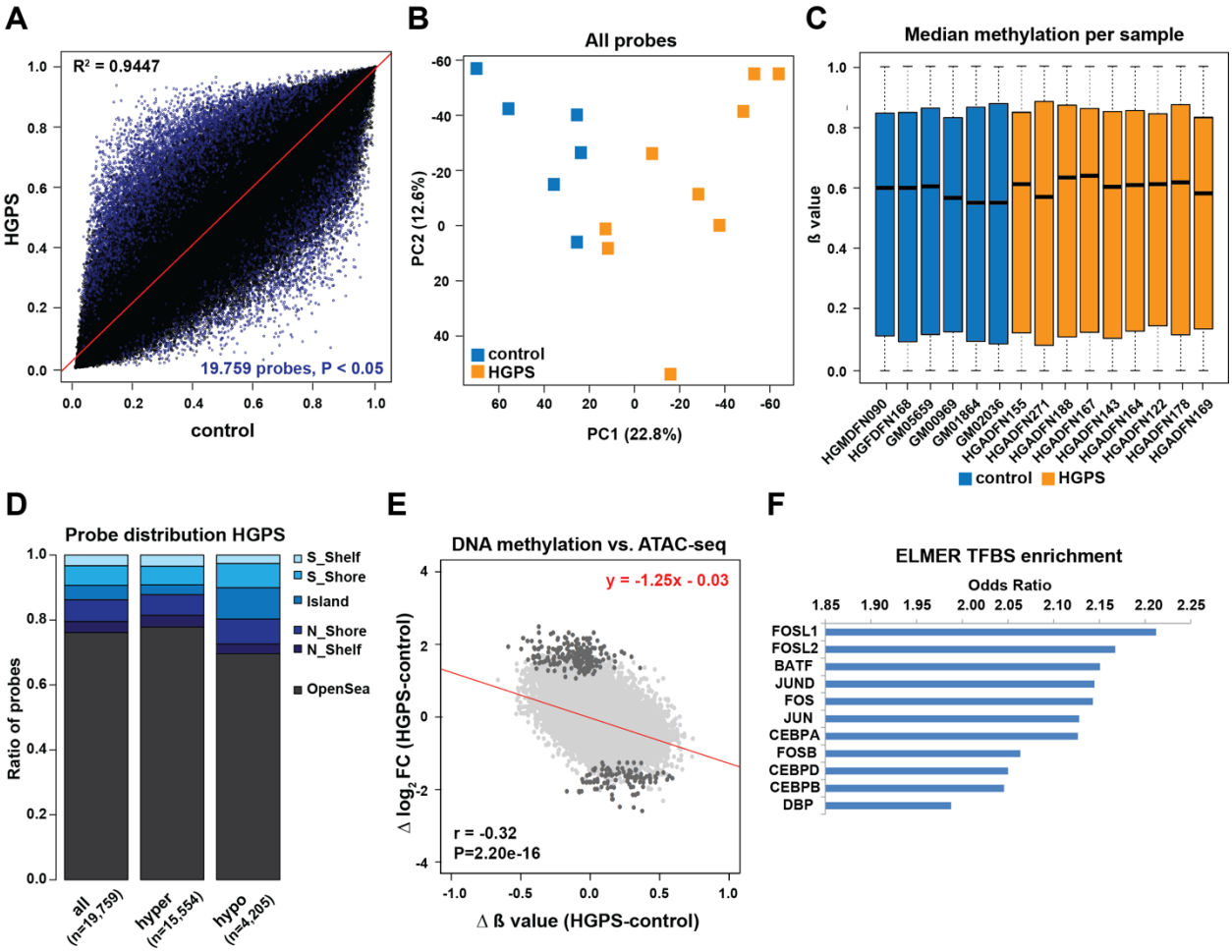

Figure 15: General features of the HGPS DNA methylome. (A) Scatter plot comparing the methylomes of HGPS and control fibroblasts. Differentially (P<0.05, F-test) methylated probes are shown in blue. **(B)** Principal component analysis (PCA) of HGPS and control samples using all probes. The variances explained by Principal Component (PC) 1 and 2 are given in brackets. **(C)** Differential methylation (β value) of all probes in sample set with median indicated as a black line. (**D)** Distribution of differentially methylated probes across North (N) and South (S) Shelves and Shores, as well as CpG Islands and Open Sea regions. **(E)** Correlation of HGPS-specific chromatin accessibility changes (Significant (q<0.05, Benjamini-Hochberg) ones in dark grey; non-significant ones in light grey) with DNA methylation (β value) changes in non-CpG island-associated regions. Linear regression of all data in red (Pearson correlation r=-0.32, P<2.20e-16). FC=Fold Change. (**F)** ELMER transcription factor binding site (TFBS) enrichment analysis reveals that members of the AP1 family are enriched in the differentially methylated (P<0.05, F-test) regions (95 % Confidence Interval).

Most of the differentially methylated probes were located in open sea regions; CpG island-, shore- and shelf-associated probes, on the other hand, only made up small proportions of the differentially (P<0.05, F-test) methylated probes, with little differences between the hyper- and hypomethylated fractions (Figure 15D).

Importantly, the DNA methylation changes were also negatively correlated with the HGPS-specific alterations in chromatin accessibility, as regions with lower chromatin accessibility tended to show increased DNA methylation and vice versa (Pearson correlation r=-0.32, P=2.20e-16, excluding CpG island probes) (Figure 15E). In addition, an analysis of TFBSs enriched in the differentially methylated regions using ELMER (Yao *et al.*, 2015; Silva *et al.*, 2018) revealed that AP1 family member TFBSs are overrepresented in parts of the genome that contain HGPS-specific differential methylation (Odds ratio >2.1, 95 % confidence interval, Figure 15F). The latter findings thus point towards the possibility that the DNA methylation alterations are involved in the epigenetic deregulation of LADs.

3.3.2. DNA methylation changes are enriched in LADs

Based on the previous findings, differential DNA methylation in regions associated with the nuclear lamina was analyzed. Interestingly, as shown in Figure 16A, probes located in Lamin A-associated regions exhibited a substantial and significant (P<0.01, Welch's Two Sample t-test) increase in median methylation levels. While this hypermethylation was also apparent in probes located in Lamin B-associated regions, it was less pronounced and more similar to the slight increase observed for non-LAD regions, as well as for all probes (Figure 16A). In line with these observations, Lamin A-associated probes were more strongly enriched (2.06-fold, P<2.20e-16, chi-squared test) than Lamin B-associated ones (1.54-fold, P<2.20e-16, chi-squared test) among the 19,759 differentially methylated probes (Figure 16B). Intriguingly, this largely resulted from an overrepresentation of both types of LAD-associated probes among hypermethylated (2.44- and 1.68-fold, P<2.20e-16 for both, chi-squared test), but not hypomethylated probes, indicating that HGPS-specific DNA methylation changes in LADs are dominated by hypermethylation (Figure 16B).

Furthermore, probes overlapping with 'solo-WCGW' PMDs, a recently identified subset of PMDs especially vulnerable to hypomethylation during development and aging (Zhou *et al.*, 2018), exhibited a significant (P<0.01, Welch's Two Sample t-test) increase in median methylation, potentially due to the large sequence overlap with LADs (Zhou *et al.*, 2018). In contrast, 'solo-WCGW' HMDs showed little differences between HGPS and control samples (Figure 16A). This result suggests that mitotic age-related hypomethylation of LADs, as

observed in a multitude of developmental lineages and aged tissues (Zhou *et al.*, 2018), is not a feature of the HGPS genome.

LADs are marked by an enrichment of H3K9me2 and H3K9me3 (Guelen *et al.*, 2008; Wen *et*

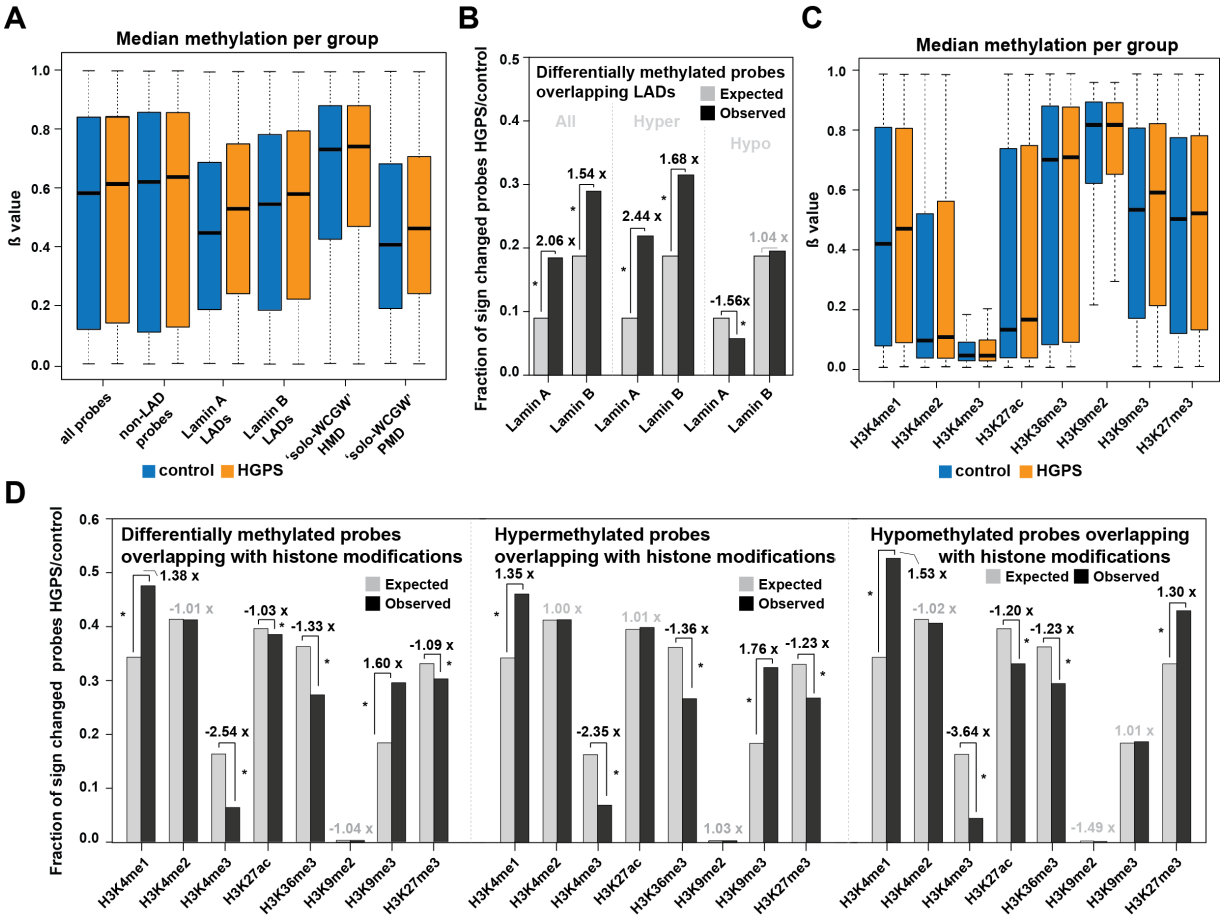

Figure 16: DNA methylation changes are enriched in lamina-associated domains (LADs). (A) Differential (β value) methylation of all probes (P<2.20e-16) and those overlapping with non-LAD (P<2.20e-16), Lamin A- (Lund *et al.,* 2015) (P<2.20e-16), Lamin B - (Guelen *et al*., 2008) (P<2.20e-16), 'solo-WCGW'-HMD- (P=4.42e-15) or 'solo-WCGW'-PMD-associated (P<2.20e-16) regions (all: Welch Two Sample t-test). Median indicated as a black line. **(B)** Enrichment of LAD-associated probes among all differentially (P<0.05, F-test) methylated probes, as well as those hyper- or hypomethylated in HGPS samples (*P<0.01; chi-squared test). Expected numbers were calculated based on the fraction of LAD-associated probes among all probes normalized to the number of differentially methylated probes. Sign = significantly. **(C)** Differential (β value) methylation of probes overlapping with different histone modifications with median indicated as black line (H3K4me1: P<2.20e-16, H3K4me2: P<2.20e-16, H3K4me3: P<2.20e-16, H3K27ac: P<2.20e-16, H3K36me3: P<8.68e-15, H3K9me2: P<2.20e-16, H3K9me3: P<2.20e-16, H3K27me3: P<2.20e-16; all: Welch Two Sample t-test). **(D)** Enrichment of probes overlapping with different histone modifications as in (B) (*P<0.01; chi-squared test). Expected numbers as in (B). Sign = significantly.

al., 2009; Kind *et al.*, 2013), while H3K27me3 is found at LAD boundaries of various cell types (Guelen *et al.*, 2008; Harr *et al.*, 2015). Hence, it was tested whether probes located in regions that are characterized by these and other histone modifications are significantly differentially methylated in HGPS cells. Consistent with the LAD probe-related findings described above, probes overlapping with regions marked by H3K9me3 showed a strong and significant (P<2.20e-16, Welch's Two Sample t-test) increase in median methylation levels (Figure 16C) and were enriched 1.76-fold (P<2.20e-16, chi-squared test) among hypermethylated probes (Figure 16D). Probes associated with H3K27me3 domains, on the other hand, showed less changes in median methylation and were slightly (1.30-fold, P<2.20e-16, chi-squared test) enriched among the hypomethylated fraction (Figure 16C and D). Interestingly, strong and significant (P<0.01, Welch's Two Sample t-test) increases in median methylation were also observed in regions marked by H3K4me1 (Figure 16C), which are generally associated with the presence of enhancers (Heintzman *et al.*, 2009). H3K4me1-associated probes also showed a significant enrichment among both hyper-and hypomethylated probes (P<2.20e-16 for both, chi-squared test) (Figure 16C), thus indicating considerable changes in the HGPS-specific enhancer landscape. Finally, probes overlapping with histone modification marks associated with active transcription, H3K4me2, H3K4me3, H3K27ac and H3K36me3, displayed little HGPS-specific DNA methylation changes (Figure 16C) and were either considerably underrepresented (H3K4me3 and H3K36me3) among the 19,759 differentially methylated probes, or in line with expectations (H3K4me2 and H3K27ac) (Figure 16D). The latter indicates that, while existent, HGPS-specific DNA methylation changes are not concentrated in regions characterized by active histone modification marks.

3.3.3. The HGPS methylome contains progeroid features

To better understand the DNA methylome changes in HGPS cells, the differential methylation patterns were further examined. For this purpose, the 5,000 most variable clusters of probes were determined and analyzed by unsupervised clustering (see Methods, Section 6.2.15.3). This separated the samples into three subgroups, with control samples forming one subgroup and HGPS samples being split into two subgroups (Figure 17A). Additionally, using the 5,000 most variable probe clusters allowed a better separation of HGPS and control samples in a PCA (Figure 17B). It is also worth noting that the probe clusters mostly contained probes located in gene bodies and intergenic regions, while only a minor number were overlapping with CpG islands, promoters, Lamin A- or Lamin B-associated regions (Figure 17A). This indicates that,

despite the considerable LAD-specific DNA methylation changes described above, many methylation changes occur in other parts of the HGPS genome.

Intriguingly, the subclassification of HGPS samples was not associated with strength of Progerin expression, sex, patient age, body site of sampling or passage number. However, with the exception of HGADFN122, it was in agreement with a subgrouping of HGPS samples based on DNA methylation age, as calculated by a recently published age predictor with improved

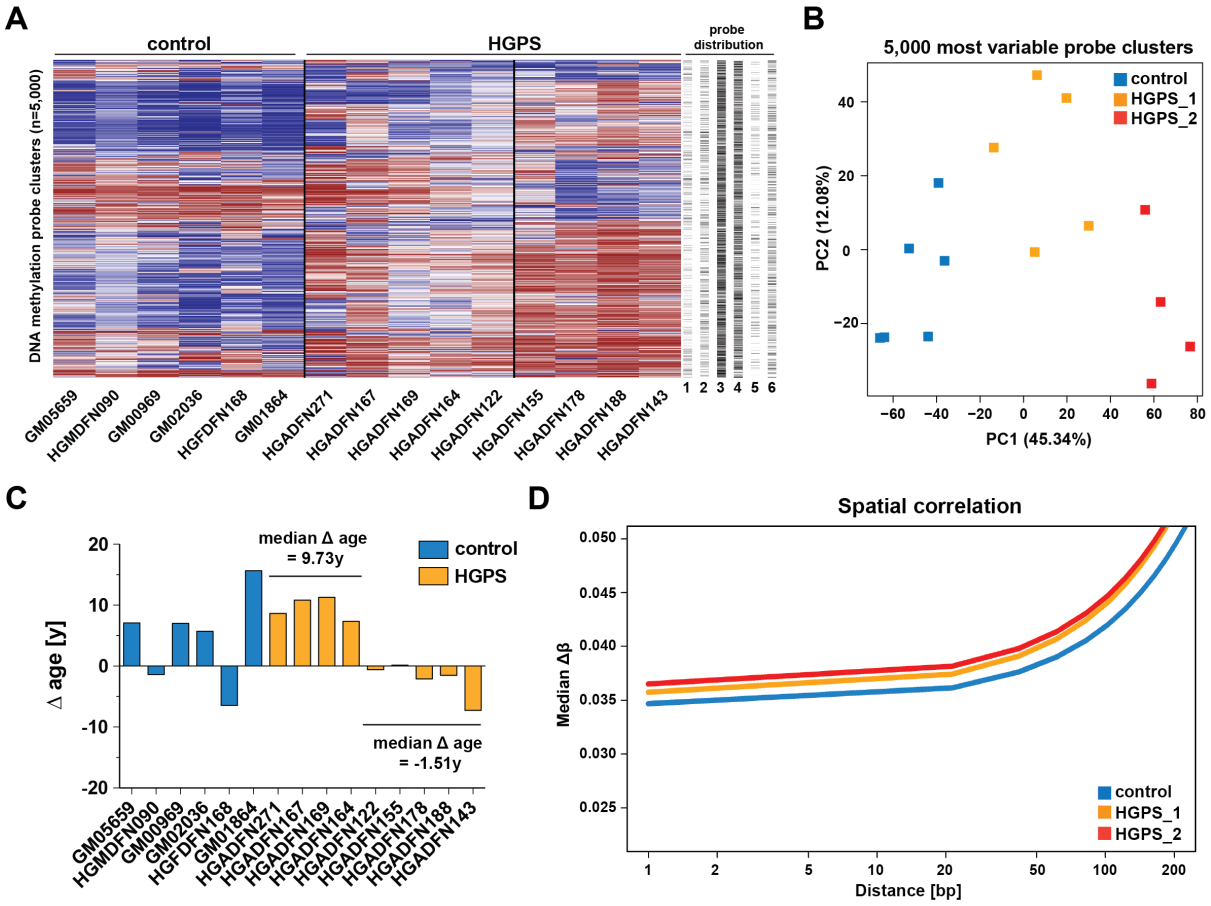

Figure 17: Progeroid features of the HGPS DNA methylome. (A) Consensus clustering based on 5,000 most variable probe clusters between HGPS and control samples (1= CpG islands, 2 = promoter, 3 = gene body, 4 = intergenic, 5 = Lamin A LAD-, 6 = Lamin B LAD-associated). β values are colored from β=0 (blue) to β=1 (red). **(B)** Principal component analysis (PCA) of HGPS and control samples using the 5,000 most variable probe clusters. The variances explained by Principal Component (PC) 1 and 2 are given in brackets. The two HGPS subgroups identified in (A) are indicated as HGPS_1 and HGPS_2. **(C)** Skin & Blood Clock classifies HGPS subgroups as accelerated and non-accelerated. The difference (= Δ age) between DNA methylation age (as calculated by the Skin & Blood Clock (Horvath *et al.*, 2018)) and chronological age in years [y] is depicted for all samples. **(D)** Spatial correlation of DNA methylation marks. Lines represent smoothened medians of distance-dependent β value differences for the indicated subgroups.

accuracy for human dermal fibroblasts (Horvath *et al.*, 2018). More precisely, one group of HGPS samples exhibited a median age acceleration of 9.73 (±1.85) years, whereas the other exhibited a slight decrease of -1.51 (±2.91) years (Figure 17C). Of note, even after adjustment for passage number, control fibroblasts obtained from the Coriell biorepository (GM05659, GM01864, GM00969, GM02036) also showed a substantial age acceleration (Figure 17C). This was in contrast to control samples obtained from the Progeria Research Foundation (PRF) (HGMDFN090 & HGFDFN168) and might result from differences in body site of origin, fibroblast subpopulation or culturing.

Loss of spatial correlation is a major characteristic of aging DNA methylomes (Bormann *et al.*, 2016). Owing to the observed differences in DNA methylation age, it was tested whether the two HGPS groups also differ with respect to the age-related erosion of DNA methylation patterns. As shown in Figure 17D, the age-accelerated group of HGPS samples showed the highest median methylation differences ($\Delta\ \beta$ value), i.e., the strongest decrease in spatial correlation of DNA methylation patterns, followed by the non-accelerated group. Control samples, in contrast, exhibited considerably lower median methylation differences, thus indicating that the loss of spatial correlation is first and foremost a feature of the HGPS methylome, and only secondarily associated with the age-acceleration in HGPS samples.

Altogether, the analysis of DNA methylation changes in HGPS fibroblasts reveals two overarching trends: while global HGPS-specific alterations in the DNA methylome seem to be limited and mostly located in gene bodies and intergenic regions, parts of the genome that are characterized by Lamin A/B-binding and the presence of H3K9me3/H3K4me1 or AP1 TFBSs show an enrichment of changes. On the other hand, features associated with an aging DNA methylome in normal cells are also present in the HGPS methylome, at least in a subgroup of patients, thus reflecting the progeroid nature of the disease.

3.4. Epidermal cancers are characterized by LAD hypomethylation and a decreased DNA methylation age

In contrast to what was observed for HGPS fibroblasts, LADs frequently become hypomethylated in cancer cells (Lister *et al.*, 2009; Hansen *et al.*, 2011; Berman *et al.*, 2012; Zhou *et al.*, 2018). In a contribution to a different work, LAD methylation patterns in cutaneous squamous cell carcinoma (cSCC), the second most common type of skin cancer, and its precancerous lesion, actinic keratosis (AK), in comparison with healthy epidermal keratinocytes was investigated. For this purpose, genomic DNA from 12 normal epidermis, 16 AK epidermis

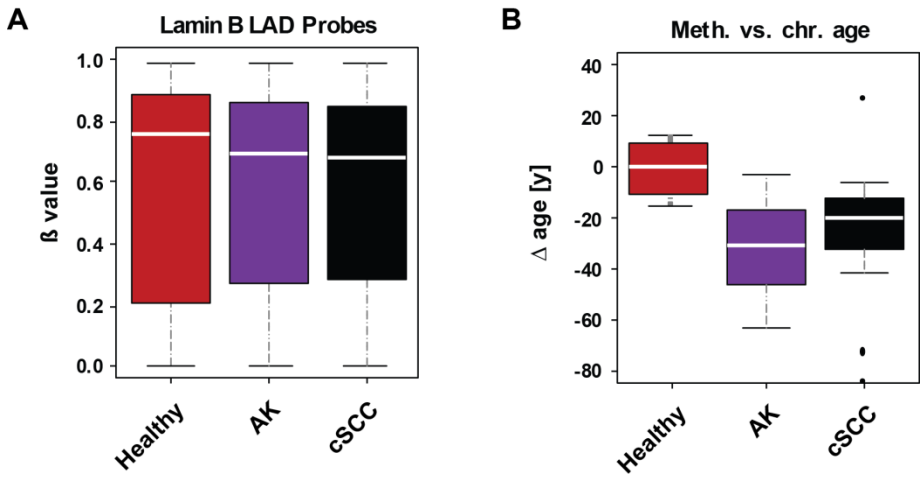

Figure 18: The epidermal cancer-specific DNA methylome differs from that of HGPS cells. (A) Probes within Lamin B LADs are significantly (P<2.20e−16, Welch Two Sample t-test) hypomethylated in AK and cSCC when compared to healthy epidermis. **(B)** Mean difference between DNA methylation age and chronological age for healthy, AK, and cSCC samples in years [y].

and 18 cSCC epidermis samples was analyzed using Infinium MethylationEPIC BeadChips (Rodríguez-Paredes *et al.*, 2018). As shown in Figure 18A, both AK and cSCC samples showed a strong and significant (P<2.20e-16, Welch Two Sample t-test) hypomethylation of Lamin B LAD-associated probes. This confirmed that the LAD hypomethylation observed in multiple other cancers (Hansen *et al.*, 2011; Berman *et al.*, 2012; Hon *et al.*, 2012; Hovestadt *et al.*, 2014; Zhou *et al.*, 2018) is also present in this epidermal cancer and in its non-cancerous precursor. Furthermore, a comparison of the chronological age of the donor with the DNA methylation age of the sample, as calculated by the original pan-tissue age estimator (Horvath, 2013), revealed that both AK and cSCC samples are characterized by a strong age deceleration (Figure 18B). These results not only confirm the previously observed DNA methylation age decrease in cancer cells (Horvath, 2013) but also underscore that the DNA methylation patterns of dermal HGPS cells are phenotypically distinct from those of skin cancer cells.

3.5. DNA adenine methyltransferase (Dam)-assisted profiling of LADs in HGPS reveals defined population-level changes

Up until this point, the identification of LAD-associated epigenetic changes in this work was based on the assumption that the dimension and distribution of LADs are conserved in the HGPS genome. However, to date Lamin A-associated genomic regions have not been

characterized in patient cells. To solve this problem, Lamin A-bound parts of the DNA were profiled in primary HGPS fibroblasts using the Dam ID technology. This technique relies on the temporary expression of a fusion protein between *E.coli* DNA adenine methyltransferase (Dam), which generates N6-methyladenine - a modification abundant in the transcriptome but absent from most eukaryotic genomes (Yue, Liu and He, 2015), and a protein of interest (here: Lamin A) (van Steensel and Henikoff, 2000). Analyzing adenine methylation in target cells by next-generation sequencing then allows the identification of regions bound by the protein of interest. Conveniently, it can be performed with a relatively small number of ~10^6 starting cells (Vogel, Peric-Hupkes and van Steensel, 2007), thus making it especially suited for the study of DNA-protein interactions in primary and disease cells.

3.5.1. The LAD landscape in the fibroblast model system

To profile regions of the HGPS fibroblast genome that are in contact with Lamin A, a Dam ID-seq experiment was performed with three HGPS and three control fibroblast samples as described in Methods, Section 6.2.19. For Dam-Lamin A samples, 20.7-33.1 million mappable reads were obtained, while for Dam-only samples, 19.5-54.2 million mappable reads were generated. Importantly, one HGPS sample had to be excluded from the analysis, due to low-quality sequencing data (see Methods, Section 6.2.19.3 and Figure S38). As a result, all HGPS LAD subsets referred to in this work represent the average of two samples, whereas control LADs were determined by averaging signal from three samples.

Figure 19 shows the chromosome-specific Lamin A enrichment calculated for both HGPS (orange) and control (blue) fibroblasts. Upon visual inspection, three major observations became evident: first, overall, the enrichment tracks of HGPS samples appeared highly similar to those of controls, with good correlation present on all chromosomes (Figure 19). Second, high similarity was also observed between regions with enriched Lamin A signal and previously published dermal fibroblast-specific LAD locations (Figure 19, grey tracks), specifically those identified with the same technique (Guelen *et al.*, 2008). This implies that LADs are largely conserved in the fibroblasts studied in this work. Third, however, some differences existed between HGPS- and control-specific tracks, on the one hand, and between previously identified LADs and the Lamin A enrichments obtained in this work, on the other hand (Figure 19). These deviations suggest that despite the general overlap, small and potentially important population-level LAD changes are detectable in HGPS cells.

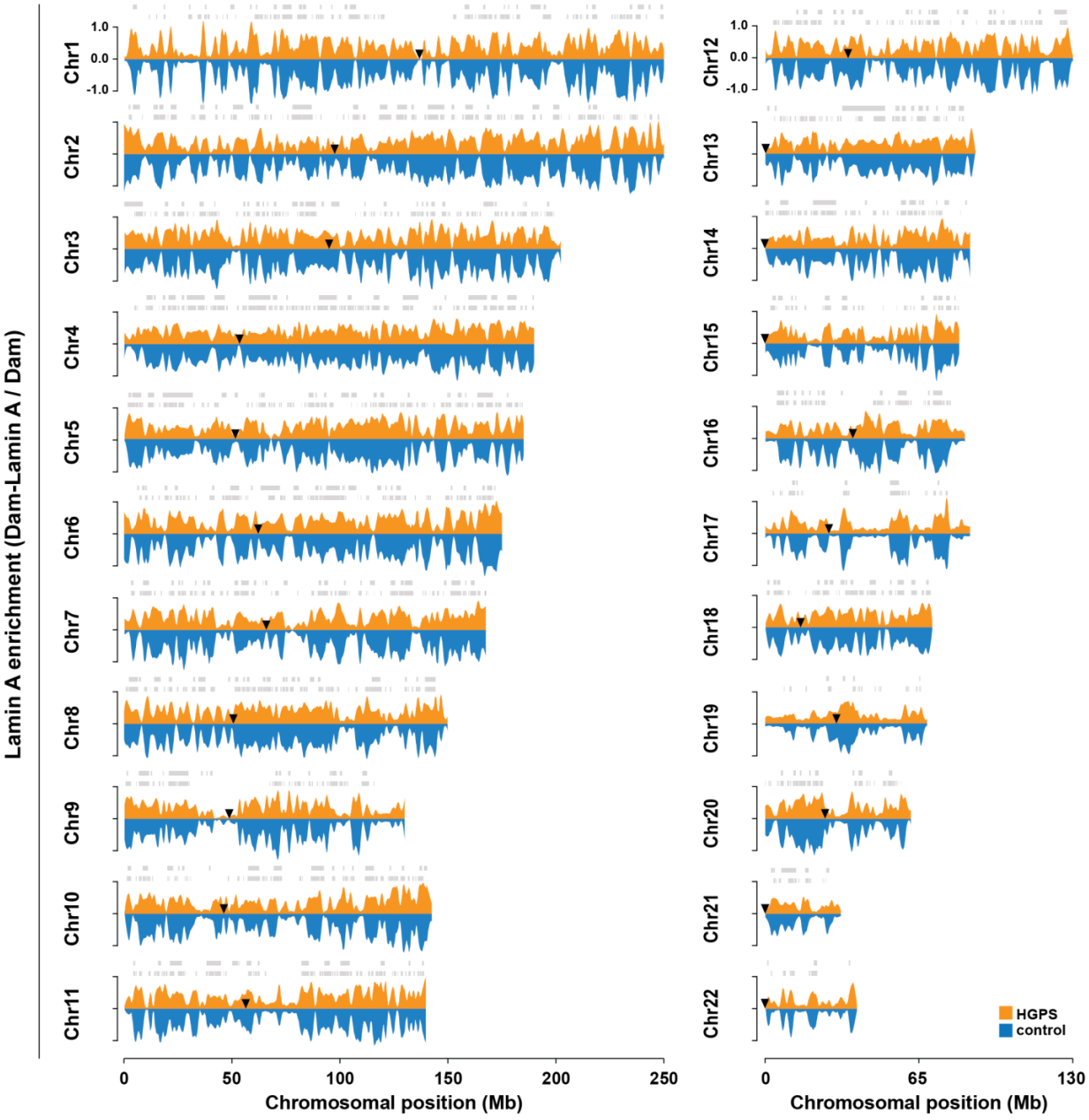

Figure 19: HGPS and control cells show similar global Lamin A enrichment profiles. Smoothed Lamin A enrichment (Dam-Lamin A / Dam) signal from HGPS (orange, top) and control (blue, bottom) samples plotted for all chromosomes. Previously identified Lamin A (top, Lund *et al*., 2015) and Lamin B (bottom, Guelen *et al.,* 2008) LADs are shown in grey. Centromere locations are indicated with black triangles.

3.5.2. HGPS-specific LAD changes

To further characterize these differences, the differential LAD enrichment between HGPS and control samples was calculated and displayed for each chromosome (Figure 20). Intriguingly, the large majority of regions on all chromosomes, especially those previously identified as LADs (Guelen *et al.*, 2008; Lund *et al.*, 2015), displayed reduced Lamin A-binding in HGPS cells, as evidenced by the slight, but widespread reduction in differential Lamin A enrichment (Figure 20). Conversely, some parts, especially telomere-proximal and pericentromeric regions, gained LAD contact in HGPS cells (Figure 20). It is also worth noting, that the similarly sized chromosomes 18 and 19, whose HGPS-specific relative chromatin accessibility changes varied drastically (Figure 13C), exhibited similarly prominent differences in differential Lamin A enrichment. While the former displayed an almost uniform reduction of Lamin A-association in HGPS cells, the latter was characterized by a more heterogeneous distribution of both gains and losses (Figure 20). Collectively, these results point towards a picture, in which the LAD landscape, while overall similar to that of unaffected dermal fibroblasts, is traceably altered in HGPS cells. Most prominently, this includes the weakening of Lamin A-binding in regions previously identified as LADs, as well as novel, but locally restricted contact sites.

As these alterations could underlie the observed DNA methylation and chromatin accessibility changes, the epigenetic data were re-analyzed with the new LAD information. For this purpose, HGPS- and control-specific LADs were defined from the respective Lamin A enrichments, applying a method developed by Gatticchi and colleagues (Gatticchi *et al.*, 2019). This resulted in the specification of distinct LAD domains for HGPS and control fibroblasts, an example of which is shown for chromosome 11 in Figure 21A. Confirming the previously described similarity in the overall Lamin A LAD landscape, HGPS and control LADs largely overlapped and closely resembled previously published LAD tracks (Guelen *et al.*, 2008; Lund *et al.*, 2015). Consistently, on a genome-scale, the total number of base pairs covered by HGPS and control LADs, closely resembled that of published Lamin B LAD tracks, while the extent of LADs overlapping between both groups was very similar to that of published Lamin A LADs (Figure 21B). Regions exclusive to HGPS or control cells, representing fractions of the genome that either lost (‘control-only’) or gained contact with the nuclear lamina (‘HGPS-only’), made up roughly one quarter of control and HGPS LADs, respectively, with slightly more regions lost than gained (Figure 21A and Figure 21B). Since these genomic stretches may provide critical insight into the disease-associated epigenetic patterns, the distribution of methylation and chromatin accessibility changes across the newly identified LAD subsets was analyzed next.

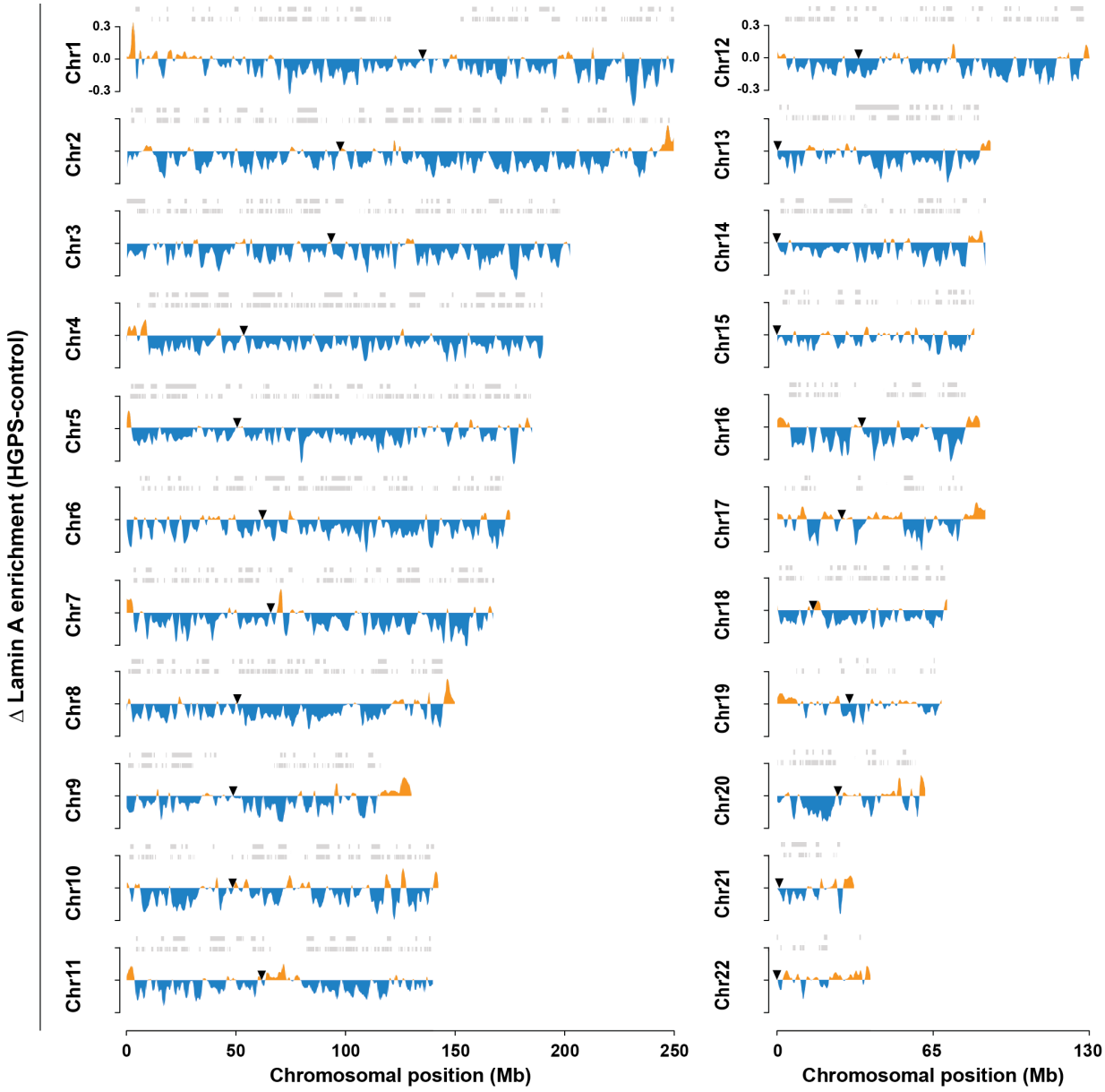

Figure 20: Differential enrichment reveals weak, but widespread HGPS-specific loss of Lamin A-binding. Smoothed differential (HGPS-control) Lamin A enrichment (Dam-Lamin A / Dam) signal plotted for all chromosomes. Positive signal (orange) indicates stronger, negative signal (blue) indicates weaker Lamin A-binding in HGPS. Previously identified Lamin A (top, Lund *et al.,* 2015) and Lamin B (bottom, Guelen *et al.,* 2008) LADs are shown in grey. Centromere locations are indicated with black triangles.

A

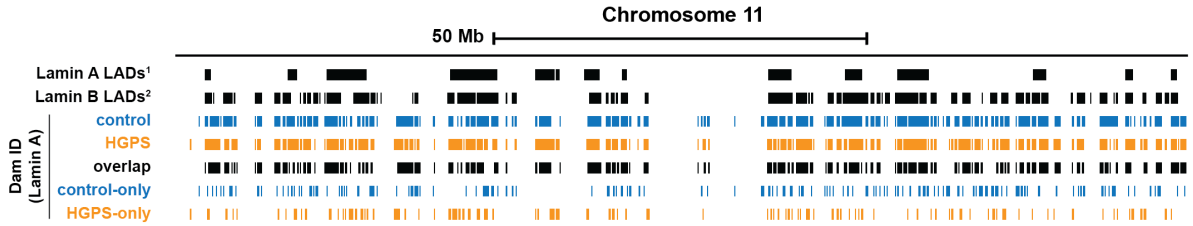

B

LAD subset	Lamin A[1]	Lamin B[2]	control	HGPS	overlapping	HGPS-only	control-only
Total # of bp	728,178,000	1,140,974,060	1,170,493,211	1,108,847,272	794,716,264	222,942,340	281,329,538

Figure 21: Definition of lamina-associated domains (LADs) in HGPS and control samples. (A) Schematic representation of LAD subsets defined using a pipeline developed by Gatticchi *et al.* (Gatticchi *et al.,* 2019) for chromosome 11. **(B)** Total genome coverage of LAD subsets shown in (A) in base pairs (bp). [1] Lund *et al.,* 2015, [2] Guelen *et al*., 2008.

3.5.3. Alterations in the LAD landscape help explain epigenetic changes observed in HGPS

The use of previously reported locations of Lamin A-associated LADs pointed towards a partial relaxation of peripheral chromatin in HGPS, as not only losses but also gains in chromatin accessibility were enriched in these regions (Figure 13B). Importantly, the HGPS-specific LAD data generated in the Dam ID-seq experiment helped to better resolve this situation.

First, based on the new information, HGPS-specific chromatin accessibility increases were not enriched in regions associated with the nuclear lamina in HGPS cells (Figure 22A, middle row), suggesting that these stretches of the genome do not undergo substantial relaxation. In fact, significant ($P<0.05$, Fisher's Exact test) chromatin accessibility gains solely occurred in regions losing LAD association in the disease, i.e. 'control-only' LADs (Figure 22A, middle row).

Second, the Dam ID-seq data more directly confirmed the heterochromatic nature of HGPS LADs, as lamina-associated regions lost chromatin accessibility. More precisely, both HGPS LADs and those overlapping between disease and control cells revealed significantly ($P<0.05$, Fisher's Exact test) enriched accessibility decreases (Figure 22A, bottom row). However, the strongest decreases occurred in parts of the genome that were identified as LADs exclusively in HGPS cells (Figure 22A, bottom row), thus indicating a heterochromatic nature of disease-specific LADs.

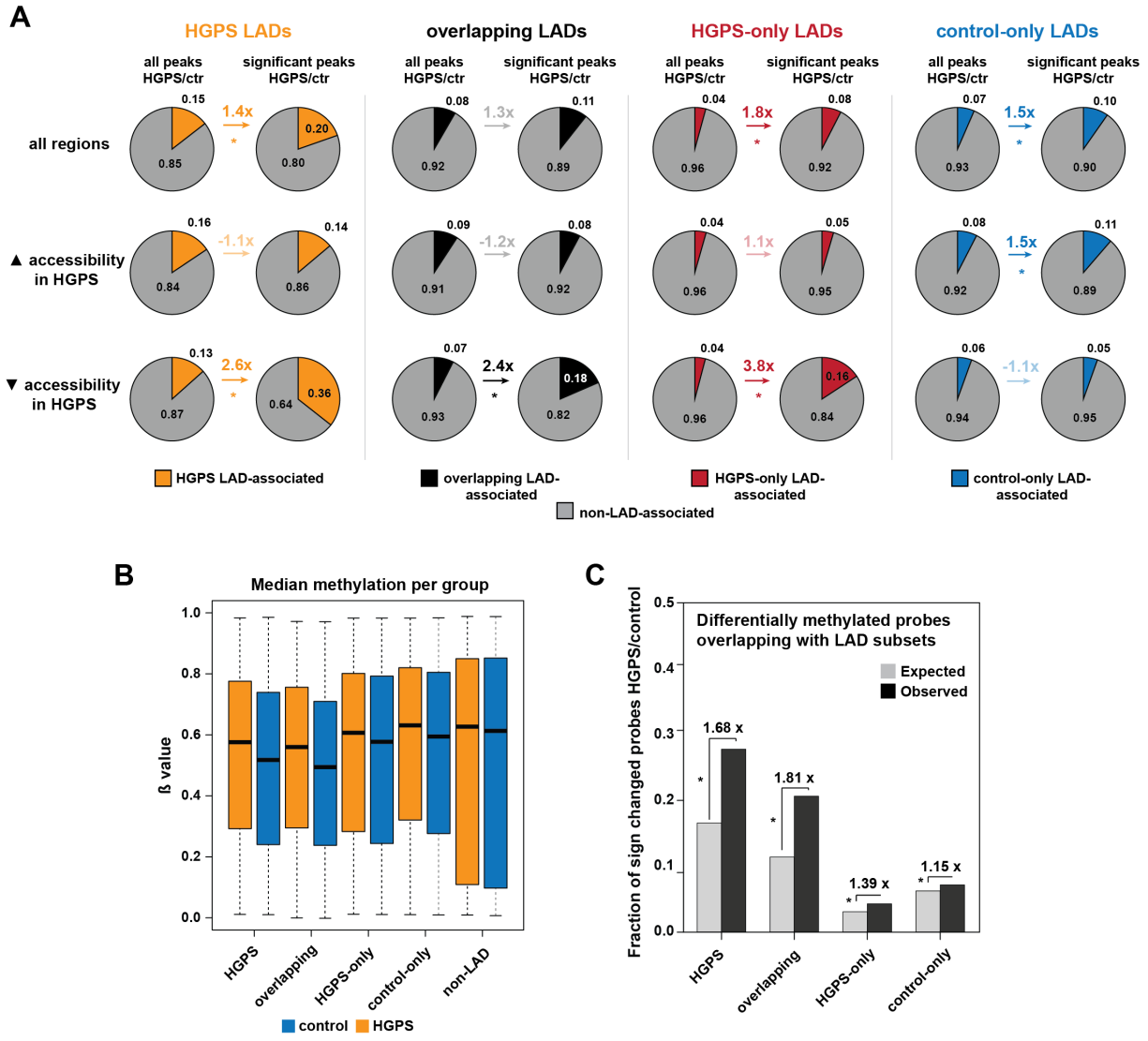

Figure 22: Dam ID-seq-defined lamina-associated domain (LAD) subsets better resolve HGPS-specific epigenetic changes. (A) Distribution of ATAC-seq peaks across LAD subsets identified in this work. The arrows indicate the observed enrichment of HGPS-specific, significantly differentially accessible regions (right) in a given LAD subset (*P<0.05; Fisher's Exact test). Ctr = control. **(B)** Differential methylation (β value) of probes overlapping with the different LAD subsets with median indicated as a black line (HGPS LADs: P<2.20e-16, overlapping LADs: P<2.20e-16, HGPS-only LADs: P=3.26e-12, control-only LADs: P<2.20e-16, non-LAD: P<2.20e-16) (Welch Two Sample t-test for all). **(C)** Enrichment of LAD subset-associated probes among differentially (P<0.05, F-test) methylated probes (*P<0.01; chi-squared test). Expected numbers were calculated based on the fraction of LAD subset-associated probes among all probes normalized to the number of differentially methylated probes.

Intriguingly, when the DNA methylation patterns were re-analyzed with the new LAD information, a different picture emerged: in agreement with the results obtained with the previously published LAD datasets (Figure 16A and B), probes located in the HGPS and overlapping LAD subsets were significantly (P<2.20e-16 for both, Chi-squared test) enriched among differentially methylated probes and showed strong and significant (P<2.20e-16 for both, Welch two sample t-test) HGPS-specific increases in median methylation (Figure 22B and C). Furthermore, non-LAD associated probes exhibited relatively little group-specific differences and higher overall methylation levels (Figure 22B). Unexpectedly, however, probes overlapping with the 'HGPS-only' and 'control-only' LAD subsets, i.e., regions gaining and losing lamina contact in HGPS cells, respectively, revealed intermediate overall methylation levels and smaller, yet significant (P=3.26e-12 and P<2.20e-16, Welch two sample t-test), disease-specific increases in median DNA methylation (Figure 22B). Consistently, they were only very slightly overrepresented among the differentially methylated probes (P<2.20e-16 and P=6.27e-08, Chi-squared test) (Figure 22C). Together, these findings imply that, at the DNA methylation level, HGPS- and control-specific LADs represent an intermediate state between the ones conserved in both groups and those not associated with the nuclear lamina.

In summary, the above data help to better resolve the landscape of epigenetic alterations in HGPS fibroblasts. More precisely, they point towards a scenario, in which the majority of HGPS LADs, including those shared with control cells, are characterized by low chromatin accessibility, partial methylation levels and HGPS-specific hypermethylation. Newly established LADs and those lost in the disease, on the other hand, exhibit methylation patterns more similar to non-LAD parts of the genome and less HGPS-specific hypermethylation but differ drastically with regard to chromatin accessibility. The latter was found to be slightly elevated in LADs lost in HGPS but to be considerably diminished in newly created ones, thus hinting at a conservation of their repressive nature in the disease.

3.6. Profiling of the HGPS transcriptome using RNA-seq

To investigate whether the identified HGPS-specific epigenomic changes affect gene expression patterns in the disease, RNA-seq was performed with fibroblasts from six HGPS patients and three controls. As shown in Figure S39, HGPS samples clustered separately from control samples in a PCA based on the transcriptomic profiles, indicating significant expression differences between both groups. These differences were subsequently further characterized.

3.6.1. The HGPS transcriptome and comparisons with earlier studies

After preprocessing (see Methods, Section 6.2.18.2), 343 genes were found to be significantly (q<0.05, Benjamini-Hochberg) differentially expressed between the HGPS and control groups, of which 160 were upregulated and 183 were downregulated in the disease, respectively (Figure 23A). Importantly, the list of differentially expressed genes included factors known to be deregulated in HGPS such as the osteoblast maturation factor '*Twist Family BHLH Transcription Factor 2*' (*TWIST2*), the extracellular matrix (ECM) protein '*Dermatopontin*' (*DPT*) or several collagens including '*Collagen Type IV Alpha 1 Chain*' (*COL4A1*) and '*Collagen Type IV Alpha 5 Chain*' (*COL4A5*) (Csoka *et al.*, 2004; Plasilova *et al.*, 2011). Further confirming the overlap with earlier studies, the data generated herein were in good correlation with data from two previous array-based reports (GSEA3860: Pearson correlation r=0.37, P<2.20e-16 (Csoka *et al.*, 2004), GSEA69391: Pearson correlation r=0.23, P<2.20e-16 (Kubben *et al.*, 2016)), especially for genes, whose expression was found to be more strongly deregulated in HGPS (Figure 23B, upper panels). Likewise, despite some deviation, many of the significantly up- or downregulated genes overlapped with genes identified in either of the two studies, or both (Figure 23B, lower panels).

In the HGPS-specific transcriptome, several processes were significantly (False Discovery Rate (FDR) q<0.05) overrepresented as measured by Gene Set Enrichment Analyses (GSEAs). Highest enrichments were observed for 'Hippo signaling' (NES=1.91, FDR q-val=0.002), a developmental signaling pathway controlling organ size (Zhao *et al.*, 2010), 'extracellular matrix receptor interaction' (NES=1.93, FDR q-val=0.01), confirming the disruption of extracellular matrix homeostasis in HGPS (Csoka *et al.*, 2004; Prokocimer, Barkan and Gruenbaum, 2013; Vidak *et al.*, 2015), and 'vascular smooth muscle contraction' (NES=1.82, FDR q-val=0.03), representing genes involved in vasoconstriction (Figure 23C). Similarly, 'UV response down' (NES=1.55, FDR q-val=0.02), containing genes downregulated upon ultraviolet (UV) light exposure such as collagens and members of the insulin-like growth factor signaling pathway, and 'Notch signaling' (NES=1.65, FDR q-val=0.03), which plays a crucial role during cardiac development (Niessen and Karsan, 2008), were significantly enriched in the transcriptome of HGPS fibroblasts (Figure 23C). Intriguingly, target genes of the AP1 transcription factor family, whose members were overrepresented in the HGPS-specific differentially accessible and differentially methylated regions (Figure 14B/C and Figure 15F), also revealed an enrichment-like pattern, despite not reaching the significance threshold (NES=1.05, FDR q-val=0.285) (Figure 23C). In accordance with this, a TRANSFAC analysis of upstream regulators driving the gene expression changes of HGPS fibroblasts included AP1 family members (Figure 23D).

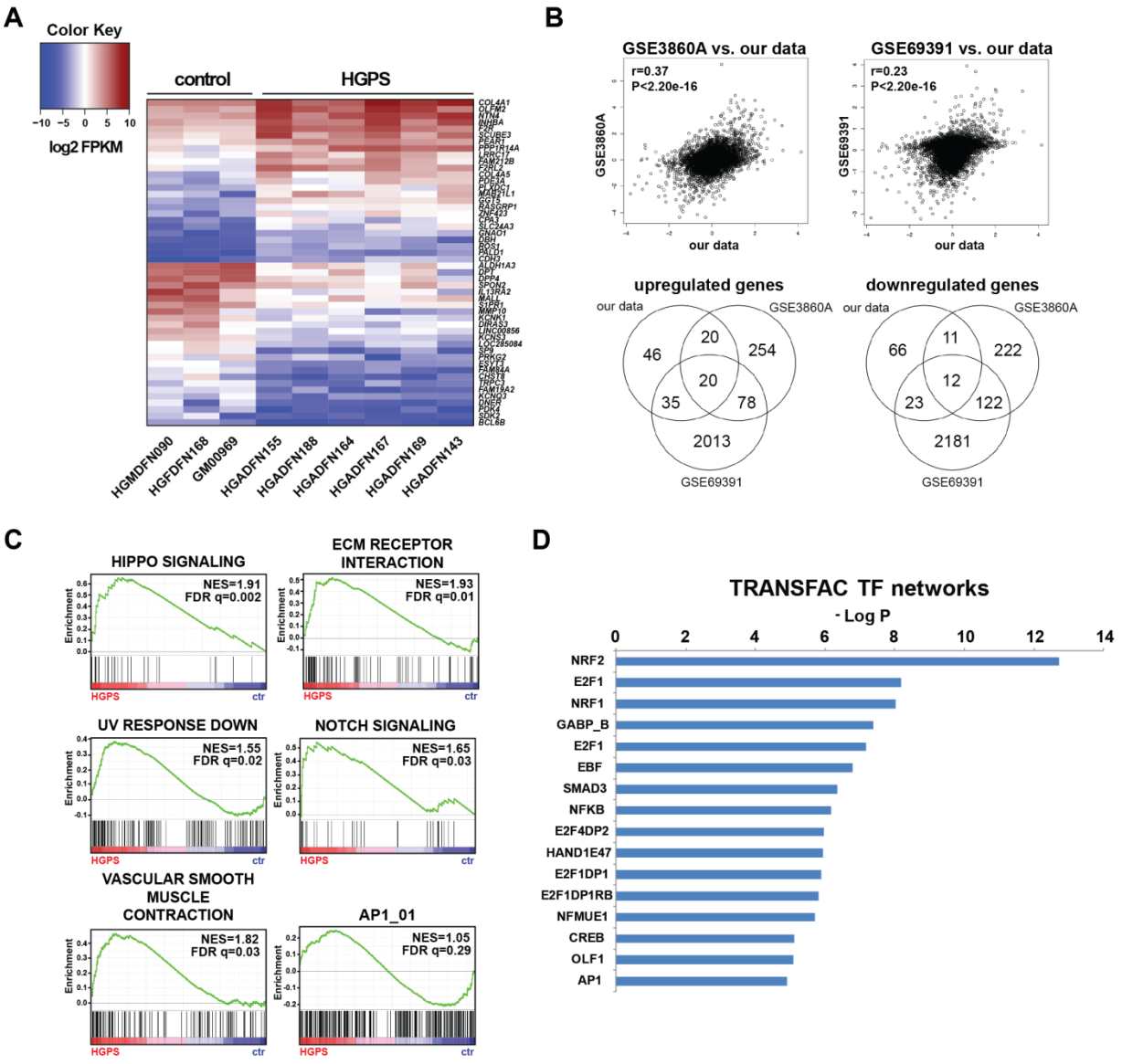

Figure 23: General features of the HGPS-specific transcriptome. (A) 50 most differentially (q<0.05, Benjamini-Hochberg) expressed genes in six HGPS vs. three control samples. Lowly expressed genes are shown in blue, highly expressed ones in red. FPKM = Fragments Per Kilobase of transcript per Million mapped reads. **(B)** Comparison of RNA-seq data with previous HGPS expression studies. Log Fold Changes (FC) of genes in GSE3860A vs. our data (Pearson correlation r=0.37, P<2.20e-16), and in GSE69391 vs. our data (Pearson correlation r=0.23, P<2.20e-16), respectively, are given in upper panels. Lower panels show the overlap of genes up- or downregulated, respectively, between our and the aforementioned studies. (**C)** Selection of Gene Ontology (GO), Kyoto Encyclopedia of Genes and Genomes (KEGG) and hallmark gene sets enriched (False Discovery Rate (FDR) q<0.05) in HGPS fibroblasts. NES=Normalized Enrichment Score. (**D)** TRANSFAC transcription factor (TF) network analysis of upstream factors controlling the observed expression changes (P<0.05 for all).

Simultaneously, it identified NRF2 as the main transcription factor behind these changes (Figure 23D), confirming an earlier report that established NRF2 as one of the key factors behind the HGPS-specific transcriptome alterations (Kubben *et al.*, 2016).

In summary, these results confirm the gene expression changes previously reported for HGPS fibroblasts and further point towards the possibility that the epigenetic changes identified herein contribute to the disease-specific transcriptome alterations.

Given the rapid progression of age-related pathologies in HGPS patients, the question arises whether cells from older patients exhibit a larger number of deregulated genes when compared to control cells. Therefore, differences in the expression patterns of fibroblasts from old and young patients were analyzed. Indeed, cells from older patients (>8 years) were characterized by the largest number of differentially expressed genes (n=397, Figure 24A). After removal of

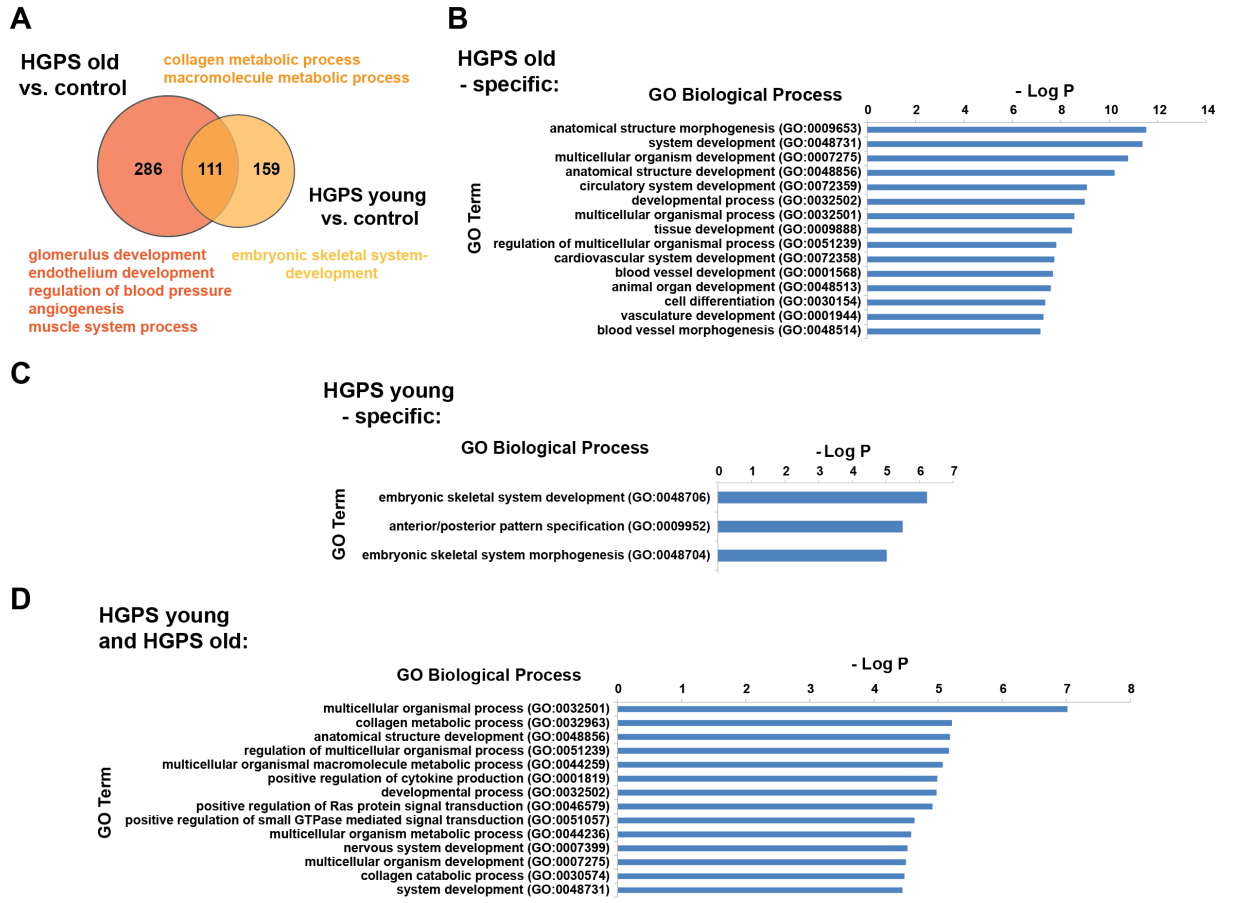

Figure 24: Transcriptomic differences between HGPS subgroups. (A) Venn diagram showing numbers of genes overlapping between HGPS young (<8 years) vs. control samples and HGPS old (>8 years) vs. control samples, respectively. The Gene Ontology (GO) processes characteristic of each comparison are given. **(B), (C) & (D)** GO processes enriched among the differentially (q<0.05, Benjamini-Hochberg) expressed genes for (B) HGPS old (>8 years) vs. control, (C) HGPS young (<8 years) vs. control and (D) genes overlapping between HGPS old vs. control and HGPS young vs. control, respectively.

those genes that were also found deregulated in cells from younger patients, the 286 remaining 'old-specific' genes were analyzed for enrichment of Gene Ontology (GO) terms. Interestingly, this yielded processes characteristic of HGPS-related pathologies such as 'glomerulus development', 'endothelium development', 'regulation of blood pressure', 'angiogenesis', and 'muscle system process' (Figure 24A and B). In contrast, the 159 genes deregulated in younger patients (<8 years), i.e., 'young-specific' ones, were associated with the GO terms 'embryonic skeletal system development' and 'anterior/posterior pattern specification' (Figure 24A and C). Lastly, the set of genes overlapping between both groups (n=111), i.e., those independent of patient age, was characterized by developmental, organismal and metabolic processes (Figure 24A and D). These results illustrate that both HGPS-related developmental changes and the aggravation of the clinical phenotype can be recapitulated at the level of gene expression *in vitro*.

3.6.2. Epigenetic changes are associated with a subset of HGPS-specific expression changes

To find out whether changes in the LAD landscape and accompanying epigenetic alterations contribute to the gene expression patterns observed in HGPS fibroblasts, the generated gene expression data were compared with the DNA methylation and ATAC-seq datasets. Out of the 343 genes with significant expression changes, 21 showed simultaneous changes in chromatin accessibility, the majority of which (n=16) gained accessibility in HGPS (Figure 25A). In comparison, 14 genes exhibited simultaneous alterations in DNA methylation, with about half (n=8) becoming hypermethylated in patient cells (Figure 25B). Finally, three genes (*EDIL3*, *RELN* and *ZNF423*) were characterized by both differential DNA methylation and differential accessibility. These limited numbers suggest that only a subset of differentially expressed genes is directly affected by the epigenetic alterations in HGPS cells.

A genomic reorganization of LADs can underlie gene expression changes in both development and disease (Perovanovic *et al.*, 2016; Poleshko *et al.*, 2017; Cheedipudi *et al.*, 2019). This raises the possibility that the epigenetic changes observed in the abovementioned gene subsets are associated with their intranuclear relocalization. To test this, fluorescence in situ hybridization (FISH) experiments were performed in HGPS fibroblasts. More specifically, the distance of specific FISH signals to the nuclear lamina was measured for a set of five genes in HGPS and control cells (Figure 25C and D, Figure S40). Two of the tested genes, '*EGF Like Repeats And Discoidin Domains 3*' (*EDIL3)* (P=3.03e-08, Welch Two Sample t-test) and '*Insulin Like Growth Factor Binding Protein 7*' (*IGFBP7)* (P=2.75e-13, Welch Two Sample t-test) were

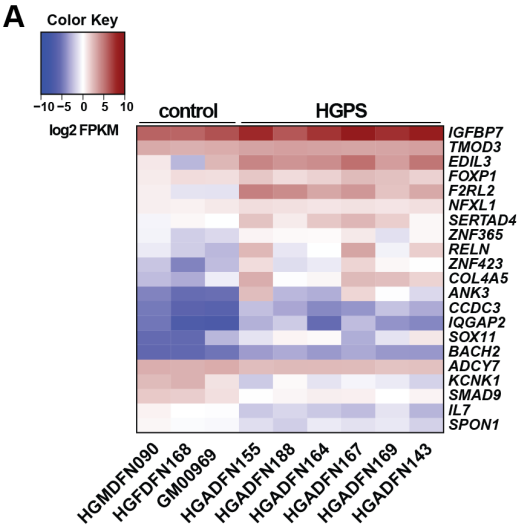
A
Color Key
−10 −5 0 5 10
log2 FPKM
control
HGPS
IGFBP7
TMOD3
EDIL3
FOXP1
F2RL2
NFXL1
SERTAD4
ZNF365
RELN
ZNF423
COL4A5
ANK3
CCDC3
IQGAP2
SOX11
BACH2
ADCY7
KCNK1
SMAD9
IL7
SPON1
HGMDFN090
HGFDFN168
GM00969
HGADFN155
HGADFN188
HGADFN164
HGADFN167
HGADFN169
HGADFN143

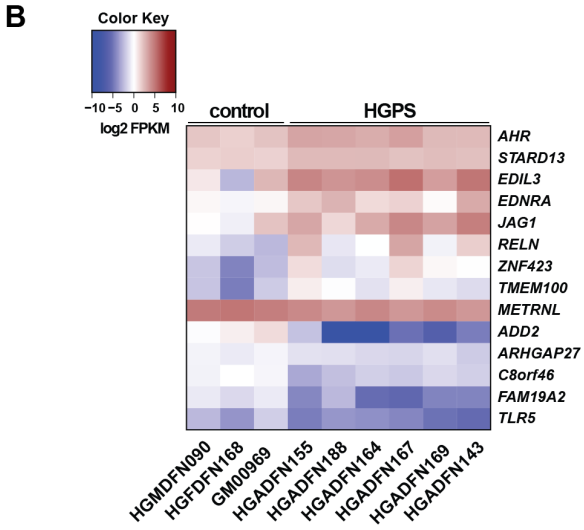
B
Color Key
−10 −5 0 5 10
log2 FPKM
control
HGPS
AHR
STARD13
EDIL3
EDNRA
JAG1
RELN
ZNF423
TMEM100
METRNL
ADD2
ARHGAP27
C8orf46
FAM19A2
TLR5
HGMDFN090
HGFDFN168
GM00969
HGADFN155
HGADFN188
HGADFN164
HGADFN167
HGADFN169
HGADFN143

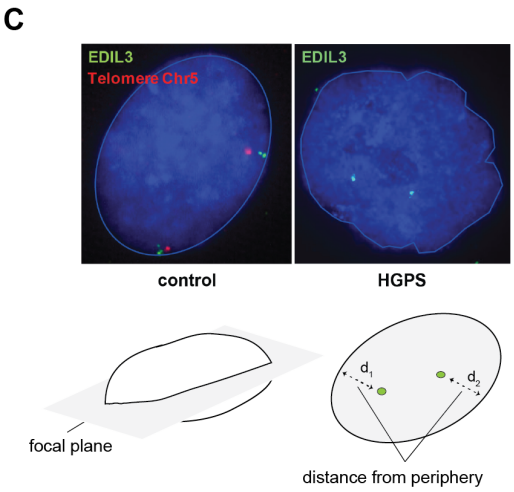
C
EDIL3
Telomere Chr5
EDIL3
control
HGPS
focal plane
d1
d2
distance from periphery

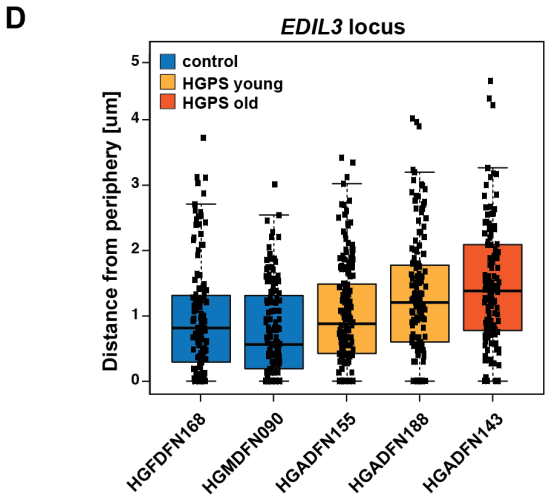
D
EDIL3 locus
control
HGPS young
HGPS old
Distance from periphery [um]
HGFDFN168
HGMDFN090
HGADFN155
HGADFN188
HGADFN143

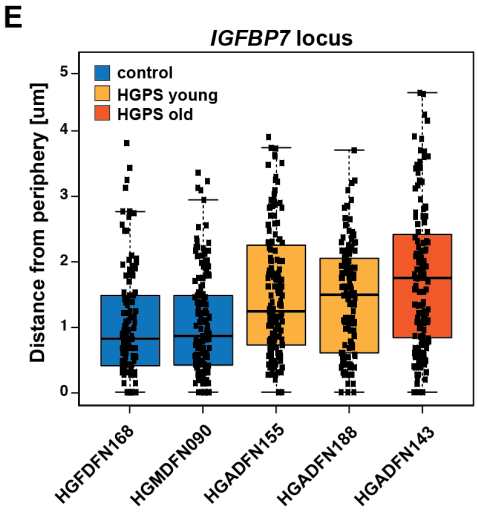
E
IGFBP7 locus
control
HGPS young
HGPS old
Distance from periphery [um]
HGFDFN168
HGMDFN090
HGADFN155
HGADFN188
HGADFN143

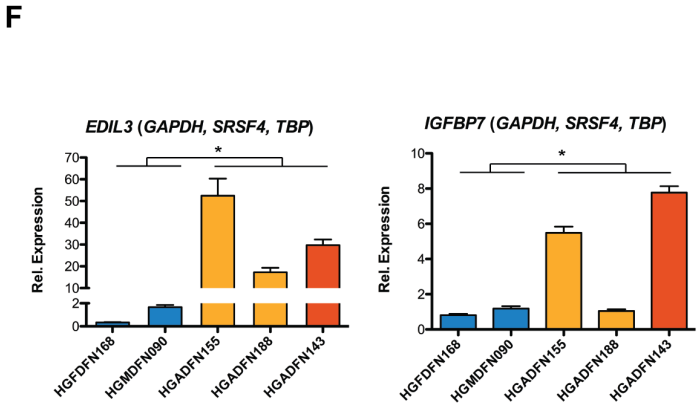
F
EDIL3 (GAPDH, SRSF4, TBP)
IGFBP7 (GAPDH, SRSF4, TBP)
Rel. Expression
*
HGFDFN168
HGMDFN090
HGADFN155
HGADFN188
HGADFN143

Figure 25: Epigenetic deregulation of lamina-associated domains (LADs) contributes to aberrant gene expression in HGPS. (A) Differentially (q<0.05, Benjamini-Hochberg) expressed genes that show concomitant HGPS-specific chromatin accessibility changes in their promoter or gene body. Lowly expressed genes are shown in blue, highly expressed ones in red. FPKM = Fragments Per Kilobase of transcript per Million mapped reads. **(B)** Differentially (q<0.05, Benjamini-Hochberg) expressed genes that show concomitant HGPS-specific DNA methylation changes in their promoter or gene body. FPKM as in (A). **(C)** Representative *EDIL3* FISH images in HGPS and control nuclei. A telomeric probe (red) on chromosome 5 (Chr5) was used as a positive staining control. The distance (d) from the FISH signal to the nuclear periphery was measured in the focal plane in cells exhibiting a clear biallelic signal. **(D) & (E)** Quantification of (C) for *EDIL3* and *IGFBP7* loci in two control and three HGPS cell lines for 60 cells per sample. *EDIL3*: P=3.03e-08, Welch Two Sample t-test. *IGFBP7:* P=2.75e-13, Welch Two Sample t-test. **(F)** *EDIL3* and *IGFBP7* expression levels relative to those of *GAPDH*, *SRSF4* and *TFB* in control (blue), HGPS young (<8 years, orange) and HGPS old (>8 years, red) cells as measured by RT-qPCR (**EDIL3*: P=2.00e-03, *IGFBP7*: P=4.00e-04, unpaired t-test).

consistently localized further away from the nuclear periphery in HGPS compared with control cells (Figure 25D&E), with the strongest locational changes occurring in cells from older patients. *EDIL3* encodes an integrin ligand with an important role in angiogenesis, vessel wall remodeling and development (Hidai *et al.*, 1998; Aoka *et al.*, 2002). *IGFBP7*, on the other hand, encodes a member of the insulin-like growth factor-binding protein family and is related to cellular senescence and modulation of angiogenesis (Wilson *et al.*, 2002; Pen *et al.*, 2008; Wajapeyee *et al.*, 2008). The increased expression of both genes in HGPS cells was subsequently verified using quantitative RT-PCR (Figure 25F). These results yield proof-of-principle evidence that intranuclear relocalization can indeed underlie both epigenetic and expression alterations observed in the disease.

To evaluate the consequences of such LAD-localization changes on a broader scale, the genomic position of genes in relation to the different HGPS-specific LAD subsets was investigated. As shown in Figure 26A, both differentially expressed genes undergoing accessibility changes, as well as those undergoing DNA methylation changes, tended to be located closer to all HGPS LAD subsets than the entirety of differentially expressed genes. Seen in isolation, this suggests that the subset of genes with epigenetic changes is predominantly located near the nuclear periphery in HGPS cells.

However, integrating the dynamics of differential Lamin A-binding (cp. Figure 20) for the same subset of genes into the analysis, better resolved this observation. Specifically, differentially expressed genes with accessibility changes showed a significant (P=2.49e-04, Wilcoxon test) reduction of Lamin A-binding in patient fibroblasts (Figure 26B). The same tendency was

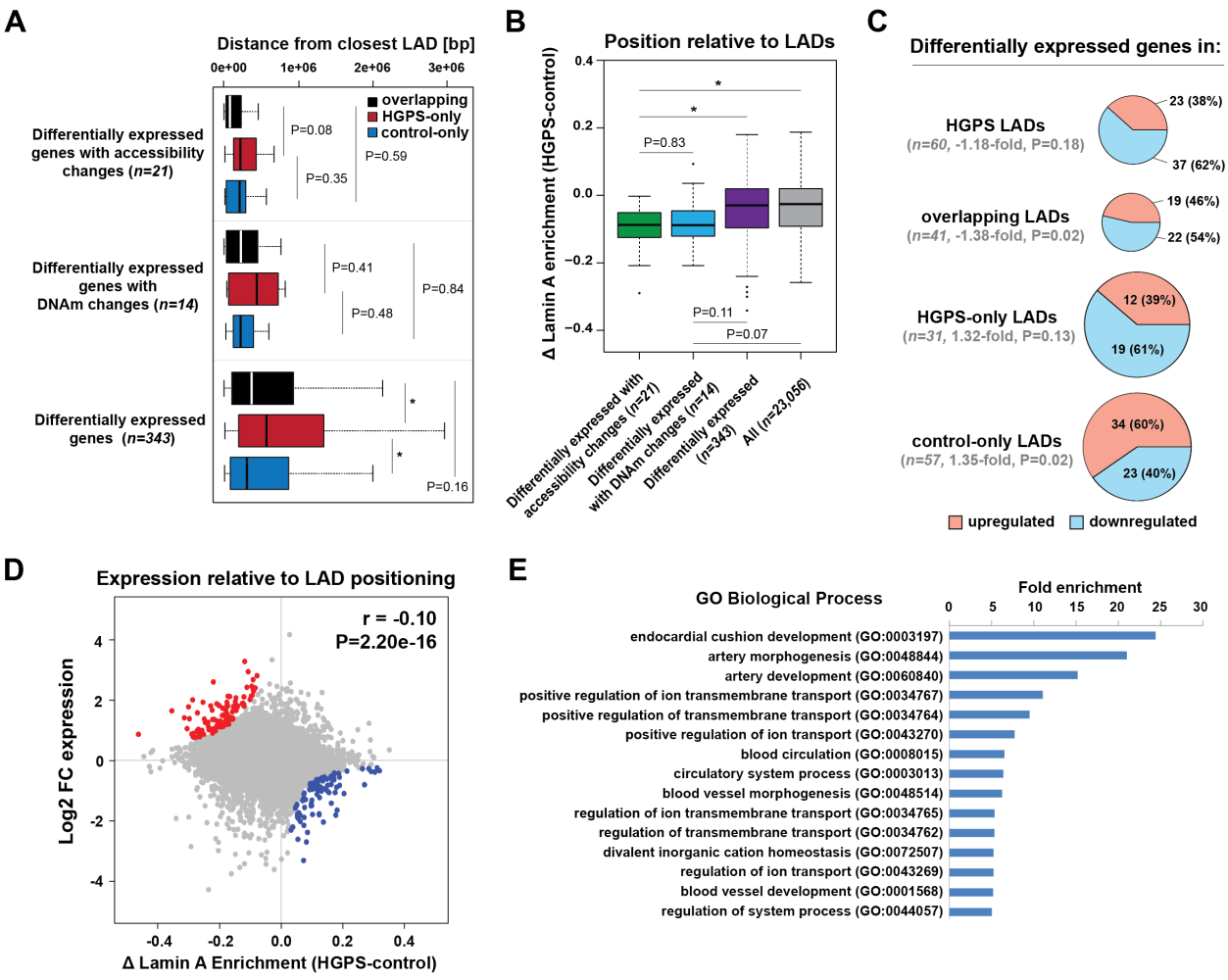

Figure 26: Lamina-associated domain (LAD) alterations are associated with a subset of HGPS-specific transcriptomic changes. (A) Distance plot showing the distance from the closest LAD for the indicated gene subsets with median indicated as a black line. Colors represent the different LAD subsets identified in this work. *P=3.79e-04 (overlapping vs. HGPS-only), *P=8.89e-07 (HGPS-only vs. control-only), Wilcoxon test for all. **(B)** Differential Lamin A enrichment (HGPS-control) (cp. Figure 20) for the different gene subsets with median indicated as a black line. *P=2.49e-04 (Diff.acc. vs. diff. expr.), *P=6.17e-05 (Diff.acc. vs. all), Wilcoxon test for all. **(C)** Number of differentially expressed genes overlapping with the different LAD subsets. The chart size reflects the fold enrichment of observed/expected (given in brackets, with Fisher's Exact test P-values). Numbers and percentages of genes up-/downregulated are also given. **(D)** Correlation of differential expression (Log2FC) and differential Lamin A enrichment (HGPS-control) on a per-gene basis. Red and blue dots represent the 100 genes exhibiting the strongest increases in expression (based on Log2 FC) and the lowest differential Lamin A enrichment in HGPS, or vice versa. **(E)** Gene Ontology processes significantly (P<0.05, Fisher's Exact test) enriched among the 100 genes exhibiting the strongest increases in expression (based on Log2 FC) and the lowest differential Lamin A enrichment in HGPS (shown in red in (D)).

present for differentially expressed genes with DNA methylation changes, despite not reaching statistical significance (P=0.11, Wilcoxon test) (Figure 26B).

In agreement with the proof-of-principle findings for *EDIL3* and *IGFBP7*, these results thus indicate that the epigenetic changes for both sets of genes tend to coincide with a detachment from the nuclear lamina. At the same time, the analysis revealed that the differential expression in patient fibroblasts is not associated with new HGPS-specific nuclear lamina contacts, as the 343 differentially expressed genes were located significantly further away from newly established HGPS LADs than from those lost in the pathology (P=8.89e-07, Wilcoxon test) or those overlapping between both groups (P=3.79e-04, Wilcoxon test) (Figure 26A).

Further evidence for these dynamics came from the quantification of differentially expressed genes in the different LAD subsets. Generally, the number of differentially expressed genes overlapping with one of the identified LAD subsets was low (Figure 26C), which is in agreement with the gene-poor nature of LADs. Nevertheless, some expression changes were found to be enriched in lamina-associated regions: while significantly (P=0.02, Fisher's Exact test) less genes than expected (-1.38-fold) were differentially expressed in LAD regions common between HGPS and control cells, significantly (P=0.02, Fisher's Exact test) more than expected (1.35-fold) were located in DNA stretches losing LAD contact in the disease (Figure 26C). Crucially, the majority of these genes (34 out of 57) were upregulated in HGPS (Figure 26C). Regions exclusively bound to Lamin A in disease fibroblasts, in contrast, contained a majority of downregulated genes (19 out of 31) (Figure 26C). Together, these findings reinforce the notion that LADs are transcriptionally inactive and that regions losing lamina association in HGPS cells become available to elevated gene expression, as observed in a proof-of-principle manner in the FISH experiments.

Finally, the set of genes, whose expression was most strongly affected by the altered lamina association in HGPS cells, was further investigated. For this purpose, the identified gene expression fold changes were correlated with the differential enrichment in Lamin A-binding (Figure 20). Overall, differential expression was weakly, but significantly negatively correlated with differential Lamin A-binding (Figure 26D, Pearson's correlation r=-0.10, P<2.20e-16), which is in agreement with the generally low expression levels of lamina-associated genes. More interestingly, analyzing the most affected genes for enrichment of GO terms yielded a striking result: no processes were significantly (P<0.05, Fisher Exact test with Bonferroni correction) enriched among the 100 genes most strongly downregulated upon increased lamina association (Figure 26D in blue). Conversely, the 100 most upregulated genes upon loss of Lamin A-binding revealed a significant enrichment of GO processes associated with cardiovascular development

(Figure 26D in red, and Figure 26E), i.e., processes involved in the formation of one of the most severely affected organ systems in the disease. These data illustrate that the increased availability of previously LAD-associated genes is an important contributor to the disease-specific gene expression.

Collectively, these results provide evidence that the HGPS-specific epigenomic changes contribute to the pathological gene expression observed in the disease. While only a subset of differentially expressed genes appears to be affected by significant chromatin accessibility and DNA methylation changes, alterations in the Lamin A-associated LAD landscape help explain a more substantial part of the HGPS fibroblast-specific transcriptome.

3.7. Lonafarnib treatment does not revert HGPS-specific DNA methylation changes

Different compounds have been shown to improve the molecular phenotype of HGPS cells (Capell *et al.*, 2005; Yang *et al.*, 2006; K. Cao *et al.*, 2011; Gabriel *et al.*, 2015; Pellegrini *et al.*, 2015; Gabriel, Gordon and Djabali, 2016; Kreienkamp *et al.*, 2016; Xiong *et al.*, 2016; Park and Shin, 2017), however, treatment with the farnesyltransferase inhibitor (FTI) Lonafarnib is currently the only intervention with demonstrated life-extending benefits for HGPS patients (Gordon *et al.*, 2014). By blocking the farnesylation step in the post-translational processing of Lamin A, this treatment has been shown to drive the accumulation of pre-Lamin A but also to activate autophagy and Progerin removal, resulting in an amelioration of the characteristic nuclear phenotype and other improvements at the cellular level (Capell *et al.*, 2005; Young *et al.*, 2013; Gabriel *et al.*, 2017). This raises the question whether treatment with a FTI alleviates the epigenetic deregulation of LADs observed in HGPS fibroblasts.

To answer this question, three HGPS and three control fibroblast cell lines were treated with 0.06 μM Lonafarnib for 7 days (see Methods, Section 6.2.2), a treatment regimen that has previously been reported to improve the nuclear phenotype of HGPS fibroblasts (Gabriel *et al.*, 2017). As expected, HGPS fibroblasts showed lower levels of Progerin and an increase in pre-Lamin A levels at the end of the treatment period (Figure 27A). Additionally, a significant ($P<0.01$, unpaired t-test) decrease in the number of lobulated nuclei was observed in two out of three HGPS samples but none of the controls (Figure 27B), hence confirming the drug's efficacy in mitigating the nuclear phenotype of HGPS fibroblasts.

Genomic DNA from DMSO- and FTI-treated cells was then tested for DNA methylation changes using Infinium MethylationEPIC arrays. Interestingly, despite the tangible phenotypic

improvement, no significantly (P<0.05, F-test) differentially methylated probes were found between FTI- and DMSO-treated HGPS cells. Consistently, no significant (P<0.05, Welch two sample t-test) methylation differences were observed between FTI- and DMSO-treated HGPS fibroblasts for probes located in the different LAD subsets, and HGPS cells retained their LAD-specific hypermethylation (Figure 27C).

Fitting this overall picture, FTI-treated HGPS cells did not show uniform or expected expression changes of some of the most strongly HGPS-specific deregulated genes (Figure

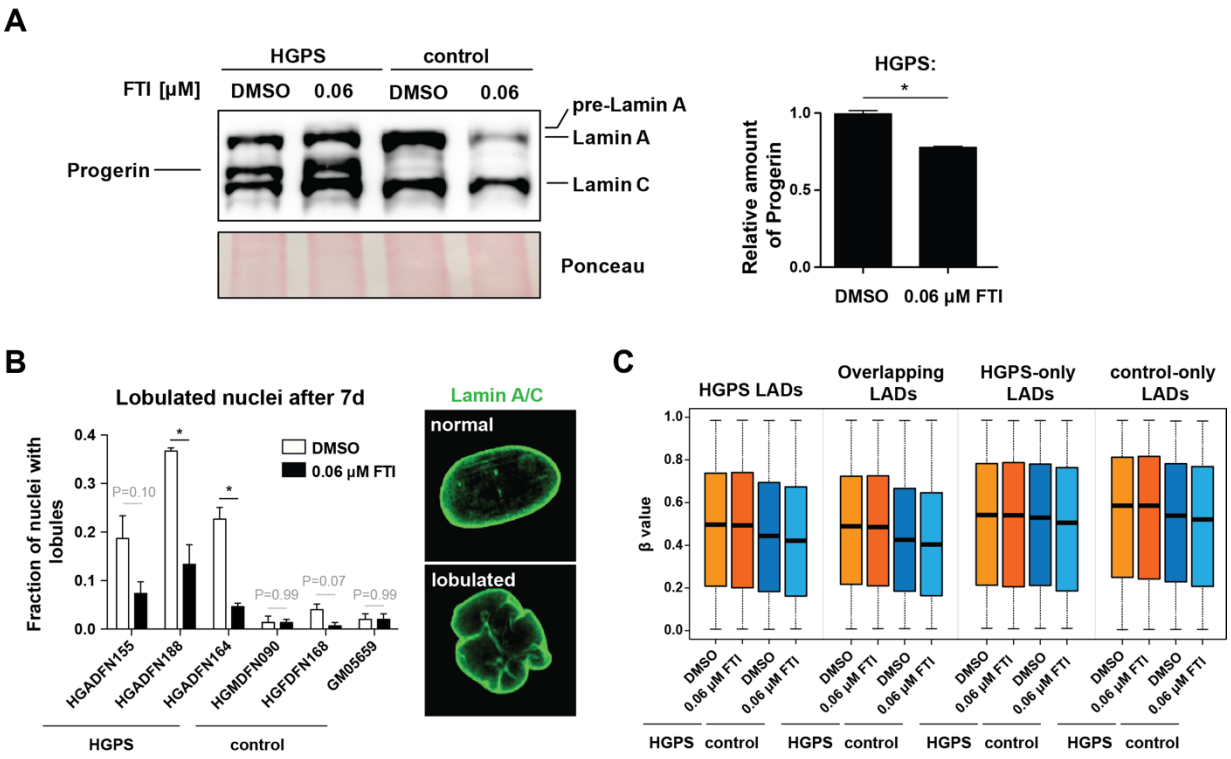

Figure 27: Lonafarnib treatment does not alleviate epigenetic deregulation of lamina-associated domains (LADs) in HGPS. (A) Left panel: Immunoblot of total protein extracts (20 µg) from HGPS (HGADFN164) and control (HGMDFN090) samples treated with DMSO or 0.06 µM Lonafarnib for 7 d. Lamin A, Progerin and Lamin C were detected using a mouse α-Lamin A/C antibody (sc7292, Santa Cruz, 1:500). Right panel: Quantification of Progerin levels relative to the amount of Lamin C in HGPS sample (triplicate measurement). *P<0.01, unpaired t-test. (**B)** Left panel: Quantification of lobulated nuclei in HGPS and control cells after 7d treatment with DMSO or 0.06 µM Lonafarnib. *P<0.01, unpaired t-test. Right panel: Representative images of normal and lobulated nuclei. (**C)** Differential methylation (ß value) of probes overlapping with the indicated LAD subsets after 7d treatment with DMSO or 0.06 µM Lonafarnib. Median indicated as a black line. HGPS LADs: P=0.11 (HGPS) and P=2.20e-16 (control); overlapping: P=0.12 (HGPS) and P=2.20e-16 (control); HGPS-only: P=0.73 (HGPS) and P=4.79e-10 (control); control-only: P=0.63 (HGPS) and P=4.38e-15 (control). Welch Two sample t-test for all.

S41). These results suggest that the Lonafarnib treatment, while effective in ameliorating the nuclear phenotype, does not alter the epigenetic and gene expression changes observed in disease cells.

3.8. A global picture emerges - epigenetic deregulation of LADs in HGPS fibroblasts

In summary, the data generated in this work paint the following picture: in normal fibroblasts, the peripheral epigenomic landscape is characterized by partially methylated, but largely inaccessible heterochromatic domains that are distinct from the highly accessible, more centrally located euchromatic compartments. In contrast, substantial remodeling takes place in lamina-associated regions of Progerin-expressing cells (Figure 28).

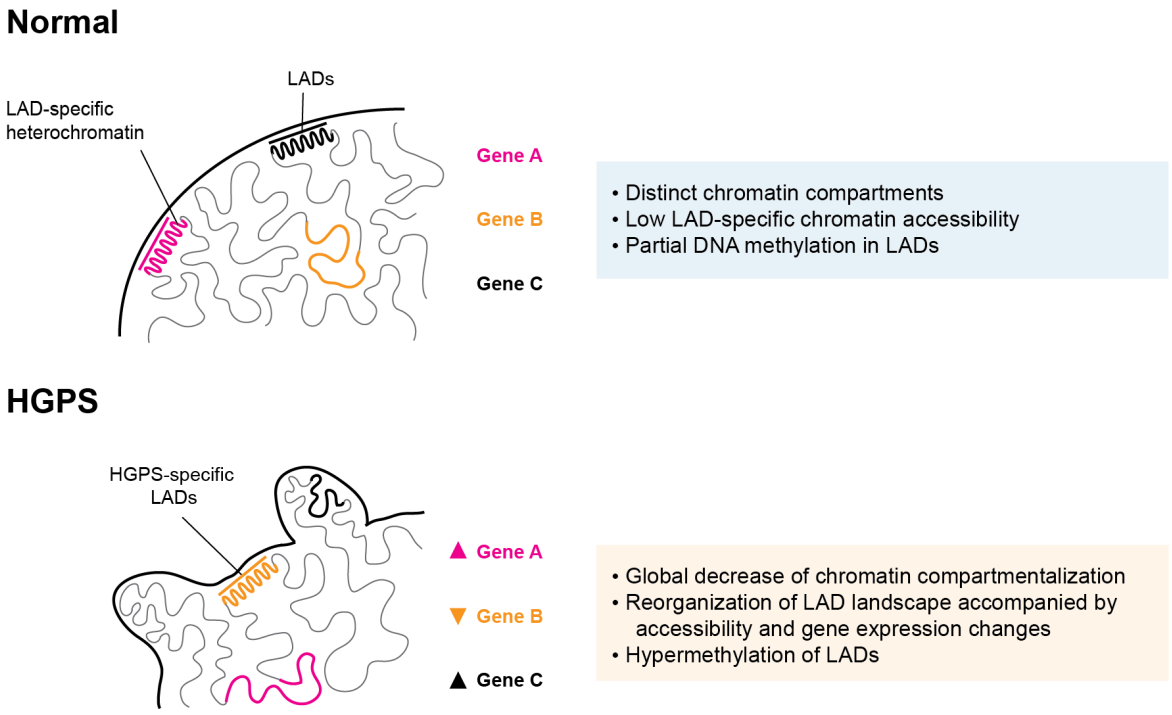

Figure 28: Epigenetic deregulation of lamina-associated domains (LADs) in HGPS. Progerin-driven nuclear malformation in HGPS nuclei causes substantial, but potentially locally stochastic epigenetic reconfiguration of LAD-specific chromatin. Chromatin accessibility and DNA methylation changes accompany a reorganization of Lamin A-binding regions. Some of the affected regions gain a more relaxed chromatin environment that is more permissive to the binding of transcription factors and might thus facilitate differential expression (Gene A). In other cases, chromatin decondensation and disease-specific differential expression of formerly LAD-associated loci coincides with a relocalization within the nucleus, as detected in the case of *EDIL3* and *IGFBP7* (Gene C). A third set of regions gains new LAD contact, followed by downregulation of the underlying genes (Gene B).

These parts of the genome exhibited significant DNA hypermethylation and chromatin accessibility changes in the HGPS populations. Critically, a widespread genomic reorganization of Lamin A-binding seems to underlie these changes; however, with different outcomes: regions losing lamina association in disease cells experience profound accessibility gains, which, in some cases, coincide with significant increases in gene expression, as detected for *EDIL3* and *IGFBP7* in a proof-of-principle manner (Figure 28, Gene A). Becoming detached from the nuclear lamina, derepressed and available to the gene expression machinery, factors unrelated to the fibroblast lineage may start to be expressed as part of this process.

Another set of loci gains LAD contact in HGPS fibroblasts, accompanied by slight decreases in chromatin accessibility and the downregulation of underlying genes (Figure 28, Gene B). Interestingly, this set of genes does not include any enriched biological processes.

Finally, the expression of a third set of genes is affected by the decondensation of peripheral heterochromatin and accompanying changes to regulatory elements and binding sites of transcription factors like AP1 and NRF2, whose differential localization can affect expression in the periphery and the nuclear interior alike (Figure 28, Gene C).

4. Discussion

Previous studies have investigated epigenetic alterations in HGPS cells but were either focused on histone modification changes (Scaffidi and Misteli, 2006; Shumaker *et al.*, 2006; McCord *et al.*, 2013) or limited by the technology of earlier DNA methylation assays (Liu *et al.*, 2011). It is therefore still unclear how global DNA methylation patterns are shaped in HGPS and whether the reported histone modification changes affect the chromatin accessibility landscape. Similarly, a link between aberrations in these regulatory layers and the pathological gene expression signature observed in Progerin-expressing cells remains to be demonstrated.

To address these questions, this work was aimed at exploring the nature and extent of HGPS-specific epigenomic alterations at the level of DNA methylation and chromatin accessibility. For this purpose, primary dermal fibroblasts from different HGPS patients were subjected to an integrated analysis using ATAC-see/-seq, DNA methylation profiling and Dam ID-seq of Lamin A-associated regions. These data were complemented with RNA-seq information, in order to identify gene expression changes that are related to the HGPS-specific epigenetic alterations.

The data obtained herein identify epigenetic deregulation of LADs as a novel, defining feature of the HGPS epigenome, which is associated with a global reorganization of the Lamin A LAD landscape and contributes to aberrant gene expression in the disease.

4.1. Chromatin accessibility and DNA methylation changes are enriched in LADs and reveal different facets of the HGPS epigenome

The central finding of this work is that HGPS-specific chromatin accessibility and DNA methylation changes are significantly enriched in genomic regions that are in contact with the nuclear lamina. This was evidenced by an accumulation of changes in both layers in regions marked by Lamin A-binding, the presence of Fos/Jun TFBSs and the absence of the active histone modification marks H3K4me3, H3K27ac and H3K36me3. The implied epigenetic reconfiguration of the nuclear periphery in HGPS fibroblasts is, in general terms, in agreement with previous reports demonstrating epigenetic changes concentrated near the nuclear lamina in Progerin-expressing cells (Goldman *et al.*, 2004; McCord *et al.*, 2013). However, a closer inspection of the nature of these changes reveals some critical differences between the two layers.

Chromatin accessibility changes were found enriched in Lamin A LADs, but the DamID-seq experiment demonstrated that they are not homogeneously distributed across the different HGPS-specific LAD subsets; instead, they reflect the underlying HGPS-specific LAD dynamics. For example, decreases in chromatin accessibility were strongly enriched in 'HGPS-only' LADs, and to a lesser extent in those conserved between HGPS and control cells. This finding suggests that lamina-associated stretches of the DNA maintain their inaccessible, i.e., compacted chromatin identity in HGPS fibroblasts, despite the widespread loss of peripheral heterochromatin in those cells (Goldman *et al.*, 2004; McCord *et al.*, 2013).

Regions losing Lamin A contact in HGPS cells, on the other hand, showed a slight, but significant enrichment of chromatin accessibility gains, implying that previously inaccessible, i.e., heterochromatic regions lose their repressive nature as they move away from the nuclear lamina. These changes are most prominently exemplified by the dynamics of intranuclear localization observed for chromosome 18. Usually located at the nuclear periphery with multiple LAD contacts in various proliferating human cell types (Croft *et al.*, 1999; Meaburn *et al.*, 2007; Kind *et al.*, 2015), this chromosome exhibited some of the highest relative changes in chromatin accessibility and a widespread decrease in Lamin A-binding in patient cells, strongly suggesting its relocalization to the nuclear interior. Not coincidentally, cytological studies have found that chromosome 18 is indeed located in the nuclear center in fibroblasts from different laminopathies including HGPS (Meaburn *et al.*, 2007; Mehta *et al.*, 2011). Moreover, the active relocalization of formerly LAD-associated loci in HGPS cells does also not appear to be restricted to single chromosomes, as the genomic loci of *IGFBP7* and *EDIL3,* located on chromosomes 4 and 5, respectively, were proven to be relocated in HGPS nuclei using FISH. Instead, these dynamics likely symbolize a larger-scale reshuffling of the LAD environment in progerin-expressing cells.

Interestingly, HGPS-specific DNA methylation changes, which were also enriched in Lamin A LADs, reveal a different characteristic of the HGPS epigenome. In contrast to the chromatin accessibility data, the highest enrichment of methylation changes, as well as considerable HGPS-specific hypermethylation, was found in Lamin A LADs conserved between HGPS and control cells. This is surprising, given that LADs largely overlap with PMDs, which have been reported to undergo progressive hypomethylation during aging in a variety of cells and tissues (Aran *et al.*, 2011; Vandiver *et al.*, 2015; Zhou *et al.*, 2018). Crucially, the decrease in DNA methylation within PMDs has been observed to coincide with an increase in heterochromatic histone marks (Salhab *et al.*, 2018), thus making it tempting to speculate that an opposite scenario may be active here. In other words, the observed HGPS-specific DNA

hypermethylation of lamina-associated regions could represent a compensatory response to the well documented decompaction of peripheral heterochromatin in HGPS cells (Goldman *et al.*, 2004; McCord *et al.*, 2013; Chandra *et al.*, 2015). Mechanistically, the loss of methylation in PMDs has been attributed to the absence of the H3K36me3 modification, which is recognized by DNMT3B's PWWP domain (Baubec *et al.*, 2015), and late replication timing in S-phase, leaving the methylation machinery with less time for the remethylation of the newly synthesized DNA strand (Aran *et al.*, 2011; Salhab *et al.*, 2018; Zhou *et al.*, 2018). Extending the above hypothesis, one would therefore expect a shift in replication timing and H3K36me3 enrichment for the loci found to be hypermethylated in HGPS cells. This seems unlikely given their conserved LAD nature. Alternatively, the relaxation of peripheral heterochromatin could render them more susceptible to the action of DNA methyltransferases in the nuclear periphery. Future experiments should therefore address the question whether these enzymes directly or indirectly interact with Lamin A or Progerin, and whether these dynamics are altered in progeria cells.

In comparison with the LAD subset discussed above, HGPS-exclusive LADs exhibited higher overall methylation levels and less pronounced HGPS-specific hypermethylation, as did those regions that lost their LAD identity in HGPS cells. From a DNA methylation perspective, both of these might therefore constitute intermediate states between the HMD-like, transcriptionally-active non-LAD regions and the more PMD-like, transcriptionally silent, conserved LADs. In other words, they could represent a fraction of more variable LAD contacts than the one overlapping between HGPS and control cells.

Altogether, although HGPS-specific differential DNA methylation and accessibility were both found to be enriched in LADs, they likely illustrate different facets of the HGPS-specific epigenome. Whereas the observed chromatin accessibility changes correlate well with alterations in the LAD landscape, the DNA methylation better define the epigenetic status of lamina-proximal DNA in HGPS fibroblasts. In combination, they underscore the pronounced deregulation of the peripheral epigenetic landscape in HGPS fibroblasts.

4.2. Additional epigenetic alterations define the progeroid nature of the HGPS epigenome

In addition to the spatial enrichment of epigenetic changes in lamina-associated parts of the genome, HGPS fibroblasts were characterized by a number of non-LAD-associated epigenetic alterations. Interestingly, these strongly suggest that the HGPS epigenome also bears characteristics, which would normally be associated with physiologically aged cells.

Most prominently, the ATAC-see experiment revealed that a significant number of HGPS nuclei are characterized by a noticeable decrease of chromatin compartmentalization. Critically, the observed loss of highly accessible regions, accompanied by an opening of previously inaccessible parts, is in agreement with previous studies showing a reduction of chromatin compartments in progeria fibroblasts based on Hi-C data (McCord *et al.*, 2013; Chandra *et al.*, 2015). Similar trends have been observed during replicative and oncogene-induced senescence (Chandra *et al.*, 2015; Criscione *et al.*, 2016), hence suggesting that some of the mechanisms contributing to this phenomenon are conserved.

Characteristics of a progeroid epigenome were also present at the level of DNA methylation. Specifically, one subgroup of HGPS fibroblasts revealed a dramatic DNA methylation age increase - an indication of an advanced biological age. As noted before, this age acceleration was not associated with the strength of Progerin expression, patient age, passage number or other parameters, thus leaving the question of the underlying mechanism unanswered. It is important to point out, that a similar age acceleration was observed in some control fibroblasts; specifically, those obtained from the Coriell biorepository. While simple biological variation may account for a portion of these observations, they might also be based on repository-related differences in cell culture and passaging procedures. To be more precise, although raw DNA methylation age estimates were corrected with a passage factor as previously suggested (Horvath *et al.*, 2018), distinctions in the number of cells seeded and harvested, for example, may still have added substantial bias, especially if aggravated over multiple passages. Support for this argument comes from the fact that samples obtained from the Coriell biorepository had significantly higher average passage numbers than those obtained from the PRF (data not shown). Validating the HGPS-specific age increases, however, the calculated data closely resemble recently reported DNA methylation age estimates for the same HGPS fibroblast samples (Horvath *et al.*, 2018). The minor deviations from the published data may, in turn, be attributable to differences in data preprocessing or the number of population doublings (Horvath *et al.*, 2018; McEwen *et al.*, 2018). Beyond that, HGPS fibroblasts have also been demonstrated to exhibit an age acceleration of 9-10 years at the transcriptomic level (Fleischer *et al.*, 2018), thus closely matching the median age difference (9.73 years) identified for the age-accelerated subset in this work.

Interestingly, a similar phenomenon has been noted in other progeroid syndromes. For example, Werner syndrome, a form of progeria with onset during adolescence (Salk, 1982), and Down syndrome, which is characterized by a number of premature aging symptoms (Devenny *et al.*, 2005; Patterson and Cabelof, 2012), are associated with average DNA methylation age

increases of 6.4 and 6.6 years, respectively (Horvath *et al.*, 2015; Maierhofer *et al.*, 2017). While the underlying age-related methylome alterations are likely to be conserved, it is interesting to see that HGPS, which is arguably characterized by the most severe progeroid phenotype as well as the shortest life expectancy of the three disorders (Yamamoto *et al.*, 2003; Coutinho *et al.*, 2009; Kazemi, Salehi and Kheirollahi, 2016), also exhibits the strongest age acceleration. Given that a DNA methylation age acceleration has been shown to be connected with increased mortality (Marioni *et al.*, 2015; Levine *et al.*, 2018), this appears plausible, even if only a subgroup of HGPS patients revealed this deviation. Emphasizing the importance of further research in this area, however, no apparent differences with regard to the severity, disease progression, or the age of death have been observed for HGPS patients to date (personal communication with PRF).

Based on the extent of epigenetic alterations in lamina-associated regions in HGPS fibroblasts, the question arises whether the epigenetic deregulation of LADs, including altered DNA methylation, contributes to the HGPS-specific acceleration of the epigenetic clock. Previous studies have shown that the majority CpG probes used in the DNA methylation age estimators are not overlapping with PMDs (Vandiver *et al.*, 2015; Zhou *et al.*, 2018). It is therefore hard to imagine that the HGPS-specific LAD deregulation is directly linked to the DNA methylation age acceleration of HGPS patients. Instead, it has been speculated that one of the contributing factors to an epigenetic age acceleration is increased epigenetic drift (Field *et al.*, 2018), i.e. the tendency of methylomes to diverge over time (Fraga *et al.*, 2005; Heyn *et al.*, 2012; Issa, 2014). During aging, these changes result in an erosion of DNA methylation patterns, which in young cells are characterized by sharply defined genomic regions with either high or low methylation (Zampieri *et al.*, 2015; Bormann *et al.*, 2016). Intriguingly, the HGPS methylome, especially of individuals with age acceleration, exhibited a decrease in spatial correlation of DNA methylation levels of neighboring CpGs, indicating that the distinct methylation patterning characteristic of young cells is diminished in progeria fibroblasts. Similar findings have been made in T-cells and keratinocytes from normal, but significantly older individuals (Heyn *et al.*, 2012; Bormann *et al.*, 2016), thus reinforcing the notion that the HGPS methylome carries characteristics of advanced biological age.

DNA methylation and chromatin regulation through the modification of histone tails are tightly interconnected (Robertson, 2002; Cedar and Bergman, 2009; Rose and Klose, 2014; Yan *et al.*, 2015). Targeting of DNA methylation, for example, is mechanistically linked to H3K9me3 through SUV39H1/HP1 (Fujita *et al.*, 2003; Fuks *et al.*, 2003) and the methylation of gene

bodies by DNMT3B is associated with intragenic H3K36me3 (Baubec *et al.*, 2015). The presence of H3K4me3 in promoters, on the other hand, is thought to block DNA methylation (Ooi *et al.*, 2007; Weber *et al.*, 2007). Given this broad cross-linkage, it is conceivable, that the progeroid DNA methylation patterns identified in this work are connected with the histone modification changes previously demonstrated for HGPS cells (Shumaker *et al.*, 2006; McCord *et al.*, 2013). In fact, the erosion of 'youthful' DNA methylation patterns is reminiscent of the loss of chromatin compartmentalization, observed in the ATAC-see experiment and in previous studies (McCord *et al.*, 2013; Chandra *et al.*, 2015). Evidence for such a connection comes from the observation that chromatin compartments can be directly predicted from DNA methylation data (Fortin and Hansen, 2015; Zhang *et al.*, 2017). However, to elucidate the specific interplay between the loss of heterochromatin markers and the erosion of DNA methylation patterns in progeria cells, future single-cell-based approaches combining the analysis of both layers are needed.

The gradual loss of DNA methylation from PMDs is a conserved characteristic of aging mammalian cells and tissues, which is aggravated in cancer cells (Lister *et al.*, 2009; Hansen *et al.*, 2011; Berman *et al.*, 2012; Vandiver *et al.*, 2015; Salhab *et al.*, 2018; Zhou *et al.*, 2018). As noted before, this loss has been attributed to a failure of the DNA methylation machinery to maintain methylation levels late during S-phase or in the absence of H3K36me3 (Zhou *et al.*, 2018). Consequently, the gradual decrease in median PMD methylation levels reflects the mitotic history of a cell or tissue. cSCC and AK cells, which were studied as part of a contribution to a different work, exhibited exactly this phenomenon. This is unsurprising, given the malignant nature of cSCC and the fact that AK displays other typical, cancer-related features including a decreased DNA methylation age and CpG island-associated hypermethylation (Rodríguez-Paredes *et al.*, 2018). Intriguingly, HGPS fibroblasts, on the other hand, were not characterized by PMD hypomethylation but instead revealed a hypermethylation of probes in these regions, which, as discussed above, likely reflects the reorganization of the LAD landscape in Progerin-expressing cells. This underscores a key distinction between the DNA methylome changes in HGPS cells and those occurring during aging and tumorigenesis.

Another characteristic hallmark of aging DNA methylomes is the hypermethylation of promoter-associated CpG islands (Heyn *et al.*, 2012; Zampieri *et al.*, 2015; Xie *et al.*, 2018). However, HGPS cells did not show any noticeable hypermethylation of promoter-associated CpG probes, as measured by the methylation of probes overlapping with promoter-enriched H3K4me3. In addition, DNA methylation and chromatin accessibility changes were

underrepresented in regions marked by the presence of H3K4me3. Hence, in contrast to the dynamics observed during physiological aging and tumorigenesis, the epigenetic reconfiguration of promoter-associated CpG-islands does not seem to represent a feature of the HGPS epigenome.

One of most fascinating questions behind this work was whether the epigenetic changes in HGPS resemble those observed during physiological aging. In summary, even though some characteristic features of aging methylomes were not detected in HGPS, there is clear evidence for the presence of an epigenomic signature associated with physiological aging. Despite the prominent nature of LAD-related alterations, which likely reflect the underlying remodeling of the LAD landscape, the HGPS epigenome also exhibits characteristics of cells from older individuals such as an increased DNA methylation age or the erosion of DNA methylation patterns.

4.3. Reorganization of the LAD landscape in HGPS

A question that arises when studying genomic and epigenomic alterations in HGPs cells, is how the expression of the mutant version of Lamin A affects the landscape of interactions between DNA and the nuclear lamina. Interestingly, while Lamin A-binding regions have been profiled in murine cardiac myocytes and embryonic fibroblasts expressing Progerin (Kubben *et al.*, 2012), these domains have never been characterized in human HGPS cells. A part of this work was therefore aimed at answering the question how the Lamin A LAD landscape is shaped in primary cells from HGPS patients.

Overall, the obtained LAD tracks were in good agreement with Lamin A and Lamin B LAD data from previous studies of human fibroblasts from skin (Lund *et al.*, 2015) or lung (Guelen *et al.*, 2008). Unexpectedly, the quantity and, to a lesser extent, the distribution of the Lamin A LADs identified herein more closely resembled that of previously profiled Lamin B LADs (Guelen *et al.*, 2008). From a technical perspective, this may simply represent a consequence of the methodological similarities to the work that identified Lamin B LADs, namely the Dam ID-seq method, whereas the data for Lamin A were produced using ChIP-seq (Lund *et al.*, 2015). Critically, the Dam ID method is based on the low-level expression of a fusion protein over a window of time (here: 48 hours), thus generating averaged binding profiles (van Steensel and Henikoff, 2000). The crosslinking-based ChIP-seq method, on the other hand, yields a picture of

temporary interactions, which likely reduces the number of consensus regions owing to the heterogeneity of cell-specific binding profiles (Kind *et al.*, 2013, 2015). From a biological perspective, there is evidence for a partial overlap of Lamin A and Lamin B LADs (Meuleman *et al.*, 2013; Kind and van Steensel, 2014; Gesson *et al.*, 2016; Forsberg *et al.*, 2019), as the two subtypes form separate, but interacting meshworks at the nuclear boundary (Shimi *et al.*, 2008, 2015; Turgay *et al.*, 2017). Taken together, the data obtained in this work likely constitute an accurate representation of the Lamin A LAD landscape in dermal fibroblasts.

Strikingly, HGPS cells exhibited a weak, but widespread loss of Lamin A enrichment that was present on almost all chromosomes. It is important to emphasize that this reduction does not represent the loss of real, bona-fide LADs but rather a decrease in the probability that a certain region is associated with Lamin A in a given cell. Nevertheless, the sheer extent of this effect raises the central question whether it represents true biological variation or a technical artifact. Arguing against methodological causes, both HGPS and control-specific Lamin A enrichments were normalized against their group-specific Dam-only background using an established read-count-based method (Marshall and Brand, 2015). Secondly, and more unambiguously, the losses in differential enrichment were not randomly distributed but exhibited biologically meaningful patterns, especially when viewed in combination with the independently obtained ATAC-seq data. For example, chromosome 18 was characterized by a widespread decrease of Lamin A-binding, which is in agreement with the relative concentration of chromatin accessibility changes on this chromosome, as well as its relocalization to the nuclear interior in HGPS fibroblasts (Meaburn *et al.*, 2007; Mehta *et al.*, 2011). In contrast, the gene-dense chromosomes 17 and 19, which in various cell types are located in the nuclear center and show little contact with the nuclear lamina (Boyle *et al.*, 2001; Mehta *et al.*, 2013; Kind *et al.*, 2015), exhibited more balanced differential enrichment signals. Together, these arguments strongly support the conclusion that the HGPS-specific Lamin A LAD patterns represent true biological alterations, rather than technical noise. Hence, the altered dynamics of lamina binding should be experimentally validated in HGPS cells, for example by FISH of candidate regions exhibiting the strongest disease-specific changes.

Assuming their validity, these data raise the intriguing question why such a large number of loci show reduced Lamin A-binding in Progerin-expressing cells. In mammals, peripheral heterochromatin is tethered to the nuclear envelope through a LBR- and a Lamin A/C-dependent mechanism (Yokochi *et al.*, 2009; Kind *et al.*, 2013; Solovei *et al.*, 2013). H3K9

methylation plays a critical role in this process, as depletion of the enzymes that catalyze these modifications relaxes or abolishes chromatin-lamina interactions (Pinheiro *et al.*, 2012; Bian *et al.*, 2013; Kind *et al.*, 2013; Harr *et al.*, 2015). Given that peripheral heterochromatin marks, including H3K9me3, are drastically diminished in HGPS fibroblasts (Goldman *et al.*, 2004; McCord *et al.*, 2013), this points towards the exciting possibility that the widespread decrease in Lamin A-binding is a consequence of the heterochromatin loss at the nuclear envelope. Support for such a conclusion comes from the observation that the decrease in Lamin A-binding largely overlapped with previously published LAD tracks, i.e., regions characterized by H3K9me2/3.

Another fascinating possibility is that diminished Lamin A-binding is, at least in part, compensated by the presence of Progerin in the nuclear envelope. In fact, in murine cardiac myocytes and embryonic fibroblasts expressing Progerin, the overwhelming majority of Lamin A-associated genes is bound by both proteins (Kubben *et al.*, 2012). One could therefore envision a scenario, in which Progerin competes with Lamin A for binding to a given genomic locus, thus diminishing the average Lamin A enrichment when analyzed in a large number of cells. A future Dam ID-seq experiment characterizing the Progerin LAD interactome should give better insight into this possibility.

Finally, the intranuclear fraction of Lamin A could also be involved in these changes. The nucleoplasmic fraction of Lamin A binds to euchromatic parts of the genome via LAP2alpha (Gesson *et al.*, 2016) but is diminished upon Progerin expression (Vidak *et al.*, 2015). Loss of interaction in these previously Lamin A-LAD-associated regions could therefore contribute to the reduced Lamin A-binding in HGPS cells.

Ultimately, it is important to keep in mind that, in comparison with control cells, HGPS fibroblasts were not characterized by a drastically decreased number of Lamin A-associated LADs, as detected through an established domain detection algorithm (Gatticchi *et al.*, 2019). This implies that, despite the striking trend towards decreased Lamin A-binding, the overall LAD structure is maintained in the population of patient fibroblasts.

The second major finding of the Dam ID-seq experiment is that pericentromeric and telomere-proximal regions show increased Lamin A-binding in HGPS fibroblasts. In somatic cells, telomeres are distributed throughout the nucleus and not preferentially located near the nuclear lamina (Crabbe *et al.*, 2012; Wood *et al.*, 2014; Moye *et al.*, 2015); however, subtelomeric repeats have been associated with peripheral localization (Ottaviani *et al.*, 2009; Gonzalo and Eissenberg, 2016). Intriguingly, this seems to be facilitated by an interaction of Lamin A/C with the shelterin component ‘telomere repeat-binding factor 2’ (TRF2) (Wood *et al.*, 2014). In

contrast, TRF2 does not bind to Progerin, leading to destabilization and, ultimately, loss of telomeres in HGPS cells (Decker *et al.*, 2009; Wood *et al.*, 2014; Gonzalo and Eissenberg, 2016). Given the results obtained in this work, it would therefore be interesting to test whether the competitive presence of Progerin in HGPS cells enhances the association of telomeric regions with the remaining fraction of Lamin A, or whether other factors are responsible for the observed increase in Lamin A-binding.

One of such factors could be the heterochromatin mark H4K20me3. It is enriched in telomeric and pericentromeric heterochromatin (Schotta *et al.*, 2004; Gonzalo *et al.*, 2005), and has been shown to accumulate in late-passage HGPS fibroblasts (Shumaker *et al.*, 2006). No direct interaction between Lamin A/C and H4K20me3 is known to date, but pericentromeric regions show a preferential positioning at the nuclear periphery (Solovei *et al.*, 2004; Guelen *et al.*, 2008) and the histone modification has been found to be associated with the nuclear lamina through binding to LBR (Olins *et al.*, 2010). It is therefore conceivable, that the HGPS-specific increase in H4K20me3 at pericentromeric and telomeric regions drives a stronger interaction with the nuclear lamina and, by association, Lamin A in patient cells. Further complicating the situation, however, pericentromeric heterochromatin undergoes relaxation and transcriptional activation in HGPS fibroblasts (Shumaker *et al.*, 2006). Additional experiments will therefore be necessary to elucidate how these regions interact with the nuclear envelope in progerin-expressing cells.

Finally, it is important to emphasize that there are some limitations to the data obtained with the Dam ID-seq technique in this work. First, while three samples were averaged to create the control tracks, the HGPS data were generated from only two samples. Although they likely give a good general impression of the HGPS-associated changes, they are somewhat biased towards the genetic and epigenetic background of the two samples and do not allow a statistically robust analysis of the disease-specific differences. Moreover, they probably do not capture the full extent of disease-specific changes in the LAD architecture. A future analysis of the LAD interactome in HGPS should therefore include additional samples, as well as a validation of the observed alterations using independent methodology such as FISH.

Second, although well established for the mapping of DNA-nuclear envelope interactions (Guelen *et al.*, 2008; Kind and van Steensel, 2014; Amendola and van Steensel, 2015), the Dam ID technique relies on the expression of an artificial fusion protein and may thus have created a certain amount of artifacts in the data, i.e., false-positive or -negative Lamin A-binding

sites. At the same time, the relatively long expression window of 48 hours may have contributed to generating false-positive findings.

Third, the data obtained are specific to cultured dermal fibroblasts. As with the rest of the results obtained in this work, their scope is limited and should be confirmed in other cell types and primary tissues to better evaluate their role in the pathology of the disease.

Fourth, and most importantly, it is critical to remember that the LAD data generated herein represent population averages from a large number of cells. On the one hand, this ensures the comparability with other population-scale data produced in this work, but, on the other hand, it probably underestimates the extent of LAD alterations occurring in the highly heterogeneous HGPS fibroblast population. Assuming that the integration of Progerin obeys at least some degree of stochasticity, a significant number of alterations are likely being missed due to an averaging over the entire cell population. Future studies will allow the study of single-cell LAD interactomes, which, in combination with other single-cell data, will not only give a better overview of the extent of aberrations in HGPS cells but also allow a better understanding of how the nuclear envelope-chromatin interplay contributes to the pathology of the disease.

4.4. Epigenetic changes have a limited direct effect on gene expression

Aside from DNA methylation, chromatin accessibility and changes in the LAD landscape, alterations at the transcriptomic level were analyzed in this work. The obtained results highlight a substantial deregulation of gene expression in HGPS fibroblasts, including an enrichment of pathways associated with key pathological features as well as an aggravation in cells from older patients.

Gene expression in progeria fibroblasts has been profiled before (Ly *et al.*, 2000; Park *et al.*, 2001; Csoka *et al.*, 2004; Kubben *et al.*, 2016). Importantly, the data generated in this work were in good correlation with those of previous genome-scale expression studies, especially for more strongly deregulated genes. In addition, they confirmed the deregulation of developmental, morphological, ECM- and cardiovascular function-related processes, as well as the central role of the transcriptional regulators NRF2 and AP1 in the disease (Csoka *et al.*, 2004; Pereira *et al.*, 2008; Marji *et al.*, 2010; Kubben *et al.*, 2016). A comparison with a more recent study establishing a transcriptome-based age predictor using HGPS fibroblasts (Fleischer *et al.*, 2018) was not performed. However, the fact that an age increase of about 10 years was identified for

HGPS cells in the same study (Fleischer *et al.*, 2018), which closely matches the DNA methylation-based age acceleration identified herein (9.73 years), suggests a good overlap with that work, as well.

One key benefit of the expansive sample set available for the present study is that gene expression profiles from HGPS samples of different age groups could be analyzed. In general, the finding that fibroblasts from older patients show an enrichment of pathology-related features is expected, as symptoms progressively worsen with advanced patient age (Merideth *et al.*, 2008). For instance, HGPS patients are affected by alopecia and severe skin abnormalities including changes in pigmentation, skin dimpling, loss of subcutaneous fat and the development of sclerotic skin (Merideth *et al.*, 2008; Rork *et al.*, 2014). The observed deregulation of core dermal fibroblast functions, such as ECM maintenance and collagen production (Sorrell and Caplan, 2004), is therefore unsurprising and may actually contribute to the skin phenotype in HGPS patients. More intriguing is the observation that HGPS fibroblasts show a deregulation of genes involved in cardiovascular development, i.e., a function not classically associated with dermal fibroblasts. Crucially, the differential expression of these genes was found to be correlated with differences in Lamin A-binding, thus offering a potential mechanistic explanation for the activation of lineage-unspecific genes, which may be conserved in other cell types.

In this respect, one of the central findings of this work is that an activation of non-dermal fibroblast-specific genes, through the redistribution of the LAD landscape in Progerin-expressing cells, contributes to the HGPS-related transcriptome changes. Conceptually, this conclusion confirms the central role that Lamin A mutations play in the reconfiguration of the LAD and chromatin layers in laminopathies (Briand and Collas, 2018). In fact, a similar mechanism, including an induction of lineage-unspecific genes, has recently been described for fibroblasts carrying a *LMNA* mutation that causes Emery-Dreifuss muscular dystrophy (Perovanovic *et al.*, 2016). Additionally, mutations in the *LMNA* gene lead to a drastic redistribution of the LAD landscape and accompanying gene expression changes in cardiac myocytes from dilated cardiomyopathy patients (Cheedipudi *et al.*, 2019). Given this evidence, it is tempting to speculate that the same mechanism may also contribute to the severe pathology affecting other Progerin-expressing cell types such as VSMCs and endothelial cells. In this respect, it has to be noted, however, that Progerin expression in endothelial cells has recently been reported to cause cardiovascular pathology more directly through an impaired mechanoresponse (Osmanagic-Myers *et al.*, 2018). In this work, the authors showed that Progerin-induced changes in mechanosignaling at the nuclear envelope contribute to excessive fibrosis and the cardiovascular pathology of HGPS mice. Although both explanations are not mutually exclusive,

future experiments with primary, non-fibroblast cell populations and HGPS *in vivo* models will be necessary to better define the role of these mechanisms in the disease.

Interestingly, the gene expression changes were only partially reflected by alterations at the chromatin accessibility and DNA methylation level in HGPS fibroblasts. In other words, the limited number of differentially expressed genes with simultaneous HGPS-specific differences in DNA methylation or chromatin accessibility appears surprising. A number of technical and biological factors may have contributed to this.

From a technical perspective, simple biological variation may have limited the effect size, as a relatively small number of samples was used for the analyses, with some HGPS samples not overlapping between different experiments. Likewise, many of the fibroblast samples were obtained from different sites of the body. Given that fibroblasts are a highly heterogeneous cell type (Sorrell and Caplan, 2004; Driskell and Watt, 2015), lineage-specific differences between the fibroblast populations may thus have hindered the detection of further HGPS-related epigenetic alterations.

From a biological perspective, the extensive population heterogeneity of HGPS cells may have had a strong impact on the observed effect size. More precisely, the ATAC-see and Lamin A/C immunofluorescence experiments revealed high degrees of cell-to-cell variation regarding nuclear malformation and chromatin accessibility in the fibroblasts. This probably limited the number of regions identified as significantly differentially accessible, which represent a consensus shared by a certain number of Progerin-expressing cells in the population. Future single-cell-based studies utilizing single-cell ATAC-seq, single-cell RNA-seq and combinatorial methods will allow us to better capture the scope of epigenetic alterations in HGPS cells and their effect on individual transcriptomes.

Another potential explanation for the relatively small effect size comes from the fact that LADs are generally gene-poor (Guelen *et al.*, 2008; van Steensel and Belmont, 2017). An accumulation of epigenetic changes in these regions may hence have little direct impact on the gene expression patterns in affected cells. But, as LADs function in the 3D organization of the genome, changes in the peripheral architecture can have consequences deep inside the nuclear interior. For example, Zheng and colleagues recently demonstrated that a knockout of all lamins in mouse embryonic stem cells leads to global transcriptional alterations not restricted to genes in LADs (Zheng *et al.*, 2018). Mechanistically, such changes can be catalyzed through altered interactions between topologically-associated chromatin domains (Zheng *et al.*, 2018) or

the release of sequestered enhancers from the nuclear lamina (Robson *et al.*, 2017), both of which were not investigated in this work.

Alternatively, the epigenetic reconfiguration of the nuclear periphery may be accompanied by an altered binding of transcription factors in these regions. The finding that binding sites of AP1 family members were highly enriched in both differentially accessible and differentially methylated regions, for instance, indicates that a special role may belong to this transcription factor family in HGPS fibroblasts. Supporting such a hypothesis, c-Fos, a member of the AP1 family, has been reported to be negatively regulated by binding to Lamin A/C at the nuclear lamina (Ivorra *et al.*, 2006). The epigenetic deregulation of the underlying binding sites may therefore explain, why AP1 target genes revealed an enrichment pattern among the HGPS-specific differentially expressed genes. Consistently, *IGFBP7* and *EDIL3*, both characterized by differential accessibility and differential expression in the disease, contain consensus binding sites for AP1 family members in their respective promoter (Wajapeyee *et al.*, 2008) or enhancer (Fishilevich *et al.*, 2017).

Another transcription factor appears to drive the HGPS-specific gene expression changes through an altered interaction with the nuclear lamina. By binding more strongly to Progerin at the nuclear rim, NRF2, a transcriptional activator of antioxidant genes (Lewis *et al.*, 2010; Ma, 2013), is sequestered away from its transcriptional targets in the nuclear interior, thus limiting the oxidative stress response in HGPS cells (Kubben *et al.*, 2016). Confirming its crucial role in the disease, the transcription factor was identified in the present work as the central driver behind the transcriptional changes of patient fibroblasts. Furthermore, NRF2 TFBSs were also enriched among the most differentially accessible regions. Together, these points underpin the conclusion that the disease-specific epigenetic deregulation of LADs affects the HGPS transcriptome at a much larger scale than the limited direct effect on gene expression might suggest.

4.5. FTI treatment does not reverse epigenetic deregulation of LADs

The farnesyltransferase inhibitor Lonafarnib is currently the only treatment option with life-extending benefits for HGPS patients (Gordon *et al.*, 2014). At the molecular level, the drug has been shown to ameliorate the characteristic nuclear phenotype by blocking Progerin farnesylation and activating autophagy (Capell *et al.*, 2005; Young *et al.*, 2013; Gabriel *et al.*, 2017). This supported the rationale that Lonafarnib treatment may reduce the epigenetic alterations observed in patient cells. Unexpectedly, the treatment regimen utilized in this work

did neither abolish the HGPS-related hypermethylation of LAD probes, nor normalize the expression patterns of a selected set of genes. The absence of an effect on these layers is surprising, as the drug proved effective in reducing Progerin protein levels and improving the characteristic nuclear phenotype. Furthermore, it raises the question why the treatment might have failed and whether alternative strategies could be used to mitigate the HGPS-specific epigenetic deregulation of LADs.

To maintain adequate growth of the HGPS and control cells, a relatively low concentration of Lonafarnib was used in this work. Previous studies were based on treatments with significantly higher concentrations of FTIs (Capell *et al.*, 2005; Marji *et al.*, 2010; Gabriel *et al.*, 2017). It is therefore theoretically possible, that higher concentrations of the drug are necessary to elicit a noticeable improvement of the studied parameters in HGPS fibroblasts. As the treatment was performed over a relatively long time period and proved effective in ameliorating nuclear lobulation, however, a strong improvement with higher FTI concentrations appears questionable.

Instead, it is plausible that the epigenetic changes are independent of the nuclear phenotype in individual cells. In support of this, loss of the heterochromatin markers H3K27me3, H3K9me3 and HP1 has been shown to precede the occurrence of nuclear malformation in patient fibroblasts (Shumaker *et al.*, 2006). It is thus conceivable that the epigenetic deregulation of LADs is elicited by minor levels of Progerin and likewise arises before detectable changes in the nuclear architecture. Testing such a time- and / or dosage-dependency will require further experiments, including the temporary expression of Progerin in non-HGPS cells or the titration of different Progerin levels using inducible constructs.

To circumvent the epigenetic deregulation of LADs and its potential downstream consequences, an efficient treatment approach should consequently be centered around limiting the expression of mutant Lamin A. While reducing ∆150 *LMNA* mRNA levels using lentivirally delivered short-hairpin RNAs (shRNAs) has proven effective in restoring proliferative capacities in HGPS fibroblasts *in vitro* (Huang *et al.*, 2005), significant advances in blocking Progerin expression *in vivo* will likely have to be based on the systemic application of gene editing techniques such as CRISPR/Cas9. Intriguingly, two recent studies in mice demonstrated that a single-dose administration of CRISPR/Cas9 components targeting Lamin A / Progerin is effective in improving some HGPS phenotypes, including weight loss, mobility and both median and maximum survival (Beyret *et al.*, 2019; Santiago-Fernández *et al.*, 2019). These studies provide an early impression of the direction the treatment of HGPS is going to take in the near future.

4.6. A novel layer for the understanding of HGPS disease mechanisms

In summary, the results obtained in this work establish the epigenetic deregulation of LADs as a previously unrecognized characteristic of the HGPS epigenome and add a novel layer to our understanding of the disease's molecular pathology. Based on the integration of different epigenomic approaches and gene expression profiling, they indicate that disease-related changes in the LAD architecture, accompanied by alterations in DNA methylation and chromatin accessibility, contribute to the pathological transcriptomic signature observed in patient fibroblasts. Illustrating the crucial role of the nuclear lamina in transcriptional regulation, these findings thus demonstrate that a disease mechanism, which has been observed in cells from other laminopathies before (Perovanovic *et al.*, 2016; Cheedipudi *et al.*, 2019), is also involved in the molecular pathology of HGPS. While requiring additional experimental verification, this mechanistic insight represents an attractive starting point for future studies of the effect that the presence of Progerin exerts on the global LAD structure, and thus, the HGPS transcriptome. If experimentally validated and confirmed in other cell types typically affected in HGPS patients, it will help close a significant gap in our understanding of the molecular foundation underlying the disease.

At the same time, these results raise a number of intriguing mechanistic and translational questions, the answers to which should help to better define the importance of HGPS-related epigenomic alterations in the future. Some of these, including the question of the mechanism behind the disease-specific PMD hypermethylation or the interconnection with previously observed histone modification changes, have already been discussed herein and will accordingly require further experimental efforts. Others, however, constitute more conceptual questions that have not been touched upon hitherto.

One of such questions, for example, is whether some parts of the LAD landscape are more vulnerable to epigenetic deregulation upon Progerin expression than others. Assuming that the accumulation of the mutant protein at the nuclear envelope obeys a somewhat stochastic pattern - an interesting question in and of itself - one would theoretically expect different LAD stretches to become deregulated in different cells. Crucially, the population-scale analyses performed in this work demonstrate that a number of loci are preferentially affected in HGPS fibroblasts and it will be interesting to discover the underlying mechanisms. In conjunction with

this, the question arises whether the relationship between the cellular quantity of Progerin and the occurrence of LAD alterations is linear and / or whether a certain threshold concentration of the mutant protein precedes the appearance of changes in the LAD structure. In the case of the latter, one would expect a sufficiently large reduction of Progerin levels below this threshold to normalize gene expression patterns in individual cells. Closely related is the question whether the observed changes in the LAD landscape are reversible, i.e., whether a reduction of Progerin levels would restore a normal LAD architecture, thereby allowing a mitigation of the pathological gene expression. While this was not tested after FTI-treatment in this work, it generally appears plausible and could be examined using Progerin knock-down/-out cells or constructs for the inducible expression of the mutant protein.

Regarding the DNA methylation dynamics observed in HGPS cells in the present study, it is surprising to see that they culminate in an epigenetic age acceleration for only a subset of patients. Although the obtained data represent a good starting point for a more thorough characterization of the two subgroups at the level of DNA methylation, a conclusive answer to this question may also involve genetic factors and will therefore require additional studies. These will also be beneficial for finding out whether the observed alterations ultimately result in differences in survival between the two subgroups.

Finally, one of the most fascinating questions with respect to the results obtained in this study is whether the epigenetic deregulation of LADs as identified in HGPS cells could also play a role in healthy aging. Such a possibility is not inconceivable, given that Progerin is expressed in healthy cells and that HGPS-related phenotypic alterations including those in the cardiovascular system resemble the ones observed in aged, unaffected individuals (McClintock *et al.*, 2007; Scaffidi and Misteli, 2006; Olive *et al.*, 2010). The available evidence for an involvement of this mechanism in physiological aging is further discussed in section 4.7.

The process of finding answers to some of the questions raised above will profit substantially from the establishment of single-cell analysis technologies in the near future. As highlighted throughout this work, the heterogeneity of individual cells in the fibroblast samples represented a key limitation of the population-based analyses performed as part of this study. Enabling the deciphering of individual changes in such highly heterogeneous populations, single-cell-based profiling methods therefore have the potential to tremendously advance our understanding of HGPS-specific mechanisms of disease.

As noted before, single-cell Dam ID-seq has already been employed successfully (Kind *et al.*, 2015). In addition, the establishment of single-cell ATAC-seq and single-cell-based DNA

methylation sequencing techniques such as single-cell bisulfite sequencing (Clark *et al.*, 2017) or single-nucleus methylcytosine sequencing (Luo *et al.*, 2017) will significantly aid in capturing the extent and nature of epigenetic alterations in the disease. Single-cell RNA-seq of primary patient cells, on the other hand, will provide further valuable information about the deterioration of gene expression patterns in cells from older patients and allow the identification of disease-specific subpopulations. Most excitingly, by connecting multiple of these layers, combinatorial approaches including the recently developed single-cell nucleosome, methylation and transcription sequencing (Clark *et al.*, 2018) will eventually permit a coherent analysis and correlation of these aberrations in individual cells.

4.7. A framework for the study of physiological aging

Progerin expression is not a feature that is exclusive to HGPS patients. Instead, as results of this work have shown, it can be detected based on the presence of the ∆150 *LMNA* in normal dermal fibroblasts, and, as others have demonstrated, at the protein level in skin biopsies from aged unaffected individuals (McClintock *et al.*, 2007). At the same time, some of the disease-specific features including the characteristic nuclear malformation, the loss of heterochromatin markers and aspects of the cardiovascular pathology also manifest as consequences of the normal aging process (Scaffidi and Misteli, 2006; Olive *et al.*, 2010). Given these analogies, it is conceivable that some of the mechanisms discovered herein play a role during physiological aging, as well.

Surprisingly little is known about the nature of changes in the LAD landscape in the context of healthy aging. Aging *Drosophila* fat bodies exhibit a loss of heterochromatin and derepression of LAD-located immune response genes as a consequence of an age-related reduction in Lamin levels (Chen, Zheng and Zheng, 2014), but data for mammalian cells is scarce. Senescent human fibroblasts and keratinocytes have been demonstrated to experience a drastic rearrangement of chromatin and a downregulation of Lamin B1 (Dreesen *et al.*, 2013; Shah *et al.*, 2013; Chandra *et al.*, 2015) but these changes may be consequential, not causative (Dreesen *et al.*, 2013). Additionally, while cellular senescence represents one outcome of the aging process in individual cells and may even contribute to it at the tissue level (Collado, Blasco and Serrano, 2007; Childs *et al.*, 2015; McHugh and Gil, 2018), it does not represent the aging process *per se*. In other words, studies with healthy, aged and non-senescent cells are needed to better decipher the importance of alterations in the LAD landscape during aging.

In the absence of such data, surrogate readouts may provide further insight into the functional role of LAD changes in the aging process. For example, an increasing transcriptomic disorder is a key characteristic of aging cells (Sen *et al.*, 2016). Given the role of the nuclear lamina in transcriptional regulation, it is conceivable that a deregulation of LADs due to structural changes at the nuclear lamina or dysfunctional heterochromatin maintenance at least partially contributes to the transcriptional noise observed in aging cells. Such a framework would predict the derepression of lineage-unspecific genes in aged cells, evidence of which exists for certain cell types. A loss of functional identity related to transcriptional changes has, for instance, been reported in aging neurons (Dönertaş *et al.*, 2017), and in both human and murine dermal fibroblasts (Salzer *et al.*, 2018; Solé-Boldo *et al.*, 2019). In the latter, advanced age results in a decrease of the expression of genes involved in ECM homeostasis and a simultaneous increase in pro-adipogenic traits (Salzer *et al.*, 2018). Whether and how alterations in the LAD interactome contribute to these changes, has yet to be defined, but it is plausible that they are part of the derepression of lineage-unspecific genes in affected cells.

Hence, while data on the presence of progeria-specific LAD dynamics are still limited, anecdotal evidence suggests that they might have a role during physiological aging, as well. A better understanding of these changes in laminopathies and the subsequent development of effective intervention strategies may therefore also advance the management of complications arising as consequences of a healthy aging process.

5. Conclusion

In this work, an integrated analysis of alterations in chromatin accessibility, DNA methylation, LAD interactome and gene expression was performed using primary dermal fibroblasts from HGPS patients. Its central finding is that both DNA methylation and chromatin accessibility changes are enriched in regions associated with the nuclear lamina in progeria cells, which establishes the epigenetic deregulation of LADs as a novel characteristic of the HGPS epigenome. Crucially, these dynamics are not only related to structural alterations in the landscape of nuclear lamina contacts but also contribute to the pathological gene expression signature observed in patient fibroblasts. Altogether, these data expand the study of cellular changes in the progeroid syndrome by a novel layer and significantly advance our understanding of the disease's molecular basis.

6. Materials and Methods

6.1. Materials

6.1.1. Chemicals, reagents and enzymes

Table 1: Chemicals, reagents and enzymes used in this work. Misc. = miscellaneous, Prep = preparation.

Name	Experiment/Purpose	Source	Reference #
ABsolute qPCR SYBR Green Mix	qRT-PCR	Thermo	AB1159A
Acetic Acid	Misc.	Merck	100063
Advantage cDNA polymerase mix	Dam ID-seq Library Prep	Clontech	639105
Ampicillin	Molecular Cloning	Sigma-Aldrich	A1593
Boric Acid	TBE Buffer	Sigma-Aldrich	B0394
Chitin Resin	ATAC-see	NEB	S6651s
Chloroform	RNA Extraction	VWR Chemicals	22711.260
Coomassie Blue	WB	SERVA	35081.01
ddH_2O	Misc.	Invitrogen	10977-035
Dextran Sulfate	FISH	G Biosciences	RC-043
DpnI	Dam ID-seq Library Prep	NEB	R0176S
DpnII	Dam ID-seq Library Prep	NEB	R0543S
DTT	ATAC-see	Sigma-Aldrich	10197777001
EcoRI	Cloning/Dam ID-seq	NEB	R0101S
EDTA	Misc.	Gerbu	#1034
Ethanol	Misc.	Fisher Scientific	E/0650DF/C17
Formamide	FISH	Merck	109684
Gateway LR Clonase II Enzyme Mix	Dam ID-seq Gateway Cloning	Invitrogen	11791-020
Genomic DNA Reagents	Library Preparation	Agilent	5067-5366
Glycerol	Misc.	Sigma-Aldrich	15523
HCl	pH Adjustment	Sigma-Aldrich	30721
HF buffer 5x (Phusion)	PCR	NEB	M0530

Name	Experiment/Purpose	Source	Reference #
Human Cot-1 DNA	FISH	Invitrogen	15279011
HyperLadder 1kb	DNA Gel Marker	Bioline	BIO-33053
HyperLadder 50bp	DNA Gel Marker	Bioline	BIO-33054
IGEPAL CA-630	Misc.	Sigma-Aldrich	13021
IPTG	ATAC-see	Sigma-Aldrich	I6758
Isopropanol	Misc.	Fisher Scientific	P/7500/PC17
KCl	Misc.	Roth	6781.1
Laemmli Pre-Mix	WB/Sample Loading	BioRad	161-0747
MESA GREEN qPCR MasterMix Plus	qRT-PCR	Eurogentec	RT-SY2X-03+NRWOU
Methanol	FISH	Fisher Scientific	M/4000/PC17
$MgCl_2$	Misc.	Sigma-Aldrich	M8266
Na_2HPO_4	FISH	neoLab	4820.1000
NaCl	Misc.	Sigma-Aldrich	31434
Na Citrate	FISH	Fluka	71405
NaH_2PO_4	FISH	AppliChem	A1939.1000
NaOH	pH Adjustment	Fluka	35256
Paraformaldehyde	Cell Fixation	Roth	0335.3
PBS 1x	Misc.	Gibco	10010023
PEI 10 %	ATAC-see	Sigma-Aldrich	P3143
Phusion Polymerase	PCR	NEB	M0530
Ponceau Staining	WB	Sigma-Aldrich	P7170
Propidium Iodide	PI staining	Sigma-Aldrich	P4170
Proteinase K	DNA Extraction	Qiagen	1019138
Protein Assay Dye Reagent Concentrate	Bradford Assay	BioRad	500-0006
RNase away	RNA extraction	Molecular BioProducts	7002
RNaseA	DNA Extraction	Sigma-Aldrich	R6513
SDS	Misc.	Roth	CN30.3
SEEBRIGHT Green 496 dUTP	FISH	Enzo	ENZ-42831

Name	Experiment/Purpose	Source	Reference #
SEEBRIGHT Red 580 dUTP	FISH	Enzo	ENZ-42844
Skim Milk Powder	WB	Gerbu	#1602.0500
Sodium Acetate	FISH	Roth	6773.2
Spectinomycin	Molecular Cloning	Sigma-Aldrich	S4014
Super Optimal Broth (S.O.C.) medium	Bacterial Transformations	Invitrogen	15544034
Taq polymerase FireTaq Blue + buffer	PCR	Steinbrenner	SL-FT blue-2500
Tris	Misc.	Sigma-Aldrich	T1503
Triton-X 100	Misc.	Gerbu	2999,0050
TRIzol	RNA extraction	Invitrogen	15596018
Tryptone/Peptone	LB Agar	Roth	8952.3
Tween 20	Misc.	Sigma-Aldrich	P1379
Vectashield with DAPI	FISH/Immunostainings	Vector Laboratories	H-1200
Western Lightning TM Plus-ECL Substrate	Chemiluminescence	Perkin Elmer	NEL103001EA
Yeast Extract	LB Agar	Fluka	70161
β-Mercaptoethanol	WB/Sample Loading	Sigma-Aldrich	M7154

6.1.2. Consumables

Table 2: Consumables used in this work. Misc. = miscellaneous, WB = Western Blot.

Name	Experiment used in	Source	Reference #
0.45 μm Minisart Cellulose Acetate Filter	Viral Transduction	Sartorius	16555
Amicon Ultra-15 Filters 30K	ATAC-see	Milipore	UFC903024
Cell Culture Dish 100/20 mm	Cell Culture	Greiner Bio-One	664160
Cell Culture Flask 250 ml, 75 cm^2	Cell Culture	Greiner Bio-One	658175
Cell Culture Flask 50 ml, 25 cm^2	Cell Culture	Greiner Bio-One	690175
Cell Culture Multiwell Plate, 6 Well	Cell Culture	Greiner Bio-One	657160
Covaris MicroTUBEs	Dam ID-seq	Covaris	PN 520045
Cover Slips	ATAC-see / FISH/ Immunofluorescence	Thermo	004711180

Name	Experiment used in	Source	Reference #
Cryotube Vials	Cryopreservation	Thermo	377267
Microcentrifuge Tubes 1.5 ml	Misc.	Sarstedt	72690
Microcentrifuge Tubes 2 ml	Misc.	Sarstedt	72691
Genomic DNA ScreenTape	Library Preparation	Agilent	5067-5365
Glass Slides	ATAC-see / FISH/ Immunofluorescence	Thermo	J2800AMNZ
Mini-PROTEAN TGX Precast protein gels	SDS-PAGE	BioRad	4561024/44
Needles Agani	Protein Extraction	Terumo	160825
Parafilm	Misc.	Bemis	PM-996
PCR Plate, 96 Well	Misc.	Thermo	AB0600
PCR Plate, 384 Well	Misc.	4titude	4ti-0382
PD10 Columns	ATAC-see	GE	17-0435-01
Slide-A-Lyzer Dialysis Cassettes	ATAC-see	Thermo	66380
Syringes	Protein Extraction	SOFT-JECT	5010.200V0
Syringes Terumo 10 ml	Viral Transduction	Th. Geyer	6088211
Trans-Blot Turbo Transfer Mini/Midi Nitrocellulose Membranes	SDS-PAGE / WB	BioRad	1704158/59
Tube, 0.2 ml	Misc.	Thermo	AB0620
Tube, 15 ml	Misc.	Greiner Bio-One	188271
Tube, 50 ml	Misc.	Greiner Bio-One	227261
Tube, FACS	PI staining	Falcon	352059

6.1.3. Equipment and devices

Table 3: Equipment and devices used in this work. Misc. = miscellaneous.

Name	Experiment used in	Manufacturer	Model
Balance	Misc.	AND / Sartorius	EK-200i / CP64
Cell Culture Hood	Cell Culture	Thermo	Herasafe KS
Centrifuge	Misc.	Eppendorf	5804R, 5415D, 5424R, 5804
Chemiluminescence	WB	Intas	ECL ChemoStar

Name	Experiment used in	Manufacturer	Model
Imager			
CO_2 Incubator	Cell Culture	Sanyo	MCO-20AIC
Confocal Microscope	FISH/ ATAC-see / Immunostainings	Olympus	FluoView FV1000
Flow Cytometer	PI staining	BD Biosciences	BD FACSCanto II
Gel Imager	Misc.	Syngene	U:Genius 3
Incubator	Misc.	New Brunswick Scientific	Innova 4200
Microcentrifuge Tube Centrifuge	Misc.	neoLab	3-1810
Microcentrifuge Tube Vortexer	Misc.	IKA	MS3
Microscope	Cell Culture	Zeiss	Axiovert A1 & Axiovert 40 CFL
Microscope + Camera	FISH/ ATAC-see / Immunostainings	Zeiss	Axioskop 2 Plus + MRc AxioCam
Nanodrop	Misc.	Thermo	Nanodrop 2000
pH Meter	Misc.	Hanna Instruments	HI2211
Photometer	SDS-PAGE	Eppendorf	BioPhotometer
Power Source	Electrophoresis	Consort	EV265
Qubit Fluorometer	Misc.	Invitrogen	3.0
Shaker	Misc.	Heidolph	Unimax 1010
Sonicator	ATAC-see	Branson	450
TapeStation	Misc.	Agilent	2200
Thermocycler	PCR	MJ Research / Biometra	PTC-200 / T3000
Thermocycler	qRT-PCR	Roche	LightCycler 480 Instrument II
Thermomixer	Misc.	Eppendorf	Thermomixer compact
Trans-Blot Turbo Transfer System	WB	BioRad	#1704150
Ultrasonicator	Dam ID-seq	Covaris	M220
UV Illuminator	Misc.	Analytik Jena	FirstLight UV Illuminator
Vortexer	Misc.	neoLab	7-2020
Water Bath	FISH	Julabo	ME-12
Water Bath	Cell Culture	Julabo	TW-12

6.1.4. Kits

Table 4: Commercial kits used in this work.

Name	Experiment/Purpose	Source	Catalog #
HiSpeed Plasmid Midi	Midi Prep	Qiagen	12643
MinElute PCR Purification	ATAC-seq	Qiagen	28004
Nextera DNA Library Prep	ATAC-see/-seq	Illumina	15028212
Nick Translation DNA Labeling System 2.0	FISH	Enzo	ENZ-GEN111-0050
pCR™8/GW/TOPO®	Dam ID-seq	Invitrogen	K250020
QIAprep Spin Miniprep	Mini Prep	Qiagen	27106
QIAquick Gel Extraction	Gel Extraction	Qiagen	28706
QIAquick PCR Purification	PCR Purification	Qiagen	28104
RNA Clean & Concentrator-5	RNA Purification	Zymo Research	R1013
SuperScript III First-Strand Synthesis System	Reverse Transcription	Invitrogen	18080051

6.1.5. Buffers and solutions

Table 5: Buffers used in this work. * = For tagmentation, 2x TD buffer (Nextera, 15028212) from Illumina was used. g = grams.

Name	Experiment/Purpose	Composition	Comments
Carnoy's Fixative	FISH	Methanol : acetic acid = 3:1	
Dialysis Buffer	ATAC-see	100 mM HEPES-KOH pH 7.2, 0.2 M NaCl, 0.2 mM EDTA, 2 mM DTT, 0.2 % Triton-X 100, 20 % (v/v) glycerol	
HEGX	ATAC-see	20 mM HEPES-KOH, 0.8 M NaCl, 1 mM EDTA, 10 % (v/v) glycerol, 0.2 % (v/v) Triton-X 100	
HEPES-KOH	ATAC-see	for 1 M: 238 g HEPES in 1 l ddH_2O	adjusted to pH 7.2 with KOH pellets
Hybridization Buffer	FISH	10 % (w/v) dextran sulfate, 50 % (v/v) formamide, 2x	

Name	Experiment/Purpose	Composition	Comments
		SSC pH 7.0	
Loading Buffer 4x	WB	900 µl Laemmli pre-mix (BioRad), 100 µl β-mercaptoethanol	
Lysis Buffer	ATAC-see	10 mM TRIS-HCl pH 7.4, 10 mM NaCl, 3 mM $MgCl_2$, 0.01 % IGEPAL CA-630	
Lysis Buffer	ATAC-seq	10 mM TRIS-HCl pH 7.4, 10 mM NaCl, 3 mM $MgCl_2$, 0.1 % IGEPAL CA-630	
PBD Washing Buffer	FISH	0.1 M NaH_2PO_4, 0.1 M Na_2HPO_4, 0.1 % (v/v) IGEPAL CA-630	
PBT	Blocking (Immunostainings)	10 % (v/v) FBS in 1x PBS with 0.1 % (v/v) Tween 20	
PFA 3.8%	Cell Fixation	3.8 % (w/v) PFA in PBS	adjusted to pH 7.4 with NaCl/HCl
Pre-Lysis Buffer	Genomic DNA Extraction	10 mM Tris-HCl pH 8.0, 5 mM EDTA, 100 mM NaCl	adjusted to pH 8.0 with NaCl/HCl
Running Buffer	WB	25 mM Tris, 192 mM glycine, 0.1 % (w/v) SDS	
SSC 20x	FISH	175.3 g of NaCl, 88.2 g sodium citrate in 1 l ddH_2O	adjusted to pH 7.0
TAE 50x	Gel Electrophoresis	40 mM Tris, 2 mM EDTA, 20 mM acetic acid	adjusted to pH 8.5
Tagmentation buffer	ATAC-see	-	from Nextera kit*
TBE 5x	Gel Electrophoresis	54 g Tris, 27.5 g boric acid, 20 ml 0.5 M EDTA pH 8.0 in 1 l ddH_2O	
Triton X-100 0.3%	Cell Permeabilization	0.3 % (v/v) Triton X-100 in 1x PBS	
Urea Buffer	WB	8 M Urea, 10 mM Tris-HCl pH 8.0	
Washing Buffer I	FISH	0.4x SSC, 0.3 % (v/v) IGEPAL CA-630	
Washing Buffer II	FISH	2x SSC, 0.1 % (v/v) IGEPAL CA-630	

6.1.6. Vectors

Table 6: Vectors used in this work.

Vector	Experiment	Description	Source	ID
pLgw-EcoDam-V5	Dam ID-seq	Expression of Dam-only	Addgene	#59210
pLgw-EcoDam-V5-Lamin A	Dam ID-seq	Expression of Dam-Lamin A	*cloned*	-

Vector	Experiment	Description	Source	ID
pLgw-EcoDam-V5-RFC1	Dam ID-seq	Destination vector for *LMNA* cDNA; Expression of Dam-fusion protein	Addgene	#59209
pMD2.G	Viral Transductions	Expression of VSV-G envelope	Addgene	#12259
psPAX2	Viral Transductions	Expression of HIV-1 gag and pol	Addgene	#12260
pTXB1-Tn5	ATAC-see	Expression of hyperactive Tn5 transposase	Addgene	#60240

6.1.7. Antibodies

Table 7: Antibodies used in this work. * = for the detection of the Dam-V5-Lamin A fusion protein after transient transfection, the α-Lamin A antibody was used in a 1:200 dilution. IF = Immunofluorescence, HRP = Horseradish peroxidase.

Antibody	Experiment	Source	Species	Reference	Dilution
Alexa Fluor 488	IF	Invitrogen	goat	A11017	1:500
α-Lamin A	WB	Santa Cruz	mouse	sc7292	1:500*
α-ms HRP-coupled IgG	WB	Jackson ImmunoResearch	goat	115-035-003	1:10,000
α-V5	WB	Santa Cruz	mouse	sc58052	1:200

6.1.8. BACs

Table 8: Bacterial Artificial Chromosomes (BACs) used in this work. All BACs were obtained from the Children's Hospital Oakland Research Institute (CHORI) (Oakland, CA, USA).

BAC Name	Reference	Chromosome	Location
Chr5 control	RP11-82M24	5	telomere
EDIL3	RP11-845G7	5	*EDIL3* gene
IGFBP7	RP11-589G9	4	*IGFBP7* gene
KCNK1	RP11-349N15	1	*KCNK1* gene
RELN	RP11-57M15	7	*RELN* gene
SMAD9	RP11-354L15	13	*SMAD9* gene
SOX11	RP11-103F8	2	*SOX11* gene

6.1.9. Primers and Oligos

Table 9: Primers and oligos used in this work. For qPCR primers, the cDNA dilution (here: for a 0.05 μg/μl stock concentration) yielding a successful amplification is given in brackets. * = Phosphorothioate linkage. Seq. = sequencing. Amplif. = amplification.

Experiment	Name	Purpose	Sequence (5'→3')
ATAC-see	Tn5MErev	Transposome assembly	*CTGTCTCTTATACACATCT
	Tn5ME-ATTO595N-A	Transposome assembly	/ATTO590/TCGTCGGCAGCGTCAGATGTGTATAAGAGACAG
	Tn5ME-ATTO590N-B	Transposome assembly	/ATTO590/GTCTCGTGGGCTCGGAGATGTGTATAAGAGACAG
ATAC-seq	PCR Primer f	PCR	AATGATACGGCGACCACCGAGATCTACACTCGTCGGCAGCGTCAGATGTG
	PCR Primer r_TAAGGCGA	PCR	CAAGCAGAAGACGGCATACGAGATTCGCCTTAGTCTCGTGGGCTCGGAGATGT
	PCR Primer r_CGTACTAG	PCR	CAAGCAGAAGACGGCATACGAGATCTAGTACGGTCTCGTGGGCTCGGAGATGT
	PCR Primer r_AGGCAGAA	PCR	CAAGCAGAAGACGGCATACGAGATTTCTGCCTGTCTCGTGGGCTCGGAGATGT
DamID-seq	AdRt	dsAdR Adaptors	CTAATACGACTCACTATAGGGCAGCGTGGTCGCGGCCGAGGA
	AdRb	dsAdR Adaptors	TCCTCGGCCG
	DamID_PCR	PCR	GGTCGCGGCCGAGGATC
	F-Prog-CDS	Dam ID-seq Cloning	ATGGAGACCCCGTCCCAGC
	R-Prog-CDS	Dam ID-seq Cloning	TTACATGATGCTGCAGTTCTGG
Sanger Seq.	M13-RP		AACAGCTATGACCATG
	pCasper-hs		GCAACTACTGAAATCTGCCAAG
qRT-PCR	Prog_RTPCR_1f	*Δ150 LMNA* amplif. (1:5)	ACCCCGCTGAGTACAACC
	Prog_RTPCR_1r	*Δ150 LMNA* amplif. (1:5)	TGGCAGGTCCCAGATTACAT
	LMNA_RTPCR_2f	*LMNA* amplif. (1:5)	CTCCCCTGTGAGCACTAGAG
	LMNA_RTPCR_2r	*LMNA* amplif. (1:5)	TGCCATCTACCATAGCCTCAG
	EDIL3_RTPCR_1f	*EDIL3* amplif. (1:50)	CCCGAGGATTTAATGGGATT
	EDIL3_RTPCR_1r	*EDIL3* amplif. (1:50)	GTGGGCCTGAGCATTTGTAT
	IGFBP7_RTPCR_1f	*IGFBP7* amplif. (1:50)	AGCTGTGAGGTCATCGGAAT
	IGFBP7_RTPCR_1r	*IGFBP7* amplif. (1:50)	CAGCACCCAGCCAGTTACTT
	F2R_RTPCR_1f	*F2R* amplif. (1:5)	GCAGGCCAGAATCAAAAGCA

Experiment	Name	Purpose	Sequence (5'→3')
	F2R_RTPCR_1r	*F2R* amplif. (1:5)	CACAACGATGGCCATGATGT
	OLFM2_RTPCR_1f	*OLFM2* amplif. (1:5)	TCGCGACCTCCAGTATGTAC
	OLFM2_RTPCR_1r	*OLFM2* amplif. (1:5)	GCACCCATCTCCTCCTGAAT
	IL13RA2_RTPCR_2f	*IL13RA2* amplif. (1:5)	CTGTTCTTGGAAACCTGGCA
	IL13RA2_RTPCR_2r	*IL13RA2* amplif. (1:5)	CTGGCGGCAAAGGTTTAACT
	KCNS3_RTPCR_1f	*KCNS3* amplif. (1:5)	AAGGGCAGAGCTTCTTGGAT
	KCNS3_RTPCR_1r	*KCNS3* amplif. (1:5)	GAGGGTGCTTTGGTCAACAG
	POSTN_RTPCR_1f	*POSTN* amplif. (1:50)	CCCAAATGTCTGTGCCCTTC
	POSTN_RTPCR_1r	*POSTN* amplif. (1:50)	GGCAGCCTTTCATTCCTTCC
	NTN4_RTPCR_2f	*NTN4* amplif. (1:5)	CCAAAGTTCAGGAGCAGCTG
	NTN4_RTPCR_2r	*NTN4* amplif. (1:5)	CGGTCATTGTATAACGGGGC
	DPT_RTPCR_2f	*DPT* amplif. (1:5)	GACAATGGAACTACGCCTGC
	DPT_RTPCR_2r	*DPT* amplif. (1:5)	AGTAAAACTGCCACTCCCGA
	S1PR1_RTPCR_4f	*S1PR1* amplif. (1:5)	TGCGGGAAGGGAGTATGTTT
	S1PR1_RTPCR_4r	*S1PR1* amplif. (1:5)	TGCAGTTCCAGCCCATGATA
	DPP4_RTPCR_3f	*DPP4* amplif. (1:5)	CTCAGCTCAGTCACCAATGC
	DPP4_RTPCR_3r	*DPP4* amplif. (1:5)	TCTTCCAACCCAGCCAGTAG
	F-SRSF4-qRT-PCR	*SRSF4* amplif. (1:50)	TGCAGCTGGCAAGACCTAAA
	R-SRSF4-qRT-PCR	*SRSF4* amplif. (1:50)	TTTTTGCGTCCCTTGTGAGC
	F-TBP-qRT-PCR	*TBP* amplif. (1:50)	CCGGCTGTTTAACTTCGCTT
	R-TBP-qRT-PCR	*TBP* amplif. (1:50)	ACGCCAAGAAACAGTGATGC
	F-GAPDH-qRT-PCR	*GAPDH* amplif. (1:50)	CGACCACTTTGTCAAGCTCA
	R-GAPDH-qRT-PCR	*GAPDH* amplif. (1:50)	GGTGGTCCAGGGGTCTTACT

6.1.10. Cell lines and bacterial strains

Primary HGPS patient (HGADFN155, HGADFN271, HGADFN188, HGADFN164, HGADFN122, HGADFN178, HGADFN167, HGADFN169 and HGADFN143) and parental skin fibroblasts (HGMDFN090 and HGFDFN168) were obtained from the PRF Cell and Tissue Bank (Boston, MA, USA). Age-matched primary skin fibroblasts (GM05659, GM02036, GM01864 and GM00969) were obtained from the Coriell Cell Repository (Camden, NJ, USA). A detailed overview of the cells used for each experiment is given in Table 10. Table 11 contains an overview of the bacterial strains used in this work.

Table 10: Human cells used in this work. PRF = Progeria Research Foundation, CCR = Coriell Cell Repository, DKFZ = German Cancer Research Center, 1 = DNA methylation profiling, 2 = ATAC-see, 3 = ATAC-seq, 4 = RNAseq, 5 = Lonafarnib, rapamycin & metformin treatment, 6 = virus production; f = female, m = male, unspecif. = unspecified, post. = posterior.

Sample ID	Status	Gender	Age [years]	Tissue	Origin	Source	Experiments
HGADFN155	HGPS	f	1.17	skin	unspecif.	PRF	1,2,3,4,5
HGADFN271	HGPS	m	1.25	skin	leg	PRF	1,3
HGADFN188	HGPS	f	2.25	skin	arm	PRF	1,2,3,4,5
HGADFN164	HGPS	f	4.67	skin	unspecif.	PRF	1,4,5
HGADFN122	HGPS	f	5.00	skin	right forearm	PRF	1
HGADFN178	HGPS	f	6.92	skin	left forearm	PRF	1
HGADFN167	HGPS	m	8.42	skin	left post. lower trunk	PRF	1,3,4
HGADFN169	HGPS	m	8.50	skin	upper back of right arm	PRF	1,3,4
HGADFN143	HGPS	m	8.83	skin	unspecif.	PRF	1,3,4
GM05659	control	m	1.00	skin	chest	CCR	1,2,5
GM00969	control	f	2.00	skin	unspecif.	CCR	1,4
GM01864	control	m	11.00	skin	unspecif.	CCR	1
GM02036	control	f	11.00	skin	unspecif.	CCR	1
HGMDFN090	control	f	37.83	skin	unspecif.	PRF	1,3,4,5
HGFDFN168	control	m	40.42	skin	unspecif.	PRF	1,2,3,4,5
HEK293T	healthy	f	fetus	kidney	embryonic	DKFZ	6

Table 11: Bacterial strains used in this work.

Strain	Species	Name	Source	Reference #	Purpose
Stbl3	*E.coli*	One Shot Stbl3	Invitrogen	C737303	Dam ID-seq-related cloning, amplification of psPAX2 & pMD2.G
TOP10	*E.coli*	One Shot TOP10	Invitrogen	C404010	Dam ID-seq-related cloning
T7 Express	*E.coli*	T7 Express	NEB	C3013I	Hyperactive Tn5 production (ATAC-see)

6.1.11. Cell culture reagents

Table 12: Cell culture reagents used in this work. Pen/Strep = Penicillin/Streptomycin.

Name	Experiment/Purpose	Source	Catalog #
DMEM high glucose	Cell Culture	Gibco	41965-039
DMSO	Drug Treatment	Sigma-Aldrich	D2650
FBS	Cell Culture	Gibco	10500-064
Lipofectamine 2000	Transfection	Invitrogen	11668030
Lonafarnib	Drug Treatment	Cayman Chemical	11746
Metformin	Drug Treatment	Sigma-Aldrich	317240
Opti-MEM	Transfection	Gibco	31985070
PBS 1x	Cell Washing	Gibco	10010023
Pen/Strep 1 %	Cell Culture	Gibco	15140-122
Polybrene	Viral Transduction	Merck	TR-1003-G
Rapamycin	Drug Treatment	Enzo	BML-A275
Trypsin 0.25 %	Cell Detachment	Gibco	25200-056

6.1.12. Software

Table 13: Software used in this work. Misc. = miscellaneous. Apr. = April. * = Software version 3.5.2 was used for the bioinformatic analysis of Dam ID-seq data.

Name	Experiment/Purpose	Source	Version
AmiGO2	GO Analyses	www.geneontology.org	2.4/2.5

Name	Experiment/Purpose	Source	Version
Axiovision	Image Acquisition	Zeiss	4.9.1.0
Chromas	Sanger sequencing analysis	www.technelysium.com.au	2.4.4
Clustal Omega	Oligonucleotide Design (Sequence Alignment)	www.ebi.ac.uk/Tools/msa/clustalo	Web Version from 2016
Fiji/ImageJ	ATAC-see, FISH, IF	Wayne Rasband (NIH)	1.51g/k
FlowJo	PI staining	FlowJo	X 10.0.7
FluoView	Image Acquisition	Olympus	4.1.2.2
Genome Browser	Dam ID-seq	UCSC	hg19/Apr. 2019
GSEA	GSEA Analyses	Broad	3.0
HOMER	Motif Analyses	http://homer.ucsd.edu/homer/	4.1
Illustrator	Figure Creation	Adobe	17.0.0
LightCycler 480	qRT-PCR Experiments & Analysis	Roche	1.5.0
Office Professional Plus 2010	Misc.	Microsoft	14.0.7232.5000
Photoshop	Figure Processing	Adobe	2015.0.0
Primer3	Oligonucleotide Design	www.bioinfo.ut.ee/primer3/	4.1.0
Prism	Misc.	GraphPad	5.0
R	Bioinformatic Analyses	The R Foundation	3.3.1/3.5.2*
SnapGene Viewer	Cloning	www.snapgene.com	2.4.3
Zen	Image Acquisition	Zeiss	Blue 2011

6.2. Methods

6.2.1. Cell Culture

Cells were cultured in DMEM high glucose medium (Gibco, 41965-039) supplemented with 10 % fetal bovine serum (FBS) (Gibco, 10500-064) and 1 % penicillin/streptomycin (Gibco, 15140-122) under standard 37°C and 5% CO_2 conditions in a CO_2 incubator (Sanyo, MCO-20AIC).

Fibroblasts were passaged every other day or upon reaching 80-90 % confluence as follows: culture medium was removed and the cells were washed once in 1x PBS (Gibco, 10010023). Then, a small volume of Trypsin (for big flasks: 1 ml, for 10 cm plates: 1 ml, for small flasks: 0.5 ml, for six-well-plates: 2 drops / well) was added and the respective flask or plate was incubated at 37°C for 5-7 min. Subsequently, trypsinized cells were resuspended in an appropriate amount of fresh growth medium and split in 1:4-1:2 ratios (depending on growth behavior) to new flasks / plates.

For cryostorage, cells were trypsinized as described above, resuspended in 1.5 ml freezing medium (complete growth medium containing 10 % (v/v) DMSO) and transferred to cryotubes (Thermo, 377267). To ensure gentle cooling, cryotubes were isolated with several layers of paper tissue and stored at -80°C overnight. The next day, they were transferred to liquid nitrogen for long-term storage.

To start culture after long-term storage in liquid nitrogen, fibroblasts were allowed to slowly thaw at room temperature. They were then resuspended in 10 ml culture medium, gently pelleted (850 g for 5 min) and resuspended in complete growth medium, before being seeded to appropriate culture plates or flasks. The next day, the culture medium was exchanged and cells were cultured as outlined above.

In general, early-passage cells were used for all experiments (Progeria Research Foundation: 8-12 passages, Coriell: 9-15 passages); however, details about the cells used for each experiment and their passage numbers are given in the respective sections.

6.2.2. Lonafarnib treatment

Early-passage fibroblasts from three HGPS patients and three unaffected donors (HGADFN155: p10, HGADFN188: p10, HGADFN164: p11, HGFDFN168: p12, HGMDFN090: p11, GM05659: p15) were grown for 7 d in the presence of either DMSO (Sigma-Aldrich, D2650) or 0.06 μM Lonafarnib (Cayman Chemical, 11746). The latter is sufficient to block a fraction of prelamin A maturation and to increase autophagy in HGPS cells while minimizing toxicity (Gabriel *et al.*, 2017). Starting with ~250,000 cells per flask, HGPS and control

fibroblasts were cultured in triplets of T25 flasks (Greiner Bio-One, 690175) per condition under standard 37°C and 5 % CO_2 conditions with growth medium changes every other day, and harvested after 7 d for DNA, RNA and protein analyses. Simultaneously, fibroblasts from every cell line (starting number: ~250,000) were grown on glass cover slips (Thermo, 004711180) in six-well-plates (Greiner Bio-One, 657160), followed by Lamin A/C immunostainings after 7 d.

6.2.3. Extraction of genomic DNA

For the extraction of genomic DNA, cell pellets were washed once in 1x PBS (Gibco, 10010023), spun down (850g, 5 min, room temperature) and resuspended in 2.25 ml pre-lysis buffer (10 mM Tris-HCl pH 8.0, 5 mM EDTA, 100 mM NaCl, adjusted to pH 8.0) in 15 ml tubes (Greiner Bio-One, 188271). 0.25 ml SDS 10 %, 25 µl Proteinase K (10 mg/ml) (Qiagen, 1019138) and 2 µl RNase A (50 mg/ml) (Sigma-Aldrich, R6513) were added and the tubes were inverted several times and incubated at 37°C overnight. The next day, 1.25 ml 5 M NaCl were added. After shaking the mixture, the tubes were centrifuged at 5,000 g for 15 min at room temperature (if a correct separation of the phases was not achieved, this procedure was repeated in microcentrifuge tubes). In a new 15 ml tube, 2.8 ml isopropanol (Fisher Scientific, P/7500/PC17) were added to the supernatant. After gently inverting the tubes several times, DNA was pelleted at 5,000 g for 10 min at room temperature. Then the supernatant was removed and the DNA pellet was washed with 1 ml of 70 % (v/v) EtOH (Fisher Scientific, E/0650DF/C17). Finally, the DNA pellet was spun down as before, air-dried and resuspended in 50-100 µl ddH_2O (Invitrogen, 10977-035).

6.2.4. Propidium iodide (PI) staining

Trypsinized and PBS-washed cells ($1x10^5$ cells per sample) were resuspended in 0.5 ml 70 % (v/v) ethanol (pre-cooled to -20°C overnight) (Fisher Scientific, E/0650DF/C17) and fixed on ice for 1 h. Cells were then spun down for 2 min at 4,000 g and resuspended in 0.5 ml 1x PBS (Gibco, 10010023) containing 0.25 % (v/v) Triton X-100 (Gerbu, 2999,0050). After a 15 min incubation on ice, they were spun down as before and resuspended in 0.5 ml PBS containing 10 µg/ml RNase A (Sigma-Aldrich, R6513) and 20 µg/ml PI stock solution (Sigma-Aldrich, P4170). Subsequently, the solution was transferred to FACS tubes (Falcon, 352059) and incubated at room temperature in the dark for 30 min. Finally, cell fluorescence was assessed on a FACS Canto II (BD Biosciences) cytometer and analyzed using FlowJo (FlowJo) software.

6.2.5. Extraction of total RNA

Trypsinized and 1x PBS-washed cells were resuspended in 1 ml of TRIzol reagent (Invitrogen, 15596018) in 2 ml microcentrifuge tubes (Sarstedt, 72691). After addition of 200 µl chloroform (VWR Chemicals, 22711.260) per ml of TRIzol, samples were centrifuged at 13,000 g for 15 min at 4°C. The upper phase was then transferred to a new 1.5 ml tube (Sarstedt, 72690) and 500 µl of isopropanol (Fisher Scientific, P/7500/PC17) were added, followed by centrifugation for 10 min at 10,000 g (4°C). In the next step, the RNA pellets were washed with 70 % (v/v) ethanol (Fisher Scientific, E/0650DF/C17) in RNase-free ddH_2O (Invitrogen, 10977-035) and finally resuspended in 20-100 µl of RNase-free ddH_2O.

6.2.6. Reverse transcription

Isolated total RNA was quantified on a Nanodrop (Thermo) and cleaned using the RNA Clean & Concentrator-5 kit (Zymo Research, R1013) following the supplied manual. Subsequently, RNA was quantified again and 1-2 µg total RNA were reverse-transcribed with the SuperScript III First-Strand Synthesis System (Invitrogen, 18080051) applying the manufacturer's instructions, yielding 0.05-0.1 µg/µl cDNA stocks. Generated cDNA was stored at -20°C until use in downstream applications.

6.2.7. qPCR

6.2.7.1. Experimental procedures

After conversion of total RNA into cDNA as outlined above, cDNA samples were diluted 1:5-1:100 (depending on amount of RNA reverse-transcribed and gene-specific primers; see Table 9) and used as templates in a qPCR reaction with ABsolute qPCR SYBR Green Mix (Thermo, AB1159A) or MESA GREEN qPCR MasterMix Plus (Eurogentec, RT-SY2X-03+NRWOU) and gene-specific primers (see Table 9; tested for generation of a single amplicon prior to use) according to the manufacturer's instructions. The experiment was performed on a LightCycler 480 Instrument II (Roche) with the following reaction settings:

qPCR protocol:

Step 1:	95°C for 15 min	
Step 2:	95°C for 15 s	50 cycles
Step 3:	60°C for 40 s	
Step 4:	40°C for 10 min	

6.2.7.2. Relative quantification and calculation of standard errors

Results were then analyzed using the LightCycler 480 software (Roche). Specifically, C_T values from triplicate measurements were obtained from the software using the 'Abs Quant/2nd Derivative Max for All Samples' analysis option and utilized to determine a ΔC_T value by subtracting the average C_T of one of the reference genes (C_{Tr}) from the average C_T of the gene of interest (C_{Ti}):

$$\Delta C_T = \overline{C_{Ti}} - \overline{C_{Tr}}$$

with $\overline{C_{T_{i/r}}}$ equaling the average of a triplicate measurement. The expression value z of the gene of interest is then:

$$z = 2^{(-\Delta C_T)}$$

which was subsequently normalized to the average expression value in control samples (i.e., expression of the gene of interest in control samples was set to equal 1) as follows:

$$Rel.Expression = \frac{z_{sample}}{z_{control}}$$

Finally, the relative expression values from different reference genes were averaged. Standard errors were calculated using the standard deviation s of C_{Tr} and C_{Ti}, respectively, given by (here: x_i = individual C_T , $\bar{x}$ = $\overline{C_{T_{i/r}}}$):

$$s = \sqrt{\frac{1}{n-1} \cdot \sum_{i=1}^{n} (x_i - \bar{x})^2}$$

in order to calculate the error e of the expression value z utilizing Gaussian error propagation:

$$e\,(z) = \sqrt{(\frac{\partial z}{\partial C_{Tr}} \cdot s(C_{Tr}))^2 + (\frac{\partial z}{\partial C_{Ti}} \cdot s(C_{Ti}))^2}$$

6.2.8. Extraction of proteins

First, trypsinized and 1x PBS-washed cells were resuspended in an appropriate volume (100 – 300 µl) of urea buffer (8 M Urea, 10 mM Tris-HCl pH 8.0). The mixture was then repeatedly aspirated through a needle (Terumo, 160825) into a syringe (SOFT-JECT, 5010.200V0) to shear DNA. Subsequently, the extracts were transferred to a new 1.5 ml microcentrifuge tube (Sarstedt, 72690) and the amount of protein was determined by Bradford assay using Protein Assay Dye Reagent Concentrate (BioRad, 500-0006) and a Biophotometer (Eppendorf).

6.2.9. SDS-PAGE and Western Blotting

Protein samples were prepared by mixing the desired amount of protein (determined in Bradford assay) from the extracts with 4x Loading buffer and ddH_2O (Invitrogen, 10977-035), followed by 5 min incubation at 95°C on a thermomixer (Eppendorf). Samples were then loaded onto 7.5 % or 12 % Mini-PROTEAN TGX Precast protein gels (BioRad, 4561024/44), run for ~ 4 h at 100 V and blotted onto Trans Blot R TurboTM Mini Nitrocellulose membranes (Biorad, 1704158/59) using a Trans-Blot Turbo Transfer System (BioRad, 1704150) with the manufacturer's predefined 'Mixed MW' transfer protocol.

The membranes were then stained with Ponceau solution (Sigma-Aldrich, P7170) to verify successful protein transfer, blocked with 5 % (w/v) milk in PBT (0.1 % (v/v) Tween 20 in 1x PBS) for 1 h at room temperature, and incubated with primary antibody (see Table 7) overnight at 4°C. The next day, they were washed three times in PBT (10 min per wash) and incubated with secondary antibody (α-mouse HRP-coupled IgG (Jackson ImmunoResearch, 115-035-003) (1:10000) in 5 % milk in PBT) for 1 h at room temperature. Ultimately, they were washed another three times in PBT, incubated with Western Lightning TM Plus-ECL Substrate (Perkin

Elmer, NEL103001EA) according to the supplier's instructions and imaged on a chemiluminescence imager (Intas).

The quantification of individual bands was performed with Fiji/ImageJ (Schindelin *et al.*, 2012; Rueden *et al.*, 2017), followed by statistical testing (unpaired t-test) in Graphpad Prism (Graphpad Software).

6.2.10. Transformations

All bacterial transformations performed as part of the methods described in this work were carried out as follows (unless noted otherwise). 30 µl of chemically competent *E.coli* cells (see Table 11) were mixed with 50 ng of the vector of interest (e.g. after ligation) and chilled on ice for 5 min. Bacterial cells were then heat-shocked by incubation at 42°C for 2 min on a thermomixer (Eppendorf) and immediately placed on ice for 5 min. Then, 1 ml of Super Optimal Broth (S.O.C.) medium (Invitrogen, 15544034) was added and the mix was incubated at 37°C for 1 h (shaking on a thermomixer). After spinning down the transformed cells (6000 rpm, 1min) in a tabletop centrifuge (Eppendorf), 900 µl of S.O.C medium were removed and Lysogeny Broth (LB) agar plates containing 100 µg/ml ampicillin (Sigma-Aldrich, A1593) were inoculated with the remaining 100 µl of bacteria. Finally, the LB agar plates were incubated at 37°C overnight in an incubator (New Brunswick Scientific) and analyzed for colony growth the next day.

6.2.11. Transfections

For transient transfections, fibroblasts were grown to 70-80 % confluence in 6-well-plates (Greiner Bio-One, 657160) and transfected using Opti-MEM reduced serum medium (Gibco, 31985070) and Lipofectamine 2000 (Invitrogen, 11668030) according to the protocol supplied by the manufacturer. 24 h after transfection, the growth medium was exchanged.

6.2.12. Transductions

For packaging and virus production, HEK293T cells (see Table 10) were transfected with the vector of interest, as well as psPAX2 (Addgene, #12260), pMD2.G (Addgene, #12259), as outlined above. More precisely, for transfection of cells in a 6-well-plate (Greiner Bio-One, 657160), 1 µg psPAX2 (Addgene), 0.3 µg pMD2.G (Addgene) and 1.3 µg of the vector of interest were mixed with 170 µl Opti-MEM medium (Gibco, 31985070) in a sterile

microcentrifuge tube (Sarstedt, 72690) (per well) and vortexed briefly. In another tube, 8 µl Lipofectamine 2000 (Invitrogen, 11668030) were mixed with 170 µl Opti-MEM medium (per well) and vortexed briefly. Subsequently, both solutions were mixed, incubated for 10 min and added dropwise to one well of HEK293T target cells. Cultureware containing transfected HEK293T cells was then transferred to a security level 2 (S2) area. 48 hours after transfection, the growth medium of transfected cells was filtered through a 0.45 µm Minisart cellulose acetate filter (Sartorius, 16555), and used to replace the growth medium of to-be-transduced fibroblasts. To maximize transduction efficiency, polybrene (Merck, TR-1003-G) was added to a final concentration of 8 µg/ml. Another 48 h later, the virus-containing medium was removed, the cells were washed twice with growth medium and, finally, grown in the same medium until downstream use. One day later, cells were transferred back to security level 1 (S1) conditions. If needed, cells were afterwards expanded to 10 cm plates (Greiner Bio-One, 664160).

6.2.13. ATAC-see

The ATAC-see experiment was performed in two stages: in the first stage, hyperactive Tn5 transposase was produced and custom transposomes containing fluorescently-labelled oligonucleotides were assembled. A detailed account of this procedure is given in the Supplementary Methods, Section 7.1.1. The second stage comprised the actual ATAC-see experiment, which is outlined below.

The ATAC-see experiment was performed by following a previously published protocol (Chen *et al.*, 2016). Specifically, early-passage fibroblasts (HGADFN188, HGADFN155 & HGFDFN168: p9, GM05659: p10) were grown on cover slips (Thermo, 004711180) until 70-80 % confluence and fixed with 3.8 % (w/v) paraformaldehyde (PFA) in 1x PBS (Gibco, 10010023) for 10 min at room temperature. They were then permeabilized with lysis buffer (10 mM TRIS-HCl pH 7.4, 10 mM NaCl, 3 mM $MgCl_2$, 0.01 % IGEPAL CA-630), washed with 1x PBS twice and incubated with the transposome mixture (100 nM assembled Tn5-Atto-590N-transposomes, 25 µl 2x TD buffer (Tagmentation Buffer, Illumina, 15028212), ddH_2O to 50 µl) at 37°C for 30 min. Subsequently, cover slips were washed three times (15 min each) with 1x PBS containing 0.01 % (v/v) SDS and 50 mM EDTA (Gerbu, #1034) at 55°C, and immunostained as outlined in Section 6.2.17. Imaging was performed using a FluoView FV1000 (Olympus) microscope.

For each sample, 50 cells from three technical replicates were analyzed using Fiji/ImageJ (Schindelin *et al.*, 2012; Rueden *et al.*, 2017) to determine nuclear malformation and the presence of ATAC-see foci. A nucleus was scored as malformed when lobulation characteristic

of HGPS cells (as shown in Figure S35) was present. Statistical significance of differences between HGPS and control cells was assessed using an unpaired t-test in GraphPad Prism (GraphPad Software).

6.2.14. ATAC-seq

6.2.14.1. Library Preparation and sequencing

ATAC-seq was performed as described previously (Buenrostro *et al.*, 2015). Specifically, 50,000 cells from early-passage fibroblasts (all: p9) were washed with ice cold 1x PBS (Gibco, 10010023) and resuspended in 50 µl lysis buffer (10 mM TRIS-HCl pH 7.4, 10 mM NaCl, 3 mM $MgCl_2$, 0.1 % IGEPAL CA-630). The lysis reaction was carried out while spinning down the samples at 500 g for 10 min at 4°C. Samples were then resuspended in transposition buffer (25 µl 2x TD buffer (Tagmentation Buffer, Illumina, 15028212), 2.5 µl TDEI (Tagment DNA Enzyme, Illumina, 15028212) and 22.5 µl ddH_2O) and incubated for 30 min at 37°C. Subsequently, samples were purified using the MinElute PCR Purification kit (Qiagen, 28004). The libraries were then PCR-amplified according to instructions given in (Buenrostro *et al.*, 2015), purified again as described above and quantified on a 2200 TapeStation (Agilent). Finally, they were submitted to the High-Throughput Sequencing Core Facility (DKFZ) for 125 bp paired-end sequencing on a HiSeq 4000 platform (Illumina).

6.2.14.2. Bioinformatic analyses

Raw reads were first trimmed by removing stretches of bases with a quality score of <30 at the ends and mapped against the hg19 assembly of the human genome using Bowtie 2 (Langmead and Salzberg, 2012). Subsequently, peaks were called using MACS2 (Zhang *et al.*, 2008), followed by the determination of differential peaks using DESeq2 (Love, Huber and Anders, 2014). Peaks with a q-value of less than 0.05 after multiple testing correction (Benjamini-Hochberg) were considered significantly differentially accessible. Peaks mapping to sex-chromosomes and haplotypes were not considered in the downstream analysis.

The distribution of significant, non-sex chromosome-associated ATAC-seq peaks across the genome was determined using the ‘subsetByOverlaps’ and ‘Genomic Regions’ functions with the ‘TxDb.Hsapiens.UCSC.hg19.knownGene’ Bioconductor annotation package (version 3.2.2) in R (The R Foundation). For the determination of peaks overlapping enhancer regions, poised enhancers were defined as regions containing pairs of H3K4me1 peaks in close proximity

(<1,500 bp) using ENCODE ChIP-seq data for dermal fibroblasts (ENCSR000ARV), while active enhancers were obtained directly from ENCODE (ENCSR871EJM). The overlap with histone modifications and Lamin A or B LADs was quantified in the same way using previously published ENCODE (ENCSR000ARX, ENCSR000ARV, ENCSR000APR, ENCSR000APN, ENCSR000APP, ENCSR000APQ, ENCSR000APO) and ChIP-seq (Guelen *et al.*, 2008; Lund *et al.*, 2015) datasets.

Significance testing of ATAC-seq peak enrichment in the respective regions was performed using Fisher's Exact test in R (The R Foundation).

Transcription factor binding sites enriched in significant, non-sex chromosome-associated ATAC-seq peaks were determined using the HOMER motif analysis tool (Heinz *et al.*, 2010) with 'known motifs' (Figure 14B) or '*de novo* motifs' (Figure 14C) using the hg19 background and the following parameters: -size: 2000, -hist: 20.

6.2.15. DNA methylation profiling

6.2.15.1. Preparation and DNA submission

For DNA methylation profiling, genomic DNA was extracted from early-passage HGPS and control fibroblasts (HGADFN122: p8, all other HGPS: p9, HGFDFN168/HGMDFN090: p9, GM01864: p11, GM05659: p9, GM00969: p12, GM02036: p13) as described in Section 6.2.3 and submitted to the Microarrays Core Facility (DKFZ). DNA methylation profiles were generated using Infinium MethylationEPIC BeadChips (Illumina), following the manufacturer's instructions.

6.2.15.2. Preprocessing and identification of significantly differentially methylated probes

Methylation data analysis was performed using the R Bioconductor package Minfi (v1.20.2) (Aryee *et al.*, 2014). Specifically, raw .IDAT files were read into R (The R Foundation) and preprocessed as follows: first, methylation loci (probes) with high detection p-values (P>0.01, as provided by Minfi), a location on sex chromosomes, the ability to self-hybridize, and those with potential SNP contamination were filtered out. Then, array normalization was carried out using the 'preprocessFunnorm' function, available in Minfi (Aryee *et al.*, 2014). After every preprocessing step, quality control was performed.

Differentially methylated probes were identified by fitting a linear model, followed by statistical analysis with an empirical Bayes method to moderate standard errors. Finally, differentially methylated probes were selected by significance threshold (P<0.05, F-test, after correction for multiple testing using the Benjamini–Hochberg method). The bioinformatic pipeline for preprocessing and identification of differentially methylated probes was programmed by Dr. Julian Gutekunst (Division of Epigenetics, German Cancer Research Center, Heidelberg, Germany).

6.2.15.3. Consensus Clustering

Probe clusters for consensus clustering were identified using the Minfi (Aryee *et al.*, 2014) function 'boundedClusterMaker' with a maximum cluster width of 1,500 bp and a maximum gap of 500 bp. Utilizing the 'ConsensusClusterPlus' package (Wilkerson and Hayes, 2010), consensus clustering was performed with the 5,000 most variable probe clusters, i.e., the 5,000 probe clusters with the highest standard deviation, using the following parameters: maxK = 6; reps = 1,000; pItem = 0.8; and pFeature = 1. Subsequently, samples were assigned to the optimal number of clusters, and, for the purpose of visualization, β values were sorted by hierarchical clustering. Finally, a PCA was created from the probe clusters with the R package FactoMineR (Lê, Josse and Husson, 2008). The Consensus Clustering analysis pipeline was programmed by Dr. Felix Bormann (Division of Epigenetics, German Cancer Research Center, Heidelberg, Germany).

6.2.15.4. Analysis of histone & LAD methylation and enrichment of TFBSs

Using the 'IlluminaHumanMethylationEPICmanifest' manifest (Hansen, 2016) and 'IlluminaHumanMethylationEPICanno.ilm10b2.hg19' annotation (Hansen, 2016), MethylationEPIC probes overlapping with a region of interest were determined in R (The R Foundation). For the comparison of LAD and 'solo-WCGW' CpG probe methylation levels, previously published locations of Lamin A LADs (Lund *et al.*, 2015), Lamin B LADs (Guelen *et al.*, 2008) and 'solo-WCGWs' CpGs (Zhou *et al.*, 2018) were used. Regions overlapping with histone modifications were obtained from previously published ENCODE datasets for dermal fibroblasts (ENCSR000ARX, ENCSR000ARV, ENCSR000APR, ENCSR000APN, ENCSR000APP, ENCSR000APQ, ENCSR000APO, ENCSR328AVV). The significance of methylation differences between groups was analyzed using Welch's Two Sample t-test in R (The R Foundation), while the significance of a probe enrichment in a region of interest was

assessed using Pearson's Chi-squared test with Yates' continuity correction in R (The R Foundation). TFBS enrichment among the differentially methylated regions was tested using ELMER 2.0 (Yao *et al.*, 2015; Silva *et al.*, 2018) with a minimum motif quality 'B' and a minimum incidence of 10.

6.2.15.5. DNA methylation age calculation

DNA methylation age estimates were obtained using a recently published algorithm (Skin & Blood Clock (Horvath *et al.*, 2018)) and corrected for passage numbers by multiplying them with a passage factor ρ, with ρ = passage number*(3.32*log(cells harvested/cells seeded)) with cells harvested = $1x10^6$ and cells seeded = $0.25x10^6$. They were then displayed as delta (Δ) age, i.e., the difference between DNA methylation age and chronological age.

6.2.15.6. DNA methylation of AK and SCC samples

For the DNA methylation analysis of epidermal cancers, genomic DNA from 12 normal epidermis, 16 AK epidermis and 18 cSCC epidermis samples was analyzed using Infinium MethylationEPIC BeadChips (further details in Rodríguez-Paredes *et al.*, 2018). LAD methylation (Lamin B LAD probes) and DNA methylation age were calculated as described above. Statistical testing was performed in R (The R foundation).

6.2.16. DNA Fluorescence In Situ Hybridization (FISH)

Bacterial Artificial Chromosomes (BACs) were obtained from the Children's Hospital Oakland Research Institute (CHORI) (Oakland, CA, USA). Table 8 contains a list with all BACs used and the genes they cover. BACs were labeled with the ENZO Nick translation DNA labeling system 2.0 (ENZO, ENZ-GEN111-0050) using SEEBRIGHT Red 580 dUTP (ENZO, ENZ-42844) and SEEBRIGHT Green 496 dUTP (ENZO, ENZ-42831), following the manufacturer's instructions. Subsequently, 500 ng of each probe were precipitated by adding 5 µl of Cot-1 DNA (1 mg/ml) (Invitrogen, 15279011), 3 µl 3 M sodium acetate pH 5.2 (Roth, 6773.2) and 150 µl EtOH (Fisher Scientific, E/0650DF/C17) and incubating the mixture at -80°C for 30 min. DNA was then pelleted by centrifugation (13,000 g at 4°C for 30 min), air-dried and resuspended in 15 µl of hybridization buffer (10 % (w/v) dextran sulfate, 50 % (v/v) formamide, 2x SSC pH7).

For the preparation of metaphase spreads, >1,000,000 cells were trypsinized, washed with 1x PBS (Gibco, 10010023) and resuspended drop by drop in 0.075 M KCl (Roth, 6781.1). After

incubation at room temperature for 20 min, they were spun down (850 g, room temperature, 5 min) and washed with 10 ml Carnoy's Fixative (methanol:acetic acid = 3:1). They were then centrifuged as before and resuspended in 1-2 ml Carnoy's Fixative for long-term storage at -20°C.

Finally, FISH was performed as previously described (Schlegelberger, B, Metzke S, Harder S, Zühlke-Jenisch R, Zhang Y, 1999). In brief, 1 µl (afterwards adjusted according to signal strength) of both red and green probes were mixed with 4 µl of hybridization buffer and incubated at 37°C for 30 min. Meanwhile, metaphase spreads were created by applying Carnoy-fixated cells dropwise to glass slides (Thermo, J2800AMNZ) from a height of >50 cm, air-dried and washed sequentially in 70 %, 80 % and 100 % (v/v) ethanol (5 min each wash). Glass slides were then air-dried thoroughly. Subsequently, the hybridization mixture was added onto the metaphase spreads, covered with cover slips (Thermo, 004711180) and incubated for 2 min on the metal surface of Thermomixer (Eppendorf) set to 78°C, before being wrapped with parafilm (Bemis, PM-996) and incubated at 37°C overnight in a humid chamber (protected from light). The next day, slides were washed once in washing buffer I (0.4x SSC 0.3 % (v/v) IGEPAL CA-630) (75°C, 2 min) and once in washing buffer II (2x SSC 0.1 % (v/v) IGEPAL CA-630) (room temperature, 5 min). After another wash with PBD washing buffer (0.1 M NaH_2PO_4, 0.1 M Na_2HPO_4, 0.1 % (v/v) IGEPAL CA-630) (room temperature, 2 min), they were air-dried, mounted with Vectashield containing 1 µg/µl DAPI (Vector Laboratories, H-1200) and stored at 4°C until imaging.

Slides were imaged using Axioskop 2 (Zeiss) and FluoView FV1000 (Olympus) microscopes. For each probe, images were acquired for 60 cells. Distance measurements were performed with Fiji/ImageJ (Schindelin *et al.*, 2012; Rueden *et al.*, 2017) using confocal sections with a clear biallelic FISH signal. For group-specific comparisons, the respective HGPS and control sample data were pooled and subjected to a Welch Two Sample t-test with a 95 % confidence interval in R (The R Foundation).

6.2.17. Immunostainings

For Lamin A immunostainings, cells were grown on coverslips (Thermo, 004711180), fixed with 3.8 % (w/v) PFA (Roth, 0335.3) in 1x PBS (Gibco, 10010023) for 10 min at room temperature and permeabilized with 0.3 % (v/v) Triton X-100 (Gerbu, 2999,0050) in 1x PBS for 15 min at room temperature. Coverslips were subsequently washed three times with 1x PBS (10 min each) and blocked with 10 % (v/v) FBS (Gibco, 10500-064) in 1x PBS with 0.1 % (v/v)

Tween 20 (Sigma-Aldrich, P1379) for 1 h at room temperature. They were then incubated with a 1:250 dilution of Lamin A/C primary antibody (Santa Cruz, sc7292) in the same solution for 90 min, washed three times with 1x PBS (10 min each) and incubated with a 1:500 dilution of Alexa 488 secondary antibody (Invitrogen, A11017) in the same solution at room temperature for 45 min. Finally, coverslips were washed three times with 1x PBS (10 min each) and mounted onto glass slides (Thermo, J2800AMNZ) with Vectashield containing 1 μg/μl DAPI (Vector Laboratories, H-1200). Slides were imaged using Axioskop 2 (Zeiss) and FluoView FV1000 (Olympus) microscopes.

Malformed nuclei were quantified by counting the number of severely misshapen nuclei (on the basis of significant blebbing and wrinkling, cp. Figure S35) in three technical replicates with 100 cells analyzed per replicate. An example of the range of nuclear aberrations scored as 'malformed' is given in Figure S35. After treatment with Lonafarnib, rapamycin or metformin, nuclear lobulation was assessed by counting the number of nuclei with ≥1 clearly visible lobules in three technical replicates with 100 cells analyzed per replicate. Significance testing was performed using an unpaired t-test in GraphPad Prism (GraphPad Software).

6.2.18. RNA-seq

6.2.18.1. Library preparation and sequencing

For RNA sequencing, total RNA was isolated from early-passage HGPS and control fibroblasts (HGADFN122: p8, all other HGPS: p9, HGFDFN168/HGMDFN090: p9, GM01864: p11, GM05659: p9, GM00969: p12, GM02036: p13) as described in Section 6.2.5. Total RNA was then purified with the RNA Clean & Concentrator-5 kit (Zymo Research, R1013) and reverse-transcribed using the SuperScript R III First-Strand Synthesis System (Invitrogen, 18080051), following the manufacturer's instructions. Finally, libraries were quantified on a 2200 TapeStation (Agilent) and submitted to the High-Throughput Sequencing Core Facility (DKFZ) for sequencing on a HiSeq 4000 machine (Illumina) using 50 bp single reads.

6.2.18.2. Preprocessing and identification of differentially expressed genes

Reads were trimmed by removing stretches of bases having a quality score of <30 at the ends. They were then mapped against the hg19 assembly of the human genome using Tophat 2.0.6 (Kim *et al.*, 2013). Differential expression analysis was performed using DESeq2 (Love, Huber and Anders, 2014) and Cuffdiff 2.0 (Trapnell *et al.*, 2013) with multiple testing corrections

(Benjamini-Hochberg). Genes with a q-value of less than 0.05 were considered significantly differentially expressed. The bioinformatic pipeline containing all these processing steps was programmed by Dr. Günter Raddatz (Division of Epigenetics, German Cancer Research Center, Heidelberg, Germany).

6.2.18.3. Gene Ontology, Gene Set Enrichment and TRANSFAC analyses

For Gene Ontology (GO) analyses, the AmiGO 2 database, version 2.4/2.5 (Ashburner *et al.*, 2000; Carbon *et al.*, 2009, 2017) was used. TRANSFAC analyses were performed using the TRANSFAC® Public 6.0 database in Match - 1.0 (Matys, 2006). Gene Set Enrichment Analysis (GSEA) (Subramanian *et al.*, 2005) was carried out by analyzing the RNA sequencing datasets of HGPS and control fibroblasts with the 'hallmark' (v5.0, Arthur Liberzon (Liberzon *et al.*, 2015), Broad Institute) and 'KEGG' (KEGG (Kyoto Encyclopedia of Genes and Genomes)) gene set collections from the Molecular Signatures Database (MSigDB), supplemented with the 'NRF2_01' (v6.0, Xiaohui Xie, Broad Institute) and 'AP1_01' (v6.0, Xiaohui Xie, Broad Institute) gene sets. Permutation parameters were set to 'gene_set permutation' and '1000 permutations'. Gene signatures with a false discovery rate (FDR) q-value of <0.05, as obtained by the software, were considered enriched.

6.2.19. Dam ID-seq

The Dam ID-seq experiment was performed in three stages: in the first stage, a Dam-Lamin A expression vector was cloned using Gateway technology; in the second stage, the Dam ID NGS libraries were prepared and sequenced; the third stage comprised the bioinformatic analysis of obtained sequencing data.

6.2.19.1. Generation of the Dam-Lamin A expression vector using Gateway cloning and verification of EcoDam-V5-Lamin A expression in dermal fibroblasts

The Dam-Lamin A expression vector (pLgw-EcoDam-V5-LaminA) was generated through Gateway cloning. A detailed account of the cloning procedure is given in the Supplementary Methods, Section 7.1.2. In brief, *LMNA* cDNA was first cloned into the the pCR™8/GW/TOPO® entry vector using the pCR™8/GW/TOPO® kit (Invitrogen, K250020), and strictly following the manufacturer's instructions. The pCR™8/GW/TOPO® entry vector containing *LMNA* cDNA together with the pLgw EcoDam-V5-RFC1 destination vector (obtained from Addgene, #59209)

was then used to generate the expression vector in an LR clonase reaction using the Gateway® LR Clonase® II Enzyme Mix (Invitrogen, 11791-020), again following the manufacturer's instructions. Additionally, a pLgw-EcoDam-V5 expression vector (for the expression of a Dam-only control) was obtained from Addgene (#59210). Both pLgw-EcoDam-V5-LaminA and pLgw-EcoDam-V5 were then sequence-verified and midi-prepped using the HiSpeed Plasmid Midi kit (Qiagen, 12643) in order to generate sufficient amounts of plasmid for downstream applications.

Expression of the EcoDam-V5-Lamin A fusion protein was then assessed through transient transfection of both HGPS and control fibroblasts. For this purpose, dermal fibroblasts were transfected with pLgw-EcoDam-V5-Lamin A as described in Section 6.2.11 and the expression of the fusion protein was verified using both α-Lamin A (Santa Cruz, sc7292) and α-V5 (Santa Cruz, sc58052) antibodies (see Supplementary Methods, Section 7.1.3).

6.2.19.2. Dam ID NGS library preparation and sequencing

Overall, Dam ID NGS libraries were prepared as previously described (Vogel, Peric-Hupkes and van Steensel, 2007) and adapted for next generation sequencing. Specifically, early-passage HGPS and control fibroblasts (passage numbers: HGFDFN168: p9, HGMDFN090: p8, GM05659: p10, HGADFN188: p9, HGADFN155: p9, HGADFN164: p9) were lentivirally transduced as outlined in Section 6.2.12 with either pEcoDam-V5 or pEcoDam-V5-Lamin A. Genomic DNA was extracted 72 h after infection as described in Section 6.2.3. 1.5 μg of genomic DNA were then *Dpn*I-digested and, after ligation of dsAdr adaptors, *Dpn*II-digested and PCR-amplified using the Advantage cDNA polymerase mix (Clontech, 639105), closely following the instructions given in Vogel, Peric-Hupkes and van Steensel, 2007. The libraries were then purified using a PCR purification kit (Qiagen, 28104), quantified using a Qubit 3 fluorometer (Invitrogen) and a 2200 TapeStation (Agilent), and sonicated on a focused-ultrasonicator (Covaris, M220) following the manufacturer's instructions to obtain a median peak size of 400 bp (400 ng/sample, 50 W Peak Incident Power, 10 % Duty Factor, 200 Cycles per Burst, 70 s Treatment Time, 130 μl microTUBEs). Finally, they were submitted to the High-Throughput Sequencing Core Facility (DKFZ) for preparation of sequencing libraries (protocol: ChIPSeq, Index Type: TruSeq HT / NEBNext Dual, Fragment Size: 400 bp) and sequenced on a HiSeq 4000 system (Illumina) using a single-read 50 bp protocol.

6.2.19.3. Bioinformatic analysis

The bioinformatic analysis was performed in collaboration with Bioinformatics.Expert UG (Dr. Felix Bormann, Berlin). In brief, adaptor sequences were first trimmed from raw reads and aligned with (v2.2.9) Bowtie 2 (Langmead and Salzberg, 2012) using the reference sequence GRCh37.87. The binary alignment files (bam-files) were then processed using the 'damidseq_pipeline' (v.1.4.5) (Marshall and Brand, 2015) with kernel density normalization and a gatc-fragment file created from the same reference (GRCh37.87). The HGPS-and control specific Dam-only backgrounds were created by merging the bam-files of Dam-only signal from two HGPS (HGADFN188 and HGADFN155) and two control (HGMDFN090 and GM05659) cell lines, respectively, prior to the analysis (Figure S38). Then, group-specific Lamin A enrichments were determined by averaging the normalized Lamin A/Dam-only signals within each group (HGPS: HGADFN188 and HGADFN164; control: HGMDFN090, HGFDFN168 and GM05659) and the differential Lamin A enrichment was calculated by subtracting the averaged Lamin A/Dam-only signal of controls from that of HGPS samples. Finally, group-specific and differential enrichments were separated by chromosome, smoothed utilizing the 'loess' function with a smoothing factor of 0.015, and plotted in R (The R Foundation).

For the definition of sample-specific LADs with a pipeline developed by Gatticchi et al. (Gatticchi *et al.*, 2019), the output bedgraph-file, which contains the enrichment of Lamin A- to Dam-only signal for each gatc-fragment, was used as a starting point. This pipeline includes a peak identification step called circular binary segmentation and uses the R (3.5.2, The R Foundation) package DNAcopy (1.56.0). Afterwards, not annotated genomic regions were excluded and negative values in the identified peaks were removed. Finally, the LAD peaks were merged, if they were closer than 5 kb, and filtered out, if they were smaller than 30 kb (Gatticchi *et al.*, 2019).

Subsequently, group-specific LADs were determined by overlapping sample-specific LADs within each group (HGPS: HGADFN188 and HGADFN164; control: HGMDFN090, HGFDFN168 and GM05659), followed by a second round of filtering (filtered out: LADs ≤30 kb in size; merged: LADs with ≤5 kb distance). The resulting control LADs were then subtracted from HGPS LADs to determine overlapping, HGPS-only or control-only LADs, which were filtered once again as outlined above. Finally, these sets were used as 'HGPS-only, 'control-only' or 'overlapping' LADs for the analysis of chromatin accessibility and DNA methylation changes (as described in Section 6.2.14 and Section 6.2.15).

6.2.20. Statistical analyses

Fisher's Exact test, Welch Two Sample t-test, Wilcoxon test, Chi-squared test and Pearson correlation were carried out in R (The R Foundation, version 3.3.1). Unpaired t-tests were performed in Graphpad Prism (Graphpad Software). A value of $P<0.05$ (95 % confidence interval) was considered statistically significant.

7. Appendix

7.1. Supplementary Methods

7.1.1. ATAC-see hyperactive Tn5 production and transposome assembly

Hyperactive Tn5 transposase production was performed using a previously published method (Picelli *et al.*, 2014), the details of which are given in the following.

First, a pTXB1-Tn5 vector (Addgene, #60240) encoding Tn5 transposase was obtained from Addgene and sequence-verified using Sanger sequencing. It was then transformed into C3013 *E.coli* cells (T7 Express, NEB, C3013I), of which 1 l of culture were grown at 37°C to an OD_{600} of 0.9 (~ 7 h). The culture was then chilled to 10°C on ice and 0.25 mM IPTG (Sigma-Aldrich, I6758) was added. Subsequently, the culture was grown at 23-26°C for 4 h. Bacterial cells were then harvested by centrifugation (13,000 g for 8 min at 4°C) of 50 ml aliquots and frozen at -80°C until further use. After thawing, pellets were kept on ice, resuspended in 80 ml HEGX buffer (20 mM HEPES-KOH pH 7.2, 0.8 M NaCl, 1 mM EDTA, 10 % (v/v) glycerol, 0.2 % (v/v) Triton-X 100) and lysed by sonication on a Branson 450 sonifier (40-45 bursts of 1 s with 1 s breaks, 10-12 cycles, output 50 %). After pelleting the lysate by centrifugation (11,000 g for 30 min at 4°C), 2.1 ml 10 % PEI (Sigma, P3143) were added to the supernatant whilst stirring and the precipitate was spun down (11,000 g for 15 min at 4°C). During centrifugation, 10 ml of a chitin resin (NEB, S6651s) were loaded onto a PD-10 column (GE, 17-0435-01) and washed with 40 ml HEGX; then, the supernatant was loaded at a rate of ~0.5 ml/min. Subsequently, the resin was washed with 200 ml HEGX at the same rate, 20 ml HEGX containing 100 mM DTT (Sigma-Aldrich, 10197777001) were added and 11 ml of eluate were allowed to flow-through. The column was then capped, sealed and incubated at 4°C for 42 h. After uncapping the column, the eluate was collected in 1 ml fractions (6 ml of HEGX buffer with 100 mM DTT were added to obtain 12 fractions), tested for presence of proteins using Bradford solution (BioRad, 500-0006) and dialyzed with dialysis buffer (100 mM HEPES-KOH pH 7.2, 0.2 M NaCl, 0.2 mM EDTA, 2 mM DTT, 0.2 % Triton-X 100, 20 % (v/v) glycerol) using Slide-A-Lyzer dialysis cassettes (Thermo, 66380) according to the manufacturer's instructions. The dialyzed protein solution was then concentrated using Amicon Ultra-15 30K filters (Milipore, UFC903024) following the manufacturer's instructions, diluted to OD_{280} = 3.0 with dialysis buffer and stored in 55 % (v/v) glycerol at -20°C. The presence of Tn5 transposase in the 55 % (v/v) glycerol mixes was then verified using Coomassie Blue (SERVA, 35081.01) staining (Figure S29).

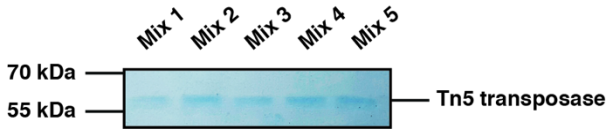

Figure S29: Detection of Tn5 transposase after dialysis. Mixes 1-5 (different 55 % (v/v) glycerol stocks) contain the ~ 55 kDa Tn5 transposase as revealed by Coomassie Blue staining.

Then, Tn5 transposome assembly using Atto-590N-labeled oligonucleotides was performed as described previously (Chen *et al.*, 2016). Specifically, 20 µl of Tn5MErev (100 µM in ddH_2O) oligonucleotides were mixed with 20 µl of either Tn5ME-ATTO590N-A (100 µM in ddH_2O) or Tn5ME-ATTO590N-B (100 µM in ddH_2O) oligonucleotides, denatured by incubation at 95°C for 5 min on a thermocycler (MJ Research / Biometra) and reannealed by gentle cooling to room temperature after turning off the thermocycler (~ 30 min). Subsequently, Tn5 transposomes were assembled by mixing 20 µl of Tn5MErev/Tn5ME-ATTO590N-A, 20 µl of Tn5MErev/Tn5ME-ATTO590N-B and 240 µl Tn5 transposase in 55 % (v/v) glycerol (OD_{280} = 3.0), and incubating this mixture at room temperature for 1 h. Assembled Tn5-Atto-590N-transposomes were then stored at -20°C until being used in the transposition reaction (see Methods, Section 6.2.13), for which they were diluted 71.5-fold to 100 nM.

7.1.2. Dam ID Gateway cloning

First, *LMNA* cDNA was cloned into the the pCR8/GW/TOPO entry vector using the pCR8/GW/TOPO kit (Invitrogen, K250020). For this purpose, *LMNA* was amplified from HGPS cDNA using the following PCR protocol:

Phusion PCR reaction:

40 ng cDNA
1.25 µl PROG f primer (10 µM)
1.25 µl PROG r primer (10 µM)
2 µl dNTP (40 µM)
5 µl 5x HF buffer
0.5 µl Phusion
to 25 µl ddH_2O

Phusion PCR protocol:

98°C	for 30 s	
98°C	for 10 s	35 cycles
70°C	for 20 s	
72°C	for 50 s	
72°C	for 10 min	
4°C	for ∞	

The PCR products were placed on ice and 3'-A overhangs were generated by adding 1 μl FireTaq polymerase (Steinbrenner, SL-FT blue-2500) to 25 μl PCR product, incubating the reaction for 9 min at 72°C and again placing it on ice. It was then used directly in the following TOPO® Cloning reaction: 1 μl salt solution and 1 μl pCR8/GW/TOPO entry vector were mixed with 4 μl PCR product, incubated for 20 min at room temperature and transformed into One Shot TOP10 *E.coli* cells (Invitrogen, C404010) (see Methods, Section 6.2.10). Bacterial colonies were grown on Spectinomycin (Sigma-Aldrich, S4014)-containing (100 μg/ml) LB Agar plates, picked and mini-prepped using the QIAprep Spin Miniprep kit (Qiagen, 27106). They were then digested with EcoRI (NEB, R0101S) following the manufacturer's instructions and run on a 0.8 % agarose gel. Colony #8 had integrated *LMNA* cDNA, while other colonies revealed the presence of Progerin-, both or no cDNA (Figure S30). The correct integration and orientation of *LMNA* cDNA into the pCR8/GW/TOPO vector in colony #8 was subsequently verified by Sanger sequencing using M13-RP.

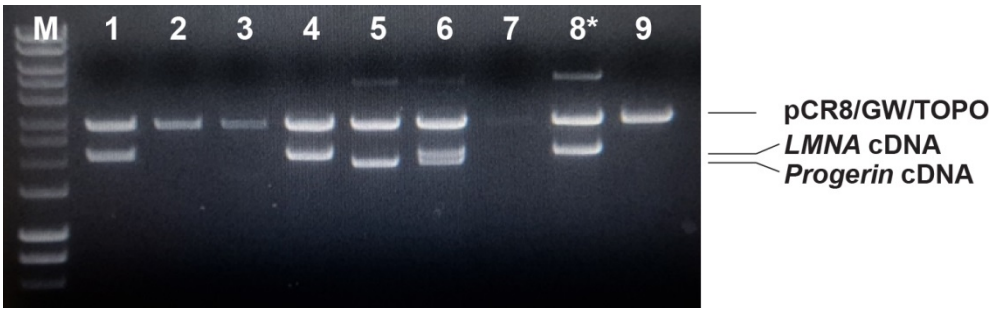

Figure S30: EcoR1-digested pCR8/GW/TOPO from nine different bacterial colonies run on a 0.8 % agarose gel. *Colony #8 showed successful integration of LMNA cDNA and, after sequence verification using Sanger sequencing, was used in downstream LR clonase reaction. M = HyperLadder 1kb (Bioline, BIO-33053). Expected sizes: LMNA cDNA: 2105 bp, Progerin cDNA: 1953 bp.

The pCR8/GW/TOPO entry vector containing *LMNA* cDNA was then used together with a destination vector (pLgw EcoDam-V5-RFC1; see Table 6) (150 ng each) in an LR clonase reaction strictly following the instructions of the pCR8/GW/TOPO kit. After incubation for 4 h at 25°C, the plasmids were transformed into One Shot Stbl3 *E.coli* cells (Invitrogen, C737303), plated onto Ampicillin (Sigma-Aldrich, A1593)-containing (100 mg/ml) LB agar plates and colonies were picked, mini-prepped as before, and tested for successful integration using the following PCR reaction:

PCR reaction:

5 μl plasmid from colony
0.5 μl PROG f primer (10 μM)
0.5 μl PROG r primer (10 μM)
2 μl dNTP (40 μM)
2.5 μl 10x buffer
0.5 μl FireTaq polymerase
to 25 μl ddH_2O

PCR protocol:

95°C for 5 min
95°C for 25 s
70°C for 20 s
72°C for 140 s
} 35 cycles
72°C for 10 min
4°C for ∞

As shown in Figure S31, in about half of the analyzed colonies the LR clonase reaction had not occurred, i.e., *LMNA* cDNA was still present in the pCR8/GW/TOPO entry vector, while colonies #8.2 and #8.20 showed a different amplification pattern. Sanger sequencing using pCasper-hs and PROG r primers verified that they contained the pLgw-EcoDam-V5-Lamin A expression vector with intact and correctly integrated *LMNA* cDNA. Both pLgw-EcoDam-V5-LaminA and the Dam only control vector (pLgw-EcoDam-V5; see Table 6) were then midi-prepped using the HiSpeed Plasmid Midi Kit (Qiagen, 12643) in order to generate sufficient amounts of plasmid for downstream applications.

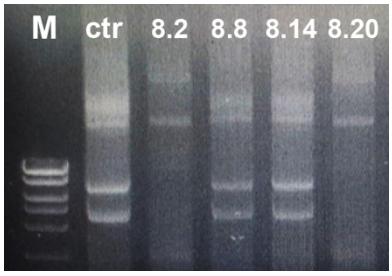

Figure S31: *LMNA* cDNA PCR with PROG cds f and r primers showing a successful LR clonase reaction in half of the analyzed colonies. While colonies 8.8 and 8.14 generated the same amplicon pattern as the control (pCR8/GW/TOPO containing *LMNA* cDNA), colonies 8.2 and 8.20 generated a different amplicon pattern and were, therefore, likely to contain a different plasmid, i.e., pLgw-EcoDam-V5-Lamin A. M = HyperLadder 50bp (Bioline, BIO-33054).

7.1.3. Verification of EcoDam-V5-Lamin A expression in dermal fibroblasts

Before the lentiviral transduction of target cells, expression of a fusion protein with the expected molecular weight was tested after transient transfection of HGPS and control fibroblasts. For this purpose, cells were transfected with pLgw-EcoDam-V5-Lamin A as described in Methods, Section 6.2.11 and total protein extracts were taken at different time points after transfection and analyzed by SDS-PAGE (as described in Methods, Section 6.2.9). As shown in Figure S32, the EcoDam-V5-Lamin A fusion protein was readily detected using an α-V5 antibody (Santa Cruz, sc58052) in both HGPS and control fibroblasts at different time points, with maximum expression 24 h after transfection. Similarly, despite considerably weaker signal due to the presence of Lamin A, Lamin C and Progerin and low transfection efficiency, the fusion protein was also detected using an α-Lamin A/C antibody (Santa Cruz, sc7292) with total protein extracts of HGADFN188 (Figure S33). Hence, expression of the desired fusion protein was considered successful and the Dam ID-seq protocol was continued with the lentiviral transduction of fibroblasts with pLgw-EcoDam-V5-Lamin A, in order to ensure stable, low-level expression (see Methods, Section 6.2.19).

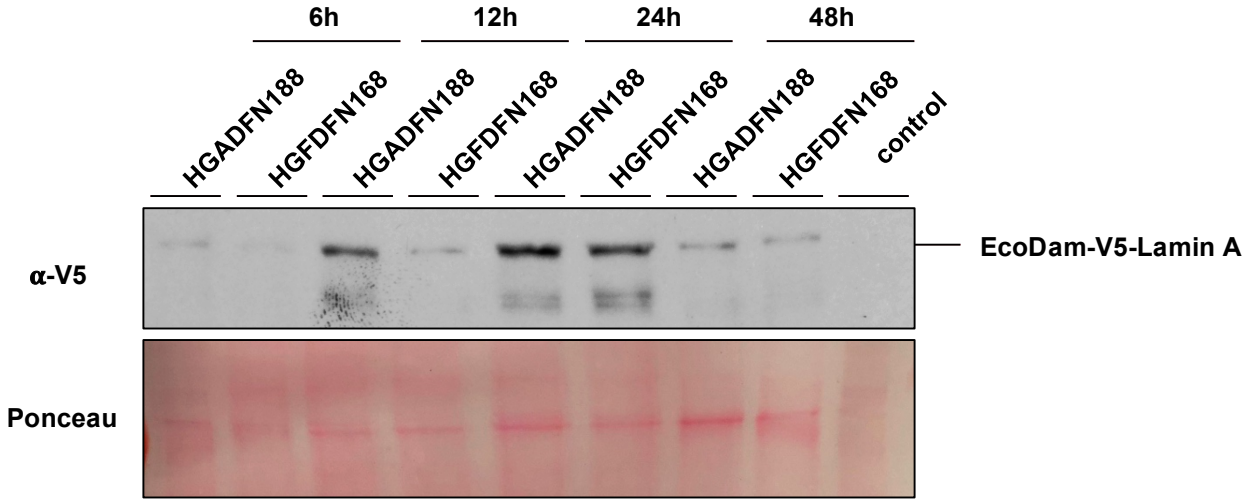

Figure S32: Detection of EcoDam-V5-Lamin A expression using an α-V5 antibody. The fusion protein was detected in total protein extracts from HGPS (HGADFN188) and control (HGFDFN168) cells at different time points after transient transfection with pLgw-EcoDam-V5-Lamin A using an antibody binding to the V5-linker (Santa Cruz, sc58052, 1:200). As expected, untransfected cells ('control', HGADFN188) do not express the fusion protein.

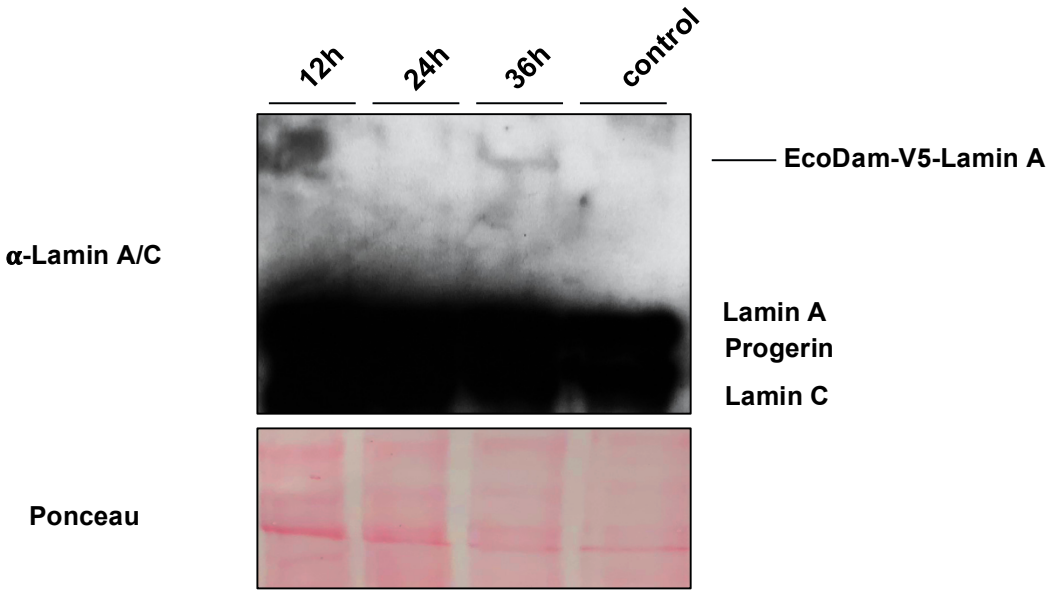

Figure S33: Detection of EcoDam-V5-Lamin A expression using an α-Lamin A/C antibody. The fusion protein was detected in total protein extracts 36 h after transient transfection of HGADFN188 with pLgw-EcoDam-V5-Lamin A but not control cells ('control', untransfected HGADFN188) using an antibody binding to Lamin A/C (Santa Cruz, sc7292, 1:200).

7.2. Additional Figures

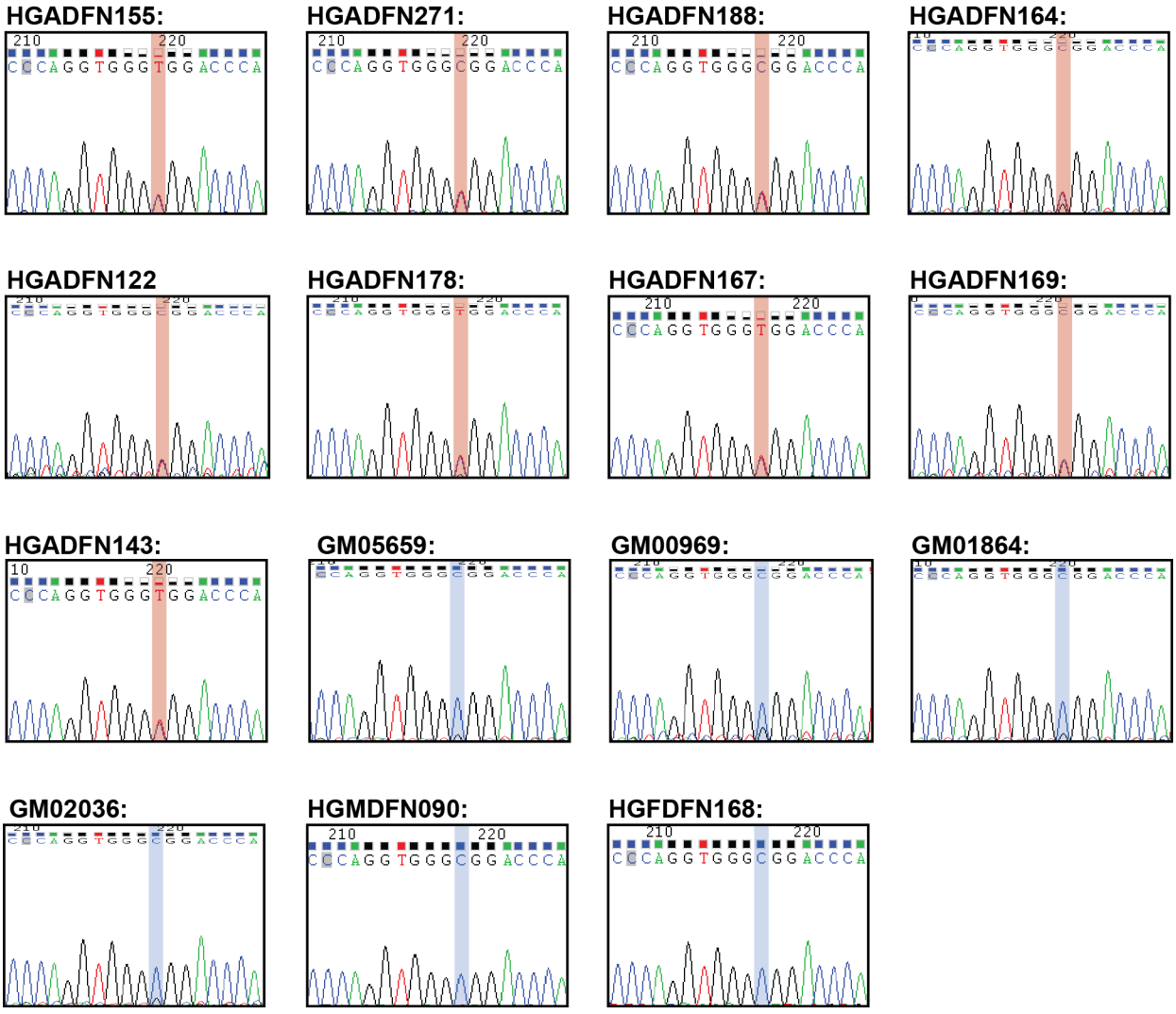

Figure S34: Verification of mutational status in fibroblast lines. A region of the *LMNA* gene spanning exon 11 was amplified with gene-specific primers and Sanger-sequenced. Presence of the heterozygous 1824C>T mutation in HGPS samples is shown in red, its absence in control samples in blue.

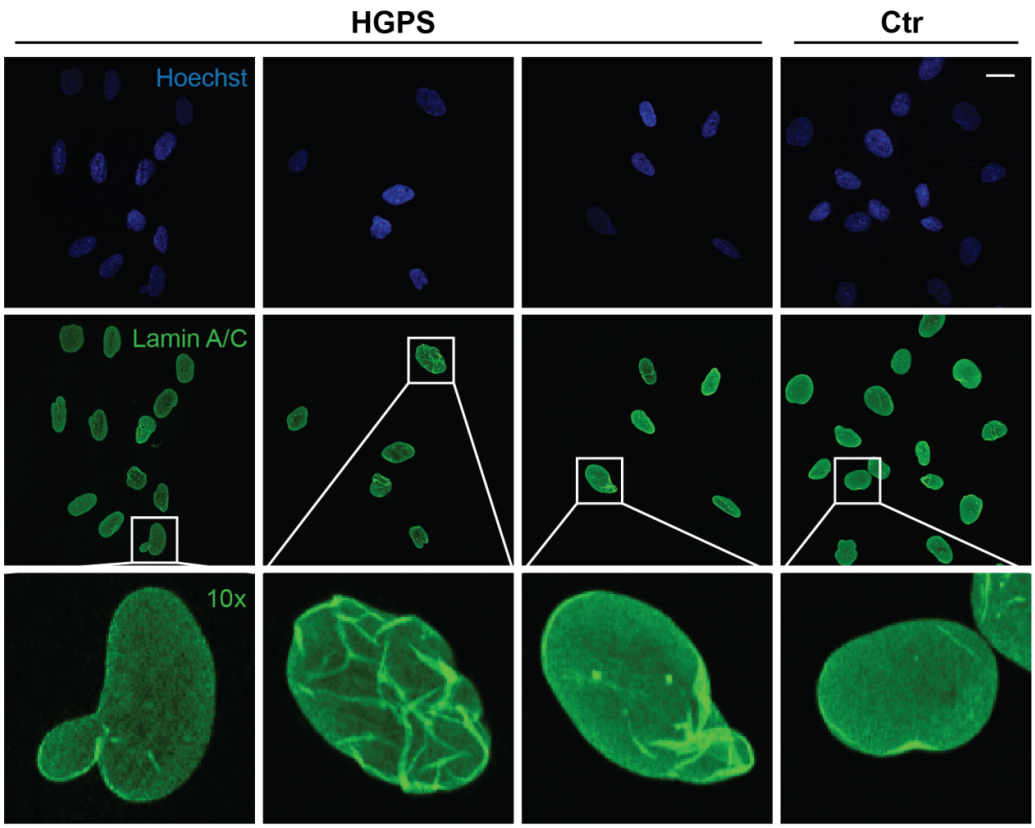

Figure S35: Range of nuclear malformations in HGPS cells. α-Lamin A/C immunofluorescence in one HGPS (HGADFN188, p9) and one control (HGMDFN090, p9) cell line. The various nuclear aberrations scored as 'malformed' are depicted for HGPS cells. Scale bar = 10 μm. Ctr = control.

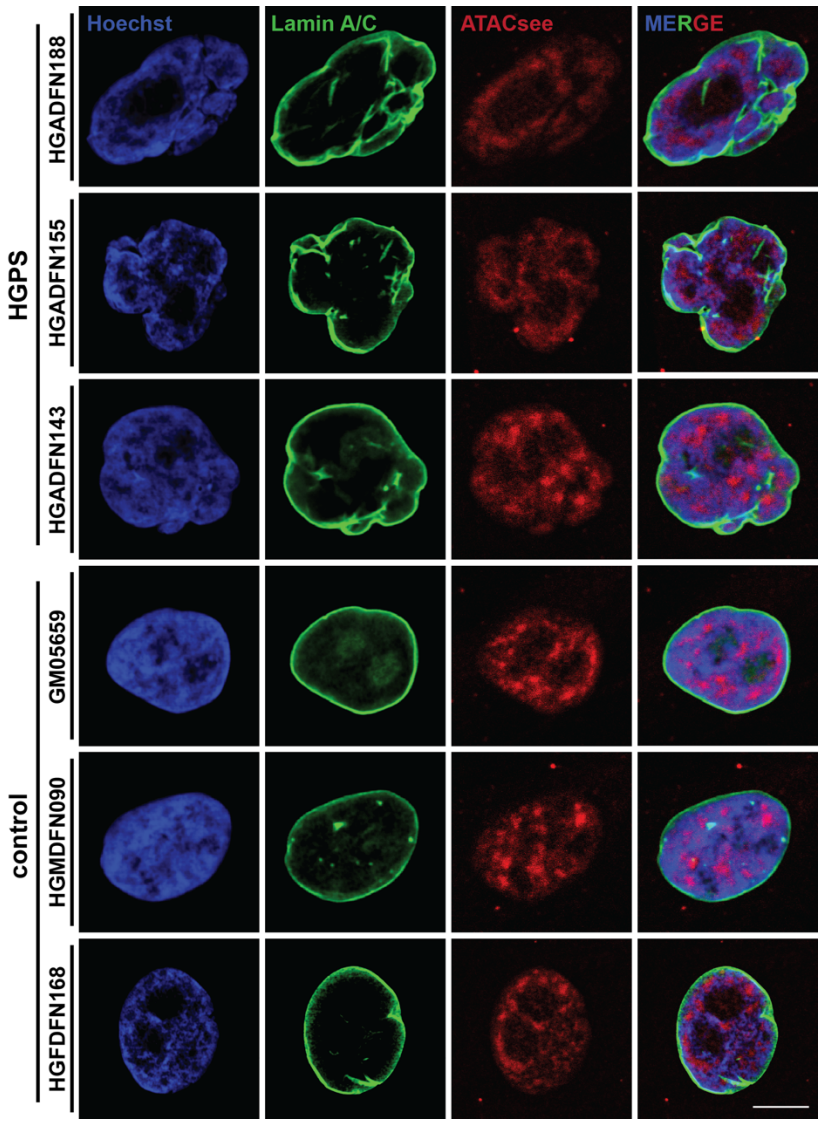

Figure S36: Typical ATAC-see signal in HGPS and control fibroblasts. Most perceivably malformed HGPS nuclei exhibited loss of bright ATAC-see foci and intermediate signal intensities, i.e., reduced dynamic range (HGADFN188 and HGADFN155). However, as shown for HGADFN143, some retained brighter regions. Scale bar = 10 μM.

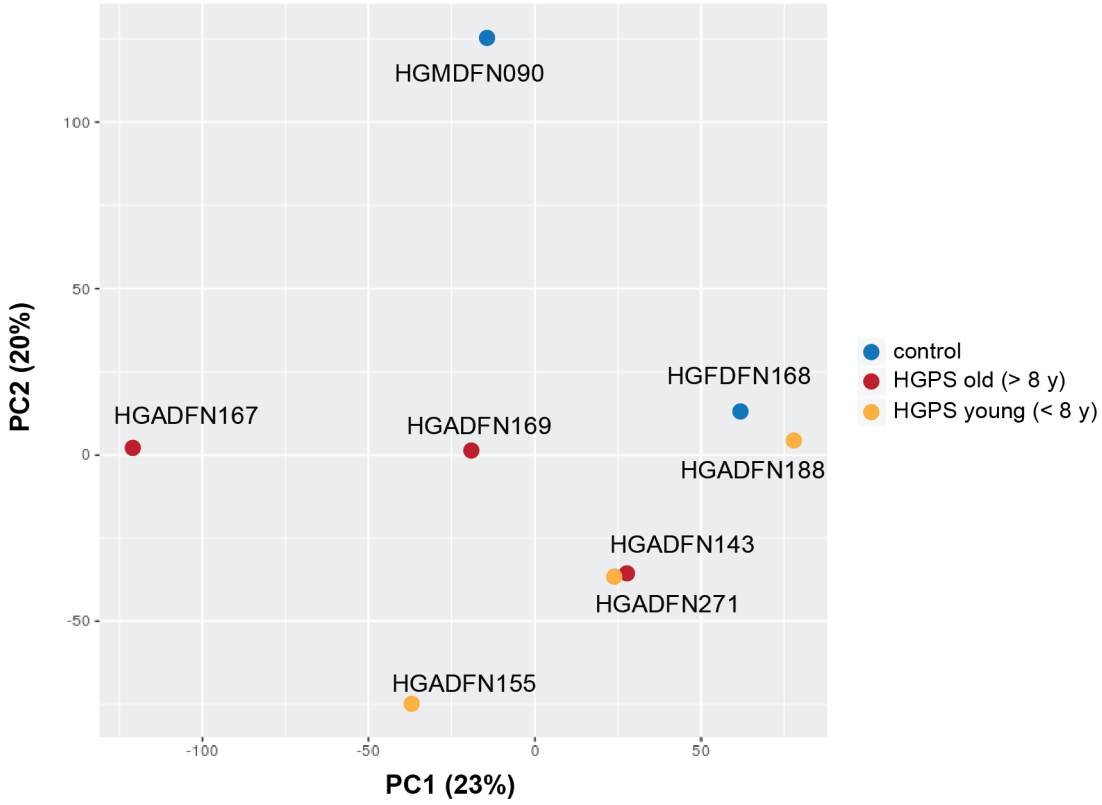

Figure S37: Principal Component Analysis (PCA) of ATAC-seq samples. Principal Component Analysis (PCA) of HGPS (with age groups as indicated) and control ATAC-seq samples. The variances explained by Principal Component (PC) 1 and 2 are given in brackets.

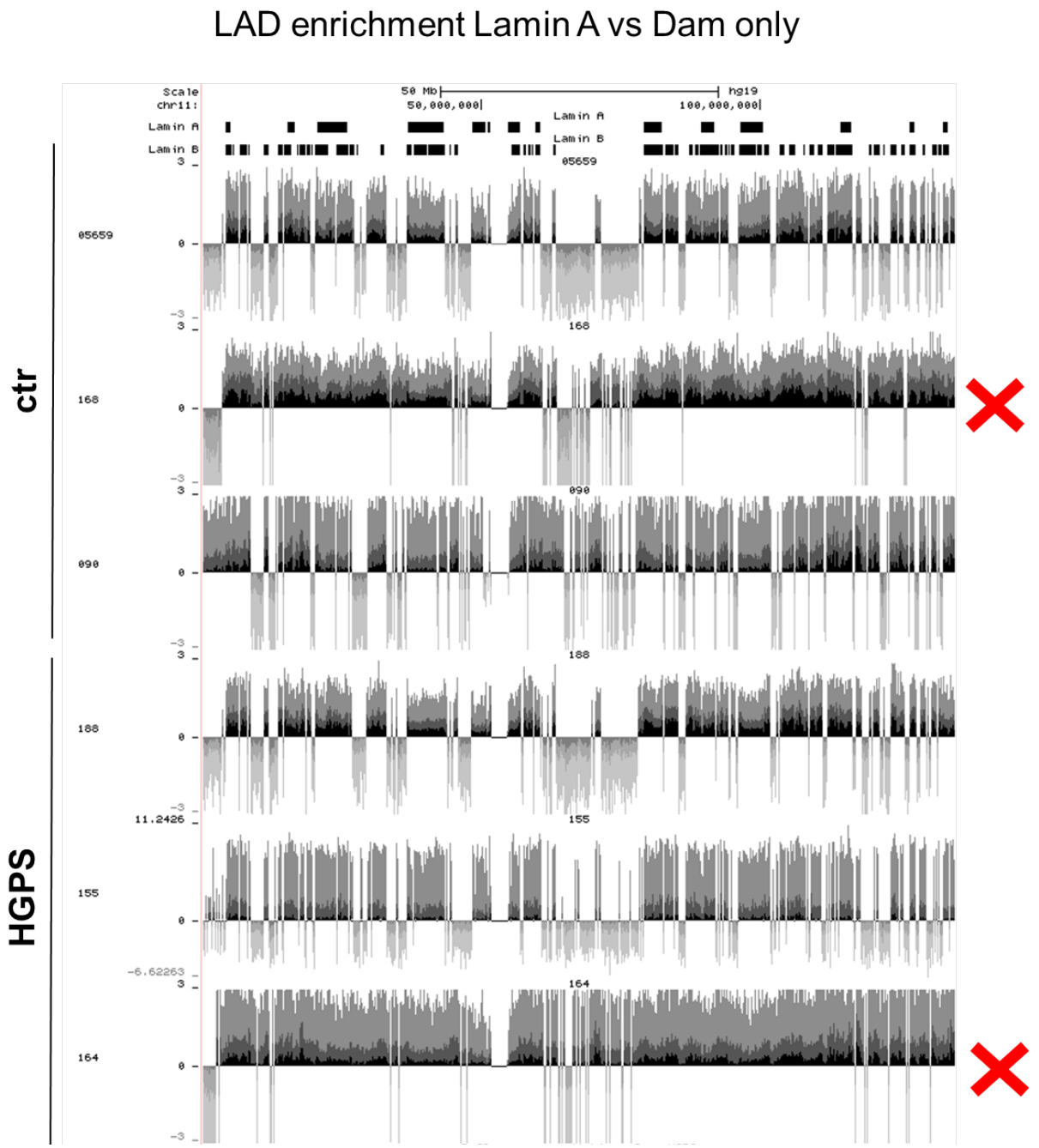

Figure S38: Dam ID-seq: Exclusion of low-quality samples. Upon visual inspection of the Dam-Lamin A vs. Dam-only enrichment tracks, three samples revealed unspecific (HGFDFN168 and HGADFN164, due to low coverage of respective Dam-only samples as marked in red) or fragmented (HGADFN155, due to low quality of Dam-Lamin A sample) binding patterns and were excluded from the analysis. Because of this, group-specific Dam-only backgrounds were created by averaging Dam-only signal from the two unaffected control and the two unaffected HGPS samples, respectively. Additionally, the HGADFN155 sample was excluded from the analysis, due to its sub-quality Dam-Lamin A signal. As a result, all HGPS LAD subsets referred to in this work were calculated using two samples (HGADFN188 and HGADFN164), whereas control LADs were determined by averaging signal from three samples (GM05659, HGFDFN168, HGMDFN090).

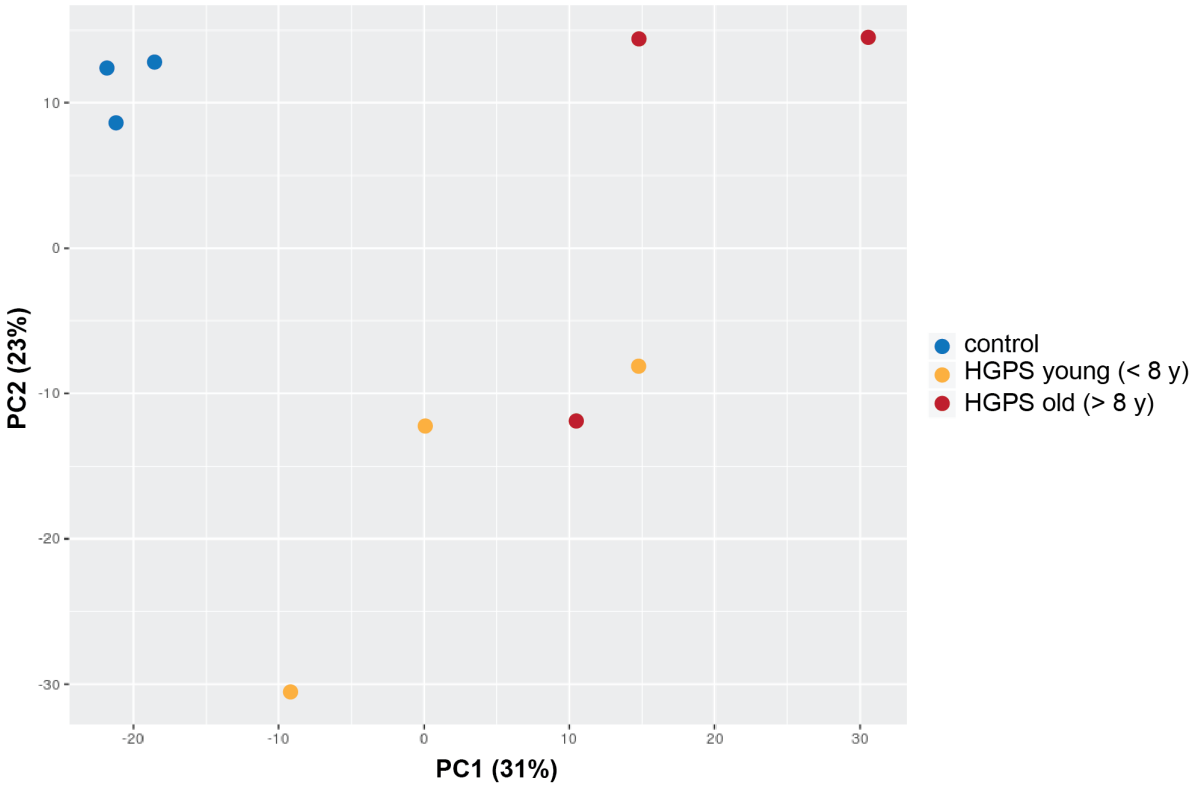

Figure S39: Principal Component Analysis (PCA) of RNA-seq samples. Principal Component Analysis (PCA) of HGPS (with age groups as indicated) and control RNA-seq samples. The variances explained by Principal Component (PC) 1 and 2 are given in brackets.

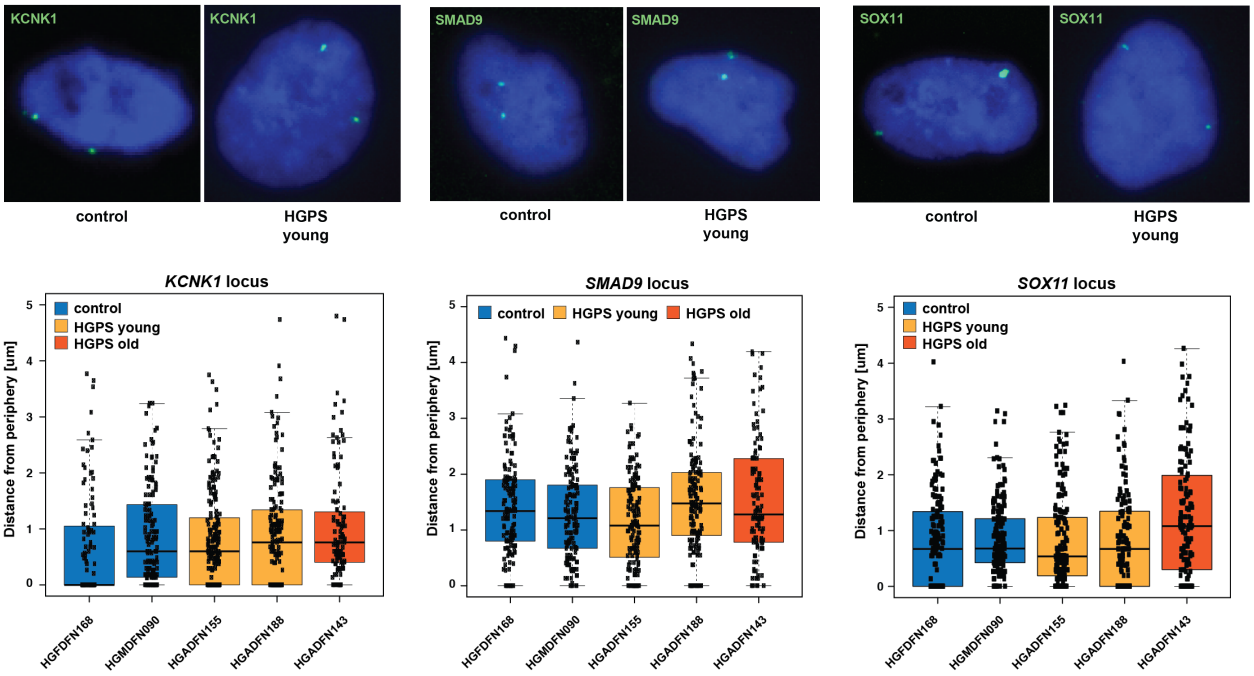

Figure S40: Additional genes tested for intranuclear relocalization using Fluorescence *In Situ* Hybridization (FISH). Upper panels: Representative FISH images of *KCNK1*, *SMAD9* and *SOX11* loci in HGPS and control nuclei. The distance from the FISH signal to the nuclear periphery was measured in the focal plane in cells exhibiting a clear biallelic signal. Lower panels: Quantification of the average distance from the periphery for in the indicated genes in two control and three HGPS cell lines (60 cells per sample). For these loci, HGPS-specific differences were found to be insignificant ($P<0.05$, Welch Two Sample t-test).

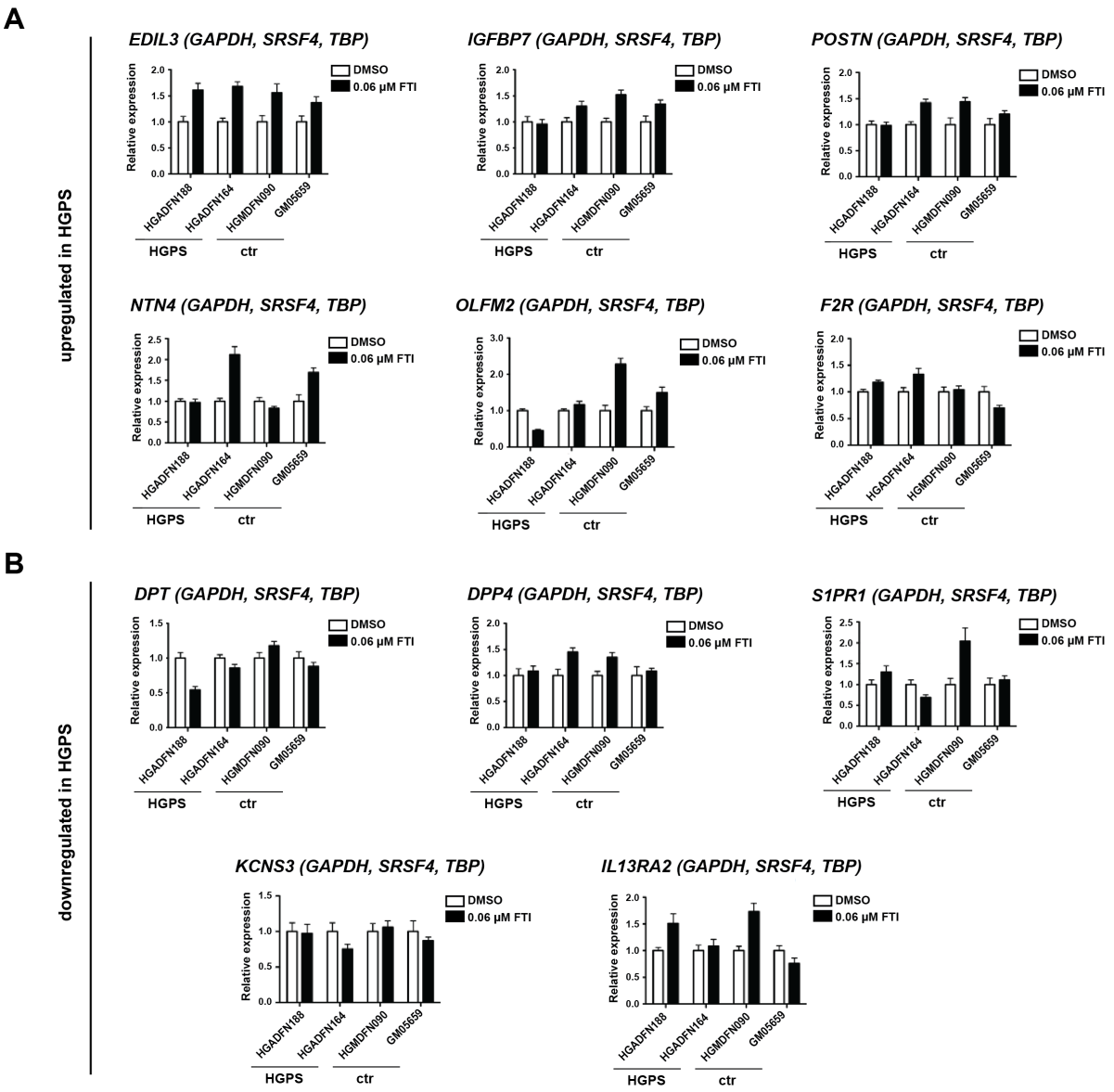

Figure S41: Lonafarnib treatment does not alter HGPS-specific expression changes. (A) & (B) Expression of indicated genes relative to *GAPDH*, *SRSF4* and *TBP* in HGPS and control cells after 7 d treatment with DMSO or 0.06 µM Lonafarnib for genes found to be upregulated (A) or downregulated (B) in HGPS.

7.3. List of Publications

Köhler F, Bormann F, Raddatz G, Gutekunst J, Musch T, Lyko F & Rodriguez-Paredes M. (2019). Epigenetic deregulation of lamina-associated domains in Hutchinson-Gilford Progeria Syndrome. *bioRxiv*; doi: https://doi.org/10.1101/520403.

Köhler F & Rodriguez-Paredes M. (2019). DNA methylation in epidermal differentiation, aging and cancer. *Journal of Investigative Dermatology*. Manuscript accepted.

Rodriguez-Paredes M, Bormann F, Raddatz G, Gutekunst J, Lucena-Porcel C, **Köhler F**, Wurzer E, Schmidt K, Gallinat S, Wenck H, Röwert-Huber J, Denisova E, Feuerbach L, Park J, Brors B, Herpel E, Nindl I, Hofmann TG, Winnefeld M & Lyko F. (2018). Methylation profiling identifies two subclasses of squamous cell carcinoma related to distinct cells of origin. *Nature Communications*, 9:577.

8. References

Akhtar, W. *et al.* (2013) 'Chromatin position effects assayed by thousands of reporters integrated in parallel.', *Cell*. Elsevier, 154(4), pp. 914–27. doi: 10.1016/j.cell.2013.07.018.

Allshire, R. C. and Madhani, H. D. (2018) 'Ten principles of heterochromatin formation and function', *Nature Reviews Molecular Cell Biology*. Nature Publishing Group, 19(4), pp. 229–244. doi: 10.1038/nrm.2017.119.

Allsopp, R. C. *et al.* (1992) 'Telomere length predicts replicative capacity of human fibroblasts.', *Proceedings of the National Academy of Sciences of the United States of America*, 89(21), pp. 10114–8. doi: 10.1073/pnas.89.21.10114.

Alvarado-Kristensson, M. *et al.* (2019) 'The Biology of the Nuclear Envelope and Its Implications in Cancer Biology', *International Journal of Molecular Sciences 2019, Vol. 20, Page 2586*. Multidisciplinary Digital Publishing Institute, 20(10), p. 2586. doi: 10.3390/IJMS20102586.

Ambatipudi, S. *et al.* (2017) 'DNA methylome analysis identifies accelerated epigenetic ageing associated with postmenopausal breast cancer susceptibility', *European Journal of Cancer*. Pergamon, 75, pp. 299–307. doi: 10.1016/J.EJCA.2017.01.014.

Amendola, M. and van Steensel, B. (2015) 'Nuclear lamins are not required for lamina-associated domain organization in mouse embryonic stem cells', *EMBO reports*. John Wiley & Sons, Ltd, 16(5), pp. 610–617. doi: 10.15252/embr.201439789.

Aoka, Y. *et al.* (2002) 'The embryonic angiogenic factor Del1 accelerates tumor growth by enhancing vascular formation', *Microvascular Research*, 64(1), pp. 148–161. doi: 10.1006/mvre.2002.2414.

Aran, D. *et al.* (2011) 'Replication timing-related and gene body-specific methylation of active human genes', *Human Molecular Genetics*. Narnia, 20(4), pp. 670–680. doi: 10.1093/hmg/ddq513.

Aryee, M. J. *et al.* (2014) 'Minfi: A flexible and comprehensive Bioconductor package for the analysis of Infinium DNA methylation microarrays', *Bioinformatics*, 30(10), pp. 1363–1369. doi: 10.1093/bioinformatics/btu049.

Ashburner, M. *et al.* (2000) 'Gene ontology: Tool for the unification of biology', *Nature Genetics*, 25(1), pp. 25–29. doi: 10.1038/75556.

Bannister, A. J. *et al.* (2001) 'Selective recognition of methylated lysine 9 on histone H3 by the HP1 chromo domain', *Nature*. Nature Publishing Group, 410(6824), pp. 120–124. doi: 10.1038/35065138.

Barateau, A. *et al.* (2017) 'A Novel Lamin A Mutant Responsible for Congenital Muscular Dystrophy Causes Distinct Abnormalities of the Cell Nucleus', *PLOS ONE*. Edited by D. Fraidenraich. Public Library of Science, 12(1), p. e0169189. doi: 10.1371/journal.pone.0169189.

Baubec, T. *et al.* (2015) 'Genomic profiling of DNA methyltransferases reveals a role for DNMT3B in genic methylation.', *Nature*, 520(7546), pp. 243–247. doi: 10.1038/nature14176.

Ben-Harush, K. *et al.* (2009) 'The Supramolecular Organization of the C. elegans Nuclear Lamin Filament', *Journal of Molecular Biology*. Academic Press, 386(5), pp. 1392–1402. doi: 10.1016/J.JMB.2008.12.024.

Benayoun, B. A., Pollina, E. A. and Brunet, A. (2015) 'Epigenetic regulation of ageing: Linking environmental inputs to genomic stability', *Nature Reviews Molecular Cell Biology*. Nature Publishing Group, 16(10), pp. 593–610. doi: 10.1038/nrm4048.

Benson, E. K., Lee, S. W. and Aaronson, S. A. (2010) 'Role of progerin-induced telomere dysfunction in HGPS premature cellular senescence', *Journal of Cell Science*. The Company of Biologists Ltd, 123(15), pp. 2605–2612. doi: 10.1242/JCS.067306.

Bergo, M. O. *et al.* (2002) 'Zmpste24 deficiency in mice causes spontaneous bone fractures, muscle weakness, and a prelamin A processing defect.', *Proceedings of the National Academy of Sciences of the United States of America*. National Academy of Sciences, 99(20), pp. 13049–54. doi: 10.1073/pnas.192460799.

Berk, J. M., Tifft, K. E. and Wilson, K. L. (2013) 'The nuclear envelope LEM-domain protein emerin', *Nucleus*. Taylor & Francis, 4(4), pp. 298–314. doi: 10.4161/nucl.25751.

Berman, B. P. *et al.* (2012) 'Regions of focal DNA hypermethylation and long-range hypomethylation in colorectal cancer coincide with nuclear lamina–associated domains', *Nature Genetics*. Nature Publishing Group, 44(1), pp. 40–46. doi: 10.1038/ng.969.

Beyret, E. *et al.* (2019) 'Single-dose CRISPR–Cas9 therapy extends lifespan of mice with Hutchinson–Gilford progeria syndrome', *Nature Medicine*, 25(3), pp. 419–422. doi: 10.1038/s41591-019-0343-4.

Bian, Q. *et al.* (2013) 'β-Globin cis-elements determine differential nuclear targeting through epigenetic modifications', *The Journal of Cell Biology*. Rockefeller University Press, 203(5), pp. 767–783. doi: 10.1083/JCB.201305027.

Bird, A. (2002) 'DNA methylation patterns and epigenetic memory', *Genes and Development*, 16(1), pp. 6–21. doi: 10.1101/gad.947102.

Black, J. C., Van Rechem, C. and Whetstine, J. R. (2012) 'Histone Lysine Methylation Dynamics: Establishment, Regulation, and Biological Impact', *Molecular Cell*. Cell Press, 48(4), pp. 491–507. doi: 10.1016/J.MOLCEL.2012.11.006.

Bollati, V. *et al.* (2009) 'Decline in genomic DNA methylation through aging in a cohort of elderly subjects', *Mechanisms of Ageing and Development*. Elsevier, 130(4), pp. 234–239. doi: 10.1016/J.MAD.2008.12.003.

Bonkowski, M. S. and Sinclair, D. A. (2016) 'Slowing ageing by design: the rise of NAD+ and sirtuin-activating compounds', *Nature Reviews Molecular Cell Biology*. Nature Publishing Group, 17(11), pp. 679–690. doi: 10.1038/nrm.2016.93.

Booth, L. N. and Brunet, A. (2016) 'The Aging Epigenome', *Molecular Cell*. Cell Press, 62(5), pp. 728–744. doi: 10.1016/J.MOLCEL.2016.05.013.

Bormann, F. *et al.* (2016) 'Reduced DNA methylation patterning and transcriptional connectivity define human skin aging', *Aging Cell*, 15(3), pp. 563–571. doi: 10.1111/acel.12470.

Boyle, S. *et al.* (2001) 'The spatial organization of human chromosomes within the nuclei of normal and emerin-mutant cells', *Human Molecular Genetics*, 10(3), pp. 211–219. doi: 10.1093/hmg/10.3.211.

Briand, N. and Collas, P. (2018) 'Laminopathy-causing lamin A mutations reconfigure lamina-associated domains and local spatial chromatin conformation', *Nucleus*. Taylor & Francis, 9(1), pp. 216–226. doi: 10.1080/19491034.2018.1449498.

Bridger, J. M. and Kill, I. R. (2004) 'Aging of Hutchinson–Gilford progeria syndrome fibroblasts is characterised by hyperproliferation and increased apoptosis', *Experimental Gerontology*, 39(5), pp. 717–724. doi: 10.1016/j.exger.2004.02.002.

Broers, J. L. V. *et al.* (2006) 'Nuclear Lamins: Laminopathies and Their Role in Premature Ageing', *Physiological Reviews*. American Physiological Society, 86(3), pp. 967–1008. doi: 10.1152/physrev.00047.2005.

Buenrostro, J. D. *et al.* (2015) 'ATAC-seq: A method for assaying chromatin accessibility genome-wide', *Current Protocols in Molecular Biology*, 2015, pp. 21.29.1-21.29.9. doi: 10.1002/0471142727.mb2129s109.

Burke, B. and Stewart, C. L. (2013) 'The nuclear lamins: flexibility in function', *Nature Reviews Molecular Cell Biology*. Nature Publishing Group, 14(1), pp. 13–24. doi: 10.1038/nrm3488.

Cantó, C. and Auwerx, J. (2009) 'Caloric restriction, SIRT1 and longevity', *Trends in Endocrinology & Metabolism*. Elsevier Current Trends, 20(7), pp. 325–331. doi: 10.1016/J.TEM.2009.03.008.

Cao, K. *et al.* (2007) 'A lamin A protein isoform overexpressed in Hutchinson-Gilford progeria syndrome interferes with mitosis in progeria and normal cells', *Proceedings of the National Academy of Sciences*, 104(12), pp. 4949–4954. doi: 10.1073/pnas.0611640104.

Cao, Kan *et al.* (2011) 'Progerin and telomere dysfunction collaborate to trigger cellular senescence in normal human

fibroblasts', *Journal of Clinical Investigation*, 121(7), pp. 2833–2844. doi: 10.1172/JCI43578.

Cao, K. *et al.* (2011) 'Rapamycin Reverses Cellular Phenotypes and Enhances Mutant Protein Clearance in Hutchinson-Gilford Progeria Syndrome Cells', *Science Translational Medicine*, 3(89), pp. 89ra58-89ra58. doi: 10.1126/scitranslmed.3002346.

Capanni, C. *et al.* (2005) 'Altered pre-lamin A processing is a common mechanism leading to lipodystrophy', *Human Molecular Genetics*. Narnia, 14(11), pp. 1489–1502. doi: 10.1093/hmg/ddi158.

Capell, B. C. *et al.* (2005) 'Inhibiting farnesylation of progerin prevents the characteristic nuclear blebbing of Hutchinson-Gilford progeria syndrome', *Proceedings of the National Academy of Sciences*, 102(36), pp. 12879–12884. doi: 10.1073/pnas.0506001102.

Capell, B. C. and Collins, F. S. (2006) 'Human laminopathies: nuclei gone genetically awry', *Nature Reviews Genetics*. Nature Publishing Group, 7(12), pp. 940–952. doi: 10.1038/nrg1906.

Carbon, S. *et al.* (2009) 'AmiGO: Online access to ontology and annotation data', *Bioinformatics*, 25(2), pp. 288–289. doi: 10.1093/bioinformatics/btn615.

Carbon, S. *et al.* (2017) 'Expansion of the gene ontology knowledgebase and resources: The gene ontology consortium', *Nucleic Acids Research*, 45((Database issue)), pp. D331–D338. doi: 10.1093/nar/gkw1108.

Cedar, H. and Bergman, Y. (2009) 'Linking DNA methylation and histone modification: patterns and paradigms', *Nature Reviews Genetics*, 10(5), pp. 295–304. doi: 10.1038/nrg2540.

Chandra, T. *et al.* (2015) 'Global reorganization of the nuclear landscape in senescent cells', *Cell Reports*, 10(4), pp. 471–484. doi: 10.1016/j.celrep.2014.12.055.

Cheedipudi, S. M. *et al.* (2019) 'Genomic Reorganization of Lamin-Associated Domains in Cardiac Myocytes Is Associated With Differential Gene Expression and DNA Methylation in Human Dilated Cardiomyopathy', *Circulation Research*, 124(8), pp. 1198–1213. doi: 10.1161/CIRCRESAHA.118.314177.

Chen, H., Zheng, X. and Zheng, Y. (2014) 'Age-Associated Loss of Lamin-B Leads to Systemic Inflammation and Gut Hyperplasia', *Cell*. Cell Press, 159(4), pp. 829–843. doi: 10.1016/J.CELL.2014.10.028.

Chen, X. *et al.* (2016) 'ATAC-see reveals the accessible genome by transposase-mediated imaging and sequencing', *Nature Methods*, 13(12), pp. 1013–1020. doi: 10.1038/nmeth.4031.

Chen, Z.-J. *et al.* (2014) 'Dysregulated interactions between lamin A and SUN1 induce abnormalities in the nuclear envelope and endoplasmic reticulum in progeric laminopathies.', *Journal of cell science*. The Company of Biologists Ltd, 127(Pt 8), pp. 1792–804. doi: 10.1242/jcs.139683.

Childs, B. G. *et al.* (2015) 'Cellular senescence in aging and age-related disease: from mechanisms to therapy.', *Nature medicine*. NIH Public Access, 21(12), pp. 1424–35. doi: 10.1038/nm.4000.

Chow, K.-H., Factor, R. E. and Ullman, K. S. (2012) 'The nuclear envelope environment and its cancer connections', *Nature Reviews Cancer*. Nature Publishing Group, 12(3), pp. 196–209. doi: 10.1038/nrc3219.

Christiansen, L. *et al.* (2016) 'DNA methylation age is associated with mortality in a longitudinal Danish twin study', *Aging Cell*. John Wiley & Sons, Ltd (10.1111), 15(1), pp. 149–154. doi: 10.1111/acel.12421.

Clark, S. J. *et al.* (2017) 'Genome-wide base-resolution mapping of DNA methylation in single cells using single-cell bisulfite sequencing (scBS-seq)', *Nature Protocols*, 12(3), pp. 534–547. doi: 10.1038/nprot.2016.187.

Clark, S. J. *et al.* (2018) 'scNMT-seq enables joint profiling of chromatin accessibility DNA methylation and transcription in single cells', *Nature Communications*. Nature Publishing Group, 9(1), p. 781. doi: 10.1038/s41467-018-03149-4.

Collado, M., Blasco, M. A. and Serrano, M. (2007) 'Cellular senescence in cancer and aging.', *Cell*. Elsevier, 130(2), pp. 223–33. doi: 10.1016/j.cell.2007.07.003.

Constantinescu, D. *et al.* (2006) 'Lamin A/C Expression Is a Marker of Mouse and Human Embryonic Stem Cell

Differentiation', *Stem Cells*. John Wiley & Sons, Ltd, 24(1), pp. 177–185. doi: 10.1634/stemcells.2004-0159.

Coutinho, H. D. M. *et al.* (2009) 'Molecular ageing in progeroid syndromes: Hutchinson-Gilford progeria syndrome as a model', *Immunity & Ageing*, 6(1), p. 4. doi: 10.1186/1742-4933-6-4.

Crabbe, L. *et al.* (2012) 'Human Telomeres Are Tethered to the Nuclear Envelope during Postmitotic Nuclear Assembly', *Cell Reports*, 2(6), pp. 1521–1529. doi: 10.1016/j.celrep.2012.11.019.

Creyghton, M. P. *et al.* (2010) 'Histone H3K27ac separates active from poised enhancers and predicts developmental state.', *Proceedings of the National Academy of Sciences of the United States of America*. National Academy of Sciences, 107(50), pp. 21931–6. doi: 10.1073/pnas.1016071107.

Criscione, S. W. *et al.* (2016) 'Reorganization of chromosome architecture in replicative cellular senescence', *Science Advances*, 2(2), p. e1500882. doi: 10.1126/sciadv.1500882.

Croft, J. A. *et al.* (1999) 'Differences in the Localization and Morphology of Chromosomes in the Human Nucleus', *The Journal of Cell Biology*, 145(6), pp. 1119–1131. doi: 10.1083/jcb.145.6.1119.

Csoka, A. B. *et al.* (2004) 'Genome-scale expression profiling of Hutchinson-Gilford progeria syndrome reveals widespread transcriptional misregulation leading to mesodermal/mesenchymal defects and accelarated atherosclerosis', *Aging Cell*, 3(4), pp. 235–243. doi: 10.1111/j.1474-9728.2004.00105.x.

Dahl, K. N. *et al.* (2006) 'Distinct structural and mechanical properties of the nuclear lamina in Hutchinson-Gilford progeria syndrome.', *Proceedings of the National Academy of Sciences of the United States of America*. National Academy of Sciences, 103(27), pp. 10271–10276. doi: 10.1073/pnas.0601058103.

Dang, W. *et al.* (2009) 'Histone H4 lysine 16 acetylation regulates cellular lifespan', *Nature*. Nature Publishing Group, 459(7248), pp. 802–807. doi: 10.1038/nature08085.

Datta, S., Snow, C. J. and Paschal, B. M. (2014) 'A pathway linking oxidative stress and the Ran GTPase system in progeria', *Molecular Biology of the Cell*. Edited by K. Weis, 25(8), pp. 1202–1215. doi: 10.1091/mbc.e13-07-0430.

Deaton, A. M. and Bird, A. (2011) 'CpG islands and the regulation of transcription', *Genes and Development*, 25(10), pp. 1010–22. doi: 10.1101/gad.2037511.

Dechat, T. *et al.* (2008) 'Nuclear lamins: major factors in the structural organization and function of the nucleus and chromatin.', *Genes & development*. Cold Spring Harbor Laboratory Press, 22(7), pp. 832–53. doi: 10.1101/gad.1652708.

Dechat, T., Gesson K. and Foisner R. (2010) 'Lamina-Independent Lamins in the Nuclear Interior Serve Important Functions', *Cold Spring Harb Symp Quant Biol.* Cold Spring Harbor Laboratory Press, 75:533-543, doi: 10.1101/sqb.2010.75.018

Dechat, T., Adam, S. A. and Goldman, R. D. (2009) 'Nuclear lamins and chromatin: When structure meets function', *Advances in Enzyme Regulation*. Pergamon, 49(1), pp. 157–166. doi: 10.1016/J.ADVENZREG.2008.12.003.

Decker, M. L. *et al.* (2009) 'Telomere length in Hutchinson-Gilford Progeria Syndrome', *Mechanisms of Ageing and Development*, 130(6), pp. 377–383. doi: 10.1016/j.mad.2009.03.001.

Deng, J. *et al.* (2009) 'Targeted bisulfite sequencing reveals changes in DNA methylation associated with nuclear reprogramming', *Nature Biotechnology*, 27(4), pp. 353–360. doi: 10.1038/nbt.1530.

Devenny, D. A. *et al.* (2005) 'Dementia of the Alzheimer's Type and Accelerated Aging in Down Syndrome', *Science of Aging Knowledge Environment*, 2005(14), pp. dn1–dn1. doi: 10.1126/sageke.2005.14.dn1.

Dhe-Paganon, S. *et al.* (2002) 'Structure of the globular tail of nuclear lamin.', *The Journal of biological chemistry*. American Society for Biochemistry and Molecular Biology, 277(20), pp. 17381–4. doi: 10.1074/jbc.C200038200.

Dittmer, T. A. and Misteli, T. (2011) 'The lamin protein family', *Genome Biology*. BioMed Central, 12(5), p. 222. doi: 10.1186/gb-2011-12-5-222.

Dönertaş, H. M. *et al.* (2017) 'Gene expression reversal toward pre-adult levels in the aging human brain and age-

related loss of cellular identity', *Scientific Reports*. Nature Publishing Group, 7(1), p. 5894. doi: 10.1038/s41598-017-05927-4.

Dreesen, O. *et al.* (2013) 'Lamin B1 fluctuations have differential effects on cellular proliferation and senescence', *The Journal of Cell Biology*, 200(5), pp. 605–617. doi: 10.1083/jcb.201206121.

Driskell, R. R. and Watt, F. M. (2015) 'Understanding fibroblast heterogeneity in the skin', *Trends in Cell Biology*, 25(2), pp. 92–99. doi: 10.1016/j.tcb.2014.10.001.

Durso, D. F. *et al.* (2017) 'Acceleration of leukocytes' epigenetic age as an early tumor and sex-specific marker of breast and colorectal cancer', *Oncotarget*. Impact Journals, 8(14), pp. 23237–23245. doi: 10.18632/oncotarget.15573.

Endisha, H. *et al.* (2015) 'Restoring SIRT6 Expression in Hutchinson-Gilford Progeria Syndrome Cells Impedes Premature Senescence and Formation of Dysmorphic Nuclei', *Pathobiology*, 82(1), pp. 9–20. doi: 10.1159/000368856.

Eriksson, M. *et al.* (2003) 'Recurrent de novo point mutations in lamin A cause Hutchinson-Gilford progeria syndrome', *Nature*, 423(6937), pp. 293–298. doi: 10.1038/nature01629.

Farooq, Z. *et al.* (2016) 'The many faces of histone H3K79 methylation', *Mutation Research/Reviews in Mutation Research*. Elsevier, 768, pp. 46–52. doi: 10.1016/J.MRREV.2016.03.005.

Fawcett, D. W. (1966) 'On the occurrence of a fibrous lamina on the inner aspect of the nuclear envelope in certain cells of vertebrates', *American Journal of Anatomy*. John Wiley & Sons, Ltd, 119(1), pp. 129–145. doi: 10.1002/aja.1001190108.

Feser, J. *et al.* (2010) 'Elevated Histone Expression Promotes Life Span Extension', *Molecular Cell*. Cell Press, 39(5), pp. 724–735. doi: 10.1016/J.MOLCEL.2010.08.015.

Field, A. E. *et al.* (2018) 'DNA Methylation Clocks in Aging: Categories, Causes, and Consequences', *Molecular Cell*. Cell Press, 71(6), pp. 882–895. doi: 10.1016/J.MOLCEL.2018.08.008.

Fisher, D. Z., Chaudhary, N. and Blobel, G. (1986) 'cDNA sequencing of nuclear lamins A and C reveals primary and secondary structural homology to intermediate filament proteins.', *Proceedings of the National Academy of Sciences of the United States of America*. National Academy of Sciences, 83(17), pp. 6450–4. doi: 10.1073/pnas.83.17.6450.

Fishilevich, S. *et al.* (2017) 'GeneHancer: genome-wide integration of enhancers and target genes in GeneCards', *Database : the journal of biological databases and curation*, 2017 Jan 1. doi: 10.1093/database/bax028.

Fleischer, J. G. *et al.* (2018) 'Predicting age from the transcriptome of human dermal fibroblasts', *Genome Biology*, 19(1), p. 221. doi: 10.1186/s13059-018-1599-6.

Forsberg, F. *et al.* (2019) 'Interplay of lamin A and lamin B LADs on the radial positioning of chromatin', *Nucleus*, 10(1), pp. 7–20. doi: 10.1080/19491034.2019.1570810.

Fortin, J.-P. and Hansen, K. D. (2015) 'Reconstructing A/B compartments as revealed by Hi-C using long-range correlations in epigenetic data', *Genome Biology*. BioMed Central, 16(1), p. 180. doi: 10.1186/s13059-015-0741-y.

Foster, C. R. *et al.* (2010) 'Lamins as cancer biomarkers', *Biochemical Society Transactions*. Portland Press Limited, 38(1), pp. 297–300. doi: 10.1042/BST0380297.

Fraga, M. F. *et al.* (2005) 'Epigenetic differences arise during the lifetime of monozygotic twins', *Proceedings of the National Academy of Sciences*. National Academy of Sciences, 102(30), pp. 10604–10609. doi: 10.1073/PNAS.0500398102.

Freund, A. *et al.* (2012) 'Lamin B1 loss is a senescence-associated biomarker', *Molecular Biology of the Cell*. Edited by T. M. Magin, 23(11), pp. 2066–2075. doi: 10.1091/mbc.e11-10-0884.

Fujita, N. *et al.* (2003) 'Methyl-CpG Binding Domain 1 (MBD1) Interacts with the Suv39h1-HP1 Heterochromatic Complex for DNA Methylation-based Transcriptional Repression', *Journal of Biological Chemistry*, 278(26), pp. 24132–24138. doi: 10.1074/jbc.M302283200.

Fuks, F. *et al.* (2003) 'The DNA methyltransferases associate with HP1 and the SUV39H1 histone methyltransferase', *Nucleic Acids Research*, 31(9), pp. 2305–2312. doi: 10.1093/nar/gkg332.

Furukawa, K. and Hotta, Y. (1993) 'cDNA cloning of a germ cell specific lamin B3 from mouse spermatocytes and analysis of its function by ectopic expression in somatic cells.', *The EMBO Journal*. John Wiley & Sons, Ltd, 12(1), pp. 97–106. doi: 10.1002/j.1460-2075.1993.tb05635.x.

Gabriel, D. *et al.* (2015) 'Sulforaphane enhances progerin clearance in Hutchinson-Gilford progeria fibroblasts', *Aging Cell*, 14(1), pp. 78–91. doi: 10.1111/acel.12300.

Gabriel, D. *et al.* (2017) 'Intermittent treatment with farnesyltransferase inhibitor and sulforaphane improves cellular homeostasis in Hutchinson-Gilford progeria fibroblasts', *Oncotarget*, 8, pp. 64809–64826.

Gabriel, D., Gordon, L. B. and Djabali, K. (2016) 'Temsirolimus Partially Rescues the Hutchinson-Gilford Progeria Cellular Phenotype', *PLOS ONE*. Edited by V. Trajkovic, 11(12), p. e0168988. doi: 10.1371/journal.pone.0168988.

Gatticchi, L. *et al.* (2019) 'Optimization of DamID for use in primary cultures of mouse hepatocytes', *Methods*. Academic Press, 157, pp. 88–99. doi: 10.1016/J.YMETH.2018.11.005.

Gerace, L. and Huber, M. D. (2012) 'Nuclear lamina at the crossroads of the cytoplasm and nucleus', *Journal of Structural Biology*. Academic Press, 177(1), pp. 24–31. doi: 10.1016/J.JSB.2011.11.007.

Gesson, K. *et al.* (2016) 'A-type lamins bind both hetero- and euchromatin, the latter being regulated by lamina-associated polypeptide 2 alpha.', *Genome research*. Cold Spring Harbor Laboratory Press, 26(4), pp. 462–73. doi: 10.1101/gr.196220.115.

Gesson, K., Vidak, S. and Foisner, R. (2014) 'Lamina-associated polypeptide (LAP)2α and nucleoplasmic lamins in adult stem cell regulation and disease', *Seminars in Cell & Developmental Biology*. Academic Press, 29, pp. 116–124. doi: 10.1016/J.SEMCDB.2013.12.009.

Ghosh, S. *et al.* (2015) 'Lamin A Is an Endogenous SIRT6 Activator and Promotes SIRT6-Mediated DNA Repair', *Cell Reports*. The Authors, 13(7), pp. 1396–1406. doi: 10.1016/j.celrep.2015.10.006.

Gibbs-Seymour, I. *et al.* (2015) 'Lamin A/C-dependent interaction with 53BP1 promotes cellular responses to DNA damage', *Aging Cell*. John Wiley & Sons, Ltd (10.1111), 14(2), pp. 162–169. doi: 10.1111/acel.12258.

Giblin, W., Skinner, M. E. and Lombard, D. B. (2014) 'Sirtuins: guardians of mammalian healthspan', *Trends in Genetics*. Elsevier Current Trends, 30(7), pp. 271–286. doi: 10.1016/J.TIG.2014.04.007.

Gilford, H. (1904) 'Progeria: A form of senilism', *Practioner*, 73, pp. 188–217.

Goldberg, M. W. *et al.* (2008) 'Filaments made from A- and B-type lamins differ in structure and organization.', *Journal of cell science*. The Company of Biologists Ltd, 121(Pt 2), pp. 215–25. doi: 10.1242/jcs.022020.

Goldman, R. D. *et al.* (2004) 'Accumulation of mutant lamin A causes progressive changes in nuclear architecture in Hutchinson-Gilford progeria syndrome', *Proceedings of the National Academy of Sciences of the United States of America*, 101(24), pp. 8963–8968. doi: 10.1073/pnas.0402943101.

Gonzalez-Suarez, I. *et al.* (2009) 'Novel roles for A-type lamins in telomere biology and the DNA damage response pathway', *The EMBO Journal*. John Wiley & Sons, Ltd, 28(16), pp. 2414–2427. doi: 10.1038/emboj.2009.196.

Gonzalo, S. *et al.* (2005) 'Role of the RB1 family in stabilizing histone methylation at constitutive heterochromatin', *Nature Cell Biology*. Nature Publishing Group, 7(4), pp. 420–428. doi: 10.1038/ncb1235.

Gonzalo, S. (2014) 'DNA Damage and Lamins', in. Springer, New York, NY, pp. 377–399. doi: 10.1007/978-1-4899-8032-8_17.

Gonzalo, S. and Eissenberg, J. C. (2016) 'Tying up loose ends: telomeres, genomic instability and lamins', *Current Opinion in Genetics & Development*. Elsevier Current Trends, 37, pp. 109–118. doi: 10.1016/J.GDE.2016.03.003.

Gordon, L. B. *et al.* (2014) 'Impact of Farnesylation Inhibitors on Survival in Hutchinson-Gilford Progeria Syndrome',

Circulation, 130(1), pp. 27–34. doi: 10.1161/CIRCULATIONAHA.113.008285.

Grewal, S. I. S. and Jia, S. (2007) 'Heterochromatin revisited', *Nature Reviews Genetics*. Nature Publishing Group, 8(1), pp. 35–46. doi: 10.1038/nrg2008.

Grossman, E., Medalia, O. and Zwerger, M. (2012) 'Functional Architecture of the Nuclear Pore Complex', *Annual Review of Biophysics*. Annual Reviews , 41(1), pp. 557–584. doi: 10.1146/annurev-biophys-050511-102328.

Gruenbaum, Y. and Foisner, R. (2015) 'Lamins: Nuclear Intermediate Filament Proteins with Fundamental Functions in Nuclear Mechanics and Genome Regulation', *Annual Review of Biochemistry*. Annual Reviews , 84(1), pp. 131–164. doi: 10.1146/annurev-biochem-060614-034115.

Guelen, L. *et al.* (2008) 'Domain organization of human chromosomes revealed by mapping of nuclear lamina interactions', *Nature*, 453(7197), pp. 948–51. doi: 10.1038/nature06947.

Guo, Y. *et al.* (2014) 'Concentration-dependent lamin assembly and its roles in the localization of other nuclear proteins', *Molecular Biology of the Cell*. Edited by M. Hetzer, 25(8), pp. 1287–1297. doi: 10.1091/mbc.e13-11-0644.

Halaschek-Wiener, J. and Brooks-Wilson, A. (2007) 'Progeria of Stem Cells: Stem Cell Exhaustion in Hutchinson-Gilford Progeria Syndrome', *The Journals of Gerontology Series A: Biological Sciences and Medical Sciences*. Narnia, 62(1), pp. 3–8. doi: 10.1093/gerona/62.1.3.

Hamczyk, M. R., del Campo, L. and Andrés, V. (2018) 'Aging in the Cardiovascular System: Lessons from Hutchinson-Gilford Progeria Syndrome', *Annual Review of Physiology*. Annual Reviews , 80(1), pp. 27–48. doi: 10.1146/annurev-physiol-021317-121454.

Hannum, G. *et al.* (2013) 'Genome-wide Methylation Profiles Reveal Quantitative Views of Human Aging Rates', *Molecular Cell*. Elsevier Inc., 49(2), pp. 359–367. doi: 10.1016/j.molcel.2012.10.016.

Hansen, K. (2016) 'IlluminaHumanMethylationEPICmanifest'. Available at: https://bioconductor.org/packages/release/data/annotation/html/IlluminaHumanMethylationEPICmanifest.html (Accessed: 15 July 2019).

Hansen, K. D. *et al.* (2011) 'Increased methylation variation in epigenetic domains across cancer types', *Nature Genetics*. Nature Publishing Group, 43(8), pp. 768–775. doi: 10.1038/ng.865.

Hansen K (2016) 'IlluminaHumanMethylationEPICanno.ilm10b2.hg19'. Available at: https://bitbucket.com/kasperdanielhansen/Illumina_EPIC.

Harborth, J. *et al.* (2001) 'Identification of essential genes in cultured mammalian cells using small interfering RNAs', *Journal of Cell Science*, 114(24).

Harr, J. C. *et al.* (2015) 'Directed targeting of chromatin to the nuclear lamina is mediated by chromatin state and A-type lamins', *Journal of Cell Biology*, 208(1), pp. 33–52. doi: 10.1083/jcb.201405110.

Heessen, S. and Fornerod, M. (2007) 'The inner nuclear envelope as a transcription factor resting place', *EMBO Reports*. doi: 10.1038/sj.embor.7401075.

Hegele, R. A. *et al.* (2006) 'Sequencing of the reannotated LMNB2 gene reveals novel mutations in patients with acquired partial lipodystrophy.', *American journal of human genetics*. Elsevier, 79(2), pp. 383–9. doi: 10.1086/505885.

Heintzman, N. D. *et al.* (2009) 'Histone Modifications at Human Enhancers Reflect Global Cell Type-Specific Gene Expression', *Nature*. NIH Public Access, 459(7243), p. 108. doi: 10.1038/NATURE07829.

Heinz, S. *et al.* (2010) 'Simple Combinations of Lineage-Determining Transcription Factors Prime cis-Regulatory Elements Required for Macrophage and B Cell Identities', *Molecular Cell*, 38(4), pp. 576–589. doi: 10.1016/j.molcel.2010.05.004.

Helman, E. *et al.* (2014) 'Somatic retrotransposition in human cancer revealed by whole-genome and exome sequencing', *Genome Research*. Cold Spring Harbor Laboratory Press, 24(7), pp. 1053–1063. doi: 10.1101/GR.163659.113.

Hennekam, R. C. M. (2006) 'Hutchinson-Gilford progeria syndrome: Review of the phenotype', in *American Journal of Medical Genetics, Part A*, pp. 2603–2624. doi: 10.1002/ajmg.a.31346.

Hergeth, S. P. and Schneider, R. (2015) 'The H1 linker histones: multifunctional proteins beyond the nucleosomal core particle', *EMBO reports*. John Wiley & Sons, Ltd, 16(11), pp. 1439–1453. doi: 10.15252/embr.201540749.

Hernandez, L. *et al.* (2010) 'Functional coupling between the extracellular matrix and nuclear lamina by wnt signaling in progeria', *Developmental Cell*, 19(3), pp. 413–425. doi: 10.1016/j.devcel.2010.08.013.

Heyn, H. *et al.* (2012) 'Distinct DNA methylomes of newborns and centenarians', *Proc Natl Acad Sci USA*, 109(26), pp. 10522–10527.

Heyn, H., Moran, S. and Esteller, M. (2013) 'Aberrant DNA methylation profiles in the premature aging disorders Hutchinson-Gilford Progeria and Werner Syndrome', *Epigenetics*, 8(1), pp. 28–33. doi: 10.4161/epi.23366.

Hidai, C. *et al.* (1998) 'Cloning and characterization of developmental endothelial locus-1: An embryonic endothelial cell protein that binds the αvβ3 integrin receptor', *Genes and Development*, 12(1), pp. 21–33. doi: 10.1101/gad.12.1.21.

Ho, C. Y. *et al.* (2012) 'Lamins at a glance.', *Journal of cell science*. The Company of Biologists Ltd, 125(Pt 9), pp. 2087–93. doi: 10.1242/jcs.087288.

Hon, G. C. *et al.* (2012) 'Global DNA hypomethylation coupled to repressive chromatin domain formation and gene silencing in breast cancer', *Genome Research*, 22(2), pp. 246–258. doi: 10.1101/gr.125872.111.

Horvath, S. (2013) 'DNA methylation age of human tissues and cell types.', *Genome biology*, 14(10), p. R115. doi: 10.1186/gb-2013-14-10-r115.

Horvath, S. *et al.* (2014) 'Obesity accelerates epigenetic aging of human liver', *Proceedings of the National Academy of Sciences*, 111(43), pp. 15538–15543. doi: 10.1073/pnas.1412759111.

Horvath, S. *et al.* (2015) 'Accelerated epigenetic aging in Down syndrome', *Aging Cell*, 14(3), pp. 491–495. doi: 10.1111/acel.12325.

Horvath, S. *et al.* (2018) 'Epigenetic clock for skin and blood cells applied to Hutchinson Gilford Progeria Syndrome and ex vivo studies.', *Aging*, 10(7), pp. 1758–1775. doi: 10.18632/aging.101508.

Horvath, S. and Levine, A. J. (2015) 'HIV-1 Infection Accelerates Age According to the Epigenetic Clock', *Journal of Infectious Diseases*. Narnia, 212(10), pp. 1563–1573. doi: 10.1093/infdis/jiv277.

Horvath, S. and Raj, K. (2018) 'DNA methylation-based biomarkers and the epigenetic clock theory of ageing', *Nature Reviews Genetics*. Nature Publishing Group, 19(6), pp. 371–384. doi: 10.1038/s41576-018-0004-3.

Hovestadt, V. *et al.* (2014) 'Decoding the regulatory landscape of medulloblastoma using DNA methylation sequencing', *Nature*, 510(7506), pp. 537–541. doi: 10.1038/nature13268.

Huang, S. *et al.* (2005) 'Correction of cellular phenotypes of Hutchinson-Gilford Progeria cells by RNA interference', *Human Genetics*, 118(3–4), pp. 444–450. doi: 10.1007/s00439-005-0051-7.

Hutchinson, J. (1886) 'Congenital Absence of Hair and Mammary Glands with Atrophic Condition of the Skin and its Appendages, in a Boy whose Mother had been almost wholly Bald from Alopecia Areata from the age of Six.', *Medico-chirurgical transactions*. Royal Society of Medicine Press, 69, pp. 473–7. doi: 10.1177/095952878606900127.

Hutchison, C. J. (2002) 'Lamins: building blocks or regulators of gene expression?', *Nature Reviews Molecular Cell Biology*. Nature Publishing Group, 3(11), pp. 848–858. doi: 10.1038/nrm950.

Hyun, K. *et al.* (2017) 'Writing, erasing and reading histone lysine methylations', *Experimental & Molecular Medicine*. Nature Publishing Group, 49(4), pp. e324–e324. doi: 10.1038/emm.2017.11.

Irianto, J. *et al.* (2016) 'Nuclear Lamins in Cancer', *Cellular and Molecular Bioengineering*. Springer US, 9(2), pp. 258–267. doi: 10.1007/s12195-016-0437-8.

Issa, J.-P. (2014) 'Aging and epigenetic drift: a vicious cycle', *The Journal of Clinical Investigation*. American Society for Clinical Investigation, 124(1), pp. 24–29. doi: 10.1172/JCI69735.

Ivorra, C. *et al.* (2006) 'A mechanism of AP-1 suppression through interaction of c-Fos with lamin A/C', *Genes and Development*, 20(3), pp. 307–320. doi: 10.1101/gad.349506.

Jamin, A. and Wiebe, M. S. (2015) 'Barrier to Autointegration Factor (BANF1): interwoven roles in nuclear structure, genome integrity, innate immunity, stress responses and progeria', *Current Opinion in Cell Biology*. Elsevier Current Trends, 34, pp. 61–68. doi: 10.1016/J.CEB.2015.05.006.

Jintaridth, P. and Mutirangura, A. (2010) 'Distinctive patterns of age-dependent hypomethylation in interspersed repetitive sequences', *Physiological Genomics*. American Physiological Society Bethesda, MD, 41(2), pp. 194–200. doi: 10.1152/physiolgenomics.00146.2009.

Johnson, B. R. *et al.* (2004) 'A-type lamins regulate retinoblastoma protein function by promoting subnuclear localization and preventing proteasomal degradation.', *Proceedings of the National Academy of Sciences of the United States of America*. National Academy of Sciences, 101(26), pp. 9677–82. doi: 10.1073/pnas.0403250101.

Jones, P. A. and Takai, D. (2001) 'The role of DNA methylation in mammalian epigenetics.', *Science (New York, N.Y.)*. American Association for the Advancement of Science, 293(5532), pp. 1068–70. doi: 10.1126/science.1063852.

Kazemi, M., Salehi, M. and Kheirollahi, M. (2016) 'Down Syndrome: Current Status, Challenges and Future Perspectives.', *International journal of molecular and cellular medicine*. Babol University of Medical Sciences, 5(3), pp. 125–133. Available at: http://www.ncbi.nlm.nih.gov/pubmed/27942498 (Accessed: 15 July 2019).

Kelley, J. B. *et al.* (2011) 'The Defective Nuclear Lamina in Hutchinson-Gilford Progeria Syndrome Disrupts the Nucleocytoplasmic Ran Gradient and Inhibits Nuclear Localization of Ubc9', *Molecular and Cellular Biology*, 31(16), pp. 3378–3395. doi: 10.1128/MCB.05087-11.

Kim, D. *et al.* (2013) 'TopHat2: accurate alignment of transcriptomes in the presence of insertions, deletions and gene fusions.', *Genome biology*, 14(1), p. R36. doi: 10.1186/gb-2013-14-4-r36.

Kim, Y. *et al.* (2011) 'Mouse B-Type Lamins Are Required for Proper Organogenesis But Not by Embryonic Stem Cells', *Science*. American Association for the Advancement of Science, 334(6063), pp. 1706–1710. doi: 10.1126/SCIENCE.1211222.

Kind, J. *et al.* (2013) 'Single-cell dynamics of genome-nuclear lamina interactions.', *Cell*. Elsevier, 153(1), pp. 178–92. doi: 10.1016/j.cell.2013.02.028.

Kind, J. *et al.* (2015) 'Genome-wide maps of nuclear lamina interactions in single human cells.', *Cell*. Elsevier, 163(1), pp. 134–47. doi: 10.1016/j.cell.2015.08.040.

Kind, J. and van Steensel, B. (2014) 'Stochastic genome-nuclear lamina interactions', *Nucleus*, 5(2), pp. 124–130. doi: 10.4161/nucl.28825.

Kohwi, M. *et al.* (2013) 'Developmentally regulated subnuclear genome reorganization restricts neural progenitor competence in Drosophila.', *Cell*. Elsevier, 152(1–2), pp. 97–108. doi: 10.1016/j.cell.2012.11.049.

van Koningsbruggen, S. *et al.* (2010) 'High-Resolution Whole-Genome Sequencing Reveals That Specific Chromatin Domains from Most Human Chromosomes Associate with Nucleoli', *Molecular Biology of the Cell*. Edited by A. G. Matera, 21(21), pp. 3735–3748. doi: 10.1091/mbc.e10-06-0508.

Kornberg, R. D. (1974) 'Chromatin structure: a repeating unit of histones and DNA.', *Science (New York, N.Y.)*. American Association for the Advancement of Science, 184(4139), pp. 868–71. doi: 10.1126/science.184.4139.868.

Kreienkamp, R. *et al.* (2016) 'Vitamin D receptor signaling improves Hutchinson-Gilford progeria syndrome cellular phenotypes', *Oncotarget*, 7(21), pp. 30018–31. doi: 10.18632/oncotarget.9065.

Kubben, N. *et al.* (2012) 'Mapping of lamin A- and progerin-interacting genome regions', *Chromosoma*, 121(5), pp. 447–464. doi: 10.1007/s00412-012-0376-7.

Kubben, N. *et al.* (2016) 'Repression of the Antioxidant NRF2 Pathway in Premature Aging', *Cell*, 165(6), pp. 1361–1374. doi: 10.1016/j.cell.2016.05.017.

Kubben, N. and Misteli, T. (2017) 'Shared molecular and cellular mechanisms of premature ageing and ageing-associated diseases', *Nature Reviews Molecular Cell Biology*. Nature Publishing Group, 18(10), pp. 595–609. doi: 10.1038/nrm.2017.68.

Lachner, M. *et al.* (2001) 'Methylation of histone H3 lysine 9 creates a binding site for HP1 proteins', *Nature*. Nature Publishing Group, 410(6824), pp. 116–120. doi: 10.1038/35065132.

Lammerding, J. *et al.* (2006) 'Lamins A and C but Not Lamin B1 Regulate Nuclear Mechanics', *Journal of Biological Chemistry*. American Society for Biochemistry and Molecular Biology, 281(35), pp. 25768–25780. doi: 10.1074/JBC.M513511200.

Langmead, B. and Salzberg, S. L. (2012) 'Fast gapped-read alignment with Bowtie 2.', *Nature methods*, 9(4), pp. 357–359. doi: 10.1038/nmeth.1923.

Lê, S., Josse, J. and Husson, F. (2008) 'FactoMineR: An R Package for Multivariate Analysis', *J. of Statistical Software*, 25(1). doi: 10.1016/j.envint.2008.06.007.

Lee, E. *et al.* (2012) 'Landscape of somatic retrotransposition in human cancers.', *Science (New York, N.Y.)*. American Association for the Advancement of Science, 337(6097), pp. 967–71. doi: 10.1126/science.1222077.

de Leeuw, R., Gruenbaum, Y. and Medalia, O. (2018) 'Nuclear Lamins: Thin Filaments with Major Functions.', *Trends in cell biology*. Elsevier, 28(1), pp. 34–45. doi: 10.1016/j.tcb.2017.08.004.

Lehnertz, B. *et al.* (2003) 'Suv39h-Mediated Histone H3 Lysine 9 Methylation Directs DNA Methylation to Major Satellite Repeats at Pericentric Heterochromatin', *Current Biology*. Cell Press, 13(14), pp. 1192–1200. doi: 10.1016/S0960-9822(03)00432-9.

Lenain, C. *et al.* (2017) 'Massive reshaping of genome-nuclear lamina interactions during oncogene-induced senescence.', *Genome research*. Cold Spring Harbor Laboratory Press, 27(10), pp. 1634–1644. doi: 10.1101/gr.225763.117.

Levine, M. E. *et al.* (2018) 'An epigenetic biomarker of aging for lifespan and healthspan.', *Aging*. Impact Journals, LLC, 10(4), pp. 573–591. doi: 10.18632/aging.101414.

Lewis, K. N. *et al.* (2010) 'Nrf2, a Guardian of Healthspan and Gatekeeper of Species Longevity', *Integrative and Comparative Biology*. Narnia, 50(5), pp. 829–843. doi: 10.1093/icb/icq034.

Li, E., Beard, C. and Jaenisch, R. (1993) 'Role for DNA methylation in genomic imprinting', *Nature*. Nature Publishing Group, 366(6453), pp. 362–365. doi: 10.1038/366362a0.

Li, Q. *et al.* (2008) 'Acetylation of Histone H3 Lysine 56 Regulates Replication-Coupled Nucleosome Assembly', *Cell*. Cell Press, 134(2), pp. 244–255. doi: 10.1016/J.CELL.2008.06.018.

Liberzon, A. *et al.* (2015) 'The Molecular Signatures Database Hallmark Gene Set Collection', *Cell Systems*, 1(6), pp. 417–425. doi: 10.1016/j.cels.2015.12.004.

Lin, F. and Worman, H. J. (1993) 'Structural organization of the human gene encoding nuclear lamin A and nuclear lamin C.', *The Journal of biological chemistry*, 268(22), pp. 16321–16326. doi: 10.1006/geno.1995.1036.

Lin F and Worman HJ (1995) 'Structural Organization of the Human Gene (LMNB1) Encoding Nuclear Lamin B1', *Genomics*, 27(2), pp. 230–236.

Lin, K. C., Park, H. W. and Guan, K.-L. (2017) 'Regulation of the Hippo Pathway Transcription Factor TEAD', *Trends in Biochemical Sciences*, 42(11), pp. 862–872. doi: 10.1016/j.tibs.2017.09.003.

Lister, R. *et al.* (2009) 'Human DNA methylomes at base resolution show widespread epigenomic differences', *Nature*. Nature Publishing Group, 462(7271), pp. 315–322. doi: 10.1038/nature08514.

Liu, B. *et al.* (2005) 'Genomic instability in laminopathy-based premature aging', *Nature medicine*, 11(7), pp. 780–5.

doi: 10.1038/nm1266.

Liu, G. *et al.* (2011) 'Recapitulation of premature ageing with iPSCs from Hutchinson-Gilford progeria syndrome', *Nature*. Nature Publishing Group, 472(7342), pp. 221–225. doi: 10.1038/nature09879.

Liu, Y. *et al.* (2008) 'Involvement of xeroderma pigmentosum group A (XPA) in progeria arising from defective maturation of prelamin A', *The FASEB Journal*. Federation of American Societies for Experimental Biology, 22(2), pp. 603–611. doi: 10.1096/fj.07-8598com.

López-Otín, C. *et al.* (2013) 'The Hallmarks of Aging', *Cell*, 153(6), pp. 1194–217. doi: 10.1016/j.cell.2013.05.039.
Love, M. I., Huber, W. and Anders, S. (2014) 'Moderated estimation of fold change and dispersion for RNA-seq data with DESeq2', *Genome Biology*, 15(12), p. 550. doi: 10.1186/s13059-014-0550-8.

Luger, K. *et al.* (1997) 'Crystal structure of the nucleosome core particle at 2.8 Å resolution', *Nature*. Nature Publishing Group, 389(6648), pp. 251–260. doi: 10.1038/38444.

Lund, E. *et al.* (2013) 'Lamin A/C-promoter interactions specify chromatin state-dependent transcription outcomes.', *Genome research*. Cold Spring Harbor Laboratory Press, 23(10), pp. 1580–9. doi: 10.1101/gr.159400.113.

Lund, E. G. *et al.* (2015) 'Distinct features of lamin A-interacting chromatin domains mapped by Chip-sequencing from sonicated or micrococcal nuclease-digested chromatin', *Nucleus*, 6(1), pp. 30–39. doi: 10.4161/19491034.2014.990855.

Luo, C. *et al.* (2017) 'Single-cell methylomes identify neuronal subtypes and regulatory elements in mammalian cortex.', *Science (New York, N.Y.)*. NIH Public Access, 357(6351), pp. 600–604. doi: 10.1126/science.aan3351.

Ly, D. H. *et al.* (2000) 'Mitotic Misregulation and Human Aging', *Science*, 287(5462), pp. 2486–2492. doi: 10.1126/science.287.5462.2486.

Lyko, F. (2018) 'The DNA methyltransferase family: A versatile toolkit for epigenetic regulation', *Nature Reviews Genetics*, 19(2), pp. 81–92. doi: 10.1038/nrg.2017.80.

Ma, Q. (2013) 'Role of Nrf2 in Oxidative Stress and Toxicity', *Annual Review of Pharmacology and Toxicology*, 53(1), pp. 401–426. doi: 10.1146/annurev-pharmtox-011112-140320.

Machiels, B. M. *et al.* (1996) 'An alternative splicing product of the lamin A/C gene lacks exon 10.', *The Journal of biological chemistry*. American Society for Biochemistry and Molecular Biology, 271(16), pp. 9249–53. doi: 10.1074/jbc.271.16.9249.

Maierhofer, A. *et al.* (2017) 'Accelerated epigenetic aging in Werner syndrome', *Aging*, 9(4), pp. 1143–1152. doi: 10.18632/aging.101217.

Maison, C. and Almouzni, G. (2004) 'HP1 and the dynamics of heterochromatin maintenance', *Nature Reviews Molecular Cell Biology*. Nature Publishing Group, 5(4), pp. 296–305. doi: 10.1038/nrm1355.

Mao, Z. *et al.* (2011) 'SIRT6 Promotes DNA Repair Under Stress by Activating PARP1', *Science*. American Association for the Advancement of Science, 332(6036), pp. 1443–1446. doi: 10.1126/SCIENCE.1202723.

Marioni, R. E. *et al.* (2015) 'DNA methylation age of blood predicts all-cause mortality in later life', *Genome Biology*. BioMed Central, 16(1), p. 25. doi: 10.1186/s13059-015-0584-6.

Marji, J. *et al.* (2010) 'Defective Lamin A-Rb Signaling in Hutchinson-Gilford Progeria Syndrome and Reversal by Farnesyltransferase Inhibition', *PLoS ONE*. Edited by M. V. Blagosklonny, 5(6), p. e11132. doi: 10.1371/journal.pone.0011132.

Marshall, O. J. and Brand, A. H. (2015) 'damidseq_pipeline: an automated pipeline for processing DamID sequencing datasets: Fig. 1.', *Bioinformatics*, 31(20), pp. 3371–3373. doi: 10.1093/bioinformatics/btv386.

Mattout, A. *et al.* (2011) 'An EDMD Mutation in C. elegans Lamin Blocks Muscle-Specific Gene Relocation and Compromises Muscle Integrity', *Current Biology*. Elsevier, 21(19), pp. 1603–1614. doi: 10.1016/J.CUB.2011.08.030.

Matys, V. (2006) 'TRANSFAC(R) and its module TRANSCompel(R): transcriptional gene regulation in eukaryotes',

Nucleic Acids Research, 34(Issue suppl_1), pp. D108-110. doi: 10.1093/nar/gkj143.

McClintock, D. *et al.* (2007) 'The Mutant Form of Lamin A that Causes Hutchinson-Gilford Progeria Is a Biomarker of Cellular Aging in Human Skin', *PLoS ONE*, 2(12), p. e1269. doi: 10.1371/journal.pone.0001269.

McCord, R. P. *et al.* (2013) 'Correlated alterations in genome organization, histone methylation, and DNA-lamin A/C interactions in Hutchinson-Gilford progeria syndrome', *Genome Research*, 23(2), pp. 260–269. doi: 10.1101/gr.138032.112.

McEwen, L. M. *et al.* (2018) 'Systematic evaluation of DNA methylation age estimation with common preprocessing methods and the Infinium MethylationEPIC BeadChip array', *Clinical Epigenetics*, 10(1), p. 123. doi: 10.1186/s13148-018-0556-2.

McHugh, D. and Gil, J. (2018) 'Senescence and aging: Causes, consequences, and therapeutic avenues.', *The Journal of cell biology*. The Rockefeller University Press, 217(1), pp. 65–77. doi: 10.1083/jcb.201708092.

Meaburn, K. J. *et al.* (2007) 'Primary laminopathy fibroblasts display altered genome organization and apoptosis', *Aging Cell*. doi: 10.1111/j.1474-9726.2007.00270.x.

Mehta, I. S. *et al.* (2011) 'Farnesyltransferase inhibitor treatment restores chromosome territory positions and active chromosome dynamics in Hutchinson-Gilford progeria syndrome cells', *Genome Biology*, 12(8), p. R74. doi: 10.1186/gb-2011-12-8-r74.

Mehta, I. S. *et al.* (2013) 'Chromosome territories reposition during DNA damage-repair response.', *Genome biology*. BioMed Central, 14(12), p. R135. doi: 10.1186/gb-2013-14-12-r135.

Merideth, M. A. *et al.* (2008) 'Phenotype and Course of Hutchinson–Gilford Progeria Syndrome', *New England Journal of Medicine*, 358(6), pp. 592–604. doi: 10.1056/NEJMoa0706898.

Meshorer, E. and Gruenbaum, Y. (2008) 'Gone with the Wnt/Notch: stem cells in laminopathies, progeria, and aging.', *The Journal of cell biology*. Rockefeller University Press, 181(1), pp. 9–13. doi: 10.1083/jcb.200802155.

Meuleman, W. *et al.* (2013) 'Constitutive nuclear lamina-genome interactions are highly conserved and associated with A/T-rich sequence.', *Genome research*. Cold Spring Harbor Laboratory Press, 23(2), pp. 270–80. doi: 10.1101/gr.141028.112.

Miller, J. D. *et al.* (2013) 'Human iPSC-based modeling of late-onset disease via progerin-induced aging.', *Cell stem cell*. NIH Public Access, 13(6), pp. 691–705. doi: 10.1016/j.stem.2013.11.006.

Moye, A. L. *et al.* (2015) 'Telomeric G-quadruplexes are a substrate and site of localization for human telomerase', *Nature Communications*. doi: 10.1038/ncomms8643.

Naetar, N., Ferraioli, S. and Foisner, R. (2017) 'Lamins in the nuclear interior − life outside the lamina', *Journal of Cell Science*. The Company of Biologists Ltd, 130(13), pp. 2087–2096. doi: 10.1242/JCS.203430.

Neri, F. *et al.* (2017) 'Intragenic DNA methylation prevents spurious transcription initiation', *Nature*. Nature Publishing Group, 543(7643), pp. 72–77. doi: 10.1038/nature21373.

Ni, Z. *et al.* (2012) 'Two SET domain containing genes link epigenetic changes and aging in Caenorhabditis elegans', *Aging Cell*. John Wiley & Sons, Ltd (10.1111), 11(2), pp. 315–325. doi: 10.1111/j.1474-9726.2011.00785.x.

Niessen, K. and Karsan, A. (2008) 'Notch Signaling in Cardiac Development', *Circulation Research*, 102(10), pp. 1169–1181. doi: 10.1161/CIRCRESAHA.108.174318.

Nissan, X. *et al.* (2012) 'Unique Preservation of Neural Cells in Hutchinson- Gilford Progeria Syndrome Is Due to the Expression of the Neural-Specific miR-9 MicroRNA', *Cell Reports*. Elsevier, 2(1), pp. 1–9. doi: 10.1016/J.CELREP.2012.05.015.

O'Sullivan, R. J. *et al.* (2010) 'Reduced histone biosynthesis and chromatin changes arising from a damage signal at telomeres', *Nature Structural & Molecular Biology*. Nature Publishing Group, 17(10), pp. 1218–1225. doi: 10.1038/nsmb.1897.

Oldenburg, A. *et al.* (2017) 'A lipodystrophy-causing lamin A mutant alters conformation and epigenetic regulation of the anti-adipogenic MIR335 locus.', *The Journal of cell biology*. Rockefeller University Press, 216(9), pp. 2731–2743. doi: 10.1083/jcb.201701043.

Olins, A. L. *et al.* (2010) 'Lamin B receptor: multi-tasking at the nuclear envelope.', *Nucleus*. Taylor & Francis, 1(1), pp. 53–70. doi: 10.4161/nucl.1.1.10515.

Olive, M. *et al.* (2010) 'Cardiovascular Pathology in Hutchinson-Gilford Progeria: Correlation With the Vascular Pathology of Aging', *Arteriosclerosis, Thrombosis, and Vascular Biology*, 30(11), pp. 2301–2309. doi: 10.1161/ATVBAHA.110.209460.

Ooi, S. K. T. *et al.* (2007) 'DNMT3L connects unmethylated lysine 4 of histone H3 to de novo methylation of DNA', *Nature*, 448(7154), pp. 714–717. doi: 10.1038/nature05987.

Osmanagic-Myers, S. *et al.* (2018) 'Endothelial progerin expression causes cardiovascular pathology through an impaired mechanoresponse', *Journal of Clinical Investigation*, 129(2), pp. 531–545. doi: 10.1172/JCI121297.

Osmanagic-Myers, S., Dechat, T. and Foisner, R. (2015) 'Lamins at the crossroads of mechanosignaling.', *Genes & development*. Cold Spring Harbor Laboratory Press, 29(3), pp. 225–37. doi: 10.1101/gad.255968.114.

Ottaviani, A. *et al.* (2009) 'Identification of a perinuclear positioning element in human subtelomeres that requires A-type lamins and CTCF', *EMBO Journal*. doi: 10.1038/emboj.2009.201.

Padiath, Q. S. *et al.* (2006) 'Lamin B1 duplications cause autosomal dominant leukodystrophy', *Nature Genetics*. Nature Publishing Group, 38(10), pp. 1114–1123. doi: 10.1038/ng1872.

Pal, S. and Tyler, J. K. (2016) 'Epigenetics and aging', *Science Advances*. American Association for the Advancement of Science, 2(7), p. e1600584. doi: 10.1126/sciadv.1600584.

Paradisi, M. *et al.* (2005) 'Dermal fibroblasts in Hutchinson-Gilford progeria syndrome with the lamin A G608G mutation have dysmorphic nuclei and are hypersensitive to heat stress.', *BMC Cell Biology*, 6(1), p. 27. doi: 10.1186/1471-2121-6-27.

Park, S.-K. and Shin, O. S. (2017) 'Metformin alleviates ageing cellular phenotypes in Hutchinson-Gilford progeria syndrome dermal fibroblasts', *Experimental Dermatology*, 26(10), pp. 889–895. doi: 10.1111/exd.13323.

Park, W.-Y. *et al.* (2001) 'Gene Profile of Replicative Senescence Is Different from Progeria or Elderly Donor', *Biochemical and Biophysical Research Communications*, 282(4), pp. 934–939. doi: 10.1006/bbrc.2001.4632.

Parry, D. A. D., Conway, J. F. and Steinert, P. M. (1986) 'Structural studies on lamin. Similarities and differences between lamin and intermediate-filament proteins', *Biochemical Journal*. Portland Press Limited, 238(1), pp. 305–308. doi: 10.1042/BJ2380305.

Patterson, D. and Cabelof, D. C. (2012) 'Down syndrome as a model of DNA polymerase beta haploinsufficiency and accelerated aging', *Mechanisms of Ageing and Development*, 133(4), pp. 133–137. doi: 10.1016/j.mad.2011.10.001.
Pellegrini, C. *et al.* (2015) 'All-trans retinoic acid and rapamycin normalize Hutchinson Gilford progeria fibroblast phenotype', *Oncotarget*, 6(30), pp. 29914–28. doi: 10.18632/oncotarget.4939.

Pen, A. *et al.* (2008) 'Glioblastoma-secreted factors induce IGFBP7 and angiogenesis by modulating Smad-2-dependent TGF-β signaling', *Oncogene*, 27(54), pp. 6834–6844. doi: 10.1038/onc.2008.287.

Pendás, A. M. *et al.* (2002) 'Defective prelamin A processing and muscular and adipocyte alterations in Zmpste24 metalloproteinase–deficient mice', *Nature Genetics*. Nature Publishing Group, 31(1), pp. 94–99. doi: 10.1038/ng871.

Pereira, S. *et al.* (2008) 'HGPS and related premature aging disorders: From genomic identification to the first therapeutic approaches', *Mechanisms of Ageing and Development*, 129(7–8), pp. 449–459. doi: 10.1016/j.mad.2008.04.003.

Pérez, R. F. *et al.* (2018) 'Distinct chromatin signatures of DNA hypomethylation in aging and cancer', *Aging Cell*. John Wiley & Sons, Ltd (10.1111), 17(3), p. e12744. doi: 10.1111/acel.12744.

Peric-Hupkes, D. *et al.* (2010) 'Molecular Maps of the Reorganization of Genome-Nuclear Lamina Interactions during

Differentiation', *Molecular Cell*, 38(4), pp. 603–613. doi: 10.1016/j.molcel.2010.03.016.

Perovanovic, J. *et al.* (2016) 'Laminopathies disrupt epigenomic developmental programs and cell fate', *Science translational medicine*. NIH Public Access, 8(335), p. 335ra58. doi: 10.1126/SCITRANSLMED.AAD4991.

Peter, M. *et al.* (1989) 'Cloning and sequencing of cDNA clones encoding chicken lamins A and B1 and comparison of the primary structures of vertebrate A- and B-type lamins', *Journal of Molecular Biology*. Academic Press, 208(3), pp. 393–404. doi: 10.1016/0022-2836(89)90504-4.

Picelli, S. *et al.* (2014) 'Tn5 transposase and tagmentation procedures for massively scaled sequencing projects', *Genome Research*, 24(12), pp. 2033–2040. doi: 10.1101/gr.177881.114.

Pickersgill, H. *et al.* (2006) 'Characterization of the Drosophila melanogaster genome at the nuclear lamina', *Nature Genetics*. Nature Publishing Group, 38(9), pp. 1005–1014. doi: 10.1038/ng1852.

Pinheiro, I. *et al.* (2012) 'Prdm3 and Prdm16 are H3K9me1 Methyltransferases Required for Mammalian Heterochromatin Integrity', *Cell*. Cell Press, 150(5), pp. 948–960. doi: 10.1016/J.CELL.2012.06.048.

Plasilova, M. *et al.* (2011) 'Discordant Gene Expression Signatures and Related Phenotypic Differences in Lamin A- and A/C-Related Hutchinson-Gilford Progeria Syndrome (HGPS)', *PLoS ONE*. Edited by K. T. Jeang, 6(6), p. e21433. doi: 10.1371/journal.pone.0021433.

Pobbati, A. V. and Hong, W. (2013) 'Emerging roles of TEAD transcription factors and its coactivators in cancers', *Cancer Biology & Therapy*, 14(5), pp. 390–398. doi: 10.4161/cbt.23788.

Poleshko, A. *et al.* (2013) 'The human protein PRR14 tethers heterochromatin to the nuclear lamina during interphase and mitotic exit.', *Cell reports*. Elsevier, 5(2), pp. 292–301. doi: 10.1016/j.celrep.2013.09.024.

Poleshko, A. *et al.* (2017) 'Genome-Nuclear Lamina Interactions Regulate Cardiac Stem Cell Lineage Restriction', *Cell*, 171(3), pp. 573-587.e14. doi: 10.1016/j.cell.2017.09.018.

Prokocimer, M., Barkan, R. and Gruenbaum, Y. (2013) 'Hutchinson-Gilford progeria syndrome through the lens of transcription', *Aging Cell*, 12(4), pp. 533–543. doi: 10.1111/acel.12070.

Pu, M. *et al.* (2015) 'Trimethylation of Lys36 on H3 restricts gene expression change during aging and impacts life span.', *Genes & development*. Cold Spring Harbor Laboratory Press, 29(7), pp. 718–31. doi: 10.1101/gad.254144.114.

Quach, A. *et al.* (2017) 'Epigenetic clock analysis of diet, exercise, education, and lifestyle factors.', *Aging*, 9(2), pp. 419–446. doi: 10.18632/aging.101168.

Rober, R. A. *et al.* (1990) 'Cells of the cellular immune and hemopoietic system of the mouse lack lamins A/C: distinction versus other somatic cells', *Journal of Cell Science*, 95(4).

Rober, R. A., Weber, K. and Osborn, M. (1989) 'Differential timing of nuclear lamin A/C expression in the various organs of the mouse embryo and the young animal: a developmental study', *Development*, 105(2).

Robertson, K. D. (2002) 'DNA methylation and chromatin – unraveling the tangled web', *Oncogene*, 21(35), pp. 5361–5379. doi: 10.1038/sj.onc.1205609.

Robson, M. I. *et al.* (2016) 'Tissue-Specific Gene Repositioning by Muscle Nuclear Membrane Proteins Enhances Repression of Critical Developmental Genes during Myogenesis', *Molecular Cell*. Cell Press, 62(6), pp. 834–847. doi: 10.1016/J.MOLCEL.2016.04.035.

Robson, M. I. *et al.* (2017) 'Constrained release of lamina-associated enhancers and genes from the nuclear envelope during T-cell activation facilitates their association in chromosome compartments.', *Genome research*. Cold Spring Harbor Laboratory Press, 27(7), pp. 1126–1138. doi: 10.1101/gr.212308.116.

Rodríguez-Paredes, M. *et al.* (2018) 'Methylation profiling identifies two subclasses of squamous cell carcinoma related to distinct cells of origin', *Nature Communications*. Nature Publishing Group, 9(1), p. 577. doi: 10.1038/s41467-018-03025-1.

Rork, J. F. *et al.* (2014) 'Initial Cutaneous Manifestations of Hutchinson-Gilford Progeria Syndrome', *Pediatric Dermatology*, 31(2), pp. 196–202. doi: 10.1111/pde.12284.

Rose, N. R. and Klose, R. J. (2014) 'Understanding the relationship between DNA methylation and histone lysine methylation', *Biochimica et Biophysica Acta (BBA) - Gene Regulatory Mechanisms*. Elsevier B.V., 1839(12), pp. 1362–1372. doi: 10.1016/j.bbagrm.2014.02.007.

Rueden, C. T. *et al.* (2017) 'ImageJ2: ImageJ for the next generation of scientific image data', *BMC Bioinformatics*, 18(1), p. 529. doi: 10.1186/s12859-017-1934-z.

Sakthivel, K. M. and Sehgal, P. (2016) 'A novel role of lamins from genetic disease to cancer biomarkers', *Oncology Reviews*, 10(2). doi: 10.4081/oncol.2016.309.

Salhab, A. *et al.* (2018) 'A comprehensive analysis of 195 DNA methylomes reveals shared and cell-specific features of partially methylated domains', *Genome Biology*. BioMed Central, 19(1), p. 150. doi: 10.1186/s13059-018-1510-5.

Salk, D. (1982) 'Can We Learn about Aging from a Study of Werner's Syndrome?', *Journal of the American Geriatrics Society*, 30(5), pp. 334–339. doi: 10.1111/j.1532-5415.1982.tb05624.x.

Salzer, M. C. *et al.* (2018) 'Identity Noise and Adipogenic Traits Characterize Dermal Fibroblast Aging.', *Cell*. Elsevier, 175(6), pp. 1575-1590.e22. doi: 10.1016/j.cell.2018.10.012.

De Sandre-Giovannoli, A. *et al.* (2003) 'Lamin A truncation in Hutchinson-Gilford progeria', *Science (New York, N.Y.)*, 300(5628), p. 2055. doi: 10.1126/science.1084125.

Santiago-Fernández, O. *et al.* (2019) 'Development of a CRISPR/Cas9-based therapy for Hutchinson–Gilford progeria syndrome', *Nature Medicine*, 25(3), pp. 423–426. doi: 10.1038/s41591-018-0338-6.

Scaffidi, P. and Misteli, T. (2005) 'Reversal of the cellular phenotype in the premature aging disease Hutchinson-Gilford progeria syndrome', *Nature Medicine*. Nature Publishing Group, 11(4), pp. 440–445. doi: 10.1038/nm1204.

Scaffidi, P. and Misteli, T. (2006) 'Lamin A-dependent nuclear defects in human aging.', *Science (New York, N.Y.)*, 312(5776), pp. 1059–63. doi: 10.1126/science.1127168.

Schindelin, J. *et al.* (2012) 'Fiji: An open-source platform for biological-image analysis', *Nature Methods*, 9(7), pp. 676–682. doi: 10.1038/nmeth.2019.

Schlegelberger, B, Metzke S, Harder S, Zühlke-Jenisch R, Zhang Y, S. R. (1999) 'Classical and molecular Cytogenetics of tumor cells', in *Diagnostic Cytogenetics*. Springer, Berlin, Heidelberg, pp. 151–185. doi: https://doi.org/10.1007/978-3-642-59918-7_9.

Schotta, G. *et al.* (2004) 'A silencing pathway to induce H3-K9 and H4-K20 trimethylation at constitutive heterochromatin.', *Genes & development*. Cold Spring Harbor Laboratory Press, 18(11), pp. 1251–62. doi: 10.1101/gad.300704.

Schroeder, D. I. *et al.* (2011) 'Large-scale methylation domains mark a functional subset of neuronally expressed genes', *Genome Research*, 21(10), pp. 1583–1591. doi: 10.1101/gr.119131.110.

Sen, P. *et al.* (2015) 'H3K36 methylation promotes longevity by enhancing transcriptional fidelity.', *Genes & development*. Cold Spring Harbor Laboratory Press, 29(13), pp. 1362–76. doi: 10.1101/gad.263707.115.

Sen, P. *et al.* (2016) 'Epigenetic Mechanisms of Longevity and Aging', *Cell*. Cell Press, 166(4), pp. 822–839. doi: 10.1016/J.CELL.2016.07.050.

Shah, P. P. *et al.* (2013) 'Lamin B1 depletion in senescent cells triggers large-scale changes in gene expression and the chromatin landscape.', *Genes & development*. Cold Spring Harbor Laboratory Press, 27(16), pp. 1787–99. doi: 10.1101/gad.223834.113.

Shevelyov, Y. Y. *et al.* (2009) 'The B-type lamin is required for somatic repression of testis-specific gene clusters.', *Proceedings of the National Academy of Sciences of the United States of America*. National Academy of Sciences, 106(9), pp. 3282–7. doi: 10.1073/pnas.0811933106.

Shiio, Y. and Eisenman, R. N. (2003) 'Histone sumoylation is associated with transcriptional repression', *Proceedings of the National Academy of Sciences*, 100(23), pp. 13225–13230. doi: 10.1073/pnas.1735528100.

Shimi, T. *et al.* (2008) 'The A- and B-type nuclear lamin networks: microdomains involved in chromatin organization and transcription.', *Genes & development*. Cold Spring Harbor Laboratory Press, 22(24), pp. 3409–21. doi: 10.1101/gad.1735208.

Shimi, T. *et al.* (2011) 'The role of nuclear lamin B1 in cell proliferation and senescence.', *Genes & development*. Cold Spring Harbor Laboratory Press, 25(24), pp. 2579–93. doi: 10.1101/gad.179515.111.

Shimi, T. *et al.* (2015) 'Structural organization of nuclear lamins A, C, B1, and B2 revealed by superresolution microscopy', *Molecular Biology of the Cell*. Edited by K. Weis, 26(22), pp. 4075–4086. doi: 10.1091/mbc.E15-07-0461.

Shimi, T., Butin-Israeli, V. and Goldman, R. D. (2012) 'The functions of the nuclear envelope in mediating the molecular crosstalk between the nucleus and the cytoplasm', *Current Opinion in Cell Biology*, 24(1), pp. 71–78. doi: 10.1016/j.ceb.2011.11.007.

Shoeman, R. L. and Traub, P. (1990) 'The in Vitro DNA-binding Properties of Purified Nuclear Lamin Proteins and Vimentin*', *Kim, Y. et al. Mouse B-type lamins are required for proper organogenesis but not by embryonic stem cells. Science 24 Nov 2011 (doi:10.1126/science.1211222)*, 265(16), pp. 9055–9061.

Shumaker, D. K. *et al.* (2006) 'Mutant nuclear lamin A leads to progressive alterations of epigenetic control in premature aging.', *Proceedings of the National Academy of Sciences of the United States of America*, 103(23), pp. 8703–8708. doi: 10.1073/pnas.0602569103.

Silva, T. C. *et al.* (2018) 'ELMER v.2: An R/Bioconductor package to reconstruct gene regulatory networks from DNA methylation and transcriptome profiles', *Bioinformatics*, 2(October), pp. 1–4. doi: 10.1093/bioinformatics/bty902.

Sinensky, M. *et al.* (1994) 'The processing pathway of prelamin A', *Journal of Cell Science*, 107(1).

Singer-Sam J, R. A. (1993) 'X chromosome inactivation and DNA methylation.', *EXS*, 64, pp. 358–84. Available at: https://www.ncbi.nlm.nih.gov/m/pubmed/7678203/ (Accessed: 15 July 2019).

Smith, Z. D. and Meissner, A. (2013) 'DNA methylation: roles in mammalian development', *Nature Reviews Genetics*. Nature Publishing Group, 14(3), pp. 204–220. doi: 10.1038/nrg3354.

Solé-Boldo, L. *et al.* (2019) 'Single-cell transcriptomes of the aging human skin reveal loss of fibroblast priming', *bioRxiv*. Cold Spring Harbor Laboratory, p. 633131. doi: 10.1101/633131.

Solovei, I. *et al.* (2004) 'Positional changes of pericentromeric heterochromatin and nucleoli in postmitotic Purkinje cells during murine cerebellum development', *Cytogenetic and Genome Research*. Karger Publishers, 105(2–4), pp. 302–310. doi: 10.1159/000078202.

Solovei, I. *et al.* (2013) 'LBR and lamin A/C sequentially tether peripheral heterochromatin and inversely regulate differentiation.', *Cell*. Elsevier, 152(3), pp. 584–98. doi: 10.1016/j.cell.2013.01.009.

Solyom, S. *et al.* (2012) 'Extensive somatic L1 retrotransposition in colorectal tumors.', *Genome research*. Cold Spring Harbor Laboratory Press, 22(12), pp. 2328–38. doi: 10.1101/gr.145235.112.

Sorrell, J. M. and Caplan, A. I. (2004) 'Fibroblast heterogeneity: more than skin deep', *Journal of Cell Science*, 117(5), pp. 667–675. doi: 10.1242/jcs.01005.

van Steensel, B. and Belmont, A. S. (2017) 'Lamina-Associated Domains: Links with Chromosome Architecture, Heterochromatin, and Gene Repression', *Cell*. Cell Press, 169(5), pp. 780–791. doi: 10.1016/J.CELL.2017.04.022.

van Steensel, B. and Henikoff, S. (2000) 'Identification of in vivo DNA targets of chromatin proteins using tethered Dam methyltransferase', *Nature Biotechnology*. doi: 10.1038/74487.

Stewart, C. and Burke, B. (1987) 'Teratocarcinoma stem cells and early mouse embryos contain only a single major lamin polypeptide closely resembling lamin B', *Cell*. Cell Press, 51(3), pp. 383–392. doi: 10.1016/0092-8674(87)90634-9.

Stubbs, T. M. *et al.* (2017) 'Multi-tissue DNA methylation age predictor in mouse', *Genome Biology*. BioMed Central, 18(1), p. 68. doi: 10.1186/s13059-017-1203-5.

Stuurman, N., Heins, S. and Aebi, U. (1998) 'Nuclear Lamins: Their Structure, Assembly, and Interactions', *Journal of Structural Biology*. Academic Press, 122(1–2), pp. 42–66. doi: 10.1006/JSBI.1998.3987.

Subramanian, A. *et al.* (2005) 'Gene set enrichment analysis: A knowledge-based approach for interpreting genome-wide expression profiles', *Proceedings of the National Academy of Sciences*, 102(43), pp. 15545–15550. doi: 10.1073/pnas.0506580102.

Sullivan, T. *et al.* (1999) 'Loss of A-type lamin expression compromises nuclear envelope integrity leading to muscular dystrophy.', *The Journal of cell biology*. Rockefeller University Press, 147(5), pp. 913–20. doi: 10.1083/jcb.147.5.913.

Sun, D. *et al.* (2014) 'Epigenomic profiling of young and aged HSCs reveals concerted changes during aging that reinforce self-renewal.', *Cell stem cell*. NIH Public Access, 14(5), pp. 673–88. doi: 10.1016/j.stem.2014.03.002.

Sun, L. *et al.* (2018) 'Chromatin Architectural Changes during Cellular Senescence and Aging', *Genes*. Multidisciplinary Digital Publishing Institute, 9(4), p. 211. doi: 10.3390/genes9040211.

Swift, J. *et al.* (2013) 'Nuclear lamin-A scales with tissue stiffness and enhances matrix-directed differentiation.', *Science (New York, N.Y.)*. American Association for the Advancement of Science, 341(6149), p. 1240104. doi: 10.1126/science.1240104.

Swift, J. and Discher, D. E. (2014) 'The nuclear lamina is mechano-responsive to ECM elasticity in mature tissue.', *Journal of cell science*. The Company of Biologists Ltd, 127(Pt 14), pp. 3005–15. doi: 10.1242/jcs.149203.

Tang, C. W. *et al.* (2008) 'The integrity of a lamin-B1-dependent nucleoskeleton is a fundamental determinant of RNA synthesis in human cells.', *Journal of cell science*. The Company of Biologists Ltd, 121(Pt 7), pp. 1014–24. doi: 10.1242/jcs.020982.

Teschendorff, A. E., West, J. and Beck, S. (2013) 'Age-associated epigenetic drift: implications, and a case of epigenetic thrift?', *Human Molecular Genetics*. Narnia, 22(R1), pp. R7–R15. doi: 10.1093/hmg/ddt375.

The Progeria Research Foundation (2019) *Progeria 101 / FAQ*. Available at: https://www.progeriaresearch.org/progeria-101faq/.

Thompson, M. J. *et al.* (2017) 'An epigenetic aging clock for dogs and wolves', *Aging*, 9(3), pp. 1055–1068. doi: 10.18632/aging.101211.

Trapnell, C. *et al.* (2013) 'Differential analysis of gene regulation at transcript resolution with RNA-seq.', *Nature biotechnology*, 31, pp. 46–53. doi: 10.1038/nbt.2450.

Tsai, M.-Y. *et al.* (2006) 'A mitotic lamin B matrix induced by RanGTP required for spindle assembly.', *Science (New York, N.Y.)*. American Association for the Advancement of Science, 311(5769), pp. 1887–93. doi: 10.1126/science.1122771.

Tsurumi, A. and Li, W. (2012) 'Global heterochromatin loss', *Epigenetics*. Taylor & Francis, 7(7), pp. 680–688. doi: 10.4161/epi.20540.

Tubio, J. M. C. *et al.* (2014) 'Extensive transduction of nonrepetitive DNA mediated by L1 retrotransposition in cancer genomes', *Science*. American Association for the Advancement of Science, 345(6196), p. 1251343. doi: 10.1126/SCIENCE.1251343.

Turgay, Y. *et al.* (2017) 'The molecular architecture of lamins in somatic cells', *Nature*. Nature Publishing Group, 543(7644), pp. 261–264. doi: 10.1038/nature21382.

Vandiver, A. R. *et al.* (2015) 'Age and sun exposure-related widespread genomic blocks of hypomethylation in nonmalignant skin', *Genome Biology*. ???, 16(1), pp. 1–15. doi: 10.1186/s13059-015-0644-y.

Verdone, L., Caserta, M. and Mauro, E. Di (2005) 'Role of histone acetylation in the control of gene expression',

Biochemistry and Cell Biology. NRC Research Press Ottawa, Canada , 83(3), pp. 344–353. doi: 10.1139/o05-041.
Verstraeten, V. L. R. M. *et al.* (2008) 'Increased mechanosensitivity and nuclear stiffness in Hutchinson-Gilford progeria cells: Effects of farnesyltransferase inhibitors', *Aging Cell*, 7(3), pp. 383–393. doi: 10.1111/j.1474-9726.2008.00382.x.

Vidak, S. *et al.* (2015) 'Proliferation of progeria cells is enhanced by lamina-associated polypeptide 2α (LAP2α) through expression of extracellular matrix proteins', *Genes and Development*, 29(19), pp. 2022–2036. doi: 10.1101/gad.263939.115.

Vidak, S. and Foisner, R. (2016) 'Molecular insights into the premature aging disease progeria', *Histochemistry and Cell Biology*. Springer Berlin Heidelberg, 145(4), pp. 401–417. doi: 10.1007/s00418-016-1411-1.

Viteri, G., Chung, Y. W. and Stadtman, E. R. (2010) 'Effect of progerin on the accumulation of oxidized proteins in fibroblasts from Hutchinson Gilford progeria patients', *Mechanisms of Ageing and Development*, 131(1), pp. 2–8. doi: 10.1016/j.mad.2009.11.006.

Vogel, M. J., Peric-Hupkes, D. and van Steensel, B. (2007) 'Detection of in vivo protein–DNA interactions using DamID in mammalian cells', *Nature Protocols*, 2(6), pp. 1467–1478. doi: 10.1038/nprot.2007.148.

Vorburger, K. *et al.* (1989) 'A second higher vertebrate B-type lamin: cDNA sequence determination and in vitro processing of chicken lamin B2', *Journal of Molecular Biology*. Academic Press, 208(3), pp. 405–415. doi: 10.1016/0022-2836(89)90505-6.

Wagner, E. J. and Carpenter, P. B. (2012) 'Understanding the language of Lys36 methylation at histone H3', *Nature Reviews Molecular Cell Biology*. Nature Publishing Group, 13(2), pp. 115–126. doi: 10.1038/nrm3274.

Wajapeyee, N. *et al.* (2008) 'Oncogenic BRAF Induces Senescence and Apoptosis through Pathways Mediated by the Secreted Protein IGFBP7', *Cell*, 132(3), pp. 363–374. doi: 10.1016/j.cell.2007.12.032.

Wang, T. *et al.* (2017) 'Epigenetic aging signatures in mice livers are slowed by dwarfism, calorie restriction and rapamycin treatment', *Genome Biology*. BioMed Central, 18(1), p. 57. doi: 10.1186/s13059-017-1186-2.

Watanabe, S. *et al.* (2018) 'Interactions of HP1 Bound to H3K9me3 Dinucleosome by Molecular Simulations and Biochemical Assays', *Biophysical Journal*. Cell Press, 114(10), pp. 2336–2351. doi: 10.1016/J.BPJ.2018.03.025.
Weber, M. *et al.* (2007) 'Distribution, silencing potential and evolutionary impact of promoter DNA methylation in the human genome', *Nature Genetics*, 39(4), pp. 457–466. doi: 10.1038/ng1990.

Wen, B. *et al.* (2009) 'Large histone H3 lysine 9 dimethylated chromatin blocks distinguish differentiated from embryonic stem cells', *Nature Genetics*, 41(2), pp. 246–250. doi: 10.1038/ng.297.

Wheaton, K. *et al.* (2017) 'Progerin-Induced Replication Stress Facilitates Premature Senescence in Hutchinson-Gilford Progeria Syndrome.', *Molecular and cellular biology*. American Society for Microbiology (ASM), 37(14). doi: 10.1128/MCB.00659-16.

Wiles, E. T. and Selker, E. U. (2017) 'H3K27 methylation: a promiscuous repressive chromatin mark', *Current Opinion in Genetics & Development*. Elsevier Current Trends, 43, pp. 31–37. doi: 10.1016/J.GDE.2016.11.001.

Wilkerson, M. D. and Hayes, D. N. (2010) 'ConsensusClusterPlus: A class discovery tool with confidence assessments and item tracking', *Bioinformatics*, 26(12), pp. 1572–1573. doi: 10.1093/bioinformatics/btq170.

Wilson, H.-M. P. *et al.* (2002) 'Insulin-like growth factor binding protein-related protein 1 inhibits proliferation of MCF-7 breast cancer cells via a senescence-like mechanism.', *Cell growth & differentiation : the molecular biology journal of the American Association for Cancer Research*, 13(5), pp. 205–213.

Wood, A. M. *et al.* (2014) 'TRF2 and lamin A/C interact to facilitate the functional organization of chromosome ends', *Nature Communications*, 5(1), p. 5467. doi: 10.1038/ncomms6467.

Wood, J. G. *et al.* (2010) 'Chromatin remodeling in the aging genome of Drosophila', *Aging Cell*. John Wiley & Sons, Ltd (10.1111), 9(6), pp. 971–978. doi: 10.1111/j.1474-9726.2010.00624.x.

Xie, W. *et al.* (2018) 'DNA Methylation Patterns Separate Senescence from Transformation Potential and Indicate Cancer Risk', *Cancer Cell*, 33(2), pp. 309-321.e5. doi: 10.1016/j.ccell.2018.01.008.

Xiong, Z.-M. *et al.* (2016) 'Methylene blue alleviates nuclear and mitochondrial abnormalities in progeria', *Aging Cell*, 15(2), pp. 279–290. doi: 10.1111/acel.12434.

Yamamoto, K. *et al.* (2003) 'A Report of Two Cases of Werner's Syndrome and Review of the Literature', *Journal of Orthopaedic Surgery*, 11(2), pp. 224–233. doi: 10.1177/230949900301100222.

Yan, H. *et al.* (2015) 'Chromatin modifications and genomic contexts linked to dynamic DNA methylation patterns across human cell types', *Scientific Reports*. Nature Publishing Group, 5(1), p. 8410. doi: 10.1038/srep08410.

Yang, S. H. *et al.* (2006) 'A farnesyltransferase inhibitor improves disease phenotypes in mice with a Hutchinson-Gilford progeria syndrome mutation', *Journal of Clinical Investigation*, 116(8), pp. 2115–2121. doi: 10.1172/JCI28968.

Yang, S. H. *et al.* (2011) 'Are B-type lamins essential in all mammalian cells?', *Nucleus (Austin, Tex.)*. Taylor & Francis, 2(6), pp. 562–9. doi: 10.4161/nucl.2.6.18085.

Yao, L. *et al.* (2015) 'Inferring regulatory element landscapes and transcription factor networks from cancer methylomes', *Genome Biology*, 16(1), p. 105. doi: 10.1186/s13059-015-0668-3.

Yokochi, T. *et al.* (2009) 'G9a selectively represses a class of late-replicating genes at the nuclear periphery.', *Proceedings of the National Academy of Sciences of the United States of America*. National Academy of Sciences, 106(46), pp. 19363–8. doi: 10.1073/pnas.0906142106.

Young, S. G. *et al.* (2013) 'Targeting protein prenylation in progeria.', *Science translational medicine*. American Association for the Advancement of Science, 5(171), p. 171ps3. doi: 10.1126/scitranslmed.3005229.

Yuan, T. *et al.* (2015) 'An Integrative Multi-scale Analysis of the Dynamic DNA Methylation Landscape in Aging', *PLOS Genetics*. Edited by J. M. Greally. Public Library of Science, 11(2), p. e1004996. doi: 10.1371/journal.pgen.1004996.

Yue, Y., Liu, J. and He, C. (2015) 'RNA N6-methyladenosine methylation in post-transcriptional gene expression regulation', *Genes & Development*, 29(13), pp. 1343–1355. doi: 10.1101/gad.262766.115.

Zampieri, M. *et al.* (2015) 'Reconfiguration of DNA methylation in aging', *Mechanisms of Ageing and Development*. Elsevier Ireland Ltd, 151, pp. 60–70. doi: 10.1016/j.mad.2015.02.002.

Zhang, F. L. and Casey, P. J. (1996) 'Protein Prenylation: Molecular Mechanisms and Functional Consequences', *Annual Review of Biochemistry*. Annual Reviews 4139 El Camino Way, P.O. Box 10139, Palo Alto, CA 94303-0139, USA , 65(1), pp. 241–269. doi: 10.1146/annurev.bi.65.070196.001325.

Zhang, H., Xiong, Z.-M. and Cao, K. (2014) 'Mechanisms controlling the smooth muscle cell death in progeria via down-regulation of poly(ADP-ribose) polymerase 1.', *Proceedings of the National Academy of Sciences of the United States of America*. National Academy of Sciences, 111(22), pp. E2261-70. doi: 10.1073/pnas.1320843111.

Zhang, J. *et al.* (2011) 'A human iPSC model of Hutchinson Gilford Progeria reveals vascular smooth muscle and mesenchymal stem cell defects.', *Cell stem cell*. Elsevier, 8(1), pp. 31–45. doi: 10.1016/j.stem.2010.12.002.

Zhang, L. *et al.* (2017) 'DNA Methylation Landscape Reflects the Spatial Organization of Chromatin in Different Cells', *Biophysical Journal*. Cell Press, 113(7), pp. 1395–1404. doi: 10.1016/J.BPJ.2017.08.019.

Zhang, R., Erler, J. and Langowski, J. (2017) 'Histone Acetylation Regulates Chromatin Accessibility: Role of H4K16 in Inter-nucleosome Interaction', *Biophysical Journal*. Cell Press, 112(3), pp. 450–459. doi: 10.1016/J.BPJ.2016.11.015.

Zhang, W. *et al.* (2015) 'Aging stem cells. A Werner syndrome stem cell model unveils heterochromatin alterations as a driver of human aging.', *Science (New York, N.Y.)*. American Association for the Advancement of Science, 348(6239), pp. 1160–3. doi: 10.1126/science.aaa1356.

Zhang, Y. *et al.* (2008) 'Model-based analysis of ChIP-Seq (MACS)', *Genome Biology*, 9(R137). doi: 10.1186/gb-2008-9-9-r137.

Zhao, B. *et al.* (2010) 'The Hippo-YAP pathway in organ size control and tumorigenesis: an updated version', *Genes*

& Development, 24(9), pp. 862–874. doi: 10.1101/gad.1909210.

Zheng, X. *et al.* (2018) 'Lamins Organize the Global Three-Dimensional Genome from the Nuclear Periphery.', *Molecular cell*. Elsevier, 71(5), pp. 802-815.e7. doi: 10.1016/j.molcel.2018.05.017.

Zheng, X., Kim, Y. and Zheng, Y. (2015) 'Identification of lamin B–regulated chromatin regions based on chromatin landscapes', *Molecular Biology of the Cell*. Edited by D. G. Drubin, 26(14), pp. 2685–2697. doi: 10.1091/mbc.E15-04-0210.

Zheng, Y. *et al.* (2016) 'Blood Epigenetic Age may Predict Cancer Incidence and Mortality', *EBioMedicine*, 5, pp. 68–73. doi: 10.1016/j.ebiom.2016.02.008.

Zhou, W. *et al.* (2018) 'DNA methylation loss in late-replicating domains is linked to mitotic cell division', *Nature Genetics*. Springer US, 50(4), pp. 591–602. doi: 10.1038/s41588-018-0073-4.

Zink, D., Fischer, A. H. and Nickerson, J. A. (2004) 'Nuclear structure in cancer cells', *Nature Reviews Cancer*. Nature Publishing Group, 4(9), pp. 677–687. doi: 10.1038/nrc1430.

9. Acknowledgements

Many people have contributed to the success of this project and I would like to acknowledge their significance accordingly. At the same time, I would like to apologize to everyone, whose role in this work I - against all intentions - might have overlooked and not honored in the following.

To begin with, this project would not have been brought to life without the crucial role of two people. On the one hand, Prof. Dr. Frank Lyko was enthusiastic about initiating another research project focused on epigenetic changes occurring during the aging process in his laboratory. He directed me throughout the duration of it with his scientific expertise and wholehearted support, all of which I am deeply grateful for. Secondly, I would like to highlight the scientific contribution of Dr. Manuel Rodriguez-Paredes in starting this project, as it was born out of his scientific curiosity. Furthermore, he provided endless and invaluable guidance throughout its duration, both technical and theoretical in nature, which I value highly.

I would also like to thank Dr. Felix Bormann, who not only performed key analyses of the Dam ID-seq experiment but also, and more importantly, selflessly assisted me during his entire time in the group in performing bioinformatic analyses whenever necessary. Similarly, I am grateful for the substantial contributions Dr. Günter Raddatz and Dr. Julian Gutekunst made to the project, especially with regard to the ATAC-seq/RNA-seq and DNA methylation analyses, respectively, but also in the countless moments when I felt the need to consult their bioinformatic expertise. Of equal importance was the role of Tanja Musch, who practically assisted me whenever needed in the laboratory and therefore contributed critically to the success of the majority of the performed experiments. I would like to further thank Dr. Francesca Tuorto, Dr. Laura Wiehle, Dr. Thomas Hofmann, Llorenç Solé Boldo, Cansu Cirzi, Dr. Carine Legrand and Dr. Vitor Coutinho Carneiro for their sustained and helpful theoretical input; Dr. Leslie Gordon, Dr. Susan Campbell and Wendy Norris from the Progeria Research Foundation for their assistance in providing biological material and information; Katharina Hanna for her unlimited willingness to assist and her thorough knowledge of the laboratory, as well as all current and former members of the Lyko laboratory for their scientific and social contributions. Not forgotten either is the support of Dr. Barbara Leuchs, Matthias Schick, Dr. Angela Schulz (plus members of the DKFZ High-Throughput Core Facility), Dr. Oliver Mücke, Bojana Kriznik and Eva-Maria Weis in making this project successful.

9. Acknowledgements

With respect to the direction and development of this project, I would finally like to thank the additional members of my Thesis Advisory Committee, Prof. Dr. Karsten Rippe, Dr. Sylvia Erhardt, Dr. Anke Lonsdorf and Dr. Michael Milsom, for their scientific input, expert guidance and critical review of the work's progress.

Besides scientific and project-related achievements, my time at the institute was also characterized by a productive learning process in the areas of project management and team leadership. Accordingly, I would like to acknowledge the role several people played in the course of it. First and foremost, I am highly thankful to Michael Persicke, Lucy Wolf, Gintvile Valinciute and Maria Bonsack for their contributions to making the 2018/19 PhD Student Council of the German Cancer Research Center such a success story. Likewise, I am grateful to the members of the 2018/19 Retreat Team (Vanessa Dieterle, Julia Mändl, Johannes Heidbüchel, Luisa Henkel, Laura Llaó Cid, Milena Simovic and Katharina Bosch) and Social Events Team (Llorenç Solé Boldo, Cansu Cirzi, Khwab Sanghvi, Oguzhan Kaya, Jasmin Mangei, Michael Bonadonna, Robin Njenga), all of which I had the pleasure to organize and spend so many stressful, amusing and deeply rewarding moments with. Lastly, I would like to thank the Helmholtz International Graduate School for Cancer Research's Graduate Office, i.e., Dr. Lindsay Murrells, Lena Hartnagel, Dr. Franziska Schmidt, Angela Hemker and Heike Riehm-Geier, who made my time as a PhD Council member such a pleasant experience.

A three-and-a-half-year doctoral research project does not only require scientific expertise and development but also motivational perseverance. I would like to emphasize the role two people played in ensuring my motivational endurance throughout this period. First, I am sincerely grateful for the deep friendship I developed to Dr. Manuel Rodriguez-Paredes over the course of my stay in the laboratory. Its value and influence on this work, my scientific education and personal development is beyond imagination. Second, having met Laura Llaó Cid has had an impact on my life - inside and outside of the laboratory - that is hard to verbalize. Scientifically, her valuable advice, critical judgment and practical support underlie a substantial share of this work. Much more importantly, however, her unconditional love, adventurous spirit, as well as her unbreakably cheerful nature have made this period of my life so worthwhile; and I am looking forward to embark on the next adventure with her.

Last but not least, I would like to underscore how thankful I am to my parents, whose love, care and unwavering support have not only allowed me to arrive at this stage of my career, but also continue to motivate me for the challenges to come.